X1998-01028
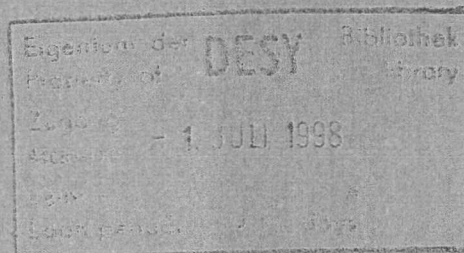
Improved QCD Perturbative Contributions and Power Corrections in Radiative and Semileptonic Rare B Decays

by

G. Hiller

To be sure that your reports and preprints are promptly included in the
HEP literature database
send them to (if possible by air mail):

DESY	DESY
Zentralbibliothek	Bibliothek
Notkestraße 85	Platanenallee 6
22603 Hamburg	15738 Zeuthen
Germany	Germany

IMPROVED QCD PERTURBATIVE CONTRIBUTIONS AND POWER CORRECTIONS IN RADIATIVE AND SEMILEPTONIC RARE B DECAYS

DISSERTATION
ZUR ERLANGUNG DES DOKTORGRADES
DES FACHBEREICHS PHYSIK
DER UNIVERSITÄT HAMBURG

VORGELEGT VON
GUDRUN HILLER
AUS HAMBURG

HAMBURG
1998

Gutachter der Dissertation:	Prof. Dr. A. Ali
	Prof. Dr. G. Kramer
Gutachter der Disputation:	Prof. Dr. A. Ali
	Prof. Dr. J. Bartels
Datum der Disputation:	16. Juni 1998
Sprecher des Fachbereichs Physik und Vorsitzender des Promotionsausschusses:	Prof. Dr. B. Kramer

Abstract

We calculate the leading power corrections to the decay rates, distributions and hadronic spectral moments in rare inclusive $B \to X_s \ell^+ \ell^-$ decays in the standard model, using heavy quark expansion (HQE) in $(1/m_b)$ and a phenomenological model implementing the Fermi motion effects of the b-quark bound in the B-hadron. We include next-to-leading order perturbative QCD corrections and work out the dependences of the spectra, decay rates and hadronic moments on the model parameters in either HQE and the Fermi motion model. In the latter, we take into account long-distance effects via $B \to X_s + (J/\psi, \psi', ...) \to X_s \ell^+ \ell^-$ with a vector meson dominance ansatz and study the influence of kinematical cuts in the dilepton and hadronic invariant masses on branching ratios, hadron spectra and hadronic moments.

We present leading logarithmic QCD corrections to the $b \to s\gamma\gamma$ amplitude. The QCD perturbative improved $B_s \to \gamma\gamma$ branching ratio is given in the standard model including our estimate of long-distance effects via $B_s \to \phi\gamma \to \gamma\gamma$ and $B_s \to \phi\psi \to \phi\gamma \to \gamma\gamma$ decays. The uncertainties due to the renormalization scale and the parameters of the HQE inspired bound state model are worked out.

Zusammenfassung

Wir berechnen im Standardmodell mit der Entwicklung schwerer Quarks (ESQ) Korrekturen in $(1/m_b)$ zu Zerfallsbreiten, Verteilungen und hadronischen Momenten des seltenen, inklusiven Zerfalls $B \to X_s \ell^+ \ell^-$. Dieselbe Analyse haben wir im phänomenologischen Fermibewegungsmodell durchgeführt, welches die Effekte des im B-Meson gebundenen b-Quarks beschreibt. In beiden Methoden zeigen wir unter Einbeziehung nicht führender QCD–Korrekturen die Abhängigkeit der Spektren, Breiten und Momente von den Modellparametern. Mit einem Vektormesondominanzansatz modellieren wir im Fermibewegungsmodell die langreichweitigen Beiträge der Charmoniumresonanzen, die durch $B \to X_s + (J/\psi, \psi', ...) \to X_s \ell^+ \ell^-$ entstehen. Wir studieren den Einfluß kinematischer Schnitte in der invarianten Masse des Leptonpaares und des hadronischen Endzustandes auf Verzweigungsverhältnisse, hadronische Verteilungen und Momente des Zerfalls $B \to X_s \ell^+ \ell^-$.

Ferner präsentieren wir führende logarithmische QCD–Korrekturen in der $b \to s\gamma\gamma$ Amplitude. Wir geben das QCD–verbesserte Verzweigungsverhältnis von $B_s \to \gamma\gamma$ im Standardmodell unter Berücksichtigung unserer Abschätzung langreichweitiger Beiträge durch die Zerfallsketten $B_s \to \phi\gamma \to \gamma\gamma$ und $B_s \to \phi\psi \to \phi\gamma \to \gamma\gamma$ an. Wir schätzen die Unsicherheiten durch die Renormierungsskala und des B_s Bindungszustandsmodelles, welches der Theorie schwerer Quarks entlehnt ist, ab.

Abstract

We calculate the leading power corrections to the decay rates, distributions and hadronic spectral moments in rare inclusive $B \to X_s \ell^+\ell^-$ decays in the standard model, using heavy quark expansion (HQE) in $(1/m_b)$ and a phenomenological model implementing the Fermi motion effects of the b-quark bound in the B-hadron. We include next-to-leading order perturbative QCD corrections and work out the dependence of the spectra, decay rates and hadronic moments on the model parameters in either HQE and the Fermi motion model. In the latter, we take into account long-distance effects via $B \to X_s + (1/\psi, \psi', ...) \to X_s \ell^+\ell^-$ with a vector meson dominance and study the influence of kinematical cuts in the dilepton and hadronic invariant masses on branching ratios, hadron spectra and hadronic moments.

We present leading logarithmic QCD corrections to the $b \to s\gamma\gamma$ amplitude. The perturbative improved $B_s \to \gamma\gamma$ branching ratio is given in the standard model including our estimate of long-distance effects via $B_s \to \phi\gamma \to \gamma\gamma$ and $B_s \to \phi\phi \to \gamma\gamma$ decays. The uncertainties due to the renormalization scale and the parameters of the HQE inspired bound state model are worked out.

Zusammenfassung

Wir berechnen im Standardmodell mit der Entwicklung schwerer Quarks (HSQ) Korrekturen in $(1/m_b)$ zu Zerfallsraten, Verteilungen und hadronischen Momenten des seltenen, inklusiven Zerfalls $B \to X_s \ell^+\ell^-$. Dieselbe Analyse haben wir im phänomenologischen Fermibewegungsmodell durchgeführt, welches die Effekte des im B-Meson gebundenen b-Quarks beschreibt. In beiden Methoden zeigen wir unter Elfwicklung nicht höherer QCD-Korrekturen die Abhängigkeit der Spektren, Breiten und Momente von den Modellparametern. Mit einem Vektormeson-dominananz modellieren wir im Fermibewegungsmodell die langreichweitigen Beiträge der Charmoniumresonanzen, die durch $B \to X_s + (1/\psi, \psi', ...) \to X_s \ell^+\ell^-$ entstehen. Wir studieren den Einfluß kinematischer Schnitte in der invarianten Masse des Leptonpaares und der hadronischen Endzustandes auf Verzweigungsverhältnisse, hadronische Verteilungen und Momente des Zerfalls $B \to X_s \ell^+\ell^-$.

Ferner präsentieren wir führende logarithmische QCD-Korrekturen in der $b \to s\gamma\gamma$ Amplitude. Wir geben das QCD-verbesserte Verzweigungsverhältnis von $B_s \to \gamma\gamma$ im Standardmodell unter Berücksichtigung unserer Abschätzung langreichweitiger Beiträge durch die Zerfallsraten $B_s \to \phi\gamma \to \gamma\gamma$ und $B_s \to \phi\phi \to \gamma\gamma$ an. Wir reduzieren die Unsicherheiten durch die Renormierungsskala und des B_s Bindungszustandsmodellns, welches der Theorie schwerer Quarks entlehnt ist, ab.

Contents

2

Chapter 1

Introduction

Rare B decays probe the flavour sector of the standard model (SM) [1] and perturbative and non-perturbative aspects of QCD. Since the first measurement of rare radiative $B \to K^* \gamma$ decays by the CLEO collaboration [2] this area of particle physics has received much experimental [3] and theoretical [4] attention. Flavour changing neutral current (FCNC) induced decays are of particular interest, since in the SM they are governed by loop effects and depend sensitively on virtual particles like, e.g., the top quark and Cabibbo Kobayashi Maskawa (CKM) matrix elements [5].

The theory of the effective Hamiltonian [6–10] (see section 2.2 for a discussion) $\mathcal{H}_{eff} \sim \sum C_i O_i$ enables a description of low energy weak processes in terms of short-distance (Wilson) coefficients C_i, which can be calculated perturbatively. The (new) vertices O_i, which are absent in the full Lagrangian, are obtained by integrating out the heavy particles (W, t, ϕ in the SM) from the full theory. Their coupling strength is given by the C_i, which characterize the short-distance dynamics of the underlying theory.

The Wilson coefficient C_7^{eff} corresponds to the effective $bs\gamma$ vertex. Its modulus $|C_7^{\text{eff}}|$ is constrained by the measurement of the inclusive $B \to X_s \gamma$ branching ratio at CLEO [11]. The CLEO result is in agreement with the present theoretical SM prediction in $B \to X_s \gamma$ decay and moreover, can exclude large parameter spaces of non-standard models.

The transition $b \to s\ell^+\ell^-$ with $\ell = e, \mu, \tau$ involves besides the electromagnetic penguin $b \to s\gamma^* \to s\ell^+\ell^-$ also electroweak penguins $b \to sZ^{0*} \to s\ell^+\ell^-$ and boxes. They give rise to two additional Wilson coefficients in the semileptonic decay $B \to X_s\ell^+\ell^-$, C_9 and C_{10}. A model independent fit of the short-distance coefficients C_9, C_{10} and C_7^{eff} is possible from the following three observables [12]: The $B \to X_s\gamma$ branching ratio $\mathcal{B}(B \to X_s\gamma)$, the (partly integrated) invariant dilepton mass spectrum and the Forward-Backward (FB) asymmetry [13] in $B \to X_s\ell^+\ell^-$ decays. They involve independent combinations of the Wilson coefficients, which allows the determination of sign and magnitude of C_7^{eff}, C_9 and C_{10} from data.

The presence of charmonium resonances in the decay $B \to X_s\ell^+\ell^-$ complicates this analysis. The $c\bar{c}$ states appear via $B \to X_s + (J/\psi, \psi', ...) \to X_s\ell^+\ell^-$ and can be taken into account in a phenomenological vector meson dominance (VMD) ansatz, which is assumed to hold near the $J/\psi, \psi', \ldots$ peaks [13]. Hence, kinematical cuts on the dilepton mass q^2 have to be imposed to remove the dominant resonance contributions and to disentangle the short-distance information from the long-distant one, e.g.,

$q^2 < m^2_{J/\psi} - \delta$. Here δ is an experimental cut-off parameter and typically of order a few hundred MeV. The restriction to certain regions of phase space explains the use of *partly* integrated spectra. The net effect of the resonances is an additional error on the distributions and hinders the determination of the short-distance coefficients C_i from experimental data. Hence, they must be evaluated by taking into account theoretical dispersion by using different phenomenological models [14] or further experimental input.

The bound state nature of heavy hadrons can be explored within the B-system. Non-perturbative power corrections in $(\Lambda_{QCD}/m_b)^n$ are systematically obtained with the heavy quark expansion (HQE) technique [15], parametrizing distributions, decay rates etc. in terms of higher order matrix elements, denoted by λ_1, λ_2 for $n = 2$. We recall the HQE relation $m_B = m_b + \bar{\Lambda} - (\lambda_1 + 3\lambda_2)/2m_b + \mathcal{O}(1/m_b^2)$ between the physical B-meson and the b-quark mass, where $\bar{\Lambda}$ accounts for the "binding energy". The HQE method has been applied to semileptonic charged current $B \to X\ell\nu_\ell$ [16] and FCNC $B \to X_s\gamma$ [17] decays, and it is known that inclusive spectra are not entirely calculable with the HQE approach [16], [18–21]. B-meson wave function effects have been estimated in $B \to X_{u,c}\ell\nu_\ell$ [22,23] and $B \to X_s\gamma$ [6,24] decays with a phenomenological Fermi motion model (FM) [22].

We present here a detailed analysis of inclusive $B \to X_s\ell^+\ell^-$ decays in the SM with $\ell = e, \mu$, (since we neglected lepton masses in our calculation the result cannot be used in the τ case), following similar studies for charged current $B \to X\ell\nu_\ell$ and radiative $B \to X_s\gamma$ decays.

This thesis contains the following points [18,25,26,14]:

- We calculate the $1/m_b^2$ power corrections using HQE techniques in $B \to X_s\ell^+\ell^-$ decays in the dilepton invariant mass distribution. This corrects an earlier calculation [17] and has been confirmed recently [27]. We find that the HQE breaks down near the high q^2 end-point, hence the spectrum cannot be used in this region.

- Alternatively, we study B-meson wave function effects with a Gaussian FM. We present the dilepton invariant mass distribution and the FB asymmetry and investigate the dependence on the FM model parameters.

- We include $c\bar{c}$ resonance effects in $B \to X_s\ell^+\ell^-$ spectra with the help of a VMD model and present the distributions including next-to-leading order perturbative QCD corrections.

- We present $1/m_b$ power corrections in the HQE approach and $\mathcal{O}(\alpha_s)$ perturbative corrections in the hadron spectra and hadronic spectral moments in $B \to X_s\ell^+\ell^-$ decays.

- The explicit dependences of the lowest moments of the hadronic energy E_H and the hadronic invariant mass S_H, $\langle E_H^n \rangle$, $\langle S_H^n \rangle$ for $n = 1, 2$ on the non-perturbative HQE parameters are worked out. We find that the first two moments of the hadronic invariant mass in $B \to X_s\ell^+\ell^-$ decay are sensitive to $\bar{\Lambda}$ and λ_1.

- We complement this profile of hadron spectra and moments in $B \to X_s\ell^+\ell^-$ decays by an analysis in the FM. The hadronic energy spectrum is found to be stable against a variation of the FM parameters, however, the hadronic invariant mass distribution depends significantly on them.

- We incorporate the charmonium resonances by means of the VMD model into the analysis of hadron spectra and moments in $B \to X_s \ell^+ \ell^-$ decays. The broadening of the resonances in the FM in the hadron spectra is worked out. Also the $c\bar{c}$ resonances turn out to be important in the moments.

- We investigate the resulting uncertainties in spectra and moments in $B \to X_s \ell^+ \ell^-$ decays from different parametrizations [28,29,18] of the resonant and non-resonant $c\bar{c}$ contributions.

- We work out hadron spectra, spectral moments and branching ratios in the FM with kinematical cuts, as used in the CLEO analysis in their search for the decays $B \to X_s \ell^+ \ell^-$, $\ell = e, \mu$ [30]. They imposed two kinds of cuts: one in the dilepton invariant mass to exclude the main bulk of the $J/\psi, \psi', \ldots$ resonances and another one in the hadronic invariant mass $S_H < 3.24 \, \text{GeV}^2$, to suppress the $B\bar{B}$ background. Our study of the $B \to X_s \ell^+ \ell^-$ branching ratios with cuts is of direct use to estimate the efficiency of the remaining signal.

To summarize, we shall present spectra, decay rates and hadronic spectral moments in inclusive rare $B \to X_s \ell^+ \ell^-$ decays in the standard model. The dilepton mass spectra and the FB asymmetry presented here are of use to extract the short-distance coefficients. We show that the uncertainties lying in different parametrizations of the charmonium resonance effects are not the dominant ones. Hadron spectra and moments in $B \to X_s \ell^+ \ell^-$ decays can be used to test HQE and FM and/or to determine their parameters. We point out that the HQE, where it is valid, and the FM show very similar behaviour. Moreover, some of their parameters can be related. In particular, the moments of the hadronic invariant mass in $B \to X_s \ell^+ \ell^-$ decays provide a complementary constraint on the non-perturbative HQE parameters $\bar{\Lambda}, \lambda_1$ to the one in charged current semileptonic $B \to X \ell \nu_\ell$ decays [31]. These decays can be used for a precise determination of these parameters. A related issue is the question of universality of the FM/HQE parameters for $b \to q$ transitions with final quarks $q = u, d, s$ or $q = c$. This remains to be tested. Finally, relating partly integrated hadron spectra of $B \to X_s \ell^+ \ell^-$ to semileptonic $B \to X_u \ell \nu_\ell$ decays, we expect the cancelation of uncertainties resulting from bound state effects, thus this offers the possibility of a precise determination of V_{ub}.

Further, we study the exclusive mode $B_s \to \gamma\gamma$, which in the SM has a branching ratio in reach of future B-facilities [3]. We improve earlier analyses [32–34] by including leading logarithmic QCD corrections to the short-distance $b \to s\gamma\gamma$ amplitudes. We use the same effective Hamiltonian [6,7] as for $b \to s\gamma$, which, as we will show, contains a complete set of operators for both decays. The $B_s \to \gamma\gamma$ decay rate gets enhanced under renormalization, like the $B \to X_s\gamma$ decay rate [6]. Likewise, we obtain a strong dependence on the renormalization scale of the $B_s \to \gamma\gamma$ observables, the branching ratio and the CP ratio [35], the latter resulting from CP-odd and CP-even parts in the FCNC 2-photon amplitude. Moreover, modeling B_s bound state effects in a HQE inspired approach, we avoid the constituent quark mass value $m_s \sim m_K$, as used in previous analyses.

In our analysis of $B_s \to \gamma\gamma$ decay we take into account long-distance (LD) effects via intermediate (neutral) vector mesons. Especially the contribution due to $B_s \to \phi\gamma$ and subsequent decay $\phi \to \gamma$ is estimated and found to sizeably reduce the $B_s \to \gamma\gamma$ branching ratio. We use QCD sum rules to evaluate the $B_s \to \phi\gamma$ form factor and include the contribution from the gluon condensate. The VMD model is employed for the ϕ-meson photon conversion.

Finally, we perform a VMD based calculation of the decay $B_s \to \phi\psi \to \phi\gamma \to \gamma\gamma$, where we abbreviate $\psi \equiv (J/\psi, \psi', ...)$. We compare the LD-contribution to $B_s \to \gamma\gamma$ decay resulting from intermediate ψ production with the one obtained by the interaction of the virtual charm loop with soft gluons [36]. We find that both amplitudes are in good agreement within the accuracy of the calculation. The contribution due to intermediate charmonium resonances changes the $B_s \to \gamma\gamma$ branching ratio including the intermediate ϕ contribution by less than 1%.

Our work in $B_s \to \gamma\gamma$ decays [37,38] can be summarized as follows:

- We present leading logarithmic QCD corrections to the short-distance amplitude in $b \to s\gamma\gamma$ decay.

- We model B_s bound state effects in a HQE inspired approach, in contrast to the constituent quark model, which is used in the literature.

- We estimate the LD effect due to the decay chain $B_s \to \phi\gamma \to \gamma\gamma$, using QCD sum rules and VMD.

- We estimate the LD contribution through $B_s \to \phi\psi \to \phi\gamma \to \gamma\gamma$ using VMD.

We present the branching ratio and the CP ratio for $B_s \to \gamma\gamma$ decay in the SM, taking into account improved perturbative $\mathcal{O}(\alpha_s)$ contributions and long-distance effects via intermediate vector mesons. Uncertainties resulting from the renormalization scale and the bound state parameters are worked out.

Organization of the work

An introduction to rare B decays and the methods used is given in Chapter 2, where we discuss the effective Hamiltonian theory, rare radiative $B \to X_s\gamma$ decays and long-distance methods in inclusive B decays (HQET, FM and VMD). Chapter 3 is based on refs. [18,25,26,14]. Here we investigate inclusive $B \to X_s\ell^+\ell^-$ decays in the SM. We present branching ratios and various spectra, furthermore hadronic spectral moments are estimated. In chapter 4 the exclusive channel $B_s \to \gamma\gamma$ is analysed [37,38]. SM based branching ratios and CP ratios in $B_s \to \gamma\gamma$ decay are given and their uncertainties are worked out. Finally, chapter 5 contains a summary and an outlook. Input parameters, Feynman rules and utilities are collected in appendix A. The power corrections to the structure functions of the hadron tensor in $B \to X_s\ell^+\ell^-$ decays are given in appendix B, together with auxiliary functions and the FM double differential Dalitz distribution in the context of the dilepton mass spectrum and the FB asymmetry. Appendix C contains analytic expressions used in the derivation of hadron spectra and hadronic spectral moment in $B \to X_s\ell^+\ell^-$ decays.

Chapter 2

Rare B Decays: Motivation and Methods

In this chapter we outline the flavour structure of the standard model (SM). We discuss the CKM mixing matrix and motivate the importance of studying flavour changing neutral current (FCNC) $b \to s$ transitions. We introduce the necessary tool to include QCD perturbative corrections in weak decays, the effective Hamiltonian theory. As an application of the former we discuss $B \to X_s\gamma$ decay as the most prominent example of a rare B decay. Finally non-perturbative methods like the heavy quark expansion technique, the Fermi motion model and vector meson dominance are sketched.

2.1 The Flavour Sector in the Standard Model

In the quark sector of the SM, there are six quarks organized in 3 families. The left-handed quarks are put into weak isospin $SU(2)_L$ doublets

$$\begin{pmatrix} q_{up} \\ q'_{down} \end{pmatrix}_{i=1,2,3} = \begin{pmatrix} u \\ d' \end{pmatrix}_L , \begin{pmatrix} c \\ s' \end{pmatrix}_L , \begin{pmatrix} t \\ b' \end{pmatrix}_L , \tag{2.1}$$

and the corresponding right-handed fields transform as singlets under $SU(2)_L$. Under the weak interaction an up-quark (with $Q_u = 2/3e$) can decay into a down-quark (with $Q_d = -1/3e$) and a W^+ boson. This charged current is given as

$$J_\mu^{CC} = \frac{e}{\sqrt{2}\sin\theta_W} (\bar{u}, \bar{c}, \bar{t})_L \gamma_\mu V_{\text{CKM}} \begin{pmatrix} d \\ s \\ b \end{pmatrix}_L , \tag{2.2}$$

where the subscript $L = (1 - \gamma_5)/2$ denotes the left-handed projector and reflects the $V - A$ structure of J_μ^{CC} in the SM. Here the weak mixing (Weinberg-)angle θ_W is a parameter of the SM, which is measured with high accuracy [39]. The so-called Cabibbo Kobayashi Maskawa (CKM) matrix V_{CKM} [5] describes the mixing between different quark flavours. It contains the angles describing the rotation between the eigen vectors of the weak interaction (q') and the mass eigen states (q)

$$\begin{pmatrix} d' \\ s' \\ b' \end{pmatrix} = V_{CKM} \begin{pmatrix} d \\ s \\ b \end{pmatrix} . \tag{2.3}$$

Symbolically, V_{CKM} can be written as

$$V_{\text{CKM}} \equiv \begin{pmatrix} V_{ud} & V_{us} & V_{ub} \\ V_{cd} & V_{cs} & V_{cb} \\ V_{td} & V_{ts} & V_{tb} \end{pmatrix}. \tag{2.4}$$

In general all the entries are complex numbers, only restricted by unitarity $V_{CKM}V_{CKM}^{\dagger} = 1$. They are parameters of the SM and can only be obtained from an experiment. Note that only three independent real parameters and one phase are left after imposing the unitarity condition. Some parametrizations of V_{CKM} can be seen in ref. [39].

A useful parametrization of the CKM matrix has been proposed by Wolfenstein [40]

$$V_{\text{Wolfenstein}} = \begin{pmatrix} 1 - \frac{1}{2}\lambda^2 & \lambda & A\lambda^3(\rho - i\eta) \\ -\lambda & 1 - \frac{1}{2}\lambda^2 & A\lambda^2 \\ A\lambda^3(1 - \rho - i\eta) & -A\lambda^2 & 1 \end{pmatrix} + \mathcal{O}(\lambda^4). \tag{2.5}$$

The parameters A, λ, ρ and the phase η are real numbers. λ is related to the Cabibbo angle through $\lambda = \sin\theta_C$ [39], which describes the quark mixing with 4 quark flavours. Since $\lambda \simeq 0.221$, the relative sizes of the matrix elements in eq. (2.4) can be read off from eq. (2.5). As can be seen, the diagonal entries are close to unity and the more off-diagonal they are, the smaller is the value of their corresponding matrix elements. The parameter A has been determined from the decays $b \to c\ell\nu_\ell$ and $B \to D^*\ell\nu_\ell$, yielding $A = 0.81 \pm 0.07$. The measurement of the ratio $|V_{ub}/V_{cb}| = 0.08 \pm 0.02$ yields $\sqrt{\rho^2 + \eta^2} = 0.36 \pm 0.09$. Likewise the mass difference $\triangle M_d \equiv M(B_d^{(1)}) - M(B_d^{(2)}) \simeq 0.46\,(ps)^{-1}$ constrains the combination $\sqrt{(1 - \rho)^2 + \eta^2}$. The observed CP-asymmetry parameter $\epsilon_K = 2.26 \cdot 10^{-3}$ constrains ρ and η. The precise determination of the parameters ρ and η is a high and important goal, since it corresponds to two important questions:

- Does CP hold in the SM ?? A non zero phase $\eta \neq 0$ in the CKM matrix directly leads to CP violating effects.

- The unitarity of the CKM matrix can be used to write down relations between its elements $\sum_{j=1}^{3} V_{ij}V_{jk}^{\dagger}$ $= \delta_{ik}$, $i, k = 1, 2, 3$. There are 6 orthogonality equations possible ($i \neq k$), and each can be represented graphically as a triangle, a so-called unitarity triangle (UT) [41]. The sides and angles of such an UT can be constrained by different types of experiments. For *the* UT given by the relation

$$V_{ud}V_{td}^* + V_{us}V_{ts}^* + V_{ub}V_{tb}^* = 0 , \tag{2.6}$$

there are 3 scenarios possible, which at present are not excluded experimentally and are a sign for *new physics*: 1. the UT does not close, i. e., $\sum_{i=1}^{3} \alpha_i \neq 0$, where α_i denotes the three angles of the triangle. 2. $\sum_{i=1}^{3} \alpha_i = 0$, but the values of the α_i are outside of their SM ranges determined by another type of experiment 3. $\sum_{i=1}^{3} \alpha_i = 0$, but the values of the angles are inconsistent with the measured sides of the triangle.

In the literature special unitarity triangles are discussed. A recent review over the present status on the CKM matrix and *the* unitarity triangle is given by [4].

2.1.1 Flavour changing neutral currents and why do we look for them in the B-system ?

In the SM, the neutral current mediated through the gauge bosons Z^0, γ, g does not change flavour. Therefore, the so-called Flavour changing neutral currents (FCNC) do not appear at tree level and are described by loop effects. The subject of the present work is an analysis of such rare (FCNC mediated) B decays in the SM. The quarks are grouped into *light* (u, d, s) and *heavy* (c, b, t) ones in the sense, that the mass of a heavy quark is much larger than the typical scale of the strong interaction, $\Lambda_{QCD} \sim 200$ MeV. The sixth quark, the top, is too heavy to build bound states because it decays too fast. The special role of the b-quark is that it is the heaviest one building hadrons. We will not discuss the "double" heavy B_c and concentrate on $B \equiv (\bar{b}q)$ meson transitions with light $q = u, d, s$. Since the b-quark is heavy, the B-system is well suited for a clean extraction of the underlying short-distance dynamics. Unlike the K-system, long-distance effects are expected to play a subdominant role in B decays except where such effects are present in a resonant form.

The motivation to investigate $b \to s(d)$ transitions is to improve the knowledge of the CKM matrix elements and to study loop effects. For the latter the interest is large, since there is no tree level FCNC decay possible in the SM. The leading loops give the leading contribution and they are sensitive to the masses and other properties of the internal virtual particles like e. g. the top. They can be heavy and therefore can be studied in a rare B decay at energies which are much lower than the ones necessary for a direct production of such particles. The idea is to compare the SM based prediction for a rare B decay with an experiment. A possible deviation gives a hint not only for the existence, but also for the structure of the "new physics" beyond the SM.

Further the B-system can be used as a testing ground for QCD, to check perturbative and non-perturbative methods. One example is the decay $B \to X_s\gamma$, which can be described in the lowest order at parton level through $b \to s\gamma$. As a 2-body decay, the photon energy in the b-quark rest frame is fixed: $E_\gamma = (m_b^2 - m_s^2)/2m_b$ for an on-shell γ. A possible non trivial spectrum can result from gluon bremsstrahlung $b \to s\gamma g$ and/or a non-perturbative mechanism, which is responsible for the motion of the b-quark inside the meson thus boosting the distribution. Such a bound state effect can be incorporated with e.g., the Fermi motion model, see section 2.4.2 for a brief discussion.

Some rare B decays have already been detected. The channel $B \to K^*\gamma$ has been measured from the CLEO collaboration some time ago [2], however the most prominent example of a rare B decay is the inclusive $B \to X_s\gamma$ [11], where X_s is any hadronic state with strangeness $s = 1$ and B is a mixture of $B^\pm$ and $B^0(\bar{B}^0)$. The branching ratios are found to be

$$B(B \to K^*\gamma)^{\text{CLEO}} = 4.2 \pm 0.8 \pm 0.6 \cdot 10^{-5} , \tag{2.7}$$

$$B(B \to X_s\gamma)^{\text{CLEO}} = 2.32 \pm 0.57 \pm 0.35 \cdot 10^{-4} . \tag{2.8}$$

Also the ALEPH collaboration has presented a preliminary result [42]

$$B(h_b \to X_s\gamma)^{\text{ALEPH}} = 3.29 \pm 0.71 \pm 0.68 \cdot 10^{-4} , \tag{2.9}$$

where h_b is any b flavoured hadron originating from Z^0 decays, $Z^0 \to h_b X$.

The calculation of the exclusive mode introduces large theoretical uncertainties due to the hadronic matrix elements. The inclusive decay is under better control, leading to the following result in the recently

completed NLO calculation [43], [44]

$$\mathcal{B}(B \to X_s\gamma)_{NLO} = 3.50 \pm 0.33 \cdot 10^{-4} \; . \tag{2.10}$$

Comparing eq. (2.8) and eq. (2.10), the CLEO measurement is found to be 2σ away from the theory, but the SM cannot be ruled out. One has to look for other decay modes, since improving the theoretical accuracy in $B \to X_s\gamma$ decay seems not at hand. After displaying the methods developed in $B \to X_s\gamma$, two other rare B decays, $B \to X_s\ell^+\ell^-$ with $\ell = e, \mu$ and the exclusive decay $B_s \to \gamma\gamma$ will be discussed in chapter 3 and chapter 4 of this work, respectively. Both candidates have branching ratios $\sim 10^{-6}$ which are in reach of future B experiments. The aim of this thesis is to analyse these decays within the framework of the SM and to present up to date predictions for measurable quantities (branching ratios, distributions, asymmetries, etc) as accurately as possible with the present available techniques.

$$W, \phi$$

$$b \qquad u, c, t \qquad s$$
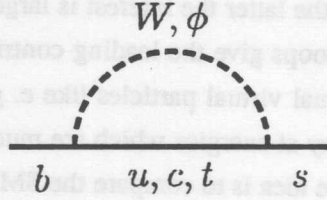
Figure 2.1: *A FCNC $b \to s$ diagram.*

A typical diagram for $b \to s$ is displayed in Fig. 2.1 from where the CKM couplings can be directly read off. The amplitude T is the sum over all internal up-quarks

$$T = \sum_{i=u,c,t} \lambda_i T_i \; ; \quad \lambda_i \equiv V_{ib}V_{is}^* \; . \tag{2.11}$$

Using the CKM unitarity $\sum_{i=u,c,t} \lambda_i = 0$ and the smallness of V_{ub} yielding $\lambda_u \ll \lambda_t$, we arrive at

$$T = \lambda_t(T_t - T_c) + \lambda_u(T_u - T_c) \simeq \lambda_t(T_t - T_c) \tag{2.12}$$

for a $b \to s$ amplitude in the SM. In the D-system the FCNC transition rates ($c \to u$) are much more suppressed due to an inbuilt GIM mechanism [45]. Here we have

$$\begin{aligned} T_{c \to u} &= \sum_{i=d,s,b} V_{ci}V_{ui}^*T_i \\ &= V_{cb}V_{ub}^*(T_b - T_s) + V_{cd}V_{ud}^*(T_d - T_s) \; , \end{aligned} \tag{2.13}$$

in which the first term is CKM suppressed and the second one GIM suppressed since $m_s^2 - m_d^2 \ll m_W^2$. The SM rates in the charm sector for decays such as $D^0 \to \gamma\gamma$, $D^0 \to \ell^+\ell^-$ are out of reach for present experiments. If one nevertheless finds something in the rare charm sector, it would be a direct hint for the desired physics beyond the SM.

2.2 The Effective Hamiltonian Theory

As a weak decay under the presence of the strong interaction, rare B decays require special techniques, to be treated economically. The main tool to calculate such rare B decays is the effective Hamiltonian theory. It is a two step program, starting with an operator product expansion (OPE) and performing a renormalization group equation (RGE) analysis afterwards. The necessary machinery has been developed over the last years, see [6–10], [46] and references therein.

The derivation starts as follows: If the kinematics of the decay are of the kind that the masses of the internal particles m_i are much larger than the external momenta p $m_i^2 \gg p^2$, then the heavy particles can be *integrated out*. This concept takes a concrete form with the functional integral formalism. It means that the heavy particles are removed as dynamical degrees of freedom from the theory, hence their fields do not appear in the (effective) Lagrangian anymore. Their residual effect lies in the generated effective vertices. In this way an effective low energy theory can be constructed from a full theory like the SM. A well known example is the four-Fermi interaction, where the W-boson propagator is made local for $q^2 \ll m_W^2$ (q denotes the momentum transfer through the W):

$$-i\frac{g_{\mu\nu}}{q^2 - m_W^2} \to ig_{\mu\nu}\left(\frac{1}{m_W^2} + \frac{q^2}{m_W^4} + \ldots\right), \tag{2.14}$$

where the ellipses denote terms of higher order in $1/m_W$. [1] Performing an OPE for QCD and electroweak interactions, the effective Hamiltonian for a FCNC $b \to s\gamma$ transition in the SM can be obtained by integrating out W, t, ϕ. Up to $\mathcal{O}(\frac{1}{m_W^4})$ it is given as:

$$\mathcal{H}_{eff}(b \to s\gamma) = -4\frac{G_F}{\sqrt{2}}\lambda_t \sum_{i=1}^{8} C_i(\mu)O_i(\mu), \tag{2.15}$$

where the weak couplings $g_W = \frac{e}{\sin\theta_W}$ are collected in the Fermi constant G_F

$$\frac{G_F}{\sqrt{2}} = \frac{g_W^2}{8m_W^2}, \tag{2.16}$$

$$G_F = 1.16639 \cdot 10^{-5} \text{ GeV}^{-2}. \tag{2.17}$$

The on-shell operator basis is chosen to be [7,6]

$$O_1 = (\bar{s}_{L\alpha}\gamma_\mu b_{L\alpha})(\bar{c}_{L\beta}\gamma^\mu c_{L\beta}),$$
$$O_2 = (\bar{s}_{L\alpha}\gamma_\mu b_{L\beta})(\bar{c}_{L\beta}\gamma^\mu c_{L\alpha}),$$
$$O_3 = (\bar{s}_{L\alpha}\gamma_\mu b_{L\alpha}) \sum_{q=u,d,s,c,b}(\bar{q}_{L\beta}\gamma^\mu q_{L\beta}),$$
$$O_4 = (\bar{s}_{L\alpha}\gamma_\mu b_{L\beta}) \sum_{q=u,d,s,c,b}(\bar{q}_{L\beta}\gamma^\mu q_{L\alpha}),$$
$$O_5 = (\bar{s}_{L\alpha}\gamma_\mu b_{L\alpha}) \sum_{q=u,d,s,c,b}(\bar{q}_{R\beta}\gamma^\mu q_{R\beta}),$$

---

[1] We remark here that the original way was reversed: The main historical step was to extrapolate the observed low energy 4-Fermi theory in nuclear β-decay to a dynamical theory of the weak interaction with heavy particle exchange.

$$O_6 = (\bar{s}_{L\alpha}\gamma_\mu b_{L\beta}) \sum_{q=u,d,s,c,b} (\bar{q}_{R\beta}\gamma^\mu q_{R\alpha}),$$

$$O_7 = \frac{e}{16\pi^2}\bar{s}_\alpha\sigma_{\mu\nu}(m_b R + m_s L)b_\alpha F^{\mu\nu},$$

$$O_8 = \frac{g}{16\pi^2}\bar{s}_\alpha T^a_{\alpha\beta}\sigma_{\mu\nu}(m_b R + m_s L)b_\beta G^{a\mu\nu}, \tag{2.18}$$

where $L(R) = 1/2(1 \mp \gamma_5)$, $\sigma_{\mu\nu} = \frac{i}{2}[\gamma_\mu, \gamma_\nu]$ and α, β are $SU(3)$ colour indices. T^a, $a = 1\ldots 8$ are the generators of QCD, some of their identities can be seen appendix A.2. Here $F^{\mu\nu}$, $G^{a\mu\nu}$ denote the electromagnetic and chromomagnetic field strength tensor, respectively. As can be seen from the operator basis, only degrees of freedom which are light compared to the heavy integrated out fields (W, t, ϕ), remain in the theory. The basis given above contains four-quark operators $O_{1\ldots 6}$, which differ by colour and left-right structure. Among them, the current-current operators O_1 and O_2 are the dominant four-Fermi operators. A typical diagram generating the so-called gluonic penguins $O_{3\ldots 6}$ is displayed in Fig. 2.2. The operators O_7 and O_8 are effective $b \to s\gamma$, $b \to sg$ vertices, respectively. All operators have dimension 6. For $b \to s\ell^+\ell^-$ transitions the basis eq. (2.18) should be complemented by two additional operators containing dileptons. They are discussed together with their corresponding Wilson coefficients in chapter 3.
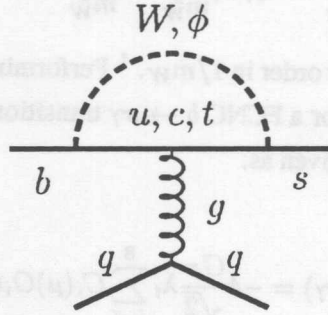
Figure 2.2: *A gluonic penguin diagram.*

The coupling strength of the introduced effective vertices O_i is given by the (c-numbers) Wilson coefficients $C_i(\mu)$. Their values at a large scale $\mu = m_W$ are obtained from a "matching" of the effective with the full theory. In the SM, the $C_i(m_W)$ read as follows [134]

$$C_{1,3\ldots 6}(m_W) = 0, \tag{2.19}$$

$$C_2(m_W) = 1, \tag{2.20}$$

$$C_7(m_W) = \frac{3x^3 - 2x^2}{4(x-1)^4}\ln x + \frac{-8x^3 - 5x^2 + 7x}{24(x-1)^3}, \tag{2.21}$$

$$C_8(m_W) = \frac{-3x^2}{4(x-1)^4}\ln x + \frac{-x^3 + 5x^2 + 2x}{8(x-1)^3}, \tag{2.22}$$

with $x = m_t^2/m_W^2$. It is convenient to define *effective* coefficients $C_{7,8}^{\text{eff}}(\mu)$ of the operators O_7 and O_8. They contain renormalization scheme dependent contributions from the four-quark operators $O_{1\ldots 6}$ in $\mathcal{H}_{eff}$ to the effective vertices in $b \to s\gamma$ and $b \to sg$, respectively. In the NDR scheme [2] , which will be

---

[2]We recall that in the naive dimensional regularization (NDR) scheme the γ_5 matrix is total anti-commuting, i. e. $\{\gamma_5, \gamma_\mu\} = 0$, thus $L\gamma_\mu = \gamma_\mu R$.

used throughout this work, they are written as [7]

$$C_7^{\text{eff}}(\mu) = C_7(\mu) + Q_d C_5(\mu) + Q_d N_c C_6(\mu) , \tag{2.23}$$
$$C_8^{\text{eff}}(\mu) = C_8(\mu) + C_5(\mu) . \tag{2.24}$$

Here N_c denotes the number of colours, $N_c = 3$ for QCD. The above expressions can be found from
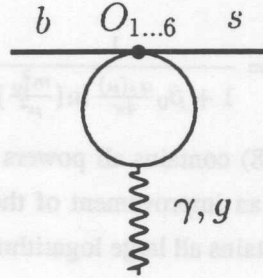
Figure 2.3: *The diagram contributing to the one loop $b \to s\gamma$, $b \to sg$ matrix element, respectively.*

evaluating the diagram shown in Fig. 2.3. Contributions from $O_{1...4}$, which correspond to an $\gamma_\mu L \otimes \gamma_\mu L$ like insertion, vanish for an on-shell photon, gluon, respectively. The Feynman rules consistent with these definitions are given in appendix A.3.

2.2.1   QCD improved α_s corrections

Our aim is now to include perturbative QCD corrections in the framework of the effective Hamiltonian theory. This can be done by writing down the renormalization group equation for the Wilson coefficients [3]

$$\mu \frac{\text{d}}{\text{d}\mu} C_i(\mu) = \gamma_{ji} C_j(\mu) , \tag{2.25}$$

where γ denotes the anomalous dimension matrix, i.e., in general the operators mix under renormalization. Solving this equation yields the running of the couplings $C_i(\mu)$ under QCD from the large matching scale (here $\mu = m_W$) down to the low scale $\mu \approx m_b$, which is the relevant one for b-decays. Eq. (2.25) can be solved in perturbation theory $g^2 = 4\pi\alpha_s$:

$$\gamma_{ji} = \frac{g^2}{16\pi^2}\gamma_{ji}^{(0)} + (\frac{g^2}{16\pi^2})^2\gamma_{ji}^{(1)} + \dots , \tag{2.26}$$

$$C_i(\mu) = C_i(\mu)^{(0)} + \frac{g^2}{16\pi^2}C_i(\mu)^{(1)} + \dots . \tag{2.27}$$

The initial values of the above RGE are the $C_i(m_W)$, which in the lowest order in the SM are given in eq. (2.19-2.22).

Let us for the moment concentrate on the special case that γ is a number. Then the lowest order solution is given by

$$C(\mu) = \eta^{\frac{\gamma^{(0)}}{2\beta_0}} C(m_W) , \tag{2.28}$$

---

[3] with $C_i = C_i(\mu, g)$ we have equivalently $\mu \frac{\text{d}}{\text{d}\mu} C_i = (\mu \frac{\partial}{\partial\mu} + \mu \frac{\text{d}g}{\text{d}\mu} \frac{\partial}{\partial g}) C_i$.

$$\eta = \frac{\alpha_s(m_W)}{\alpha_s(\mu)} , \qquad (2.29)$$

which can be easily checked by substituting it into eq. (2.25). In the derivation we have used the QCD β function, which describes the running of the strong coupling:

$$\beta(g) = \mu \frac{d}{d\mu} g = -g \left(\frac{g^2}{16\pi^2} \beta_0 + \left(\frac{g^2}{16\pi^2} \right)^2 \beta_1 \right) + \cdots , \qquad (2.30)$$

with its lowest order solution

$$\frac{\alpha_s(m_W)}{\alpha_s(\mu)} = \frac{1}{1 + \beta_0 \frac{\alpha_s(\mu)}{4\pi} \ln\left(\frac{m_W^2}{\mu^2} \right)} . \qquad (2.31)$$

We see that our obtained solution eq. (2.28) contains all powers of $\alpha_s(\mu) \ln\left(\frac{\mu}{m_W} \right)$. It is called leading logarithmic (LLog) approximation and is an improvement of the conventional perturbation theory. In general such a QCD improved solution contains all large logarithms like $n = 0, 1, \ldots$ (here with $\mu = m_b$)

$$\alpha_s^n(m_b) \ln^m\left(\frac{m_b}{m_W} \right) , \qquad (2.32)$$

where $m = n$ corresponds to LLog. A calculation including the next to lowest order terms is called next to leading order (NLO) and would result in a summation of all terms with $m = n - 1$ and so on. In the following we use the 2-loop expression for $\alpha_s(\mu)$ which can be always cast into the form

$$\alpha_s(\mu) = \frac{4\pi}{\beta_0 \ln(\mu^2/\Lambda_{QCD}^2)} \left[1 - \frac{\beta_1 \ln \ln(\mu^2/\Lambda_{QCD}^2)}{\beta_0^2 \ln(\mu^2/\Lambda_{QCD}^2)} \right] . \qquad (2.33)$$

With $N_f = 5$ *active* flavours (note that we integrated out the top) and $SU(N_c = 3)$ the values of the coefficients of the β function are

$$\beta_0 = \frac{23}{3} , \qquad \beta_1 = \frac{116}{3} . \qquad (2.34)$$

They are given in appendix A.2 for arbitrary N_c and N_f. The strong scale parameter $\Lambda_{QCD} \equiv \Lambda_{QCD}^{(N_f=5)}$ is chosen to reproduce the measured value of $\alpha_s(\mu)$ at the Z^0 pole. For $\alpha_s(m_Z) = 0.112, 0.117, 0.122$ we have $\Lambda_{QCD}^{(5)} = 160, 214, 280$ MeV, corresponding to the values of the input parameters listed in appendix A.1.

We recall that in LLog the calculation of the anomalous dimension and the matching conditions at lowest order, $\gamma^{(0)}, C_i^{(0)}(m_W)$ is required. In NLO a further evaluation of higher order diagrams yielding $\gamma^{(1)}, C_i^{(1)}(m_W)$ is necessary and in addition the hadronic matrix elements $\langle O_i \rangle$ have also to be known in $\mathcal{O}(\alpha_s)$.

In a general theory and also in the one relevant for rare radiative b decays given in eq. (2.15), the operators mix and the matrix γ has to diagonalized. In the latter case the (8×8) matrix $\gamma^{(0)}$ has been obtained by [8,9] and the running of the $C_i(\mu)$ in LLog approximation cannot be given analytically. The LLog solution for the Wilson coefficients ready for numerical analysis can be taken from [47]. We display the C_i for different values of the scale μ in Table 2.1. As can be seen, there is a strong dependence on the renormalization scale μ, especially for C_1 and C_7^{eff}. Other sources of uncertainty in the short-distance coefficients C_i are the top mass and the value of $\alpha_s(m_Z)$. We keep them fixed to their central values given in appendix A.1.

$C_i(\mu)$	$\mu = m_W$	$\mu = 10$ GeV	$\mu = 5$ GeV	$\mu = 2.5$ GeV
C_1	0	-0.161	-0.240	-0.347
C_2	1	1.064	1.103	1.161
C_3	0	0.007	0.011	0.016
C_4	0	-0.017	-0.025	-0.035
C_5	0	0.005	0.007	0.010
C_6	0	-0.019	-0.030	-0.046
C_7^{eff}	-0.196	-0.277	-0.311	-0.353
C_8^{eff}	-0.098	-0.134	-0.148	-0.164

Table 2.1: *Leading order Wilson coefficients in the Standard Model as a function of the renormalization scale μ.*

Here a comment about power counting in our effective theory is in order: As can be seen from Fig. 2.3 with an external photon, the insertion of four-Fermi operators generates a contribution to $b \rightarrow s\gamma$, which is also called a "penguin". It is a 1-loop diagram, but unlike "normal" perturbation theory, of order α_s^0. To get the α_s^1 contribution, one has to perform already 2 loops and so on. That means, the calculation of the LO(NLO) anomalous dimension matrix was a 2(3)-loop task.

A comprehensive discussion of weak decays beyond leading logarithms can be seen in ref. [46]. The main results of the NLO calculation in $B \rightarrow X_s\gamma$ decay will be given in section 2.3.

The advantages of the effective theory compared to the full theory can be summarized as follows:

- The effective theory is the more appropriate way to include QCD corrections. Large logarithms like $\ln(\mu/m_W)$ multiplied by powers of the strong coupling $\alpha_s(\mu)$, which spoil the perturbation series in the full theory, can be resummed with the help of the RGE.

- On the level of a generic amplitude $A = \langle \mathcal{H}_{eff} \rangle \sim \sum_i C_i(\mu)\langle O_i \rangle(\mu)$ the problem can be factorized into two parts: The short-distance (SD) information, which can be calculated perturbatively, is encoded in the C_i, and it is independent of the external states, i.e. quarks or hadrons. The long-distance (LD) contribution lies in the hadronic matrix elements. Both are separated by the renormalization scale μ. Of course the complete physical answer should not depend on the scale μ, truncating the perturbation series causes such a remaining dependence, which can be reduced only after including higher order terms or a full resummation of the theory.

- As long as the basis is complete, the effective Hamiltonian theory enables one to write down a model independent analysis in terms of the SD coefficients C_i. This is true for SM *near* extensions like the two Higgs doublet model (2HDM) and the minimal supersymmetric model (MSSM). Here one can try to fit the C_i from the data [12]. However, new physics scenarios like, e.g., the left-right symmetric model (LRM) require an extended operator set [48,49,50]. Wilson coefficients in the 2HDM and in supersymmetry (SUSY) can be seen in ref. [51] and ref. [52], respectively.

2.3 $B \to X_s \gamma$ in the Effective Hamiltonian Theory

The effective Hamiltonian theory displayed in the previous section is applied to $B \to X_s \gamma$ decay. Several groups have worked on the completion of the LLog calculation [8,9]. The anomalous dimension matrix at leading order $\gamma^{(0)}$ and the lowest order matching conditions (eq. (2.19-2.22)) govern the running of the LLog Wilson coefficients, denoted in this and only this section by $C_i^{(0)}(\mu)$, to separate them from the NLO coefficients. We discuss the improvement of the theory in $B \to X_s \gamma$ obtained from NLO analysis. In the remainder of this work we treat the Wilson coefficients C_i, $i = 1, \ldots 8$ in LLog approximation.

In the spectator model, the branching ratio for $B \to X_s \gamma$ in LLog approximation can be written as

$$\mathcal{B}(B \to X_s \gamma) = \mathcal{B}_{sl} \frac{\Gamma(b \to s\gamma)}{\Gamma(b \to ce\bar{\nu}_e)} = \frac{|\lambda_t|^2}{|V_{cb}|^2} \frac{6\alpha}{\pi f(\hat{m}_c)} |C_7^{(0)\mathrm{eff}}(\mu)|^2 \,, \tag{2.35}$$

where a normalization to the semileptonic decay $B \to X_c \ell \nu_\ell$ to reduce the uncertainty in the b-quark mass has been performed. Here $\mathcal{B}_{sl}$ denotes the measured semileptonic branching ratio and the phase space factor $f(\hat{m}_c)$ with $\hat{m}_c = m_c/m_b$ for $\Gamma(B \to X_c \ell \nu_\ell)$ can be seen in eq. (3.30).

As the branching ratio for $B \to X_s \gamma$ is mainly driven by $C_7^{(0)\mathrm{eff}}(\mu)$, several effects can be deduced:

- Including LLog QCD corrections enhance the branching ratio for $B \to X_s \gamma$ about a factor $2 - 3$, as can be seen in Table 2.1 (here denoted by $C_i(\mu)$) and changing the scale from $\mu = m_W$ down to $\mu \sim m_b$.

- While the sign of $C_7^{(0)\mathrm{eff}}$ is fixed within the SM, i.e. negative, it can be plus or minus in possible extensions of the SM. A measurement of $\mathcal{B}(B \to X_s \gamma)$ alone is not sufficient to determine the sign of $C_7^{(0)\mathrm{eff}}$, or in general, the sign of C_7^{eff} resulting from possible higher order calculations.

- The strong scale dependence of the value of $C_7^{(0)\mathrm{eff}}(\mu)$ causes serious problems in the accuracy of the LLog prediction. Varying the scale between $\frac{m_b}{2} \leq \mu \leq 2m_b$, results in an error in the branching ratio of $\pm 25\%$ [53], [7].

Because of the last point the NLO calculation was required. Several steps have been necessary for a complete NLO analysis. Let us illustrate how the individual pieces look like: At NLO, the matrix element for $b \to s\gamma$ renormalized around $\mu = m_b$ can be written as [7]:

$$\mathcal{M}(b \to s\gamma) = -4 \frac{G_F}{\sqrt{2}} \lambda_t D \langle O_7(m_b) \rangle_{tree} \,, \tag{2.36}$$

with

$$D = C_7^{\mathrm{eff}}(\mu) + \frac{\alpha_s(m_b)}{4\pi} \sum_i \left(C_i^{(0)\mathrm{eff}}(\mu) \gamma_{i7}^{(0)} \ln \frac{m_b}{\mu} + C_i^{(0)\mathrm{eff}}(\mu) r_{i7} \right) \,. \tag{2.37}$$

The r_{i7} are computed in ref. [43]. They contain the bremsstrahlung corrections [6], [54] $b \to s\gamma g$ and virtual corrections to the O_7 matrix element [43]. Especially the latter with an O_2 operator insertion demands an involved 2-loop calculation, see Figs. 1-4 in [43], where the corresponding diagrams are shown. It is consistent to keep the pieces in the parentheses in eq. (2.37), which are multiplied by $\alpha_s(m_b)$, in LLog approximation.

Now $C_7^{\mathrm{eff}}(\mu)$ has be be known at NLO precision,

$$C_7^{\mathrm{eff}}(\mu) = C_7^{(0)\mathrm{eff}}(\mu) + \frac{\alpha_s(m_b)}{4\pi}C_7^{(1)\mathrm{eff}}(\mu) \,. \tag{2.38}$$

As this job consists out of two parts, the work has been done by two groups: The $\mathcal{O}(\alpha_s^2)$ anomalous dimension matrix was obtained in ref. [44], which required the calculation of the residue of a large number of 3-loop diagrams, describing the mixing between the four-Fermi operators $O_{1\ldots6}$ and $O_{7,8}$. The second part, the NLO matching at $\mu = m_W$ has been done in ref. [55] and confirmed in ref. [56]. The NLO calculation reduces the $\mu = \mathcal{O}(m_b)$ scale uncertainty in varying μ in the range $\frac{m_b}{2} \leq \mu \leq 2m_b$ drastically to $\pm 4.3\%$ [57] and suggests for $B \to X_s\gamma$ a scale $\mu = \frac{m_b}{2}$ as an "effective" NLO calculation through

$$\Gamma(B \to X_s\gamma)_{LO}(\mu = \frac{m_b}{2}) \approx \Gamma(B \to X_s\gamma)_{NLO} \,. \tag{2.39}$$

As a final remark on scale uncertainties it should be noted that in the foregoing the top quark and the W have been integrated out at the same scale $\mu = m_W$, which is an approximation to be tested. It is justified by the fact that the difference between $\alpha_s(m_W)$ and $\alpha_s(m_t)$ is much smaller than the one between $\alpha_s(m_W)$ and $\alpha_s(m_b)$. [4] The authors of [57] analysed the dependencies on both the W matching scale $\mu_W = \mathcal{O}(m_W)$ and the one at which the running top mass is defined: $\bar{m}_t(\mu_t)$ and $\mu_W \neq \mu_t$. Similar to the m_b scale they allowed for μ_W, μ_t a possible range: $\frac{m_x}{2} \leq \mu_x \leq 2m_x$ where $x = W, t$. Their findings are that the μ_W, μ_t uncertainty is much smaller (namely $\pm 1.1\%, \pm 0.4\%$ at $\mu \sim m_b$ in NLO, respectively) than the uncertainty in the scale around m_b and therefore negligible.

2.4 Long-Distance Effects in Inclusive B Decays

In this section we sketch the methods to treat the LD effects in inclusive B decays. We have effects due to the confinement of the quarks in a bound state and due to resonances. They will be explained more detailed in the following chapters when and where necessary. For the evaluation of the exclusive channels we refer to chapter 4 in which the rare mode $B_s \to \gamma\gamma$ is discussed, especially section 4.2.

There are mainly two different approaches to take into account the effects of the B-meson bound state, the heavy quark expansion (HQE) and the phenomenologically motivated Fermi motion model (FM). While the former is a field theory in the framework of the heavy quark limit of QCD and has an interest of its own, the latter serves as a model of the data and has no intrinsic problems like end-point singularities etc. like HQE. Both models have parameters which can be related to each other and as they are used as *inclusive* methods, no form factors appear in the amplitudes. Inclusive decays are good from theoretical point of view and a challenge for experimentalists: An inclusive final state X is an average over a sufficiently high number of exclusive single (resonances) and continuous multi body states with the same quantum numbers as X. Inclusive decays involve the calculation of quark level processes. The underlying assumption of quark-hadron duality requires a large and dense populated phase space. By means of a "smearing" procedure, the singular behaviour in a local form is avoided and the differential spectra can be measured in a distribution sense.

---

[4]Using eq. (2.33) and the input parameters in Table A.1, we have $\alpha_s(m_W) = 0.12$, $\alpha_s(m_t) = 0.11$ and $\alpha_s(m_b) = 0.21$.

Another type of LD effect beside the bound state effect mentioned above, is due to resonances. A $(q\bar{q})$ spin 1 state can hadronize from a virtual q-loop. The conversion of such a vector meson into a photon is described by the phenomenological vector meson dominance (VMD) model.

2.4.1 The heavy quark expansion of QCD

Consider a hadron containing one heavy quark Q in the limit $m_Q \to \infty$. The other ingredients, light quarks and gluons, are seen as a light cloud around the heavy quark, sometimes also called the "light brown muck" [58], which exchanges small momenta of order Λ_{QCD} with Q for which a perturbative expansion is not useful. The parameter Λ_{QCD} characterizes the soft hadronic interaction scale. The heavy quark inside the bound state is treated as a static source of gauge charge (colour and electric charge): Q is so heavy compared to Λ_{QCD}, that it does not recoil as a result of the soft exchanges, it sits at rest in the hadron rest frame. This is the heavy quark limit of QCD.

New symmetries can be explored which are exact in the limit of an infinitely heavy quark: The light degrees of freedom are insensitive to the mass, flavour and spin of the heavy quark! This brings an enormous simplification of certain aspects of QCD, like the calculation of heavy quark matrix elements and hadron spectroscopy. However, for a firm phenomenological analysis we need to go from the predictions of heavy quark symmetry in the strict limit $m_Q \to \infty$ to a theory which provides a controlled expansion around this (academic) case. This can be done with the heavy quark expansion technique (HQET) in the limit $m_Q \gg \Lambda_{QCD}$. The necessary technology has been developed over the last decade and can be seen in a selection of papers [15,16] and references therein. A nice review on the HQE technique is given in ref. [59].

$1/m_b$ power corrections

Let us now switch to the system under consideration, the B-mesons. Since the b-quark is heavy, i. e. $m_b \sim 4.8\text{GeV} \gg \Lambda_{QCD} \sim 200\,\text{MeV}$, the success of the spectator model in $B \equiv (\bar{b}q)$ meson decays can be understood. Moreover, corrections in inverse powers of m_b to this can be systematically obtained with the help of the HQET.

The light degrees of freedom in the B-meson give rise to the parameter $\bar{\Lambda}$ which accounts for the binding energy of the bound state. In the limit of an infinitely heavy b-quark, i. e. $m_b \to \infty$ we have

$$m_B = m_b + \bar{\Lambda}\,, \tag{2.40}$$

where m_B denotes the B-meson mass. Corrections to this can be calculated within the following set up of HQE: The heavy b-quark momentum is written as $p_b = m_b v + k$, where k is a small residual momentum of order Λ_{QCD}. v denotes the velocity of the meson with momentum $P = m_B v$, which at rest is $v = (1, 0, 0, 0)$. It follows that the relative movement between the heavy quark and the meson is suppressed by powers of k/m_b. Performing an operator product expansion up to operators with canonical field dimension 5, the HQET mass relation modifies to [60]

$$m_B = m_b + \bar{\Lambda} - \frac{1}{2m_b}(\lambda_1 + 3\lambda_2) + \dots\,, \tag{2.41}$$

Reference	Method	$\bar{\Lambda}$ [GeV]	λ_1 [GeV^2]
Falk et al. [66]	Hadron Spectrum	≈ 0.45	≈ -0.1
Gremm et al. [31]	Lepton Spectrum	0.39 ± 0.11	-0.19 ± 0.10
Chernyak [67]	($\bar{B} \rightarrow X \ell \bar{\nu}$)	0.28 ± 0.04	-0.14 ± 0.03
Gremm, Stewart [68]		0.33 ± 0.11	-0.17 ± 0.10
Li, Yu [69]	Photon Spectrum ($\bar{B} \rightarrow X_s \gamma$)	$0.65^{+0.42}_{-0.30}$	$-0.71^{+0.70}_{-1.16}$

Table 2.2: *Determinations of the parameters $\bar{\Lambda}$ and λ_1 from inclusive decay spectra.*

likewise for B^* vector mesons

$$m_{B^*} = m_b + \bar{\Lambda} - \frac{1}{2m_b}(\lambda_1 - \lambda_2) + \dots , \qquad (2.42)$$

where the ellipses denote terms higher order in $1/m_b$. In general, the next to leading power corrections in HQET are parameterized in terms of these matrix elements of the kinetic energy and the magnetic moment operators λ_1 and λ_2, respectively. We can get the value of λ_2 from spectroscopy

$$\lambda_2 \simeq \frac{m_{B^*}^2 - m_B^2}{4} = 0.12 \, \text{GeV}^2 . \qquad (2.43)$$

The quantity λ_1 is subject to a theoretical dispersion. Its value has been determined from QCD sum rules, yielding $\lambda_1 = -(0.52 \pm 0.12)$ GeV^2 (Ball and Braun in [61]) and $\lambda_1 = -(0.10 \pm 0.05)$ GeV^2 (Neubert [62]). Further, the value for λ_1 has been extracted from an analysis of data on semileptonic B decays ($B \rightarrow X\ell\nu_\ell$), yielding $\lambda_1 = -0.20$ GeV^2 with a corresponding value $\bar{\Lambda} = 0.39$ GeV, as the two are correlated [31]. For a review on the spread in the present values of these non-perturbative parameters extracted from inclusive decay spectra, see Table 2.2, which is adopted from [63].

Now there is an intrinsic difficulty in the relation eq. (2.41). One can ask for the meaning of the "pole" mass m_b and $\bar{\Lambda}$? First of all, they are non-perturbative parameters and they add up in the combination given by eq. (2.41) to the physical B-meson mass. However, while the sum is fixed, there is a scheme dependent "renormalon" ambiguity of order Λ_{QCD} in both m_b and $\bar{\Lambda}$, which cancels out in physically measurable quantities [64]. Assuming universality, the parameters $m_b, \bar{\Lambda}$ determined by one experiment can be used to help the analysis of another decay, provided that one uses the same renormalization scheme prescription.

The power corrections in $B \rightarrow X_s\gamma$ decay including $1/m_b^2$ terms have been calculated in ref. [17]. The $1/m_b^3$ corrections have been recently reported in ref. [65]. However, the use of the last calculation is limited by the fact, that the matrix elements of the higher dimensional operators are almost unknown. In $B \rightarrow X_s\ell^+\ell^-$ decay the $1/m_b^2$ have been first calculated in ref. [17] (with massless s-quark) and corrected in ref. [18] with full m_s. The latter has been confirmed recently in the massless s-quark case in ref. [27]. Details of the HQET calculation are given in chapter 3.

$1/m_c$ **power corrections**

With $m_c \sim 1.4 \text{GeV} \gg \Lambda_{QCD}$ the charm is still a heavy quark and also $1/m_c$ power corrections are subject of present B-physics. A theoretically interesting structure, an effective $bs\gamma g$-vertex appears from the diagrams displayed in Fig. 2.4 [36]. The amplitude of this operator can be expanded in $1/m_c$. The power corrections in Λ_{QCD}/m_c to the $B \to X_s\gamma$ decay rate have been calculated first in ref. [70] and [71], however with the wrong sign. This has been settled now in favor of [72,73,27]. The resulting correction to the decay rate is found to be small:

$$\frac{\delta\Gamma(B \to X_s\gamma)}{\Gamma(B \to X_s\gamma)} = -\frac{C_2\lambda_2}{9C_7^{\text{eff}}m_c^2} \sim +0.03 \ . \tag{2.44}$$

The $1/m_c$ expansion is an alternative description of the virtual charm loop to the traditional vector meson
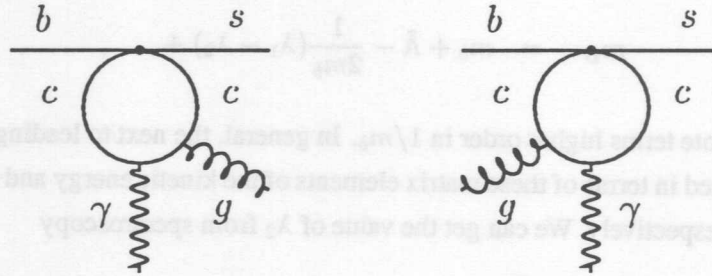

Figure 2.4: *The $bs\gamma g$-vertex at lowest order in QCD.*

dominance ansatz, (see section 2.4.3, Fig. 2.5) in regions of momentum transfer q^2 far away from the resonances.

Pros and cons of the HQE approach

- systematic expansion in $\Lambda_{QCD}/m_{c,b}$

- well-defined limit of QCD

- unknown matrix elements of higher order operators

- expansion breaks down in some regions of the phase space

The last point above corresponds to an uncomfortable property of the HQE method: The development of end-point singularities in inclusive decay spectra [16,18], hence only quantities smeared over a sufficiently large phase space interval are calculable. Such a smearing is incorporated, e.g., in the Fermi motion model [22], discussed in the next section.

2.4.2 The Fermi motion model

Another model to handle the effects of the bound state is the phenomenological Fermi motion model (FM) [22]. The FM is defined through the requirement that the $\bar{b}$-quark and the spectator quark q four-momenta add up to the $B = (\bar{b}q)$-meson four-momentum. In the rest frame of the B-meson the quarks fly back to

back with momentum $\vec{p} \equiv \vec{p_b} = -\vec{p_q}$. From energy conservation follows than that either the spectator or the $\bar{b}$ quark has to have a momentum dependent mass. In this work we choose m_q to be a parameter of the model and the $\bar{b}$ quark to have a p dependent mass. It reads

$$m_b^2(p) = m_B{}^2 + m_q{}^2 - 2m_B\sqrt{p^2 + m_q{}^2} \quad ; \quad p = |\vec{p}|. \tag{2.45}$$

The next assumption is that the momentum p obeys the Gaussian distribution function $\phi(p)$ weighted with the Fermi momentum p_F

$$\phi(p) = \frac{4}{\sqrt{\pi}p_F{}^3} \exp(\frac{-p^2}{p_F{}^2}), \tag{2.46}$$

with the normalization $\int_0^\infty dp\, p^2\, \phi(p) = 1$. The procedure to implement these wave function effects to a general parton model distribution obtained in the $\bar{b}$ quark rest frame is as follows:

1. replace the $\bar{b}$ quark mass by $m_b(p)$
2. boost the distribution into the B-meson rest frame and
3. fold the result with the wave function given in eq. (2.46).

For subsequent use in working out the normalization (decay widths) in the FM model, we also define an *effective* b-quark mass by

$$m_b^{\text{eff}} \equiv (\int_0^\infty dp\, p^2\, m_b(p)^5 \phi(p))^{1/5}. \tag{2.47}$$

The two parameters of the FM model, the Fermi momentum p_F and the spectator mass m_q can be fitted from data, however, up to now this procedure has not been very conclusive as still large ranges of the parameters are possible. The question appears here whether the FM parameters do depend on flavour, i. e., are they universal for $B \rightarrow X_f + (\gamma, leptons)$ with $f = d, u, s, c$ transitions. Further relations between the FM parameters (p_F, m_q) and the HQET parameters $(\lambda_1, \bar{\Lambda})$ can be obtained. However, there is no analogue of the magnetic moment coupling λ_2 in the FM.

We will return to the FM in chapter 3 to model the wave function effects in $B \rightarrow X_s \ell^+ \ell^-$ decay.

2.4.3 Vector meson dominance

Vector meson dominance (VMD) provides a mechanism to convert a spin 1 meson, here generically denoted by $V \equiv (q\bar{q})$ into a photon [74]. The creation of a $(q\bar{q})$ bound state from a virtual $q, \bar{q}$ pair and its subsequent conversion into a photon is displayed in Fig. 2.5. The intermediate vector meson propagator
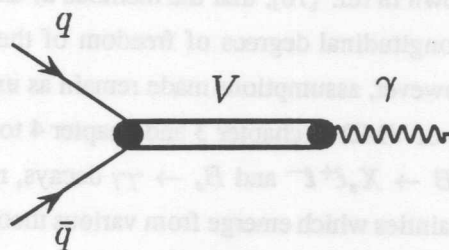

Figure 2.5: *The VMD conversion.*

equals $1/(m_V^2 - q^2 - im_V \Gamma_V^{tot})$, where the imaginary parts takes the effect of a finite total width Γ_V^{tot} of the V into account. The matrix element of the constituent current is defined as

$$< 0|\bar{q}\gamma_\mu q|V(q, \epsilon^V) > = f_V(q^2)m_V \epsilon_\mu^V , \qquad (2.48)$$

and the photon interacts with the (neutral) bound state through the electromagnetic current $J_\mu^{em} = eQ_q \bar{q}\gamma_\mu q$ as:

$$< 0|J_\mu^{em}|V(q, \epsilon^V) > = eQ_q f_V(q^2)m_V \epsilon_\mu^V . \qquad (2.49)$$

Here q, ϵ^V are the momentum and the polarization vector of the vector meson V, respectively and Q_q denotes the charge of the quark q in units of e. VMD conversion means that while $V \to \gamma$ also $\epsilon_\mu^V \to \epsilon_\mu$, where ϵ_μ is the polarization vector of the photon. The form factor at $q^2 = m_V^2$ can be obtained from measurement of the leptonic width

$$\Gamma(V \to e^+ e^-) = f_V^2 \frac{Q_q^2 4\pi \alpha^2}{3m_V} . \qquad (2.50)$$

What about $f_V(q^2)$ at $q^2 \neq m_V^2$? For the calculation of the form factor at $0 \leq q^2 \leq m_V^2$, there exist different ways, which are neither straightforward nor unique. a) First of all data on photo production $\gamma N \to VN$ at $q^2 = 0$ can be used. They indicate a large suppression of $f_V(0)$ compared to $f_V(m_V^2)$ only if the vector meson is heavy such as $V = J/\psi, \psi'$. As in this case $q^2 = m_{J/\psi}^2, m_{\psi'}^2$, to $q^2 = 0$ involves a large extrapolation in q^2. It is not expected to be so significant for $V = \rho, \omega, \phi$ as $q^2 = m_\rho^2$ etc. is not far away from $q^2 = 0$. This is what all the methods listed here share, that $f_V(q^2)$ decreases with decreasing q^2. b) Often a single-pole form is assumed to extrapolate the form factor to smaller values of the momentum transfer

$$f_V(q^2) = \frac{f_V(0)}{1 - q^2/m_{pole}^2} , \qquad (2.51)$$

where m_{pole} corresponds to the masses of higher resonances of the V. c) The approach by [75] is based on a dispersion relation calculation. It yields an interpolation formula between $f_V(0)$ and $f_V(m_V^2)$ where both can be fixed by data. The situation for $q^2 > m_V^2$ is unclear.

The VMD mechanism has been applied to $B \to X_s \gamma$ decay to estimate the long distance contribution through $B \to X_s \psi^i \to X_s \gamma$ by [76,77]. Here $\psi^i = J/\psi, \psi', \dots \psi^{(v)}$ are the known six charmonium resonances, see [39]. The $\psi^i \to \gamma$ conversion requires the knowledge of the form factor at $q^2 = 0$ for an on-shell photon. It has been shown in ref. [76], that the methods a) and c) listed above yield a consistent suppression at $q^2 = 0$. The longitudinal degrees of freedom of the ψ^i have been removed using the procedure proposed by [77]. However, assumptions made remain as uncertainties in the calculation.

We will make extensive use of VMD in chapter 3 and chapter 4 to include long-distance effects from intermediate vector mesons in $B \to X_s \ell^+ \ell^-$ and $B_s \to \gamma\gamma$ decays, respectively. However, in chapter 3 we estimate the resulting uncertainties which emerge from various theoretical approaches in implementing the q^2-dependence of the VMD-dominated amplitude.

Chapter 3

Inclusive $B \to X_s \ell^+ \ell^-$ Decay

This chapter contains a comprehensive analysis of $B \to X_s \ell^+ \ell^-$ decay in the standard model (SM). We include QCD improved $\mathcal{O}(\alpha_s)$ corrections, use heavy quark expansion techniques (HQET) and apply the Fermi motion model (FM). Further, the long-distance effects via intermediate $J/\psi, \psi', ...$ resonances are taken into account with a vector meson dominance (VMD) ansatz.

3.1   Introduction

Flavour changing neutral current (FCNC) decays $B \to X_s \ell^+ \ell^-$ and $B \to X_s \gamma$ are governed in the SM by loop effects. They provide a sensitive probe of the flavour sector in the SM and search for physics beyond. In the context of rare B decays the radiative mode $B \to X_s \gamma$ has been extensively discussed in chapter 2.

In this chapter we address inclusive $B \to X_s \ell^+ \ell^-$ decay with $\ell = e, \mu$. Since we are neglecting finite lepton masses we cannot apply our results to the τ-case. The $b \to s \ell^+ \ell^-$ transition has been studied earlier in the free quark model in refs. [78–80] in the lowest order in the SM context. The NLO $\mathcal{O}(\alpha_s)$ improvement in the invariant dilepton mass distribution and the decay rate has been worked out in refs. [9,47]. Leading $(1/m_b^2)$ power corrections in the HQET framework [15,16] in the invariant dilepton spectrum in $B \to X_s \ell^+ \ell^-$ decay have been reported in ref. [18], correcting an earlier calculation [17]. This has been recently confirmed in ref. [27] for the massless s-quark case. Another interesting quantity in $B \to X_s \ell^+ \ell^-$ is the FB asymmetry [13], also known at $1/m_b^2$ [18]. It can be used together with the branching ratio of $B \to X_s \gamma$ and the dilepton spectrum in $B \to X_s \ell^+ \ell^-$ for a model independent analysis of the short-distance coefficients [12] in the search for SUSY effects [81–83], [50]. The $1/m_b^2$ power corrections to the left-right asymmetry [84,85] have been presented in [86] correcting an earlier calculation of the same [85]. Both the FB asymmetry and the left-right asymmetry are defined in section 3.1.3. The longitudinal polarization of the lepton, P_L, in $B \to X_s \tau^+ \tau^-$ at the partonic level has been worked out [87]; the other two orthogonal polarization components P_T (the component in the decay plane) and P_L (the component normal to the decay plane) were subsequently worked out in [28]. The $\mathcal{O}(1/m_c^2)$ correction to the dilepton invariant mass spectrum in $B \to X_s \ell^+ \ell^-$ has also been calculated in [88], however, the result differs in sign from the one in [27]. This controversy, which goes back to the corresponding one in $B \to X_s \gamma$ decay (see section 2.4.1 for a discussion) has been settled in favor

of [27]. It is known that inclusive decay spectra are not entirely calculable with HQET [19–21], [16], especially, the expansion in powers of $1/m_b$ diverges in the high dilepton mass q^2 region in $B \to X_s \ell^+ \ell^-$ decay [18]. An alternative approach to take into account B-meson bound state effects is the FM model [22]. In the FM a prediction for the entire q^2 range for the dilepton mass distribution and FB asymmetry in $B \to X_s \ell^+ \ell^-$ decay has been given ref. [18]. The sensitivity of the distributions on the FM parameters is worked out there. Long-distance effects due to intermediate $B \to X_s + (J/\psi, \psi', ...) \to X_s \ell^+ \ell^-$ have been discussed in refs. [89,28,90] and recently [14]. Hadron spectra and hadronic spectral moments are presented in refs. [25,26,14] in both the HQE approach and the FM.

This chapter is divided into two parts. The first one (this section up to and including section 3.4) based on ref. [18], contains an introduction to $B \to X_s \ell^+ \ell^-$ decay, basic definitions and the $\mathcal{O}(\alpha_s)$ and $1/m_b^2$ corrected matrix element for $b \to s \ell^+ \ell^-$. Is is mainly devoted to the analysis of the dilepton invariant mass distribution and the FB asymmetry. In doing that, we derive leading power corrections to the decay rates and q^2 distributions in the decay $B \to X_s \ell^+ \ell^-$ using heavy quark expansion (HQE) in $(1/m_b)$. Further, wave function effects of the b-quark bound in the B-hadron are studied by us in the phenomenologically motivated Gaussian Fermi motion model. Using this model for estimating the non-perturbative effects, we include the dominant long-distance (LD) contributions from the decays $B \to X_s + (J/\psi, \psi', ...) \to X_s \ell^+ \ell^-$. Further, taking into account the next-to-leading order perturbative QCD corrections in $b \to s \ell^+ \ell^-$, we present the decay rates and distributions for the inclusive process $B \to X_s \ell^+ \ell^-$ in the SM.

The second part, starting from section 3.5 complements the study of $B \to X_s \ell^+ \ell^-$ decay and investigates hadron spectra and hadronic spectral moments. It is mainly based on refs. [25,26,14]. We compute the leading order (in α_s) perturbative QCD and power $(1/m_b^2)$ corrections to the hadronic invariant mass and hadron energy spectra in the decay $B \to X_s \ell^+ \ell^-$. The computations are carried out using HQET and a perturbative-QCD improved Fermi motion model which takes into account B-meson bound state effects. We also present results for the first two hadronic moments $\langle S_H^n \rangle$ and $\langle E_H^n \rangle$, $n = 1, 2$, working out their sensitivity on the HQET and FM model parameters. In the FM, also the LD effects due to intermediate charmonium resonances are taken into account. We study uncertainties in the parametrization of the $c\bar{c}$ effects. Further, we investigated the effect of the experimental cuts, used recently by the CLEO collaboration in searching for the decay $B \to X_s \ell^+ \ell^-$ [30], on the branching ratios, hadron spectra and hadronic invariant mass moments using the FM model.

3.1.1 Kinematics

We start with the definition of the kinematics of $B \to X_s \ell^+ \ell^-$ decay at parton level,

$$b(p_b) \to s(p_s)(+g(p_g)) + \ell^+(p_+) + \ell^-(p_-) , \tag{3.1}$$

where g denotes a gluon from the $O(\alpha_s)$ correction (see Fig. 3.2). We define the momentum transfer to the lepton pair and the invariant mass of the dilepton system, respectively, as

$$q \equiv p_+ + p_- , \tag{3.2}$$

$$s \equiv q^2 . \tag{3.3}$$

The dimensionless variables with a hat are related to the dimensionful variables by the scale m_b, the b-quark mass, e.g.,

$$\hat{s} = \frac{s}{m_b^2} \,, \quad \hat{m}_s = \frac{m_s}{m_b} \,, \tag{3.4}$$

etc.. Further, we define a 4-vector v, which denotes the velocity of both the b-quark and the B-meson, $p_b = m_b v$ and $p_B = m_B v$. We shall also need the variable u and the scaled variable $\hat{u} = \frac{u}{m_b^2}$, defined as:

$$u \equiv -(p_b - p_+)^2 + (p_b - p_-)^2 \,, \tag{3.5}$$

$$\hat{u} = 2v \cdot (\hat{p}_+ - \hat{p}_-) \,, \tag{3.6}$$

and further the kinematical phase factor

$$u(s, m_s) = \sqrt{(s - (m_b + m_s)^2)(s - (m_b - m_s)^2)} \,. \tag{3.7}$$

The scaled variables $\hat{s}$ and $\hat{u}$ in the decay $b \to s\ell^+\ell^-$ are bounded as follows,

$$-\hat{u}(\hat{s}, \hat{m}_s) < \hat{u} < +\hat{u}(\hat{s}, \hat{m}_s) \,,$$
$$\hat{u}(\hat{s}, \hat{m}_s) = \sqrt{[\hat{s} - (1 + \hat{m}_s)^2][\hat{s} - (1 - \hat{m}_s)^2]} \,,$$
$$4\hat{m}_l^2 < \hat{s} < (1 - \hat{m}_s)^2 \,. \tag{3.8}$$

3.1.2 NLO-corrected amplitude for $b \to s\ell^+\ell^-$

Next, the explicit expressions for the matrix element and (partial) branching ratios in the decays $b \to s\ell^+\ell^-$ are presented in terms of the Wilson coefficients of the effective Hamiltonian obtained by integrating out the top quark and the $W^\pm$ bosons,

$$\mathcal{H}_{eff}(b \to s + \ell^+\ell^-) = \mathcal{H}_{eff}(b \to s + \gamma) - \frac{4G_F}{\sqrt{2}} V_{ts}^* V_{tb} \left[C_9(\mu)O_9 + C_{10}O_{10} \right], \tag{3.9}$$

where $\mathcal{H}_{eff}(b \to s + \gamma)$ together with the operators $O_{1...8}$ and their corresponding Wilson coefficients $C_i(\mu)$ [7,6] can be seen in section 2.2. The two additional operators involving the dileptons O_9 and O_{10} are defined as:

$$O_9 = \frac{e^2}{16\pi^2} \bar{s}_\alpha \gamma^\mu L b_\alpha \bar{\ell} \gamma_\mu \ell \,,$$

$$O_{10} = \frac{e^2}{16\pi^2} \bar{s}_\alpha \gamma^\mu L b_\alpha \bar{\ell} \gamma_\mu \gamma_5 \ell \,. \tag{3.10}$$

A usual, CKM unitarity has been used in factoring out the product $V_{ts}^* V_{tb}$. Note that the chromomagnetic operator O_8 does not contribute to the decay $B \to X_s \ell^+\ell^-$ in the approximation which we use here. The Wilson coefficients are given in the literature (see, for example, [9,47]). They depend, in general, on the renormalization scale μ, except for C_{10}. At leading logarithmic (LLog) approximation, we use the values of the C_i given in Table 3.1.

With the help of the effective Hamiltonian in eq. (3.9) the matrix element for the decay $b \to s\ell^+\ell^-$ can be factorized into a leptonic and a hadronic part as,

$$\mathcal{M}(b \to s\ell^+\ell^-) = \frac{G_F \alpha}{\sqrt{2}\pi} V_{ts}^* V_{tb} \left[\left(C_9^{\text{eff}} - C_{10} \right) (\bar{s}\gamma_\mu L b)(\bar{\ell}\gamma^\mu L \ell) \right.$$

C_1	C_2	C_3	C_4	C_5	C_6	C_7^{eff}	C_9	C_{10}	$C^{(0)}$
-0.240	$+1.103$	$+0.011$	-0.025	$+0.007$	-0.030	-0.311	$+4.153$	-4.546	$+0.381$

Table 3.1: *Values of the Wilson coefficients used in the numerical calculations corresponding to the central values of the parameters given in Table A.1. Here, $C_7^{\text{eff}} \equiv C_7 - C_5/3 - C_6$, and for C_9 we use the NDR scheme and $C^{(0)} \equiv 3C_1 + C_2 + 3C_3 + C_4 + 3C_5 + C_6$.*

$$+ \left(C_9^{\text{eff}} + C_{10} \right) \left(\bar{s} \, \gamma_\mu \, L \, b \right) \left(\bar{\ell} \, \gamma^\mu \, R \, \ell \right)$$
$$- 2 C_7^{\text{eff}} \left(\bar{s} \, i \, \sigma_{\mu\nu} \frac{q^\nu}{q^2} (m_s L + m_b R) \, b \right) \left(\bar{\ell} \, \gamma^\mu \, \ell \right) \right] , \quad (3.11)$$

where we abbreviate $C_9^{\text{eff}} \equiv C_9^{\text{eff}}(\hat{s})$. We have kept the s-quark mass term in the matrix element explicitly and this will be kept consistently in the calculation of power corrections and phase space. The above matrix element can be written in a compact form,

$$\mathcal{M}(b \to s \ell^+ \ell^-) = \frac{G_F \alpha}{\sqrt{2}\pi} V_{ts}^* V_{tb} \left(\Gamma_\mu^L L^{L\mu} + \Gamma_\mu^R L^{R\mu} \right) , \quad (3.12)$$

with

$$L^{L/R}{}_\mu \equiv \bar{\ell} \, \gamma_\mu \, L(R) \, \ell , \quad (3.13)$$

$$\Gamma^{L/R}{}_\mu \equiv \bar{s} \left[R \gamma_\mu \left(C_9^{\text{eff}} \mp C_{10} + 2 C_7^{\text{eff}} \frac{\hat{q}}{\hat{s}} \right) + 2 \hat{m}_s \, C_7^{\text{eff}} \gamma_\mu \frac{\hat{q}}{\hat{s}} L \right] b . \quad (3.14)$$

where we have already used massless leptons in substituting $-2i\sigma_{\mu\nu}q^\nu = [\gamma_\mu, \hat{q}]$ by $2\gamma_\mu \hat{q}$ in the term proportional to C_7^{eff}.

The effective Wilson coefficient $C_9^{\text{eff}}(\hat{s})$ receives contributions from various pieces. The resonant $c\bar{c}$ states also contribute to $C_9^{\text{eff}}(\hat{s})$ and will be discussed in section 3.4; hence the contribution given below is just the perturbative part:

$$C_9^{\text{eff}}(\hat{s}) = C_9 \eta(\hat{s}) + Y(\hat{s}) . \quad (3.15)$$

The function $Y(\hat{s})$ represents the one-loop matrix element of the four-Fermi operators [47,9], see Fig. 3.1.
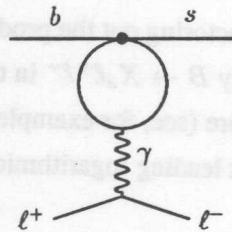

Figure 3.1: *The Feynman diagram responsible for the four-Fermi-operator contribution (depicted by the blob) to the operator O_9.*

It is written as:

$$
\begin{aligned}
Y(\hat{s}) =\ & g(\hat{m}_c, \hat{s})\,(3\,C_1 + C_2 + 3\,C_3 + C_4 + 3\,C_5 + C_6) \\
& - \frac{1}{2}g(1, \hat{s})\,(4\,C_3 + 4\,C_4 + 3\,C_5 + C_6) - \frac{1}{2}g(0, \hat{s})\,(C_3 + 3\,C_4) \\
& + \frac{2}{9}\,(3\,C_3 + C_4 + 3\,C_5 + C_6) - \xi\frac{4}{9}\,(3\,C_1 + C_2 - C_3 - 3\,C_4)\,,
\end{aligned}
\tag{3.16}
$$

$$
\xi = \begin{cases} 0 & \text{(NDR)}\,, \\ -1 & \text{(HV)}\,, \end{cases}
\tag{3.17}
$$

where (NDR) and (HV) correspond to the naive dimensional regularization and the 't Hooft-Veltman schemes, respectively. We recall that while C_9 is a renormalization scheme-dependent quantity, this dependence cancels out with the corresponding one in the function $Y(\hat{s})$ (the value of ξ, see above). The function $g(z, \hat{s})$ includes the quark-antiquark pair contribution [9,47]:

$$
\begin{aligned}
g(z, \hat{s}) =\ & -\frac{8}{9}\ln\left(\frac{m_b}{\mu}\right) - \frac{8}{9}\ln z + \frac{8}{27} + \frac{4}{9}y - \frac{2}{9}(2 + y)\sqrt{|1 - y|} \\
& \times \left[\Theta(1 - y)\left(\ln\frac{1 + \sqrt{1 - y}}{1 - \sqrt{1 - y}} - i\pi\right) + \Theta(y - 1)2\arctan\frac{1}{\sqrt{y - 1}}\right]\,,
\end{aligned}
\tag{3.18}
$$

$$
g(0, \hat{s}) = \frac{8}{27} - \frac{8}{9}\ln\left(\frac{m_b}{\mu}\right) - \frac{4}{9}\ln\hat{s} + \frac{4}{9}i\pi\,,
\tag{3.19}
$$

where $y = 4z^2/\hat{s}$. As can be seen from the above equations, internal b-quarks $\sim g(1, \hat{s})$, c-quarks $\sim g(\hat{m}_c, \hat{s})$ and light quarks q, (with $m_q = 0$ for $q = u, d, s$) $\sim g(0, \hat{s})$ contribute to the function $Y(\hat{s})$; only the charm loop involves the dominant "current-current" operators O_1 and O_2.

The $O(\alpha_s)$ correction [91] from the one-gluon exchange in the matrix element of O_9 in the invariant dilepton mass $\hat{s}$ is represented by

$$
\eta(\hat{s}) = 1 + \frac{\alpha_s(\mu)}{\pi}\omega(\hat{s})\,,
\tag{3.20}
$$

where

$$
\begin{aligned}
\omega(\hat{s}) =\ & -\frac{2}{9}\pi^2 - \frac{4}{3}\mathrm{Li}_2(\hat{s}) - \frac{2}{3}\ln\hat{s}\ln(1 - \hat{s}) - \frac{5 + 4\hat{s}}{3(1 + 2\hat{s})}\ln(1 - \hat{s}) \\
& - \frac{2\hat{s}(1 + \hat{s})(1 - 2\hat{s})}{3(1 - \hat{s})^2(1 + 2\hat{s})}\ln\hat{s} + \frac{5 + 9\hat{s} - 6\hat{s}^2}{6(1 - \hat{s})(1 + 2\hat{s})}\,.
\end{aligned}
\tag{3.21}
$$

Note that the function $\omega(\hat{s})$ is given with $m_s = 0$. The one-gluon correction to O_9 with respect to the final partonic energy and the invariant mass will be presented below in section 3.6.

In the order we are working only O_9 is subject to α_s corrections since the renormalization group improved perturbation series for C_9 is $\mathcal{O}(1/\alpha_s) + \mathcal{O}(1) + \mathcal{O}(\alpha_s) + \ldots$, due to the large logarithm in C_9 represented by $\mathcal{O}(1/\alpha_s)$ [47]. The Feynman diagrams, which contribute to the matrix element of O_9 in $O(\alpha_s)$, corresponding to the virtual one-gluon and bremsstrahlung corrections, are shown in Fig. 3.2.

With the help of the above expressions, the differential decay width becomes on using $p_\pm = (E_\pm, \boldsymbol{p}_\pm)$,

$$
d\Gamma = \frac{1}{2m_B}\frac{G_F^2\,\alpha^2}{2\pi^2}|V_{ts}^*V_{tb}|^2\frac{d^3\boldsymbol{p}_+}{(2\pi)^3 2E_+}\frac{d^3\boldsymbol{p}_-}{(2\pi)^3 2E_-}\left(W^L_{\mu\nu}L^{L\mu\nu} + W^R_{\mu\nu}L^{R\mu\nu}\right)\,,
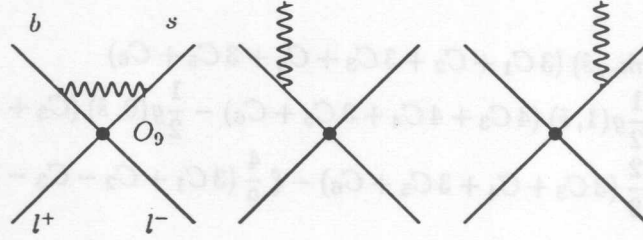\tag{3.22}
$$

Figure 3.2: *Feynman diagrams contributing to the explicit order α_s corrections of the operator O_9. Curly lines denote a gluon. Wave function corrections are not shown.*

where $W_{\mu\nu}$ and $L_{\mu\nu}$ are the hadronic and leptonic tensors, respectively. The hadronic tensor $W_{\mu\nu}^{L/R}$ is related to the discontinuity in the forward scattering amplitude, denoted by $T_{\mu\nu}^{L/R}$, through the relation $W_{\mu\nu} = 2 \, \mathrm{Im} \, T_{\mu\nu}$. Transforming the integration variables to $\hat{s}$, $\hat{u}$ and $v \cdot \hat{q}$, one can express the Dalitz distribution in $b \to s \ell^+ \ell^-$ (neglecting the lepton masses) as:

$$\frac{d\Gamma}{d\hat{u}\,d\hat{s}\,d(v \cdot \hat{q})} = \frac{1}{2\,m_B} \frac{G_F^2 \, \alpha^2}{2\,\pi^2} \frac{m_b^{\,4}}{256\,\pi^4} |V_{ts}^* V_{tb}|^2 \, 2\,\mathrm{Im}\left(T^L_{\ \mu\nu} L^{L\mu\nu} + T^R_{\ \mu\nu} L^{R\mu\nu}\right), \tag{3.23}$$

with

$$T^{L/R}_{\ \mu\nu} \equiv i \int d^4 y \, e^{-i\,\hat{q}\cdot y} \left\langle B \left| \mathrm{T} \left\{ \Gamma_{1\mu}^{L/R}(y), \Gamma_{2\nu}^{L/R}(0) \right\} \right| B \right\rangle, \tag{3.24}$$

$$L^{L/R\mu\nu} \equiv \sum_{spin} \left[\bar{v}^{L/R}(p_+) \, \gamma^\mu \, u^{L/R}(p_-) \right] \left[\bar{u}^{L/R}(p_-) \, \gamma^\nu \, v^{L/R}(p_+) \right]$$

$$= 2 \left[p_+^{\ \mu} p_-^{\ \nu} + p_-^{\ \mu} p_+^{\ \nu} - g^{\mu\nu}(p_+ \cdot p_-) \mp i\epsilon^{\mu\nu\alpha\beta} p_{+\alpha} p_{-\beta} \right], \tag{3.25}$$

where $\Gamma_{1\mu}^{L/R\dagger} = \Gamma_{2\mu}^{L/R} = \Gamma_\mu^{L/R}$, given in eq. (3.14). The Dalitz distribution eq. (3.23) contains the explicit $O(\alpha_s)$-improvement, and the distributions in which we are principally interested in can be obtained by straight-forward integrations.

Using Lorentz decomposition, the tensor $T_{\mu\nu}$ can be expanded in terms of three structure functions [1],

$$T_{\mu\nu} = -T_1 \, g_{\mu\nu} + T_2 \, v_\mu \, v_\nu + T_3 \, i\epsilon_{\mu\nu\alpha\beta} \, v^\alpha \, \hat{q}^\beta, \tag{3.26}$$

where the structure functions which do not contribute to the amplitude in the limit of massless leptons have been neglected. After contracting the hadronic and leptonic tensors, one finds

$$T^{L/R}_{\ \mu\nu} L^{L/R\mu\nu} = m_b^{\,2} \left\{ 2\,\hat{s}\,T_1^{L/R} + \left[(v \cdot \hat{q})^2 - \frac{1}{4}\hat{u}^2 - \hat{s} \right] T_2^{L/R} \mp \hat{s}\,\hat{u}\,T_3^{L/R} \right\}. \tag{3.27}$$

We remark here that the T_3 term will contribute to the FB asymmetry but not to the branching ratio or the dilepton invariant mass spectrum in the decay $B \to X_s \ell^+ \ell^-$.

---

[1] We use the convention $Tr(\gamma^\mu \gamma^\nu \gamma^\alpha \gamma^\beta \gamma_5) = -4i\epsilon^{\mu\nu\alpha\beta}$, with $\epsilon^{0123} = -1$.

Normalization

It has become customary to express the branching ratio for $B \to X_s \ell^+ \ell^-$ in terms of the well-measured semileptonic branching ratio $\mathcal{B}_{sl}$ for the decays $B \to (X_c, X_u)\ell\nu_\ell$ according to

$$d\mathcal{B}(B \to X_s \ell^+ \ell^-) = \mathcal{B}_{sl} \frac{d\Gamma(B \to X_s \ell^+ \ell^-)}{\Gamma(B \to (X_c, X_u)\ell\nu_\ell)} . \tag{3.28}$$

This fixes the normalization constant $\mathcal{B}_0$, which will be used throughout the following sections to be,

$$\mathcal{B}_0 \equiv \mathcal{B}_{sl} \frac{3}{16\pi^2} \frac{\alpha^2}{|V_{cb}|^2} \frac{|V_{ts}^* V_{tb}|^2}{f(\hat{m}_c)\kappa(\hat{m}_c)} . \tag{3.29}$$

Here $f(\hat{m}_c)$ is the phase space factor for $\Gamma(B \to X_c \ell \nu_\ell)$ and the function $\kappa(\hat{m}_c)$ accounts for both the $O(\alpha_s)$ QCD correction to the semileptonic decay width [92] and the leading order $(1/m_b)^2$ power correction [15]. They read as:

$$f(\hat{m}_c) = 1 - 8\,\hat{m}_c^2 + 8\,\hat{m}_c^6 - \hat{m}_c^8 - 24\,\hat{m}_c^4 \ln \hat{m}_c \tag{3.30}$$

and

$$\kappa(\hat{m}_c) = 1 + \frac{\alpha_s(m_b)}{\pi} g(\hat{m}_c) + \frac{h(\hat{m}_c)}{2m_b^2} , \tag{3.31}$$

where

$$g(\hat{m}_c) = \frac{A_0(\hat{m}_c)}{f(\hat{m}_c)} , \tag{3.32}$$

$$h(\hat{m}_c) = \lambda_1 + \frac{\lambda_2}{f(\hat{m}_c)} \left[-9 + 24\hat{m}_c^2 - 72\hat{m}_c^4 + 72\hat{m}_c^6 - 15\hat{m}_c^8 - 72\hat{m}_c^4 \ln \hat{m}_c \right] , \tag{3.33}$$

and the analytic form of $A_0(\hat{m}_c)$ can be seen in ref. [93]. Note that the frequently used approximation $g(z) \approx -\frac{2}{3}((\pi^2 - \frac{31}{4})(1-z)^2 + \frac{3}{2})$ holds within 1.4% accuracy in the range $0.2 \leq z \leq 0.4$. The equation $g(z) = -1.671 + 2.04(z - 0.3) - 2.15(z - 0.3)^2$ is accurate for $0.2 \leq z \leq 0.4$ to better than one per mille accuracy.

3.1.3 Asymmetries in $B \to X_s \ell^+ \ell^-$ Decay

Besides the differential branching ratio, $B \to X_s \ell^+ \ell^-$ decay offers other distributions (with different combinations of Wilson coefficients) to be measured. An interesting quantity is the Forward-Backward (FB) asymmetry defined in [13,12]

$$\frac{d\mathcal{A}(\hat{s})}{d\hat{s}} = \int_0^1 \frac{d^2\mathcal{B}}{d\hat{s}\,dz}\,dz - \int_{-1}^0 \frac{d^2\mathcal{B}}{d\hat{s}\,dz}\,dz , \tag{3.34}$$

where $z \equiv \cos\theta$ is the angle of ℓ^+ measured w.r.t. the b-quark direction in the dilepton c.m. system. From the experimental point of view, a more useful quantity is the normalized FB asymmetry, obtained by normalizing $d\mathcal{A}/d\hat{s}$ with the dilepton mass distribution, $d\mathcal{B}/d\hat{s}$,

$$\frac{d\overline{\mathcal{A}}}{d\hat{s}} = \frac{d\mathcal{A}}{d\hat{s}} \Big/ \frac{d\mathcal{B}}{d\hat{s}} . \tag{3.35}$$

The asymmetry $\bar{A}$, which we recall is defined in the dilepton c.m.s. frame, is identical to the energy asymmetry A_E introduced in [81], as shown in ref. [18]. It is defined in the B rest frame as

$$A_E \equiv \frac{(N(E_- > E_+) - N(E_+ > E_-))}{(N(E_- > E_+) + N(E_+ > E_-))} . \tag{3.36}$$

Here $N(E_- > E_+)$ denotes the number of lepton pairs whose negatively charged member is more energetic than its positive partner, where $E_\pm$ denote the $\ell^\pm$ charged lepton energy in the B rest frame. The FB asymmetry is odd under charge conjugation in contrary to the differential branching ratio, which is charge conjugation even. Both observables contain non overlapping information which together can be used to test the SM.

Another quantity is the left-right-asymmetry [84,85,86], defined as

$$\frac{\mathrm{d}\mathcal{A}^{LR}}{\mathrm{d}\hat{s}} = \frac{\mathrm{d}B^L}{\mathrm{d}\hat{s}} - \frac{\mathrm{d}B^R}{\mathrm{d}\hat{s}} , \tag{3.37}$$

with $\mathrm{d}B^L/\mathrm{d}\hat{s}$ ($\mathrm{d}B^R/\mathrm{d}\hat{s}$) denoting the invariant dilepton mass distribution for $B \to X_s \ell^+ \ell^-$ decay into purely left-handed (right-handed) leptons. We can obtain $\mathrm{d}B^{L/R}/\mathrm{d}\hat{s}$ from the dilepton invariant mass distribution $\mathrm{d}B/\mathrm{d}\hat{s}$ by the replacements

$$C_9^{\mathrm{eff}} \to \frac{C_9^{\mathrm{eff}} \mp C_{10}}{2} , \quad C_{10} \to \frac{C_{10} \mp C_9^{\mathrm{eff}}}{2} , \quad |C_7^{\mathrm{eff}}|^2 \to \frac{1}{2}|C_7^{\mathrm{eff}}|^2 . \tag{3.38}$$

Measurement of these asymmetries provides additional information on the underlying short-distance physics.

3.1.4 Leading power $(1/m_b)$ corrections in the decay $B \to X_s \ell^+ \ell^-$

We start with a discussion of the analyticity properties of the forward scattering amplitude $T_{\mu\nu}$. They are determined by cuts, depending on the external states. We consider real particle production in the inclusive decay $B \to X_s \ell^+ \ell^-$, thus we have $p_B = p_X + q$, where p_B, p_X denotes the 4-momentum of the B-meson, final hadronic state X_s, respectively. The hadronic invariant mass is in the range

$$m_K^2 \leq p_X^2 \leq m_B^2 , \tag{3.39}$$

and the physical cut runs along the real axis in the complex $v \cdot q$ plane in the limits

$$\sqrt{q^2} \leq v \cdot q \leq \frac{m_B^2 + q^2 - m_K^2}{2m_B} . \tag{3.40}$$

The phase space integration, which follows the above cut, is over intermediate physical states and hence, depends on long-distance QCD. Moreover, at the upper bound of the cut, where $p_X^2 \sim m_s^2$, resonances are dominating. In order to perform a reliable expansion in perturbative QCD, the contour of the integration has to be deformed in such a way that a) it encloses the cut and b) stays away from it by a distance large compared to Λ_{QCD} (see Fig. 1 in [16] for the contour of integration). The expansion is valid except in the corner of the Dalitz plot, where the hadronic invariant mass of the final state is small (the s-quark in Fig. 3.3 is almost on-shell.) However, results of perturbative QCD are expected to be recovered after suitable smearing.

Operator product expansion

The next task is to expand the forward scattering amplitude $T_{\mu\nu}$ in eq. (3.26) in inverse powers of m_b. We employ HQE techniques which have been already sketched in section 2.4.1. The leading term in this expansion, i.e., $\mathcal{O}(m_b^0)$ reproduces the parton model result. Let us describe how to get next to leading power corrections. First we write the momentum of the heavy b-quark as $p_{b\mu} = m_b v_\mu + k_\mu$, fix the four-velocity of the external b-quark field to be v_μ and treat the components of the "residual momentum" k_μ of order Λ_{QCD}. We obtain the condition $p_b^2 = m_b^2 + 2m_b v.k + k^2$, which yields $p_b^2 = m_b^2 + \mathcal{O}(k/m_b)$. The heavy quark remains almost on-shell under soft gluon exchange with the light degrees of freedom, there is no anti-quark generated and the total b-number is conserved.

It is customary to define a field h with fixed velocity v through

$$h(x) = e^{im_b v.x} P_+ b(x) \,, \tag{3.41}$$

with inversion

$$b(x) = e^{im_b v.x} \left[1 + i\frac{\slashed{D}}{2m_b} + ... \right] h(x) \,, \tag{3.42}$$

and the projection operators $P_\pm = (1 \pm \slashed{v})/2$. For the Dirac field $b(x)$ the following identities hold $P_+ b(x) = b(x)$ and $P_- b(x) = 0$, which are corrected by terms of $\mathcal{O}(1/m_b)$. Inserting this into the usual QCD Lagrangian $\mathcal{L} = \bar{b}(i\slashed{D} - m_q)b$ we get the one in the HQET:

$$\mathcal{L}_{HQET} = \bar{h}iv.Dh + \delta\mathcal{L} \,, \tag{3.43}$$

with $\delta\mathcal{L}$ containing the corrections in $1/m_b$:

$$\delta\mathcal{L} = \frac{1}{2m_b}\bar{h}(iD)^2 h - \frac{1}{2m_b}Z_1(\mu)\bar{h}(iv.D)^2 h + \frac{1}{2m_b}Z_2(\mu)\bar{h}\frac{-i}{2}\sigma^{\mu\nu}G_{\mu\nu}h + \mathcal{O}(1/m_b^2) \,. \tag{3.44}$$

Here, $G_{\mu\nu} \equiv [iD_\mu, iD_\nu]$ denotes the gluon field strength tensor. [2] For definition of the renormalization constants $Z_{1,2}(\mu)$ we refer to [17] and references therein. For the sake of completeness we give the Feynman rules in the HQET in appendix A.3.1. The matrix elements of the above higher dimensional operators are given as

$$\left\langle B \left| \bar{h}(iD)^2 h \right| B \right\rangle \equiv 2m_B\lambda_1 \,,$$
$$\left\langle B \left| \bar{h}\frac{-i}{2}\sigma^{\mu\nu}G_{\mu\nu}h \right| B \right\rangle \equiv 6m_B\lambda_2 \,, \tag{3.45}$$

where B denotes the pseudoscalar B-meson, see section 2.4.1 for a discussion of the values of the parameters λ_1 and λ_2. The second term on the r.h.s. of eq. (3.44) vanishes by the lowest order equation of motion $iv.Dh = 0$. The on-shell condition of the heavy quark is $m_b^2 = m_b^2 + 2m_b v.k + k^2$. Neglecting the last term, we have the simple condition $v.k = 0$. This is equivalent to the lowest order EOM of a heavy quark, thus we have the correspondence $k \leftrightarrow iD$.

---

[2]Note that here and only in this section we use this definition of the gluon field strength tensor $G = G^{FLS}$, following the conventions of ref. [17]. It is not consistent with the usual one appearing in QCD text books, eq. (A.10), denoted here by G^{QCD}. The two are related by $G^{FLS} = igG^{QCD}$.
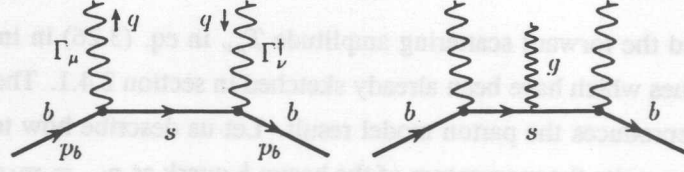
Figure 3.3: *The diagrams contributing to the operator product expansion.*

Suppressing the Lorentz indices for the time being, this operator product expansion (OPE) can be formally represented as:

$$\int d^4 y\, e^{-i\,\hat{q}\cdot y}\, \langle B\,|\mathrm{T}\left\{\Gamma_1(y),\Gamma_2(0)\right\}|\,B\rangle \;=\; -\frac{1}{m_b}\left[\langle B\,|\mathcal{O}_0|\,B\rangle + \frac{1}{2\,m_b}\,\langle B\,|\mathcal{O}_1|\,B\rangle \right.$$
$$\left. +\frac{1}{4\,m_b{}^2}\,\langle B\,|\mathcal{O}_2|\,B\rangle + \cdots\right]. \tag{3.46}$$

The expressions for the operators $\mathcal{O}_0, \mathcal{O}_1$ and $\mathcal{O}_2$ have been first derived in ref. [17], which we have checked and confirm. They are given as:

$$\mathcal{O}_0 \;=\; \frac{1}{x}\bar{b}\Gamma_1(\slashed{v}-\slashed{q}+\hat{m}_s)\Gamma_2 b\,, \tag{3.47}$$

$$\mathcal{O}_1 \;=\; \frac{2}{x}\bar{h}\Gamma_1\gamma^\alpha\Gamma_2 iD_\alpha h - \frac{4}{x^2}(v-\hat{q})^\alpha\bar{h}\Gamma_1(\slashed{v}-\slashed{q}+\hat{m}_s)\Gamma_2 iD_\alpha h\,, \tag{3.48}$$

and

$$\mathcal{O}_2 \;=\; \mathcal{O}_2^{(2)} + \mathcal{O}_2^{(g)} + \mathcal{O}_2^{(1)}\,, \tag{3.49}$$

where

$$\mathcal{O}_2^{(2)} \;=\; \frac{16}{x^3}(v-\hat{q})^\alpha(v-\hat{q})^\beta\bar{h}\Gamma_1(\slashed{v}-\slashed{q}+\hat{m}_s)\Gamma_2 iD_\alpha iD_\beta h - \frac{4}{x^2}\bar{h}\Gamma_1(\slashed{v}-\slashed{q}+\hat{m}_s)\Gamma_2(iD)^2 h$$
$$-\frac{4}{x^2}(v-\hat{q})^\beta\bar{h}\Gamma_1\gamma^\alpha\Gamma_2(iD_\alpha iD_\beta + iD_\beta iD_\alpha)h\,, \tag{3.50}$$

$$\mathcal{O}_2^{(g)} \;=\; \frac{2}{x^2}\hat{m}_s\bar{h}\Gamma_1 i\sigma_{\alpha\beta}\Gamma_2 G^{\alpha\beta}h + \frac{2}{x^2}i\epsilon^{\mu\lambda\alpha\beta}(v-\hat{q})_\lambda\bar{h}\Gamma_1\gamma_\mu\gamma_5\Gamma_2 G_{\alpha\beta}h\,, \tag{3.51}$$

$$\mathcal{O}_2^{(1)} \;=\; \frac{2}{x}\bar{h}(\gamma^\beta\Gamma_1\gamma^\alpha\Gamma_2 + \Gamma_1\gamma^\beta\Gamma_2\gamma^\alpha)iD_\beta iD_\alpha h - \frac{4}{x^2}(v-\hat{q})^\alpha\bar{h}\gamma^\beta\Gamma_1(\slashed{v}-\slashed{q}+\hat{m}_s)\Gamma_2 iD_\beta iD_\alpha h$$
$$-\frac{4}{x^2}(v-\hat{q})^\alpha\bar{h}\Gamma_1(\slashed{v}-\slashed{q}+\hat{m}_s)\Gamma_2\gamma^\beta iD_\alpha iD_\beta h\,. \tag{3.52}$$

Here $x \equiv 1 + \hat{s} - 2\,(v\cdot\hat{q}) - \hat{m}_s^2 + i\,\epsilon$. The operator O_3 responsible for $1/m_b^3$ corrections can be seen in ref. [65].

The above $\mathcal{O}_i$, $i = 0, 1, 2$ are obtained by expanding the Feynman diagrams shown in Fig. 3.3, which contributes to the time-ordered product on the l.h.s. of eq. (3.46). The diagram on the left is responsible for the operators $\mathcal{O}_0, \mathcal{O}_1, \mathcal{O}_2^{(1)}$ and $\mathcal{O}_2^{(2)}$. To be definite, we write the intermediate s-quark propagator using 4-momentum conservation $p_s = p_b - q = m_b v - q + k$ as

$$i\frac{\slashed{p}_s + m_s}{p_s^2 - m_s^2 + i\epsilon} = i\frac{1}{m_b}\frac{\slashed{v} - \slashed{q} + \slashed{k}/m_b + \hat{m}_s}{x - 2\hat{q}\cdot k/m_b + 2v\cdot k/m_b + k^2/m_b^2}\,. \tag{3.53}$$

and insert this into the diagrams Fig. 3.3. Expanding as well the propagator as the Dirac field b, which sandwiches the amplitudes, as the normalization of the states in powers of k/m_b, we obtain the desired OPE. Note that the leading operator $\mathcal{O}_0$ is defined in terms of the "full" four-component field b. The other two subleading operators $\mathcal{O}_1$ and $\mathcal{O}_2$ are, however, written in terms of the two-component effective fields h. In rewriting the operator $\mathcal{O}_1$ from $b \rightarrow h$ fields by means of eq. (3.42), we obtain the operator $\mathcal{O}_2^{(1)}$. Evaluation of the one-gluon diagram in Fig. 3.3 results in the operator $\mathcal{O}_2^{(g)}$.

The results of the power corrections to the structure functions T_i, $i = 1, 2, 3$ can be decomposed into the sum of various terms, denoted by $T_i^{(j)}$, which can be traced back to well defined pieces in the evaluation of the time-ordered product given above [18]:

$$T_i(v.\hat{q}, \hat{s}) = \sum_{j=0,1,2,s,g,\delta} T_i^{(j)}(v.\hat{q}, \hat{s}) . \tag{3.54}$$

The expressions for $T_i^{(j)}(v.\hat{q}, \hat{s})$ calculated up to $O(m_B/m_b^3)$ are given in appendix B.1. They contain the parton model expressions $T_i^{(0)}(v.\hat{q}, \hat{s})$ and the power corrections in the HQE approach which depend on the two HQE-specific parameters λ_1 and λ_2 defined in eqs. (3.45). Note that the s-quark mass terms are explicitly kept in $T_i^{(j)}(v.\hat{q}, \hat{s})$. The origin of the various terms in the expansion given in eq. (3.54) can be specified, as follows:

$$\begin{aligned}
T_i^{(0)}(v.\hat{q}, \hat{s}) &= \langle B|\mathcal{O}_0|B\rangle \quad \text{for} \quad \lambda_1 = \lambda_2 = 0 , \\
T_i^{(s)}(v.\hat{q}, \hat{s}) &= \langle B|\mathcal{O}_0|B\rangle - T_i^{(0)}(v.\hat{q}, \hat{s}) , \\
T_i^{(j)}(v.\hat{q}, \hat{s}) &= \langle B|\mathcal{O}_2^{(j)}|B\rangle \quad \text{for} \quad j = 1, 2, g , \\
T_i^{(\delta)}(v.\hat{q}, \hat{s}) &= \langle B|\mathcal{O}_1|B\rangle .
\end{aligned} \tag{3.55}$$

In the leading order in $(1/m_b)$ the matrix element of $\mathcal{O}_1$ vanishes, but in the sub-leading order it receives a non-trivial contribution which can be calculated by using the equation of motion [17]. The contributions $T_i^{(s)}$ arise from the matrix element of the scalar operator $\bar{b}b$, i.e use of eq. (3.58) given below. We recall that the scalar current can be written in terms of the vector current plus higher dimensional operators as [15]

$$\bar{b}b = v_\mu \bar{b}\gamma^\mu b + \frac{1}{2m_b^2}\bar{h}\left[(iD)^2 - (v.iD)^2 - (i/2)\sigma^{\mu\nu}G_{\mu\nu}\right]h + \dots . \tag{3.56}$$

With our normalization:

$$\langle B|\bar{b}\gamma_\mu b|B\rangle = 2(p_B)_\mu , \tag{3.57}$$

it follows then

$$\langle B|\bar{b}b|B\rangle = 2m_B(1 + \frac{1}{2m_b^2}(\lambda_1 + 3\lambda_2)) + \mathcal{O}(m_B/m_b^3) . \tag{3.58}$$

Other possible Lorentz structures like γ_5, $\gamma_5\gamma_\mu$, $\gamma_\mu\gamma_\nu$ sandwiched between $\bar{b}$ and b give zero after taking the B-meson matrix element.

From the expressions for $T_i^{(j)}$ given in appendix B.1, we see that $T_i^{(0)}$ ($i = 1, 2, 3$) are of order m_B/m_b and the rest $T_i^{(1)}$, $T_i^{(\delta)}$, $T_i^{(2)}$, $T_i^{(s)}$ and $T_i^{(g)}$ are all of order $m_B\lambda_1/m_b^3$ or $m_B\lambda_2/m_b^3$. Since the ratio $m_B/m_b = 1 + O(1/m_b)$, we note that the Dalitz distribution in $B \rightarrow X_s\ell^+\ell^-$ has linear corrections in $1/m_b$.

3.2 Power Corrections to the Dilepton Invariant Mass Distribution and FB Asymmetry

The integration in the complex plane $v \cdot \hat{q}$ can be done using the relation

$$\text{Im} \frac{1}{x^n} \propto \frac{(-1)^{n-1}}{(n-1)!} \delta^{(n-1)}(1 - 2v \cdot \hat{q} + \hat{s} - \hat{m}_s^2) \,. \tag{3.59}$$

Further, the integrand should be multiplied by the function $\theta(4v \cdot \hat{q}^2 - 4\hat{s}^2 - \hat{u}^2)$ responsible for the correct integration boundary. [3] The resulting double differential branching ratio in $B \to X_s \ell^+ \ell^-$ can be expressed as,

$$
\begin{aligned}
\frac{d\mathcal{B}}{d\hat{s}\, d\hat{u}} \;=\; & \mathcal{B}_0 \Bigg(\Bigg\{ \Bigg[\Big(1 - \hat{m}_s^2 \Big)^2 - \hat{s}^2 - \hat{u}^2 - \frac{1}{3} \Big(2\,\hat{\lambda}_1(-1 + 2\hat{m}_s^2 - \hat{m}_s^4 - 2\,\hat{s} + \hat{s}^2) \\
& + 3\,\hat{\lambda}_2(-1 + 6\hat{m}_s^2 - 5\hat{m}_s^4 - 8\,\hat{s} + 5\,\hat{s}^2) \Big) \Bigg] \Big(|C_9^{\text{eff}}|^2 + |C_{10}|^2 \Big) \\
& + \Bigg[4 \Big(1 - \hat{m}_s^2 - \hat{m}_s^4 + \hat{m}_s^6 - 8\hat{m}_s^2\hat{s} - \hat{s}^2 - \hat{m}_s^2\hat{s}^2 + \hat{u}^2 + \hat{m}_s^2\hat{u}^2 \Big) \\
& - \frac{4}{3} \Big(2\,\hat{\lambda}_1(-1 + \hat{m}_s^2 + \hat{m}_s^4 - \hat{m}_s^6 + 2\,\hat{s} + 10\hat{m}_s^2\hat{s} + \hat{s}^2 + \hat{m}_s^2\hat{s}^2) \\
& + 3\,\hat{\lambda}_2(3 + 5\hat{m}_s^2 - 3\hat{m}_s^4 - 5\hat{m}_s^6 + 4\,\hat{s} + 28\hat{m}_s^2\hat{s} + 5\,\hat{s}^2 + 5\hat{m}_s^2\hat{s}^2) \Big) \Bigg] \frac{|C_7^{\text{eff}}|^2}{\hat{s}} \\
& - 8 \Bigg[\Big(\hat{s}(1 + \hat{m}_s^2) - (1 - \hat{m}_s^2)^2 \Big) + \frac{2}{3}\hat{\lambda}_1(-1 + 2\hat{m}_s^2 - \hat{m}_s^4 + \hat{s} + \hat{m}_s^2\hat{s}) \\
& + \hat{\lambda}_2(5\hat{m}_s^2 - 5\hat{m}_s^4 + 2\hat{s} + 5\hat{m}_s^2\hat{s}) \Bigg] Re(C_9^{\text{eff}})\, C_7^{\text{eff}} \\
& + 2 \Big[2 + \hat{\lambda}_1 + 5\,\hat{\lambda}_2 \Big] \hat{u}\,\hat{s}\, Re(C_9^{\text{eff}})\, C_{10} \\
& + 4 \Big[2 \Big(1 + \hat{m}_s^2 \Big) + \hat{\lambda}_1(1 + \hat{m}_s^2) + \hat{\lambda}_2(3 + 5\hat{m}_s^2) \Big] \hat{u}\, Re(C_{10})\, C_7^{\text{eff}} \Bigg\} \theta \Big[\hat{u}(\hat{s}, \hat{m}_s)^2 - \hat{u}^2 \Big] \\
& - E_1(\hat{s}, \hat{u})\, \delta \Big[\hat{u}(\hat{s}, \hat{m}_s)^2 - \hat{u}^2 \Big] - E_2(\hat{s}, \hat{u})\, \delta' \Big[\hat{u}(\hat{s}, \hat{m}_s)^2 - \hat{u}^2 \Big] \Bigg) \,,
\end{aligned}
\tag{3.60}
$$

where $\hat{\lambda}_1 = \lambda_1/m_b^2$ and $\hat{\lambda}_2 = \lambda_2/m_b^2$. The auxiliary functions $E_i(\hat{s}, \hat{u})$ $(i = 1, 2)$, introduced here for ease of writing, are given explicitly in appendix B.2. The boundary of the Dalitz distribution is as usual determined by the argument of the θ-function and in the $(\hat{u}, \hat{s})$-plane it has been specified in eq. (3.8). The analytic form of the result (3.60) is very similar to the corresponding double differential distributions derived by Manohar and Wise in [16] for the semileptonic decays $B \to (X_c, X_u)\ell\nu_\ell$. Further comparisons with this work in the $V - A$ limit for the single differential and integrated rates are given a little later at the end of this section.

Finally, after integrating over the variable $\hat{u}$, we derive the differential branching ratio in the scaled dilepton invariant mass for $B \to X_s \ell^+ \ell^-$,

$$
\begin{aligned}
\frac{d\mathcal{B}}{d\hat{s}} \;=\; & 2\,\mathcal{B}_0 \Bigg\{ \Bigg[\frac{2}{3}\hat{u}(\hat{s}, \hat{m}_s)((1 - \hat{m}_s^2)^2 + \hat{s}(1 + \hat{m}_s^2) - 2\hat{s}^2) + \frac{1}{3}(1 - 4\hat{m}_s^2 + 6\hat{m}_s^4 - 4\hat{m}_s^6 + \hat{m}_s^8 - \hat{s} \\
& + \hat{m}_s^2\hat{s} + \hat{m}_s^4\hat{s} - \hat{m}_s^6\hat{s} - 3\hat{s}^2 - 2\hat{m}_s^2\hat{s}^2 - 3\hat{m}_s^4\hat{s}^2 + 5\hat{s}^3 + 5\hat{m}_s^2\hat{s}^3 - 2\hat{s}^4)\frac{\hat{\lambda}_1}{\hat{u}(\hat{s}, \hat{m}_s)} \\
& + \Big(1 - 8\hat{m}_s^2 + 18\hat{m}_s^4 - 16\hat{m}_s^6 + 5\hat{m}_s^8 - \hat{s} - 3\hat{m}_s^2\hat{s} + 9\hat{m}_s^4\hat{s} - 5\hat{m}_s^6\hat{s} - 15\hat{s}^2 - 18\hat{m}_s^2\hat{s}^2
\end{aligned}
$$

---
[3] This corresponds to $q_{max}^2 = 4E_+ E_-$, with lepton energies $E_\pm = v \cdot q/2 \pm u/(4m_b)$.

$$-15\hat{m}_s^4\hat{s}^2 + 25\hat{s}^3 + 25\hat{m}_s^2\hat{s}^3 - 10\hat{s}^4 \Big) \frac{\hat{\lambda}_2}{\hat{u}(\hat{s}, \hat{m}_s)} \Bigg] \left(|C_9^{\text{eff}}|^2 + |C_{10}|^2 \right)$$

$$+ \Bigg[\frac{8}{3}\hat{u}(\hat{s}, \hat{m}_s)(2(1 + \hat{m}_s^2)(1 - \hat{m}_s^2)^2 - (1 + 14\hat{m}_s^2 + \hat{m}_s^4)\hat{s} - (1 + \hat{m}_s^2)\hat{s}^2)$$

$$+ \frac{4}{3}(2 - 6\hat{m}_s^2 + 4\hat{m}_s^4 + 4\hat{m}_s^6 - 6\hat{m}_s^8 + 2\hat{m}_s^{10} - 5\hat{s} - 12\hat{m}_s^2\hat{s} + 34\hat{m}_s^4\hat{s} - 12\hat{m}_s^6\hat{s} - 5\hat{m}_s^8\hat{s} + 3\hat{s}^2$$

$$+ 29\hat{m}_s^2\hat{s}^2 + 29\hat{m}_s^4\hat{s}^2 + 3\hat{m}_s^6\hat{s}^2 + \hat{s}^3 - 10\hat{m}_s^2\hat{s}^3 + \hat{m}_s^4\hat{s}^3 - \hat{s}^4 - \hat{m}_s^2\hat{s}^4) \frac{\hat{\lambda}_1}{\hat{u}(\hat{s}, \hat{m}_s)} + 4 \left(-6 + 2\hat{m}_s^2 \right)$$

$$+ 20\hat{m}_s^4 - 12\hat{m}_s^6 - 14\hat{m}_s^8 + 10\hat{m}_s^{10} + 3\hat{s} + 16\hat{m}_s^2\hat{s} + 62\hat{m}_s^4\hat{s} - 56\hat{m}_s^6\hat{s} - 25\hat{m}_s^8\hat{s} + 3\hat{s}^2$$

$$+ 73\hat{m}_s^2\hat{s}^2 + 101\hat{m}_s^4\hat{s}^2 + 15\hat{m}_s^6\hat{s}^2 + 5\hat{s}^3 - 26\hat{m}_s^2\hat{s}^3 + 5\hat{m}_s^4\hat{s}^3 - 5\hat{s}^4 - 5\hat{m}_s^2\hat{s}^4) \frac{\hat{\lambda}_2}{\hat{u}(\hat{s}, \hat{m}_s)} \Bigg] \frac{|C_7^{\text{eff}}|^2}{\hat{s}}$$

$$+ \Bigg[8\hat{u}(\hat{s}, \hat{m}_s)((1 - \hat{m}_s^2)^2 - (1 + \hat{m}_s^2)\hat{s}) + 4(1 - 2\hat{m}_s^2 + \hat{m}_s^4 - \hat{s} - \hat{m}_s^2\hat{s}) \hat{u}(\hat{s}, \hat{m}_s) \hat{\lambda}_1$$

$$+ 4 \left(-5 + 30\hat{m}_s^4 - 40\hat{m}_s^6 + 15\hat{m}_s^8 - \hat{s} + 21\hat{m}_s^2\hat{s} + 25\hat{m}_s^4\hat{s} - 45\hat{m}_s^6\hat{s} + 13\hat{s}^2 + 22\hat{m}_s^2\hat{s}^2 \right.$$

$$\left. + 45\hat{m}_s^4\hat{s}^2 - 7\hat{s}^3 - 15\hat{m}_s^2\hat{s}^3 \right) \frac{\hat{\lambda}_2}{\hat{u}(\hat{s}, \hat{m}_s)} \Bigg] Re(C_9^{\text{eff}}) C_7^{\text{eff}} \Bigg\}. \tag{3.61}$$

The leading power corrected expression for the FB-asymmetry $\mathcal{A}(\hat{s})$ is:

$$\frac{d\mathcal{A}(\hat{s})}{d\hat{s}} = -2 \, \mathcal{B}_0 \Bigg\{ \Bigg[2(\hat{u}(\hat{s}, \hat{m}_s))^2\hat{s} + \frac{\hat{s}}{3}(3 - 6\hat{m}_s^2 + 3\hat{m}_s^4 + 2\hat{s} - 6\hat{m}_s^2\hat{s} + 3\hat{s}^2)\hat{\lambda}_1$$

$$+ \hat{s}(-9 - 6\hat{m}_s^2 + 15\hat{m}_s^4 - 14\hat{s} - 30\hat{m}_s^2\hat{s} + 15\hat{s}^2)\hat{\lambda}_2 \Bigg] Re(C_9^{\text{eff}}) C_{10}$$

$$+ \Bigg[4(\hat{u}(\hat{s}, \hat{m}_s))^2(1 + \hat{m}_s^2) + \frac{2}{3}(1 + \hat{m}_s^2)(3 - 6\hat{m}_s^2 + 3\hat{m}_s^4 + 2\hat{s} - 6\hat{m}_s^2\hat{s} + 3\hat{s}^2)\hat{\lambda}_1 \tag{3.62}$$

$$+ 2(-7 - 3\hat{m}_s^2 - 5\hat{m}_s^4 + 15\hat{m}_s^6 - 10\hat{s} - 24\hat{m}_s^2\hat{s} - 30\hat{m}_s^4\hat{s} + 9\hat{s}^2 + 15\hat{m}_s^2\hat{s}^2)\hat{\lambda}_2 \Bigg] Re(C_{10}) C_7^{\text{eff}} \Bigg\}.$$

The results derived for the $O(\alpha_s)$-improved and power-corrected Dalitz distribution, dilepton invariant mass, and FB-asymmetry in $B \to X_s\ell^+\ell^-$ are the principal new results in this section. It is useful to write the corresponding expressions in the limit $m_s = 0$. For the dilepton invariant mass distribution, we get

$$\frac{d\mathcal{B}}{d\hat{s}} = 2 \, \mathcal{B}_0 \Bigg\{ \Bigg[\frac{1}{3}(1 - \hat{s})^2(1 + 2\hat{s})(2 + \hat{\lambda}_1) + (1 - 15\hat{s}^2 + 10\hat{s}^3)\hat{\lambda}_2 \Bigg] \left(|C_9^{\text{eff}}|^2 + |C_{10}|^2 \right)$$

$$+ \Bigg[\frac{4}{3}(1 - \hat{s})^2(2 + \hat{s})(2 + \hat{\lambda}_1) + 4(-6 - 3\hat{s} + 5\hat{s}^3)\hat{\lambda}_2 \Bigg] \frac{|C_7^{\text{eff}}|^2}{\hat{s}}$$

$$+ \Bigg[4(1 - \hat{s})^2(2 + \hat{\lambda}_1) + 4(-5 - 6\hat{s} + 7\hat{s}^2)\hat{\lambda}_2 \Bigg] Re(C_9^{\text{eff}}) C_7^{\text{eff}} \Bigg\}. \tag{3.63}$$

The (unnormalized) FB asymmetry reads as,

$$\frac{d\mathcal{A}}{d\hat{s}} = -2 \, \mathcal{B}_0 \Bigg\{ \Bigg[2(1 - \hat{s})^2\hat{s} + \frac{\hat{s}}{3}(3 + 2\hat{s} + 3\hat{s}^2)\hat{\lambda}_1 + \hat{s}(-9 - 14\hat{s} + 15\hat{s}^2)\hat{\lambda}_2 \Bigg] Re(C_9^{\text{eff}}) C_{10}$$

$$+ \Bigg[4(1 - \hat{s})^2 + \frac{2}{3}(3 + 2\hat{s} + 3\hat{s}^2)\hat{\lambda}_1 + 2(-7 - 10\hat{s} + 9\hat{s}^2)\hat{\lambda}_2 \Bigg] Re(C_{10}) C_7^{\text{eff}} \Bigg\}. \tag{3.64}$$

Our result [18] for the dilepton invariant mass distribution given in eq. (3.63) has been confirmed recently by [27] in the $m_s = 0$ limit and is in disagreement with an earlier publication [17]. (The differences between the previous result eq. (3.21) of the paper by [17] have been discussed at length in [18].)

Concerning the invariant dilepton mass spectrum derived by us and given in eq. (3.61), we would like to make the following observations: First, the leading order power corrections in the dilepton mass

distribution are found to be small over a good part of the dilepton mass $\hat{s}$. However, we find that the power corrections become increasingly large and negative as one approaches $\hat{s} \to \hat{s}^{max}$, where $\hat{s}^{max} = (1 - \hat{m}_s)^2$. Since the parton model spectrum falls steeply near the end-point $\hat{s} \to \hat{s}^{max}$, this leads to the uncomfortable result that the power corrected dilepton mass distribution becomes negative for the high dilepton masses. We show in Fig. 3.4 this distribution in the parton model and the HQE approach, using the central values of the parameters in Table A.1. Further, the power-corrected dilepton invariant mass distribution retains the characteristic $1/\hat{s}$ behaviour following from the one-photon exchange in the parton model. We note that the correction proportional to the kinetic energy term $\hat{\lambda}_1$ renormalizes the parton model invariant mass distribution multiplicatively by approximately the factor $(1 + \lambda_1/(2m_b^2))$, which is exact in the limit $m_s = 0$ and no new functional dependence in $\hat{s}$ is introduced (moreover, this factor is hardly different from 1). Hence, the negative probability near the end-point is largely driven by the magnetic moment term $\hat{\lambda}_2$.

The normalized FB asymmetry, $d\bar{A}(\hat{s})/d\hat{s}$, in the HQE-approach and the parton model are shown in Fig. 3.5. We find that this asymmetry is stable against leading order power corrections up to $\hat{s} \leq 0.6$, but the corrections become increasingly large due to the unphysical behaviour of the HQE-based dilepton mass distribution as $\hat{s}$ approaches $\hat{s}^{max}$ (see Fig. 3.4). Based on these investigations, we must conclude that the HQE-based approach has a restrictive kinematical domain for its validity. In particular, it breaks down for the high dilepton invariant mass region in $B \to X_s \ell^+ \ell^-$. This behaviour of the dilepton

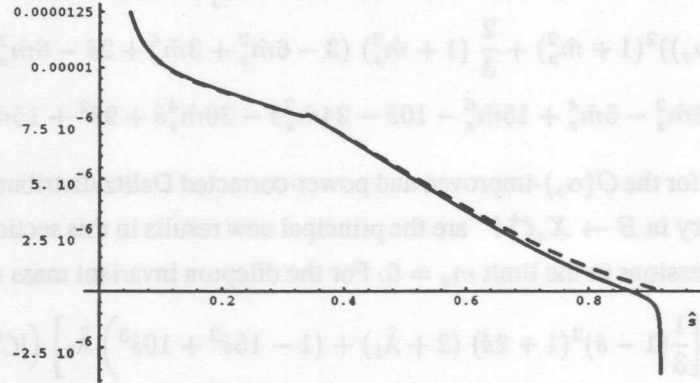Figure 3.4: *Dilepton invariant mass spectrum* $\mathrm{d}B(B \to X_s e^+ e^-)/\mathrm{d}\hat{s}$ *in the parton model (dashed curve) and with leading power corrections calculated in the HQE approach (solid curve). The parameters used are given in Table A.1.*

mass spectrum in $B \to X_s \ell^+ \ell^-$ is not unexpected, as similar behaviours have been derived near the end-point of the lepton energy spectra in the decays $B \to X \ell \nu_\ell$ in the HQE approach [16]. To stress these similarities, we show the power correction in the dilepton mass distribution as calculated in the HQE approach compared to the parton model through the ratio defined as:

$$R^{\mathrm{HQE}}(\hat{s}) \equiv \frac{\mathrm{d}\mathcal{B}/\mathrm{d}\hat{s}(\mathrm{HQE}) - \mathrm{d}\mathcal{B}/\mathrm{d}\hat{s}(\mathrm{Parton\ Model})}{\mathrm{d}\mathcal{B}/\mathrm{d}\hat{s}(\mathrm{Parton\ Model})} . \tag{3.65}$$

The correction factor $R^{\mathrm{HQE}}(\hat{s})$ for $B \to X_s \ell^+ \ell^-$ shown in Fig. 3.6 is qualitatively similar to the corresponding factor in the lepton energy spectrum in the decay $B \to X_c \ell \nu_\ell$, given in Fig. 6 of [16]. We
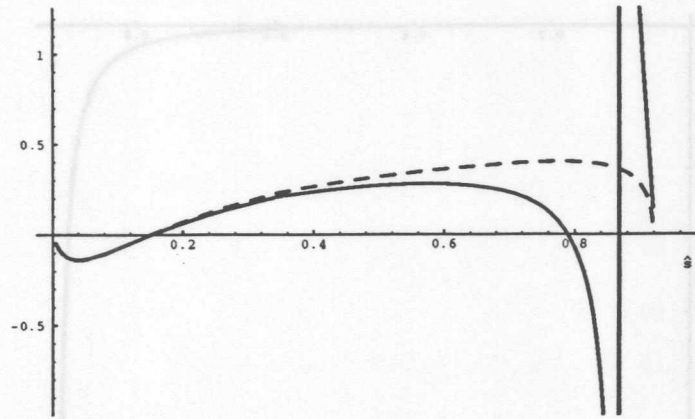
Figure 3.5: *FB asymmetry (normalized)* $\mathrm{d}\overline{\mathcal{A}}(B \to X_s e^+ e^-)/\mathrm{d}\hat{s}$ *in the parton model (dashed curve) and with power corrections calculated in the HQE approach (solid curve). The parameters used are given in Table A.1.*

note that we have been able to derive the power corrected rate for the semileptonic decays $B \to X_c \ell \nu_\ell$ obtained by Manohar and Wise in [16]. [4] In doing this, we shall reduce the matrix element for the decay $B \to X_s \ell^+ \ell^-$ to the one encountered in $B \to X_c \ell \nu_\ell$, obtained by the replacements ($V - A$ limit):

$$C_9^{\mathrm{eff}} = -C_{10} = \frac{1}{2}, \tag{3.66}$$

$$C_7^{\mathrm{eff}} = 0, \tag{3.67}$$

$$\left(\frac{G_F \alpha}{\sqrt{2}\,\pi} V_{ts}^* V_{tb}\right) \to \left(-\frac{4\,G_F}{\sqrt{2}} V_{cb}\right). \tag{3.68}$$

This amounts to keeping only the charged current $V - A$ contribution in $B \to X_s \ell^+ \ell^-$ decays.

Finally, since the HQE-improved expression for the decay rate cannot be given analytically due to the Wilson coefficient $C_9^{\mathrm{eff}}(\hat{s})$ which is a complicated function of $\hat{s}$, we give below the results in numerical form:

$$\Gamma^{\mathrm{HQE}} = \Gamma^b(1 + c_1\hat{\lambda}_1 + c_2\hat{\lambda}_2), \tag{3.69}$$

where Γ^b is the parton model decay width for $b \to s\ell^+\ell^-$ and the coefficients depend on the input parameters. For the central values of the parameters given in Table A.1, they have the values $c_1 = 0.501$ and $c_2 = -7.425$. This leads to a reduction in the decay width by -4.1%, using the values of λ_1 and λ_2 given in Table A.1. Moreover, this reduction is mostly contributed by the λ_2-dependent term. We recall that the coefficient of the $\hat{\lambda}_1$ term c_1 is (almost) the same as in the semileptonic width $\Gamma(B \to X_u \ell \nu_\ell)$ obtained by Bigi et al [15]

$$\Gamma_{sl}^{\mathrm{HQE}} = \Gamma_{sl}^b\left(1 + \frac{1}{2}\hat{\lambda}_1 - \frac{9}{2}\hat{\lambda}_2\right), \tag{3.70}$$

where Γ_{sl}^b is the parton model decay width. This points towards the universality of this coefficient. The coefficient of the $\hat{\lambda}_2$ term c_2 for $b \to s\ell^+\ell^-$ decay is larger than the corresponding one in the semileptonic decay width. Hence, the power corrections in $\Gamma(B \to X_u \ell \nu_\ell)$ and $\Gamma(B \to X_s \ell^+ \ell^-)$ are rather similar but not identical.

---

[4]The HQE matrix elements in our convention and the MW ones are related by $\lambda_1 = -2m_b^2 K_b$, $3\lambda_2 = -2m_b^2 G_b$ and $\lambda_1 + 3\lambda_2 = -2m_b^2 E_b = -2m_b^2(K_b + G_b)$, likewise we have for the normalization of states $|B\rangle = \sqrt{2m_B}|B\rangle^{MW}$.
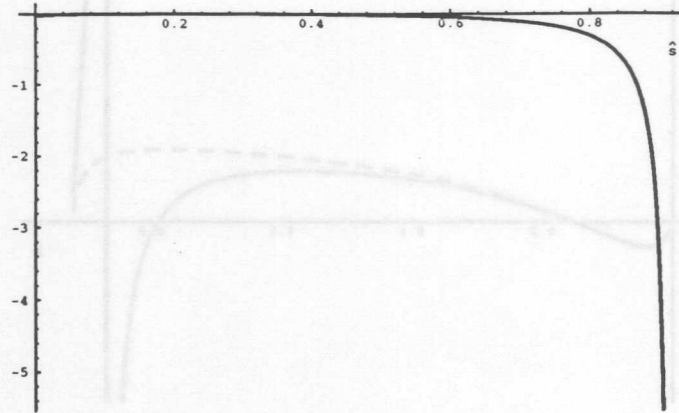
Figure 3.6: *The correction factor $R^{HQE}(\hat{s})$ (in percentage) as defined in eq. (3.65) for the dilepton mass spectrum $\mathrm{d}B(B \to X_s \ell^+ \ell^-)/\mathrm{d}\hat{s}$. The parameters used are given in Table A.1.*

3.3 Dilepton Invariant Mass and the FB Asymmetry in the Fermi Motion Model

In this section, we present our estimates of the non-perturbative effects on the decay distributions in $B \to X_s \ell^+ \ell^-$. These effects are connected with the bound state nature of the B-hadron and the physical threshold in the $B \to X_s \ell^+ \ell^-$ in the final state. In order to implement these effects on the decay distributions in $B \to X_s \ell^+ \ell^-$, we resort to the Gaussian Fermi motion (FM) model [22] introduced in section 2.4.2.

In the Fermi motion model, the problem of negative probabilities encountered in the HQE approach for the high dilepton masses near $s \to s_{max}$ is not present, which motivates us to use this model as a reasonable approximation of the non-perturbative effects in the entire dilepton mass range. The success of this model in describing the inclusive lepton energy spectra in $B \to (X_c, X_u)\ell\nu_\ell$ and $B \to X_s \gamma$ strengthens this hope.

In the decay $B \to X_s \ell^+ \ell^-$, the distribution $dB/d\hat{s}$ depends on the Lorentz-invariant variable $\hat{s}$ only. So, the Lorentz boost involved in the Fermi motion model (Doppler shift) leaves the dilepton mass distribution invariant. However, since the b-quark mass $m_b(p)$ is now a momentum-dependent quantity, this distribution is affected due to the difference $(m_b(p) - m_b)$ (mass defect), which rescales the variable $\hat{s}$ and hence smears the dilepton distribution calculated in the parton model. For different choices of the model parameters (p_F, m_q) corresponding to the same effective b-quark mass, m_b^{eff} which is defined in eq. (2.47) the dilepton mass distributions should be very similar [23], which indeed is the case as we have checked numerically but do not show the resulting distributions here.

The situation with the FB asymmetry is, however, quite different. Being an angle-dependent quantity, it is not Lorentz-invariant and is sensitive to both the Doppler shift and the mass defect. We give in appendix B.3, the Dalitz distribution $d^2\Gamma(B \to X_s \ell^+ \ell^-)/dsdu$ in the Fermi motion model.

As we calculate the branching ratio for the inclusive decay $B \to X_s \ell^+ \ell^-$ in terms of the semilep-tonic decay branching ratio $B(B \to X \ell\nu_\ell)$, we have to correct the normalization due to the variable b-quark mass in both the decay rates. We recall that the decay widths for $B \to X_s \ell^+ \ell^-$ and $B \to X \ell\nu_\ell$
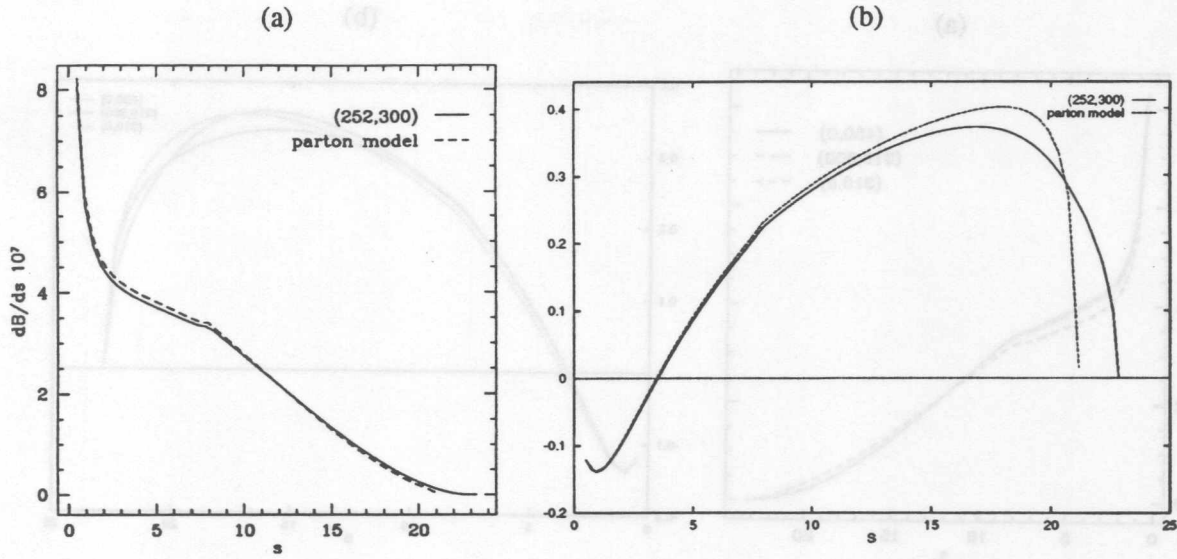
(a)   (b)

Figure 3.7: *Differential branching ratio dB/ds for $B \to X_s \ell^+ \ell^-$ (a) and normalized differential FB asymmetry $d\overline{\mathcal{A}}(s)/ds$ (b) in the SM including the next-to-leading order QCD corrections. The dashed curve corresponds to the parton model with the parameters given in Table A.1 and the solid curve results from the Fermi motion model with the model parameters $(p_F, m_q) = (252, 300)$ MeV, yielding an effective b-quark mass $m_b^{eff} = 4.85$ GeV.*

in this model are proportional to $(m_b^{\text{eff}})^5$ [24,6,53]. Hence the decay widths for both the decays individually are rather sensitive to m_b^{eff}. This dependence largely (but not exactly) cancels out in the branching ratio $\mathcal{B}(B \to X_s \ell^+ \ell^-)$. Thus, varying m_b^{eff} in the range $m_b^{\text{eff}} = 4.8 \pm 0.1$ GeV results in $\Delta\Gamma(B \to X_s \ell^+ \ell^-)/\Gamma = \pm 10.8\%$. However, the change in the branching ratio itself is rather modest, namely $\Delta\mathcal{B}(B \to X_s \ell^+ \ell^-)/\mathcal{B} = \pm 2.3\%$. This is rather similar to what we have obtained in the HQE approach.

The theoretical uncertainties in the branching ratios for $B \to X_s \ell^+ \ell^-$ from the perturbative part, such as the ones from the indeterminacy in the top quark mass, the QCD scale Λ_{QCD} and the renormalization scale μ, have been investigated in the literature [9,47]. We have recalculated them for the indicated ranges of the parameters in Table A.1. The resulting (SD) branching ratios and their present uncertainties are found to be:

$$\mathcal{B}(B \to X_s e^+ e^-) = (8.4 \pm 1.9) \times 10^{-6},$$
$$\mathcal{B}(B \to X_s \mu^+ \mu^-) = (5.7 \pm 0.9) \times 10^{-6},$$
$$\mathcal{B}(B \to X_s \tau^+ \tau^-) = (2.6 \pm 0.4) \times 10^{-7}, \tag{3.71}$$

where in calculating the branching ratio $\mathcal{B}(B \to X_s \tau^+ \tau^-)$, we have included the τ-lepton mass terms in the matrix element [28]. These uncertainties, typically $\pm 20\%$, are much larger than the wave function-dependent uncertainties, and so the theoretical accuracy of the SD-part in the SM in these decays is not compromised by the non-perturbative effects.

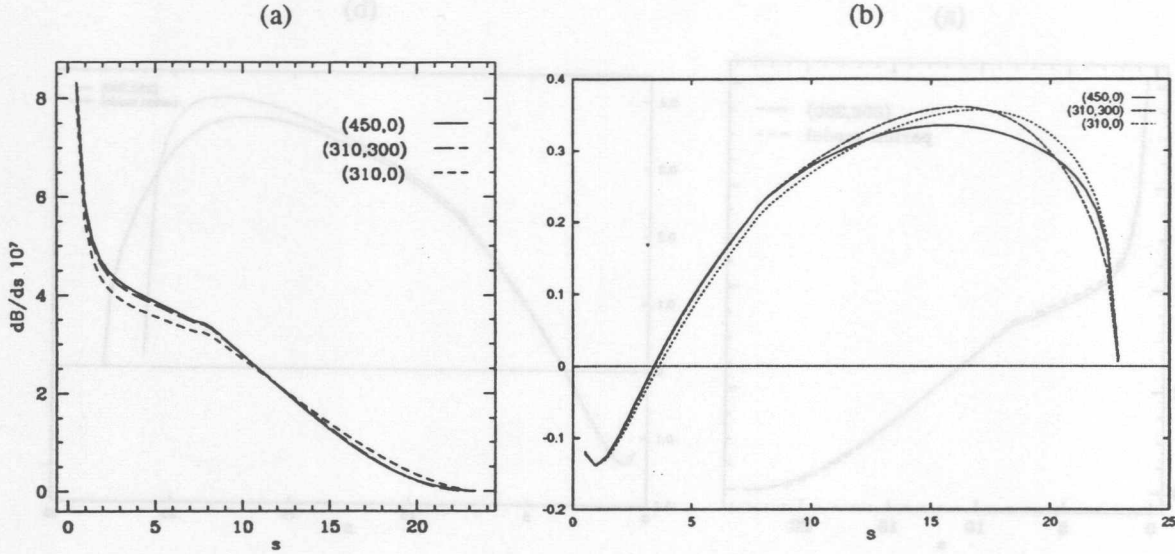We show the resulting dilepton invariant mass distribution in Fig. 3.7 (a) and the **FB-asymmetry**

(a)   (b)

Figure 3.8: *Differential branching ratio dB/ds for $B \to X_s \ell^+ \ell^-$ (a) and normalized differential FB asymmetry $d\overline{A}(s)/ds$ (b) using the Fermi motion model for three different pairs of the model parameters $(p_F, m_q) = (450, 0)$ MeV (solid curve), $(310, 300)$ MeV (long dashed curve), and $(p_F, m_q) = (310, 0)$ MeV (short dashed curve) yielding the effective b-quark masses $m_b^{eff} = 4.76$ GeV, 4.80 GeV, and 4.92 GeV, respectively.*

in Fig. 3.7 (b), where for the sake of illustration we have used the values $(p_F, m_q) = (252, 300)$ in (MeV,MeV), which correspond to an allowed set of parameters obtained from the analysis of the measured photon energy spectrum in $B \to X_s \gamma$, using the same model [94]. We see that the dilepton mass distribution is stable against Fermi motion effects over most part of this spectrum, as expected. We emphasize here that the end-point spectrum extends to the physical kinematic limit in $B \to X_s \ell^+ \ell^-$ $s^{max} = (m_B - m_X)^2$ with $m_X = max(m_K, m_s + m_q)$ (m_q is the spectator mass), which has to be imposed on the FM program. It corresponds to the invariant hadronic mass of the lowest physical state with total strangeness number $s = 1$, $m(X_s) = m_K$, as opposed to the parton model, in which $s^{max} = (m_b - m_s)^2$. The two thresholds can be made to coincide for only unrealistically values of m_b and m_s. The FB-asymmetry shows a more marked dependence on the model parameters, which becomes significant in the high dilepton mass region.

As the parameters of the Fermi motion model are not presently very well-determined from the fits of the existing data [94,95], one has to vary these parameters and estimate the resulting dispersion on the distributions in $B \to X_s \ell^+ \ell^-$. We show in Figs. 3.8 the dilepton mass distribution (a) and the FB asymmetry (b), respectively, indicating also the ranges of the parameters (p_F, m_q). The resulting theoretical uncertainty in the distributions is found to be modest.

3.4 LD Contributions in $B \to X_s \ell^+ \ell^-$ (I)

Next, we implement the effects of LD contributions in the processes $B \to X_s \ell^+ \ell^-$. The issues involved here have been discussed in [96,28,90]. The LD contributions due to the vector mesons J/ψ and ψ'
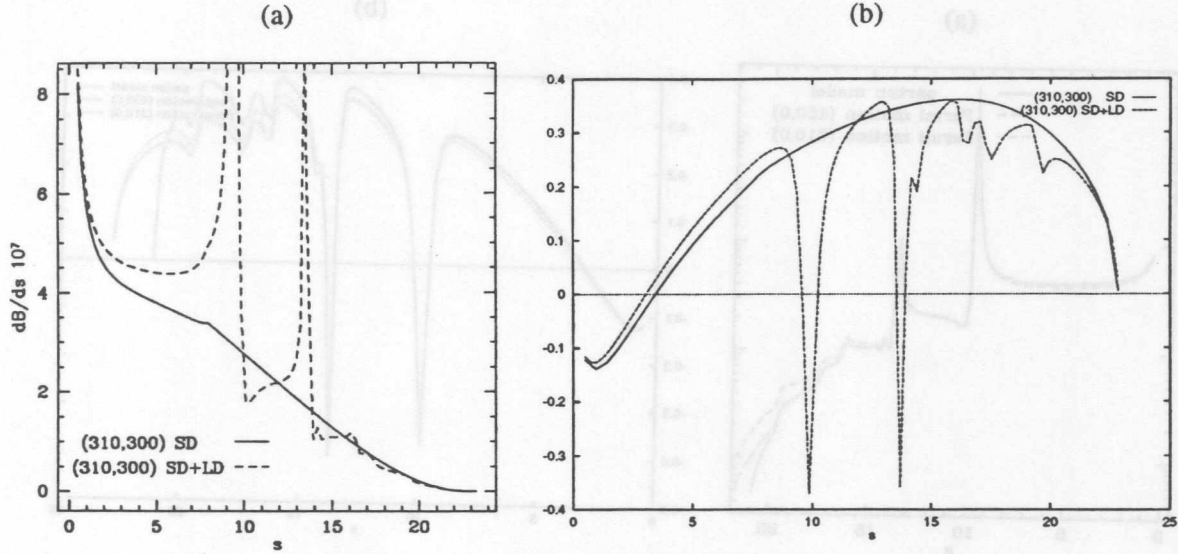
(a)　　(b)

Figure 3.9: *Differential branching ratio dB/ds for $B \to X_s \ell^+ \ell^-$ (a) and normalized differential FB asymmetry $d\overline{\mathcal{A}}(s)/ds$ (b) calculated in the SM using the next-to-leading order QCD corrections and Fermi motion effect (solid curve), and including the LD-contributions (dashed curve). The Fermi motion model parameters (p_F, m_q) in MeV are displayed in the figure.*

and higher resonances, as well as the $(c\bar{c})$ continuum contribution, which we have already included in the coefficient C_9^{eff}, appear in the $(\bar{s}_L \gamma_\mu b_L)(\bar{e}\gamma^\mu e)$ interaction term only, i.e., in the coefficient of the operator O_9. This implies that such LD-contributions should change C_9 effectively, but keep C_7^{eff} and C_{10} unchanged. In principle, one has also a LD contribution in the effective coefficient C_7^{eff}; this, however, has been discussed extensively in the context of the $B \to X_s \gamma$ decay and estimated to be small [97,77,76,98]. The LD-contribution is negligible in C_{10}. Hence, the three-coefficient fit of the data on $B \to X_s \ell^+ \ell^-$ and $B \to X_s \gamma$, proposed in ref. [12] on the basis of the SD-contributions, can be carried out also including the LD-effects.

In accordance with this, to incorporate the LD-effects in $B \to X_s \ell^+ \ell^-$, the function $Y(\hat{s})$ introduced earlier is replaced by,

$$Y(\hat{s}) \to Y'(\hat{s}) \equiv Y(\hat{s}) + Y_{res}(\hat{s}) , \qquad (3.72)$$

where $Y_{res}(\hat{s})$ accounts for the charmonium resonance contribution via $B \to X_s(J/\Psi, \Psi', \ldots) \to X_s \ell^+ \ell^-$. Its origin lies in the diagram displayed in Fig. 3.1, where the internal charm loop hadronizes before decaying into a photon. We take the representation [13],

$$Y_{res}(\hat{s}) = \frac{3}{\alpha^2} \kappa\, C^{(0)} \sum_{V_i = \psi(1s),\ldots,\psi(6s)} \frac{\pi\, \Gamma(V_i \to \ell^+ \ell^-)\, m_{V_i}}{m_{V_i}^2 - \hat{s}\, m_b^2 - i m_{V_i} \Gamma_{V_i}}, \qquad (3.73)$$

where $C^{(0)} \equiv 3C_1 + C_2 + 3C_3 + C_4 + 3C_5 + C_6$. We adopt $\kappa = 2.3$ for the numerical calculations [96]. This is a fair representation of present data in the factorization approach [99]; also the phase of κ, which is fixed in eq. (3.73), is now supported by data which finds it close to its perturbative value [100]. Of course, the data determines only the combination $\kappa\, C^{(0)} = 0.88$. The relevant parameters of the charmonium
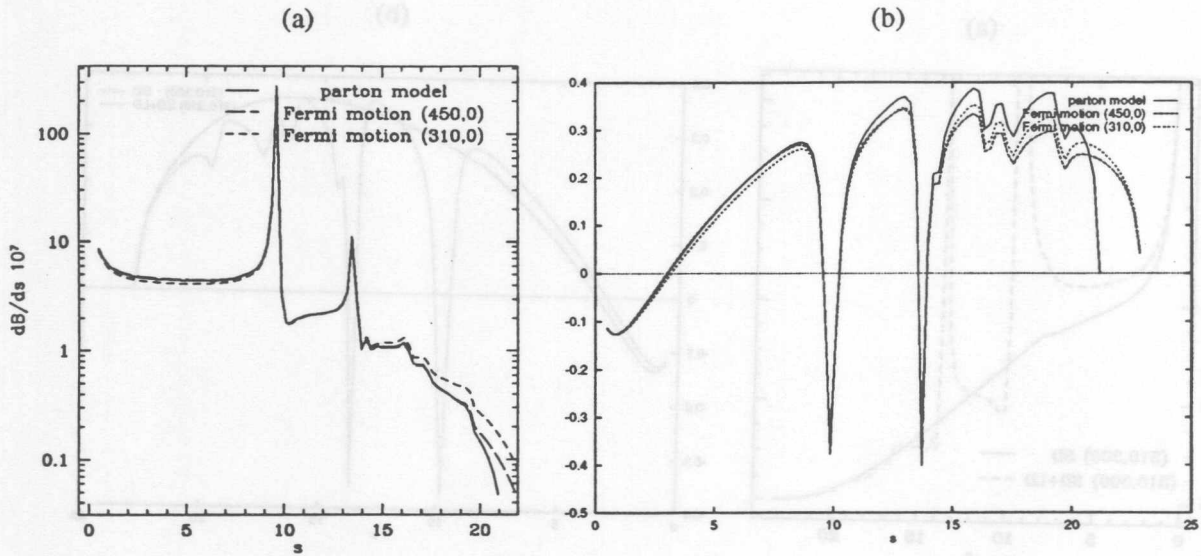
(a)   (b)

Figure 3.10: *Dilepton invariant mass distribution in $B \to X_s \ell^+ \ell^-$ (a) and normalized differential FB asymmetry $d\overline{\mathcal{A}}(s)/ds$ (b) in the SM including next-to-leading order QCD correction and LD effects. The solid curve corresponds to the parton model and the short-dashed and long-dashed curves correspond to including the Fermi motion effects. The values of the FM parameters in MeV are indicated in the figure.*

resonances $(1S, \ldots, 6S)$ are given in the Particle Data Group [39], and we have averaged the leptonic widths for the decay modes $V \to \ell^+ \ell^-$ for $\ell = e$ and $\ell = \mu$. Note that in extrapolating the dilepton masses away from the resonance region, no extra q^2-dependence is included in the $\gamma^*(q^2)$-V_i junction. (The q^2-dependence written explicitly in eq. (3.73) is due to the Breit-Wigner shape of the resonances.) This is an assumption and may lead to an underestimate of the LD-effects in the low-s region. However, as the present phenomenology is not equivocal on this issue, any other choice at this stage would have been on a similar footing.

The resulting dilepton mass spectrum and the FB asymmetry are shown in Fig. 3.9 (a) and Fig. 3.9 (b), respectively. We recall that the two curves labeled SD and SD+LD include explicit $O(\alpha_s)$-improvement, calculated in the parton model [9,47] and non-perturbative effects related with the bound state nature of the B-hadrons and the physical threshold in the final state in $B \to X_s \ell^+ \ell^-$, using the Fermi motion model. In addition, the SD+LD case also includes the LD-effects due to the vector resonances, contributing to C_9^{eff} as discussed earlier. The parametric dependence due to the FM is shown in Figs. 3.10 for the dilepton mass spectrum (a) and the FB asymmetry (b), respectively, and compared with the case of the parton model in which case no wave function effects are included. These figures give a fair estimate of the kind of uncertainties present in these distributions from non-perturbative effects. In particular, we draw attention to the marked dependence of the FB asymmetry to both the LD-(resonances) and wave function effects, which is particularly noticeable in the region $s > m_{\psi'}^2$. The dilepton invariant mass spectrum, on the other hand, is very stable except at the very end of the spectrum, which is clearly different in all three cases shown. This closes the first part of this chapter.

Bridge

Concerning our approach to include resonant charm effects eq. (3.72), we compare it in section 3.10 with two other LD prescriptions, given in ref. [28] and [29] and estimate the resulting uncertainties in the dilepton mass spectrum and the FB asymmetry. Further, we discuss a possible double counting, inherent in our procedure adding SD and LD amplitudes. The determination of these uncertainties is very important, as a measurement of the partly integrated spectra $\triangle \mathcal{B}$, $\triangle \mathcal{A}$ in $B \to X_s \ell^+ \ell^-$ decay will be used to extract the SD coefficients, testing the SM.

3.5 Introduction to Hadron Spectra and Spectral Moments in the Decay $B \to X_s \ell^+ \ell^-$

In this second part of this chapter we present spectra in inclusive $B \to X_s \ell^+ \ell^-$ decay in kinematical variables different from the dilepton invariant mass q^2, the hadronic energy and the hadronic invariant mass. Further, we calculate lowest moments in these hadronic variables. We include perturbative $\mathcal{O}(\alpha_s)$ corrections, $1/m_b$ power corrections by means of the heavy quark expansion technique (HQET) and studies in the Fermi motion model (FM). This part is based on refs. [25,26,14].

A similar program of investigations [93,23], [101–103] has been run for the charged current induced semileptonic $B \to X_{u,c} \ell \nu_\ell$ decay. Here the main interest is focused on testing HQET and on the determination of the CKM matrix elements V_{cb} and V_{ub}. To be more specific, the HQE parameters λ_1 and $\bar{\Lambda}$ have been extracted from moments of the hadronic invariant mass spectrum in $B \to X_{u,c} \ell \nu_\ell$ decay [66]. We recall that these non-perturbative parameters appear in the relation $m_B = m_b + \bar{\Lambda} - (\lambda_1 + 3\lambda_2)/2m_b$ between the mass of the B-meson to the b-quark mass (see section 2.4.1). Explicit calculation [25,26] shows that also in $B \to X_s \ell^+ \ell^-$ decay the hadronic invariant mass moments are sensitive to the HQET parameters λ_1 and $\bar{\Lambda}$. This provides potentially an independent determination of these quantities. We think that the hadron spectra in $B \to X_s \ell^+ \ell^-$ and $B \to X_u \ell \nu_\ell$ can be related to each other over limited phase space and this could help in improving the present precision on V_{ub} [39] and the parameters λ_1 and $\bar{\Lambda}$ [31,63]. Of course, $B \to X_{u,c} \ell \nu_\ell$ decays involve much less problems than FCNC $B \to X_s \ell^+ \ell^-$ decay, as the charged current mode has simpler short-distance (SD) couplings and no $c\bar{c}$ resonances present in the spectra. Besides these obvious differences, we will point out in the following sections similarities between rare $B \to X_s \ell^+ \ell^-$ and the charged current $B \to X_{u,c} \ell \nu_\ell$ decays.

What can we learn from the study of hadron spectra and moments in $B \to X_s \ell^+ \ell^-$? Our motivation is manifold:

1. Hadron spectra have an interest on their own, they complete the profile of $B \to X_s \ell^+ \ell^-$ decay which has been given in the previous sections, i. e. the dilepton invariant mass distribution and the FB asymmetry.

2. In their search for $B \to X_s \ell^+ \ell^-$ the CLEO collaboration [30] imposed a cut on the hadronic invariant mass S_H to suppress the $B\bar{B}$ background in measuring the dilepton invariant mass distribution. The hadronic invariant mass spectrum is absolutely necessary to acquire control over the signal after a cut in S_H.

3. A possible determination of non-perturbative HQE parameters $\lambda_1, \bar{\Lambda}$ from the first two moments of the hadronic invariant mass in $B \rightarrow X_s \ell^+ \ell^-$ decay, complementing the constraint from the charged current $B \rightarrow X_c \ell \nu_\ell$ decay. The constraints from these decays can be used to reduce the present dispersion on λ_1 and $\bar{\Lambda}$.

4. Test of the Fermi motion model in $B \rightarrow X_s \ell^+ \ell^-$ decay.

The power corrections presented here in the hadron spectrum and hadronic spectral moments in $B \rightarrow X_s \ell^+ \ell^-$ are the first results in this decay.

3.5.1   Hadron kinematics

Besides the parton level kinematics already introduced in section 3.1.1, the corresponding kinematics at hadron level can be written as:

$$B(p_B) \rightarrow X_s(p_H) + \ell^+(p_+) + \ell^-(p_-) . \tag{3.74}$$

The hadronic invariant mass is denoted by $S_H \equiv p_H^2$ and E_H denotes the hadron energy in the final state. The corresponding quantities at parton level are the invariant mass s_0 and the scaled parton energy $x_0 \equiv \frac{E_0}{m_b}$. In parton model without gluon bremsstrahlung, this simplifies to $s_0 = m_s^2$ and x_0 becomes directly related to the dilepton invariant mass $x_0 = 1/2(1 - \hat{s} + \hat{m}_s^2)$. From momentum conservation the following equalities hold in the b-quark, equivalently B-meson, rest frame ($v = (1, 0, 0, 0)$):

$$x_0 = 1 - v \cdot \hat{q} , \quad \hat{s}_0 = 1 - 2v \cdot \hat{q} + \hat{s} , \tag{3.75}$$

$$E_H = m_B - v \cdot q , \quad S_H = m_B^2 - 2m_B v \cdot q + s . \tag{3.76}$$

The relations between the kinematic variables of the parton model and the hadronic states , using the HQET mass relation, can be written as

$$E_H = \bar{\Lambda} - \frac{\lambda_1 + 3\lambda_2}{2m_B} + \left(m_B - \bar{\Lambda} + \frac{\lambda_1 + 3\lambda_2}{2m_B} \right) x_0 + \dots ,$$

$$S_H = m_s^2 + \bar{\Lambda}^2 + (m_B^2 - 2\bar{\Lambda} m_B + \bar{\Lambda}^2 + \lambda_1 + 3\lambda_2)(\hat{s}_0 - \hat{m}_s^2)$$

$$+ (2\bar{\Lambda} m_B - 2\bar{\Lambda}^2 - \lambda_1 - 3\lambda_2)x_0 + \dots , \tag{3.77}$$

where the ellipses denote terms higher order in $1/m_b$.

3.6   Perturbative $O(\alpha_s)$ Corrected Hadron Spectra in $B \rightarrow X_s \ell^+ \ell^-$ Decay

In this section the $O(\alpha_s)$ corrections to the hadron spectra are investigated. Following the argument given in section 3.1.2, only O_9 is subject to α_s corrections and the corresponding Feynman diagrams can be seen in Fig. 3.2. The effect of a finite s-quark mass on the $\mathcal{O}(\alpha_s)$ correction function is found to be very small. After showing this, we have neglected the s-quark mass in the numerical calculations of the $\mathcal{O}(\alpha_s)$ terms.

3.6.1 Hadron energy spectrum

The explicit order α_s correction to O_9 can be obtained by using the existing results in the literature as follows: The vector current O_9 can be decomposed as $V = (V - A)/2 + (V + A)/2$. We recall that the $(V - A)$ and $(V + A)$ currents yield the same hadron energy spectrum [104] and there is no interference term present in this spectrum for massless leptons. So, the correction for the vector current case in $B \to X_s \ell^+ \ell^-$ can be taken from the corresponding result for the charged $(V - A)$ case [22,91], yielding

$$C_9^{\text{eff}}(x_0) = C_9 \rho(x_0) + Y(x_0) \tag{3.78}$$

with

$$\rho(x) = 1 + \frac{\alpha_s}{\pi} \sigma(x) , \tag{3.79}$$

$$\sigma(x) = \frac{1}{(3x - 4x^2 - 2\hat{m}_s^2 + 3\hat{m}_s^2 x)} \frac{G_1(x)}{3\sqrt{x^2 - \hat{m}_s^2}} , \tag{3.80}$$

where $Y(x_0) \equiv Y(\hat{s})$ with $\hat{s} = 1 - 2x_0 + \hat{m}_s^2$. The expression for $G_1(x)$ with $m_s \neq 0$ has been calculated in [91]. The effect of a finite m_s is negligible in $G_1(x)$, as can be seen in Fig. 3.11, where this function is plotted both with a finite s-quark mass, $m_s = 0.2$ GeV, and for the massless case, $m_s = 0$. A numerical difference occurs at the lowest order end-point $x_0^{max} = 1/2(1 + \hat{m}_s^2)$ (for $m_l = 0$), where the function develops a singularity from above $(x_0 > x_0^{max})$ and the position of which depends on the value of m_s. The function $G_1(x)$ for a massless s-quark is given and discussed below [91].

$$G_1(x) = x^2 \{ \frac{1}{90}(16x^4 - 84x^3 + 585x^2 - 1860x + 1215) + (8x - 9)\ln(2x)$$

$$+ 2(4x - 3)\left[\frac{\pi^2}{2} + Li_2(1 - 2x)\right] \} \quad \text{for } 0 \leq x \leq 1/2 ,$$

$$G_1(x) = \frac{1}{180}(1 - x)(32x^5 - 136x^4 + 1034x^3 - 2946x^2 + 1899x + 312)$$

$$- \frac{1}{24}\ln(2x - 1)(64x^3 - 48x^2 - 24x - 5)$$

$$+ x^2(3 - 4x)\left[\frac{\pi^2}{3} - 4Li_2(\frac{1}{2x}) + \ln^2(2x - 1) - 2\ln^2(2x)\right] \quad \text{for } 1/2 < x \leq 1 . \tag{3.81}$$

The $\mathcal{O}(\alpha_s)$ correction has a double logarithmic (integrable) singularity for $x_0 \to 1/2$ from above $(x_0 > 1/2)$. Further, the value of the order α_s corrected Wilson coefficient $C_9^{\text{eff}}(x_0)$ is reduced compared to its value with $\alpha_s = 0$, therefore also the hadron energy spectrum is reduced after including the explicit order α_s QCD correction for $0 < x_0 < 1/2$. Note that the hadron energy spectrum for $B \to X_s \ell^+ \ell^-$ receives contributions for $1 \geq x > 1/2$ only from the order α_s bremsstrahlung corrections.

3.6.2 Hadronic invariant mass spectrum

We have calculated the order α_s perturbative QCD correction for the hadronic invariant mass in the range $\hat{m}_s^2 < \hat{s}_0 \leq 1$. Since the decay $b \to s + \ell^+ + \ell^-$ contributes in the parton model only at $\hat{s}_0 = \hat{m}_s^2$, only the bremsstrahlung graphs $b \to s + g + \ell^+ + \ell^-$ contribute in this range. This makes the calculation much simpler than in the full $\hat{s}_0$ range including virtual gluon diagrams. We find

$$\frac{dB}{d\hat{s}_0} = \frac{2}{3}B_0 \frac{\alpha_s}{\pi} \frac{1}{\hat{s}_0} \{ \frac{(\hat{s}_0 - 1)}{27}(93 - 41\hat{s}_0 - 95\hat{s}_0^2 + 55\hat{s}_0^3) + \frac{4}{9}\ln \hat{s}_0(-3 - 5\hat{s}_0 + 9\hat{s}_0^2 - 2\hat{s}_0^4) \} C_9^2 . \tag{3.82}$$
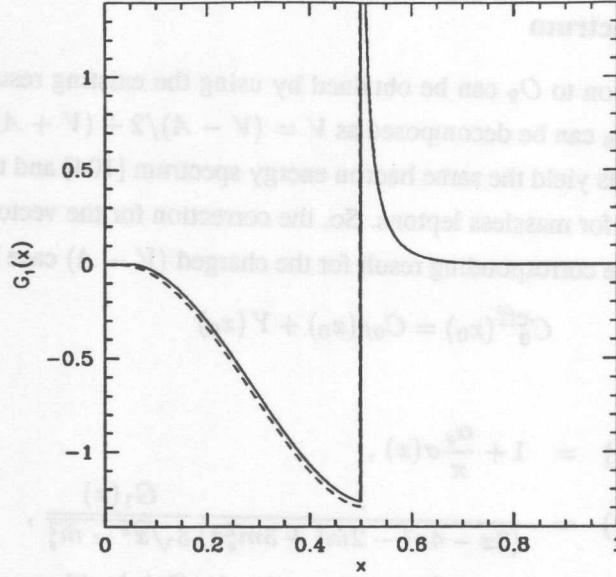
Figure 3.11: *The function $G_1(x)$ is shown for $m_s = 0.2\,\text{GeV}$ (solid line) and for the massless case corresponding to eq. (3.81) (dashed line).*

Our result for the spectrum in $B \to X_s \ell^+ \ell^-$ is in agreement with the corresponding result for the $(V - A)$ current obtained for the decay $B \to X_q \ell \nu_\ell$ in the $m_q = 0$ limit in [93] (their eq. (3.8)), once one takes into account the difference in the normalizations. We display the hadronic invariant mass distribution in Fig. 3.12 as a function of s_0 (with $s_0 = m_b^2 \hat{s}_0$), where we also show the Sudakov improved spectrum, obtained from the $\mathcal{O}(\alpha_s)$ spectrum in which the double logarithms have been resummed. For the decay $B \to X_u \ell \nu_\ell$, this has been derived in [23], where all further details can be seen. We confirm eq. (17) of [23] for the Sudakov exponentiated double differential decay rate $\frac{d^2\Gamma}{dxdy}$ and use it after changing the normalization $\Gamma_0 \to \mathcal{B}_0 \frac{2}{3} C_9^2$ for the decay $B \to X_s \ell^+ \ell^-$. The constant $\mathcal{B}_0$ is given in eq. (3.29). Defining the kinematic variables (x, y) as

$$q^2 = x^2 m_b^2 ,$$
$$v \cdot q = (x + \frac{1}{2}(1 - x)^2 y) m_b , \tag{3.83}$$

the Sudakov-improved Dalitz distribution is given by

$$\frac{d^2 B}{dxdy}(B \to X_s \ell^+ \ell^-) = -\mathcal{B}_0 \frac{8}{3} x (1 - x^2)^2 (1 + 2x^2) \exp\left(-\frac{2\alpha_s}{3\pi} \ln^2(1 - y)\right) \tag{3.84}$$

$$\times \left\{ \frac{4\alpha_s}{3\pi} \frac{\ln(1 - y)}{(1 - y)} \left[1 - \frac{2\alpha_s}{3\pi}(G(x) + H(y)) \right] - \frac{2\alpha_s}{3\pi} \frac{dH}{dy}(y) \right\} C_9^2 ,$$

where [23]

$$G(x) = \frac{[8x^2(1 - x^2 - 2x^4)\ln x + 2(1 - x^2)^2(5 + 4x^2)\ln(1 - x^2) - (1 - x^2)(5 + 9x^2 - 6x^4)]}{2(1 - x^2)^2(1 + 2x^2)}$$
$$+ \pi^2 + 2Li_2(x^2) - 2Li_2(1 - x^2) , \tag{3.85}$$

$$H(y) = \int_0^y dz \left(\frac{4}{1 - z} \ln \frac{2 - z(1 - x) + \kappa}{2} \right.$$
$$\left. - \frac{(1 - x)(3 + x + xz - z)}{(1 + x)^2} \left[\ln(1 - z) - 2 \ln \frac{2 - z(1 - x) + \kappa}{2} \right] \right)$$
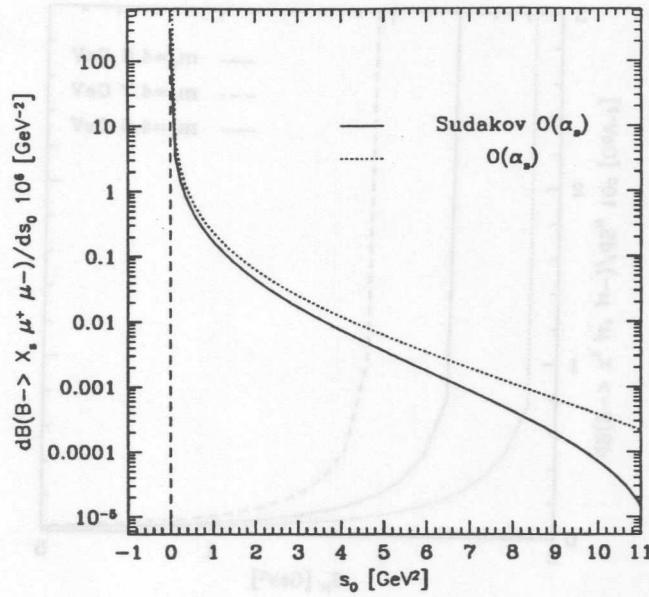
Figure 3.12: *The differential branching ratio $\frac{\mathrm{d}\mathcal{B}(B \to X_s \ell^+ \ell^-)}{\mathrm{d}s_0}$ in the parton model is shown in the $\mathcal{O}(\alpha_s)$ bremsstrahlung region. The dotted (solid) line corresponds to eq. (3.82), (eq. (3.87)). The vertical line denotes the one particle pole from $b \to s\ell^+\ell^-$. We do not show the full spectra in the range $0 \leq s_0 \leq m_b^2$ as they tend to zero for larger values of s_0.*

$$-\frac{\kappa}{2(1+x)^2(1+2x^2)}\left[\frac{7(1+x)(1+2x^2)}{1-z} + (1-x)(3-2x^2)\right]\right). \tag{3.86}$$

The quantity κ in eq. (3.86) is defined as $\kappa \equiv \sqrt{z^2(1-x)^2 + 4xz}$.

To get the hadronic invariant mass spectrum for a b-quark decaying at rest we change variables from (x, y) to (q^2, s_0) followed by an integration over q^2,

$$\frac{\mathrm{d}\mathcal{B}}{\mathrm{d}s_0} = \int_{4m_l^2}^{(m_b - \sqrt{s_0})^2} \mathrm{d}q^2 \frac{\mathrm{d}^2\mathcal{B}}{\mathrm{d}x\mathrm{d}y} \frac{1}{2m_b^4 x(1-x)^2}. \tag{3.87}$$

The most significant effect of the bound state is the difference between m_B and m_b, which is dominated by $\bar{\Lambda}$. Neglecting λ_1, λ_2, i.e., using $\bar{\Lambda} = m_B - m_b$, the spectrum $\frac{\mathrm{d}\mathcal{B}}{\mathrm{d}S_H}$ is obtained along the lines as given above for $\frac{\mathrm{d}\mathcal{B}}{\mathrm{d}s_0}$, after changing variables from (x, y) to (q^2, S_H) and performing an integration over q^2. It is valid in the region $m_B \frac{m_B\bar{\Lambda} - \bar{\Lambda}^2 + m_s^2}{m_B - \bar{\Lambda}} < S_H \leq m_B^2$ (or $m_B\bar{\Lambda} \leq S_H \leq m_B^2$, neglecting m_s) which excludes the zeroth order and virtual gluon kinematics ($s_0 = m_s^2$), yielding

$$\frac{\mathrm{d}\mathcal{B}}{\mathrm{d}S_H} = \int_{4m_l^2}^{(m_B - \sqrt{S_H})^2} \mathrm{d}q^2 \frac{\mathrm{d}^2\mathcal{B}}{\mathrm{d}x\mathrm{d}y} \frac{1}{2m_b^3 m_B x(1-x)^2}. \tag{3.88}$$

The hadronic invariant mass spectrum thus found depends rather sensitively on m_b (or equivalently $\bar{\Lambda}$), as can be seen from Fig. 3.13. An analogous analysis for the charged current semileptonic B decays $B \to X_u \ell \nu_\ell$ has been performed in [101], with similar conclusions.
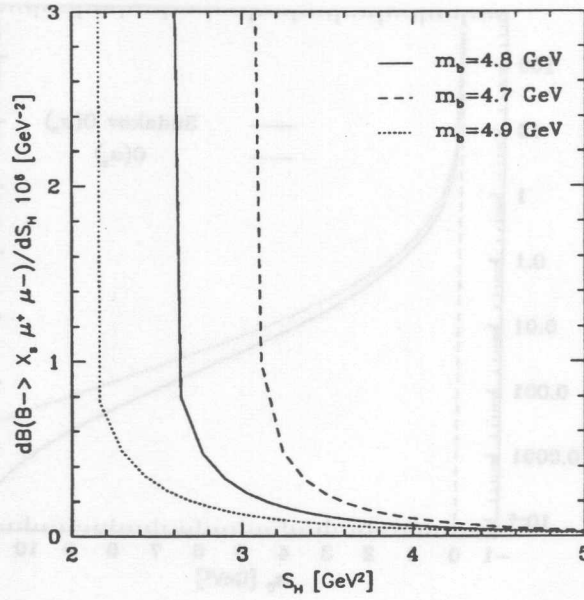
Figure 3.13: *The differential branching ratio $\frac{d\mathcal{B}(B \to X_s \ell^+ \ell^-)}{dS_H}$ in the hadronic invariant mass, S_H, shown for different values of m_b in the range where only bremsstrahlung diagrams contribute. We do not show the result in the full kinematic range as the spectra tend monotonically to zero for larger values of $S_H \leq m_B^2$.*

3.7   Power Corrected Hadron Spectra in $B \to X_s \ell^+ \ell^-$ Decay

We start directly with the structure functions T_i of the hadronic tensor, which are calculated up to $O(m_B/m_b^3)$ in [18]. They have been decomposed into a sum of various terms, $T_i(v.\hat{q}, \hat{s}) = \sum_{j=0,1,2,s,g,\delta} T_i^{(j)}(v.\hat{q}, \hat{s})$ where the individual parts $T_i^{(j)}$ can be seen in appendix B.1. After contracting the hadronic and leptonic tensors, one arrives at eq. (3.27). Now we are interested in a different set of kinematical variables. We transform $(v \cdot \hat{q}, \hat{s}) \to (x_0, \hat{s}_0)$ with the help of the kinematic identities given in eq. (3.75), and make the dependence on x_0 and $\hat{s}_0$ explicit,

$$T^{L/R}{}_{\mu\nu} L^{L/R\mu\nu} = m_b{}^2 \left\{ 2(1 - 2x_0 + \hat{s}_0) T_1^{L/R} + \left[x_0^2 - \frac{1}{4}\hat{u}^2 - \hat{s}_0 \right] T_2^{L/R} \mp (1 - 2x_0 + \hat{s}_0)\hat{u}\, T_3^{L/R} \right\}. \tag{3.89}$$

With this we are able to derive the double differential power corrected spectrum $\frac{d\mathcal{B}}{dx_0 \, d\hat{s}_0}$ for the decay $B \to X_s \ell^+ \ell^-$. Integrating eq. (3.23) over $\hat{u}$ first, where the variable $\hat{u}$ is bounded by

$$-2\sqrt{x_0^2 - \hat{s}_0} \leq \hat{u} \leq +2\sqrt{x_0^2 - \hat{s}_0} \,, \tag{3.90}$$

we arrive at the following expression [26]

$$\frac{d^2\mathcal{B}}{dx_0 \, d\hat{s}_0} = -\frac{8}{\pi} B_0 \mathrm{Im}\sqrt{x_0^2 - \hat{s}_0} \left\{ (1 - 2x_0 + \hat{s}_0) T_1(\hat{s}_0, x_0) + \frac{x_0^2 - \hat{s}_0}{3} T_2(\hat{s}_0, x_0) \right\} + \mathcal{O}(\lambda_i; \alpha_s) \,, \tag{3.91}$$

where

$$T_1(\hat{s}_0, x_0) = \frac{1}{x} \left\{ \left(8x_0 - 4(\frac{\lambda_1}{3} + \hat{\lambda}_2) \right) \left(|C_9^{\mathrm{eff}}(\hat{s})|^2 + |C_{10}|^2 \right) \right.$$

$$+ \left(32(-2\hat{m}_s^2 - 2\hat{s}_0 - 4\hat{m}_s^2\hat{s}_0 + x_0 + 5\hat{m}_s^2 x_0 + \hat{s}_0 x_0 + \hat{m}_s^2\hat{s}_0 x_0) + 16(\frac{\hat{\lambda}_1}{3} + \hat{\lambda}_2) \right.$$

$$\times \left. (-5 - 11\hat{m}_s^2 + 5\hat{s}_0 - \hat{m}_s^2\hat{s}_0 + 10x_0 + 22\hat{m}_s^2 x_0 - 10x_0^2 - 10\hat{m}_s^2 x_0^2) \right) \frac{|C_7^{\text{eff}}|^2}{(\hat{s}_0 - 2x_0 + 1)^2}$$

$$+ \left(\frac{-32}{\hat{s}_0 - 2x_0 + 1}(\hat{m}_s^2 + \hat{s}_0 - x_0 - \hat{m}_s^2 x_0) - 48(\frac{\hat{\lambda}_1}{3} + \hat{\lambda}_2) \right) Re(C_9^{\text{eff}}(\hat{s}))\, C_7^{\text{eff}} \Bigg\}$$

$$+ \frac{1}{x^2} \left\{ \left(\frac{8\hat{\lambda}_1}{3}(-2\hat{s}_0 - 3x_0 + 5x_0^2) + 8\hat{\lambda}_2(-2\hat{s}_0 + x_0 + 5x_0^2) \right) \left(|C_9^{\text{eff}}(\hat{s})|^2 + |C_{10}|^2 \right) \right.$$

$$+ \left(\frac{32\hat{\lambda}_1}{3}(6\hat{m}_s^2 + 12\hat{s}_0 + 18\hat{m}_s^2\hat{s}_0 - 2\hat{s}_0^2 - 2\hat{m}_s^2\hat{s}_0^2 - 3x_0 - 21\hat{m}_s^2 x_0 - 13\hat{s}_0 x_0 - 19\hat{m}_s^2\hat{s}_0 x_0 \right.$$

$$- 3x_0^2 + 9\hat{m}_s^2 x_0^2 + 5\hat{s}_0 x_0^2 + 5\hat{m}_s^2\hat{s}_0 x_0^2 + 4x_0^3 + 4\hat{m}_s^2 x_0^3)$$

$$+ 32\hat{\lambda}_2(-2\hat{m}_s^2 - 2\hat{m}_s^2\hat{s}_0 - 2\hat{s}_0^2 - 2\hat{m}_s^2\hat{s}_0^2 + x_0 - \hat{m}_s^2 x_0 - 5\hat{s}_0 x_0 - 11\hat{m}_s^2\hat{s}_0 x_0 + x_0^2$$

$$+ 13\hat{m}_s^2 x_0^2 + 5\hat{s}_0 x_0^2 + 5\hat{m}_s^2\hat{s}_0 x_0^2) \bigg) \frac{|C_7^{\text{eff}}|^2}{(\hat{s}_0 - 2x_0 + 1)^2}$$

$$+ \left(\frac{-32\hat{\lambda}_1}{3}(-3\hat{m}_s^2 - 5\hat{s}_0 + 2\hat{m}_s^2\hat{s}_0 + 3x_0 + 6\hat{m}_s^2 x_0 + 3\hat{s}_0 x_0 - x_0^2 - 5\hat{m}_s^2 x_0^2) \right.$$

$$- \left. 32\hat{\lambda}_2(\hat{m}_s^2 + \hat{s}_0 + 2\hat{m}_s^2\hat{s}_0 - x_0 + 2\hat{m}_s^2 x_0 + 3\hat{s}_0 x_0 - 3x_0^2 - 5\hat{m}_s^2 x_0^2) \right) \frac{Re(C_9^{\text{eff}}(\hat{s}))\, C_7^{\text{eff}}}{\hat{s}_0 - 2x_0 + 1} \Bigg\}$$

$$+ \frac{1}{x^3}\hat{\lambda}_1(\hat{s}_0 - x_0^2) \left\{ \frac{32x_0}{3} \left(|C_9^{\text{eff}}(\hat{s})|^2 + |C_{10}|^2 \right) \right.$$

$$+ \frac{128}{3}(-2\hat{m}_s^2 - 2\hat{s}_0 - 4\hat{m}_s^2\hat{s}_0 + x_0 + 5\hat{m}_s^2 x_0 + \hat{s}_0 x_0 + \hat{m}_s^2\hat{s}_0 x_0) \frac{|C_7^{\text{eff}}|^2}{(\hat{s}_0 - 2x_0 + 1)^2}$$

$$+ \left. \frac{-128}{3}(\hat{m}_s^2 + \hat{s}_0 - x_0 - \hat{m}_s^2 x_0) \frac{Re(C_9^{\text{eff}}(\hat{s}))\, C_7^{\text{eff}}}{\hat{s}_0 - 2x_0 + 1} \right\} \,,$$

$$T_2(\hat{s}_0, x_0) = \frac{1}{x} \left\{ \left(16 - 40(\frac{\hat{\lambda}_1}{3} + \hat{\lambda}_2) \right) \left(|C_9^{\text{eff}}(\hat{s})|^2 + |C_{10}|^2 \right) \right.$$

$$+ \left. \left(-64 + 160(\frac{\hat{\lambda}_1}{3} + \hat{\lambda}_2) \right) (1 + \hat{m}_s^2) \frac{|C_7^{\text{eff}}|^2}{\hat{s}_0 - 2x_0 + 1} \right\}$$

$$+ \frac{1}{x^2} \left\{ \left(\frac{112\hat{\lambda}_1}{3}(-1 + x_0) + 16\hat{\lambda}_2(-3 + 5x_0) \right) \left(|C_9^{\text{eff}}(\hat{s})|^2 + |C_{10}|^2 \right) \right.$$

$$+ \left. \left(\frac{448\hat{\lambda}_1}{3}(1 - x_0) + 64\hat{\lambda}_2(5x_0 - 1) \right) (1 + \hat{m}_s^2) \frac{|C_7^{\text{eff}}|^2}{\hat{s}_0 - 2x_0 + 1} - 64\hat{\lambda}_2 Re(C_9^{\text{eff}}(\hat{s}))\, C_7^{\text{eff}} \right\}$$

$$+ \frac{1}{x^3}\hat{\lambda}_1(\hat{s}_0 - x_0^2) \left\{ \frac{64}{3} \left(|C_9^{\text{eff}}(\hat{s})|^2 + |C_{10}|^2 \right) + \frac{-256}{3}(1 + \hat{m}_s^2) \frac{|C_7^{\text{eff}}|^2}{\hat{s}_0 - 2x_0 + 1} \right\} \,. \qquad (3.92)$$

Here, $x = \hat{s}_0 - \hat{m}_s^2 + i\epsilon$, $\hat{\lambda}_1 = \lambda_1/m_b^2$ and $\hat{\lambda}_2 = \lambda_2/m_b^2$. As the structure function T_3 does not contribute to the branching ratio, we did not consider it in the calculation of the hadron spectra. The Wilson coefficient $C_9^{\text{eff}}(\hat{s})$ depends both on the variables x_0 and $\hat{s}_0$ arising from the matrix element of the four-Fermi-operators. Here the normalization constant $\mathcal{B}_0$, defined in eq. (3.29), expresses the branching ratio for $B \to X_s \ell^+ \ell^-$ as usual in terms of the semileptonic decays $B \to X_c \ell \nu_\ell$. The double differential ratio given in eq. (3.91) agrees in the $(V - A)$ limit given in eqs. (3.66) - (3.68) with the corresponding expression

derived for $B \to X_c \ell \nu_\ell$ decay in [93] (their eq. (3.2)).

The hadron energy spectrum can now be obtained by integrating over $\hat{s}_0$. Using eq. (3.59), the following replacements are equivalent to taking the imaginary part

$$
\begin{aligned}
\frac{1}{x} &\to \delta(\hat{s}_0 - \hat{m}_s^2) \,, \\
\frac{1}{x^2} &\to -\delta'(\hat{s}_0 - \hat{m}_s^2) \,, \\
\frac{1}{x^3} &\to \frac{1}{2}\delta''(\hat{s}_0 - \hat{m}_s^2) \,.
\end{aligned}
\tag{3.93}
$$

The kinematic boundaries are given as:

$$
max(\hat{m}_s^2, -1 + 2x_0 + 4\hat{m}_l^2) \leq \hat{s}_0 \leq x_0^2 \,,
$$
$$
\hat{m}_s \leq x_0 \leq \frac{1}{2}(1 + \hat{m}_s^2 - 4\hat{m}_l^2) \,.
\tag{3.94}
$$

Here we keep $\hat{m}_l$ as a regulator wherever it is necessary and abbreviate $C_9^{\text{eff}} \equiv C_9^{\text{eff}}(\hat{s} = 1 - 2x_0 + \hat{m}_s^2)$. Including the leading power corrections, the hadron energy spectrum in the decay $B \to X_s \ell^+ \ell^-$ is given below:

$$
\begin{aligned}
\frac{dB}{dx_0} &= B_0 \left\{ \left[g_0^{(9,10)} + \hat{\lambda}_1 g_1^{(9,10)} + \hat{\lambda}_2 g_2^{(9,10)} \right] \left(|C_9^{\text{eff}}|^2 + |C_{10}|^2 \right) \right. \\
&+ \left[g_0^{(7)} + \hat{\lambda}_1 g_1^{(7)} + \hat{\lambda}_2 g_2^{(7)} \right] \frac{|C_7^{\text{eff}}|^2}{x_0 - \frac{1}{2}(1 + \hat{m}_s^2)} + \left[g_0^{(7,9)} + \hat{\lambda}_1 g_1^{(7,9)} + \hat{\lambda}_2 g_2^{(7,9)} \right] Re(C_9^{\text{eff}}) \, C_7^{\text{eff}} \\
&+ (\hat{\lambda}_1 h_1^{(9)} + \hat{\lambda}_2 h_2^{(9)}) \frac{d|C_9^{\text{eff}}|^2}{d\hat{s}_0} + \hat{\lambda}_1 k_1^{(9)} \frac{d^2|C_9^{\text{eff}}|^2}{d\hat{s}_0^2} \\
&+ (\hat{\lambda}_1 h_1^{(7,9)} + \hat{\lambda}_2 h_2^{(7,9)}) \frac{dRe(C_9^{\text{eff}})}{d\hat{s}_0} C_7^{\text{eff}} + \hat{\lambda}_1 k_1^{(7,9)} \frac{d^2 Re(C_9^{\text{eff}})}{d\hat{s}_0^2} C_7^{\text{eff}} \right\} \\
&+ \delta(x_0 - \frac{1}{2}(1 + \hat{m}_s^2 - 4\hat{m}_l^2)) f_\delta(\hat{\lambda}_1, \hat{\lambda}_2) + \delta'(x_0 - \frac{1}{2}(1 + \hat{m}_s^2 - 4\hat{m}_l^2)) f_{\delta'}(\hat{\lambda}_1, \hat{\lambda}_2) \,.
\end{aligned}
\tag{3.95}
$$

The functions $g_i^{(9,10)}, g_i^{(7)}, g_i^{(7,9)}, h_i^{(9)}, h_i^{(7,9)}, k_1^{(9)}, k_1^{(7,9)}$ in the above expression are the coefficients of the $1/m_b^2$ power expansion for different combinations of Wilson coefficients, with $g_0^{(j,k)}$ being the lowest order (parton model) functions. They are functions of the variables x_0 and $\hat{m}_s$ and are given in appendix C.1. The singular functions δ, δ' have support only at the lowest order end-point of the spectrum, i.e., at $x_0^{max} \equiv \frac{1}{2}(1 + \hat{m}_s^2 - 4\hat{m}_l^2)$. The auxiliary functions $f_\delta(\hat{\lambda}_1, \hat{\lambda}_2)$ and $f_{\delta'}(\hat{\lambda}_1, \hat{\lambda}_2)$ vanish in the limit $\hat{\lambda}_1 = \hat{\lambda}_2 = 0$. They are given in appendix C.2. The derivatives of C_9^{eff} are defined as $\frac{d^n C_9^{\text{eff}}}{d\hat{s}_0^n} \equiv \frac{d^n C_9^{\text{eff}}}{d\hat{s}^n}(\hat{s} = 1 - 2x_0 + \hat{s}_0; \hat{s}_0 = \hat{m}_s^2)$ $(n = 1, 2)$. In the $(V - A)$ limit our eq. (3.95) for the hadron energy spectrum in $B \to X_s \ell^+ \ell^-$ agrees with the corresponding spectrum in $B \to X \ell \nu_\ell$ given in ref. [93] (their eq. (A1)). Integrating also over x_0 the resulting total width for $B \to X_s \ell^+ \ell^-$ agrees again in the $(V - A)$ limit with the well known result [15].

The power-corrected hadron energy spectrum $\frac{dB(B \to X_s \ell^+ \ell^-)}{dE_0}$ (with $E_0 = m_b x_0$) is displayed in Fig. 3.14 through the solid curve, however, without the singular δ, δ' terms. Note that before reaching the kinematic lower end-point, the power-corrected spectrum becomes negative, as a result of the $\hat{\lambda}_2$ term. This behavior is analogous to what has already been reported for the dilepton mass spectrum
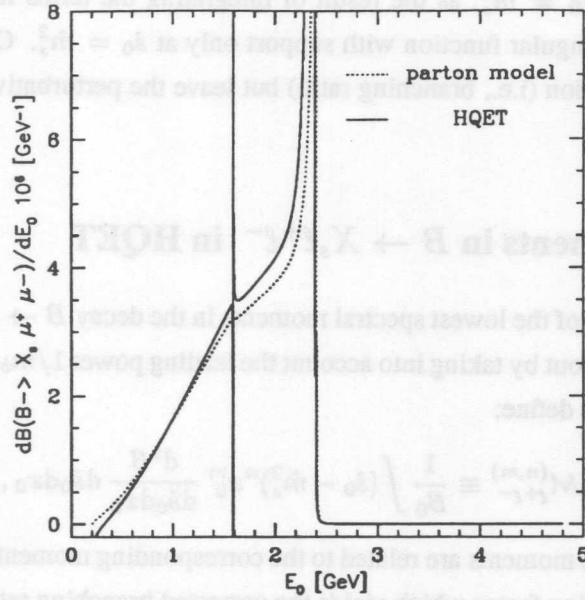
Figure 3.14: *Hadron energy spectrum* $\frac{d\mathcal{B}(B \to X_s \ell^+ \ell^-)}{dE_0}$ *in the parton model (dotted line) and including leading power corrections (solid line). For $m_b/2 < E_0 \leq m_b$ the distributions coincide. The parameters used for this plot are the central values given in Table A.1 and the default values of the HQET parameters specified in text.*

$\frac{d\mathcal{B}(B \to X_s \ell^+ \ell^-)}{dq^2}$ in the high q^2 region [18], signaling a breakdown of the $\frac{1}{m_b}$ expansion in this region. The terms with the derivatives of C_9^{eff} in eq. (3.95) give rise to a singularity in the hadron energy spectrum at the charm threshold due to the cusp in the function $Y(\hat{s})$, when approached from either side. The hadron energy spectrum for the parton model is also shown in Fig. 3.14, which is finite for all ranges of E_0.

What is the region of validity of the hadron energy spectrum derived in HQET? It is known that in $B \to X_s \ell^+ \ell^-$ decay there are resonances present, from which the known six [39] populate the x_0 (or E_0) range between the lower end-point and the charm threshold. Taking this into account and what has been remarked earlier, one concludes that the HQET spectrum cannot be used near the resonances, near the charm threshold and around the lower endpoint. Excluding these regions, the spectrum calculated in HQET is close to the partonic perturbative spectrum as the power corrections are shown to be small. The authors of [27], who have performed an $1/m_c$ expansion for the dilepton mass spectrum $\frac{d\mathcal{B}(B \to X_s \ell^+ \ell^-)}{dq^2}$ and who also found a charm-threshold singularity, expect a reliable prediction of the spectrum for $q^2 \leq 3m_c^2$ corresponding to $E_0 \geq \frac{m_b}{2}(1 + \hat{m}_s^2 - 3\hat{m}_c^2) \approx 1.8$ GeV. In this region, the effect of the $1/m_b$ power corrections on the energy spectrum is small and various spectra in $B \to X_s \ell^+ \ell^-$ calculated here and in [18] can be compared with data.

The leading power corrections to the invariant mass spectrum is found by integrating eq. (3.91) with respect to x_0. We have already discussed the non-trivial hadronic invariant mass spectrum which results from the $\mathcal{O}(\alpha_s)$ bremsstrahlung and its Sudakov-improved version. Since we have consistently dropped everywhere terms of $\mathcal{O}(\lambda_i \alpha_s)$ (see eq. (3.91)), this is the only contribution to the invariant mass spectrum

also in HQET away from $\hat{s}_0 = \hat{m}_s^2$, as the result of integrating the terms involving power corrections in eq. (3.91) over x_0 is a singular function with support only at $\hat{s}_0 = \hat{m}_s^2$. Of course, these corrections contribute to the normalization (i.e., branching ratio) but leave the perturbative spectrum intact for $\hat{s}_0 \neq \hat{m}_s^2$.

3.8 Hadronic Moments in $B \to X_s \ell^+ \ell^-$ in HQET

We start with the derivation of the lowest spectral moments in the decay $B \to X_s \ell^+ \ell^-$ at the parton level. These moments are worked out by taking into account the leading power $1/m_b$ and the perturbative $\mathcal{O}(\alpha_s)$ corrections. To that end, we define:

$$\mathcal{M}_{\ell^+\ell^-}^{(n,m)} \equiv \frac{1}{B_0} \int (\hat{s}_0 - \hat{m}_s^2)^n x_0^m \frac{\mathrm{d}^2 B}{\mathrm{d}\hat{s}_0 \mathrm{d}x_0} \, \mathrm{d}\hat{s}_0 \mathrm{d}x_0 , \tag{3.96}$$

for integers n and m. These moments are related to the corresponding moments $\langle x_0^m (\hat{s}_0 - \hat{m}_s^2)^n \rangle$ obtained at the parton level by a scaling factor which yields the corrected branching ratio $B = B_0 \mathcal{M}_{\ell^+\ell^-}^{(n,m)}$. Thus,

$$\langle x_0^m (\hat{s}_0 - \hat{m}_s^2)^n \rangle = \frac{B_0}{B} \mathcal{M}_{\ell^+\ell^-}^{(n,m)} . \tag{3.97}$$

The correction factor B_0/B is given below in eq. (3.103). We remind that one has to Taylor expand it in terms of the $\mathcal{O}(\alpha_s)$ and power corrections. The moments can be expressed as double expansion in $\mathcal{O}(\alpha_s)$ and $1/m_b$ and to the accuracy of our calculations can be represented in the following form:

$$\mathcal{M}_{\ell^+\ell^-}^{(n,m)} = D_0^{(n,m)} + \frac{\alpha_s}{\pi} C_9^2 A^{(n,m)} + \hat{\lambda}_1 D_1^{(n,m)} + \hat{\lambda}_2 D_2^{(n,m)} , \tag{3.98}$$

with a further decomposition into pieces from different Wilson coefficients for $i = 0, 1, 2$:

$$D_i^{(n,m)} = \alpha_i^{(n,m)} C_7^{\mathrm{eff}^2} + \beta_i^{(n,m)} C_{10}^2 + \gamma_i^{(n,m)} C_7^{\mathrm{eff}} + \delta_i^{(n,m)} . \tag{3.99}$$

The terms $\gamma_i^{(n,m)}$ and $\delta_i^{(n,m)}$ in eq. (3.99) result from the terms proportional to $Re(C_9^{\mathrm{eff}})C_7^{\mathrm{eff}}$ and $|C_9^{\mathrm{eff}}|^2$ in eq. (3.91), respectively. The results for $\alpha_i^{(n,m)}, \beta_i^{(n,m)}, \gamma_i^{(n,m)}, \delta_i^{(n,m)}$ are presented in appendix C.3. Out of these, the functions $\alpha_i^{(n,m)}$ and $\beta_i^{(n,m)}$ are given analytically, but the other two $\gamma_i^{(n,m)}$ and $\delta_i^{(n,m)}$ are given in terms of a one-dimensional integral over x_0, as these latter functions involve the coefficient C_9^{eff}, which is a complicated function of x_0.

The leading perturbative contributions for the hadronic invariant mass and hadron energy moments can be obtained analytically by integrating eq. (3.82) and eq. (3.81), respectively, yielding

$$A^{(0,0)} = \frac{25 - 4\pi^2}{9} , \quad A^{(1,0)} = \frac{91}{675} , \quad A^{(2,0)} = \frac{5}{486} ,$$

$$A^{(0,1)} = \frac{1381 - 210\pi^2}{1350} , \quad A^{(0,2)} = \frac{2257 - 320\pi^2}{5400} . \tag{3.100}$$

The zeroth moment $n = m = 0$ is needed for the normalization and we recall that the result for $A^{(0,0)}$ was derived some time ago [92]. Likewise, the first mixed moment $A^{(1,1)}$ can be extracted from the results given in [93] for the decay $B \to X \ell \nu_\ell$ after changing the normalization,

$$A^{(1,1)} = \frac{3}{50} . \tag{3.101}$$

For the lowest order parton model contribution $D_0^{(n,m)}$, we find, in agreement with [93], that the first two hadronic invariant mass moments $\langle \hat{s}_0 - \hat{m}_s^2 \rangle$, $\langle (\hat{s}_0 - \hat{m}_s^2)^2 \rangle$ and the first mixed moment $\langle x_0(\hat{s}_0 - \hat{m}_s^2) \rangle$ vanish:

$$D_0^{(n,0)} = 0 \text{ for } n = 1, 2 \text{ and } D_0^{(1,1)} = 0 . \tag{3.102}$$

We remark that we have included the s-quark mass dependence in the leading term and in the power corrections, but omitted it throughout our work in the calculation of the explicit α_s term. All the expressions derived here for the moments agree in the $V - A$ limit (and with $\hat{m}_s = 0$ in the perturbative α_s correction term) with the corresponding expressions given in ref. [93]. From here the full $\mathcal{O}(\alpha_s m_s)$ expressions can be inferred after adjusting the normalization $\Gamma_0 \rightarrow \mathcal{B}_0 \frac{2}{3} C_9^2$. We have checked that a finite s-quark mass effects the values of the $A^{(n,m)}$ given in eqs. (3.100-3.101) by less than 8% for $m_s = 0.2$ GeV.

We can eliminate the hidden dependence on the non-perturbative parameters resulting from the b-quark mass in the moments $\mathcal{M}_{\ell^+\ell^-}^{(n,m)}$ with the help of the HQET mass relation. As m_s is of order Λ_{QCD}, to be consistent we keep only terms up to order m_s^2/m_b^2 [66]. An additional m_b-dependence is in the mass ratios $\hat{m}_l = \frac{m_l}{m_b}$. Substituting m_b by the B-meson mass using the HQET relation introduces additional $\mathcal{O}(1/m_B, 1/m_B^2)$ terms in the Taylor expansion of eq. (3.97). We get for the following normalization factor for $\mathcal{B}/\mathcal{B}_0 = \mathcal{M}_{\ell^+\ell^-}^{(0,0)}$:

$$
\begin{aligned}
\frac{\mathcal{B}}{\mathcal{B}_0} &= \frac{32}{9m_B^2}(-4m_B^2 - 13m_s^2 - 3(m_B^2 - 2m_s^2)\ln(4\frac{m_l^2}{m_B^2}))C_7^{\text{eff}^2} + \frac{2}{3m_B^2}(m_B^2 - 8m_s^2)C_{10}^2 \\
&+ \int_{m_s/m_B}^{\frac{1}{2}(1+m_s^2/m_B^2)} dx_0 \frac{64}{m_B^2}(-m_s^2 - 4m_s^2 x_0 + 2m_B^2 x_0^2 + 2m_s^2 x_0^2) Re(C_9^{\text{eff}}) C_7^{\text{eff}} \\
&+ \int_{m_s/m_B}^{\frac{1}{2}(1+m_s^2/m_B^2)} dx_0 \frac{16}{3m_B^2}(-3m_s^2 + 6m_B^2 x_0^2 + 6m_s^2 x_0^2 - 8m_B^2 x_0^3)|C_9^{\text{eff}}|^2 \\
&+ \frac{\alpha_s}{\pi} A^{(0,0)} C_9^2 + \frac{-64}{3} C_7^{\text{eff}^2} \frac{\bar{\Lambda}}{m_B} + \frac{-32}{3} C_7^{\text{eff}^2} \frac{\bar{\Lambda}^2}{m_B^2} + \Big[\frac{16}{9}(2 - 3\ln(4\frac{m_l^2}{m_B^2}))C_7^{\text{eff}^2} + \frac{C_{10}^2}{3} \\
&+ \int_0^{\frac{1}{2}} dx_0(64 x_0^2 Re(C_9^{\text{eff}})C_7^{\text{eff}} + \frac{16}{3}(3 - 4x_0)x_0^2|C_9^{\text{eff}}|^2) \Big] \frac{\lambda_1}{m_B^2} \\
&+ \Big[\frac{16}{3}(4 + 9\ln(4\frac{m_l^2}{m_B^2}))C_7^{\text{eff}^2} - 3C_{10}^2 \\
&+ \int_0^{\frac{1}{2}} dx_0(64(-1 - 4x_0 + 7x_0^2)Re(C_9^{\text{eff}})C_7^{\text{eff}} + 16(-1 + 15x_0^2 - 20x_0^3)|C_9^{\text{eff}}|^2) \Big] \frac{\lambda_2}{m_B^2} .
\end{aligned}
\tag{3.103}
$$

Here, the $\frac{\bar{\Lambda}}{m_B}$ and $\frac{\bar{\Lambda}^2}{m_B^2}$ terms proportional to $C_7^{\text{eff}^2}$ result from the expansion of $\hat{m}_l$

$$\ln\Big(\frac{4m_l^2}{m_b^2}\Big) = \ln\Big(\frac{4m_l^2}{m_B^2}\Big) + 2\frac{\bar{\Lambda}}{m_B} + \frac{\bar{\Lambda}^2}{m_B^2} - \frac{\lambda_1 + 3\lambda_2}{m_B^2} + \dots . \tag{3.104}$$

The first two moments and the first mixed moment, $\langle x_0 \rangle \mathcal{B}/\mathcal{B}_0$, $\langle x_0^2 \rangle \mathcal{B}/\mathcal{B}_0$, $\langle \hat{s}_0 - \hat{m}_s^2 \rangle \mathcal{B}/\mathcal{B}_0$, $\langle (\hat{s}_0 - \hat{m}_s^2)^2 \rangle \mathcal{B}/\mathcal{B}_0$ and $\langle x_0(\hat{s}_0 - \hat{m}_s^2) \rangle \mathcal{B}/\mathcal{B}_0$ are presented in appendix C.4.

With this we obtain the moments for the physical quantities valid up to $\mathcal{O}(\alpha_s/m_B^2, 1/m_B^3)$, where the second equation corresponds to a further use of $m_s = \mathcal{O}(\Lambda_{QCD})$. We get for the first two hadronic

invariant mass moments [5]

$$\langle S_H \rangle = m_s^2 + \bar{\Lambda}^2 + (m_B^2 - 2\bar{\Lambda} m_B)\langle \hat{s}_0 - \hat{m}_s^2 \rangle + (2\bar{\Lambda} m_B - 2\bar{\Lambda}^2 - \lambda_1 - 3\lambda_2)\langle x_0 \rangle \,,$$

$$\langle S_H^2 \rangle = m_s^4 + 2\bar{\Lambda}^2 m_s^2 + 2m_s^2(m_B^2 - 2\bar{\Lambda} m_B)\langle \hat{s}_0 - \hat{m}_s^2 \rangle + 2m_s^2(2\bar{\Lambda} m_B - 2\bar{\Lambda}^2 - \lambda_1 - 3\lambda_2)\langle x_0 \rangle$$

$$+ (m_B^4 - 4\bar{\Lambda} m_B^3)\langle (\hat{s}_0 - \hat{m}_s^2)^2 \rangle + 4\bar{\Lambda}^2 m_B^2 \langle x_0^2 \rangle + 4\bar{\Lambda} m_B^3 \langle x_0(\hat{s}_0 - \hat{m}_s^2) \rangle \,, \qquad (3.105)$$

$$= (m_B^4 - 4\bar{\Lambda} m_B^3)\langle (\hat{s}_0 - \hat{m}_s^2)^2 \rangle + 4\bar{\Lambda}^2 m_B^2 \langle x_0^2 \rangle + 4\bar{\Lambda} m_B^3 \langle x_0(\hat{s}_0 - \hat{m}_s^2) \rangle \,,$$

and for the hadron energy moments:

$$\langle E_H \rangle = \bar{\Lambda} - \frac{\lambda_1 + 3\lambda_2}{2m_B} + \left(m_B - \bar{\Lambda} + \frac{\lambda_1 + 3\lambda_2}{2m_B} \right)\langle x_0 \rangle \,,$$

$$\langle E_H^2 \rangle = \bar{\Lambda}^2 + (2\bar{\Lambda} m_B - 2\bar{\Lambda}^2 - \lambda_1 - 3\lambda_2)\langle x_0 \rangle \qquad (3.106)$$

$$+ (m_B^2 - 2\bar{\Lambda} m_B + \bar{\Lambda}^2 + \lambda_1 + 3\lambda_2)\langle x_0^2 \rangle \,.$$

3.8.1   Numerical estimates of the hadronic moments in HQET

Using the expressions for the HQET moments given in appendix C.4, we present the numerical results for the hadronic moments in $B \to X_s \ell^+ \ell^-$, valid up to $\mathcal{O}(\alpha_s/m_B^2, 1/m_B^3)$. We find:

$$\langle x_0 \rangle = 0.367 \left(1 + 0.148\frac{\alpha_s}{\pi} - 0.204\frac{\bar{\Lambda}}{m_B}\frac{\alpha_s}{\pi} - 0.030\frac{\bar{\Lambda}}{m_B} - 0.017\frac{\bar{\Lambda}^2}{m_B^2} + 0.884\frac{\lambda_1}{m_B^2} + 3.652\frac{\lambda_2}{m_B^2} \right),$$

$$\langle x_0^2 \rangle = 0.147 \left(1 + 0.324\frac{\alpha_s}{\pi} - 0.221\frac{\bar{\Lambda}}{m_B}\frac{\alpha_s}{\pi} - 0.058\frac{\bar{\Lambda}}{m_B} - 0.034\frac{\bar{\Lambda}^2}{m_B^2} + 1.206\frac{\lambda_1}{m_B^2} + 4.680\frac{\lambda_2}{m_B^2} \right),$$

$$\langle x_0(\hat{s}_0 - \hat{m}_s^2) \rangle = 0.041\frac{\alpha_s}{\pi}\left(1 + 0.083\frac{\bar{\Lambda}}{m_B} \right) + 0.124\frac{\lambda_1}{m_B^2} + 0.172\frac{\lambda_2}{m_B^2} \,,$$

$$\langle \hat{s}_0 - \hat{m}_s^2 \rangle = 0.093\frac{\alpha_s}{\pi}\left(1 + 0.083\frac{\bar{\Lambda}}{m_B} \right) + 0.641\frac{\lambda_1}{m_B^2} + 0.589\frac{\lambda_2}{m_B^2} \,,$$

$$\langle (\hat{s}_0 - \hat{m}_s^2)^2 \rangle = 0.0071\frac{\alpha_s}{\pi}\left(1 + 0.083\frac{\bar{\Lambda}}{m_B} \right) - 0.196\frac{\lambda_1}{m_B^2} \,. \qquad (3.107)$$

As already discussed earlier, the normalizing factor $\mathcal{B}/\mathcal{B}_0$ is also expanded in a Taylor series. Thus, in deriving the above results, we have used

$$\frac{\mathcal{B}}{\mathcal{B}_0} = 25.277 \left(1 - 1.108\frac{\alpha_s}{\pi} - 0.083\frac{\bar{\Lambda}}{m_B} - 0.041\frac{\bar{\Lambda}^2}{m_B^2} + 0.546\frac{\lambda_1}{m_B^2} - 3.439\frac{\lambda_2}{m_B^2} \right).$$

The parameters used in arriving at the numerical coefficients are given in Table A.1 and Table 3.1.

Inserting the expressions for the moments calculated at the partonic level into eq. (3.105) and eq. (3.106), we find the following expressions for the short-distance hadronic moments, valid up to $\mathcal{O}(\alpha_s/m_B^2, 1/m_B^3)$:

$$\langle S_H \rangle = m_B^2\left(\frac{m_s^2}{m_B^2} + 0.093\frac{\alpha_s}{\pi} - 0.069\frac{\bar{\Lambda}}{m_B}\frac{\alpha_s}{\pi} + 0.735\frac{\bar{\Lambda}}{m_B} + 0.243\frac{\bar{\Lambda}^2}{m_B^2} + 0.273\frac{\lambda_1}{m_B^2} - 0.513\frac{\lambda_2}{m_B^2} \right),$$

---

[5]Our first expression for $\langle S_H^2 \rangle$, eq. (3.105), does not agree in the coefficient of $\langle \hat{s}_0 - \hat{m}_s^2 \rangle$ with the one given in ref. [93] (their eq. (4.1)). We point out that m_B^2 should have been replaced by m_b^2 in this expression. This has been confirmed by Adam Falk (private communication). Dropping the higher order terms given in their expressions, the hadronic moments in HQET derived here and in [93] agree.

$$\langle S_H^2 \rangle = m_B^4 (0.0071 \frac{\alpha_s}{\pi} + 0.138 \frac{\bar{\Lambda}}{m_B} \frac{\alpha_s}{\pi} + 0.587 \frac{\bar{\Lambda}^2}{m_B^2} - 0.196 \frac{\lambda_1}{m_B^2}) , \qquad (3.108)$$

$$\langle E_H \rangle = 0.367 m_B (1 + 0.148 \frac{\alpha_s}{\pi} - 0.352 \frac{\bar{\Lambda}}{m_B} \frac{\alpha_s}{\pi} + 1.691 \frac{\bar{\Lambda}}{m_B} + 0.012 \frac{\bar{\Lambda}^2}{m_B^2} + 0.024 \frac{\lambda_1}{m_B^2} + 1.070 \frac{\lambda_2}{m_B^2}) ,$$

$$\langle E_H^2 \rangle = 0.147 m_B^2 (1 + 0.324 \frac{\alpha_s}{\pi} - 0.128 \frac{\bar{\Lambda}}{m_B} \frac{\alpha_s}{\pi} + 2.954 \frac{\bar{\Lambda}}{m_B} + 2.740 \frac{\bar{\Lambda}^2}{m_B^2} - 0.299 \frac{\lambda_1}{m_B^2} + 0.162 \frac{\lambda_2}{m_B^2}) .$$

One sees that there are linear power corrections, $\mathcal{O}(\bar{\Lambda}/m_B)$, present in all these hadronic quantities except $\langle S_H^2 \rangle$ which starts in $\frac{\alpha_s}{\pi} \frac{\bar{\Lambda}}{m_B}$.

Setting $m_s = 0$ changes the numerical value of the coefficients in the expansion given above (in which we already neglected $\alpha_s m_s$) by at most 1%. With the help of the expressions given above, we have calculated numerically the hadronic moments in HQET for the decay $B \to X_s \ell^+ \ell^-$, $\ell = \mu, e$ and have estimated the errors by varying the parameters within their $\pm 1\sigma$ ranges given in Table A.1. They are presented in Table 3.2 where we have used $\bar{\Lambda} = 0.39\,\text{GeV}$, $\lambda_1 = -0.2\,\text{GeV}^2$ and $\lambda_2 = 0.12\,\text{GeV}^2$. Further, using $\alpha_s(m_b) = 0.21$, the explicit dependence of the hadronic moments given in eq. (3.108) on the HQET parameters λ_1 and $\bar{\Lambda}$ can be worked out [25]

$$\langle S_H \rangle = 0.0055 m_B^2 (1 + 132.61 \frac{\bar{\Lambda}}{m_B} + 44.14 \frac{\bar{\Lambda}^2}{m_B^2} + 49.66 \frac{\lambda_1}{m_B^2}) ,$$

$$\langle S_H^2 \rangle = 0.00048 m_B^4 (1 + 19.41 \frac{\bar{\Lambda}}{m_B} + 1223.41 \frac{\bar{\Lambda}^2}{m_B^2} - 408.39 \frac{\lambda_1}{m_B^2}) , \qquad (3.109)$$

$$\langle E_H \rangle = 0.372 m_B (1 + 1.64 \frac{\bar{\Lambda}}{m_B} + 0.01 \frac{\bar{\Lambda}^2}{m_B^2} + 0.02 \frac{\lambda_1}{m_B^2}) ,$$

$$\langle E_H^2 \rangle = 0.150 m_B^2 (1 + 2.88 \frac{\bar{\Lambda}}{m_B} + 2.68 \frac{\bar{\Lambda}^2}{m_B^2} - 0.29 \frac{\lambda_1}{m_B^2}) .$$

While interpreting these numbers, one should bear in mind that there are two comparable expansion parameters $\bar{\Lambda}/m_B$ and α_s/π and we have fixed the latter in showing the numbers. As expected, the dependence of the energy moments $\langle E_H^n \rangle$ on $\bar{\Lambda}$ and λ_1 is very weak. The correlations on the HQET parameters λ_1 and $\bar{\Lambda}$ which follow from (assumed) fixed values of the hadronic invariant mass moments $\langle S_H \rangle$ and $\langle S_H^2 \rangle$ are shown in Fig. 3.15. We have taken the values for the decay $B \to X_s \mu^+ \mu^-$ from Table 3.2 for the sake of illustration and have also shown the presently irreducible theoretical errors on these moments following from the input parameters m_t, α_s and the scale μ, given in Table A.1. The errors were calculated by varying these parameters in the indicated range, one at a time, and adding the individual errors in quadrature. Further the correlation following from the analysis of data on semileptonic $B \to X \ell \nu_\ell$ decays [31] is shown in Fig. 3.15 (ellipse). As can be seen, it gives a complementary constraint to the one from $B \to X_s \ell^+ \ell^-$ decay [25], which allows in principle a precise determination of $\bar{\Lambda}$, λ_1 from data on the latter.

The theoretical stability of the moments has to be checked against higher order corrections and the error estimates presented here will have to be improved. The "BLM-enhanced" two-loop corrections [105] proportional to $\alpha_s^2 \beta_0$, where $\beta_0 = 11 - 2n_f/3$ is the first coefficient in the QCD beta function, can be included at the parton level as has been done in other decays [93,68], but not being crucial to our point we have not done this. More importantly, higher order corrections in α_s and $1/m_b^3$ are not included here. While we do not think that the higher orders in α_s will have a significant influence, the second

moment $\langle S_H^2 \rangle$ is susceptible to the presence of $1/m_b^3$ corrections as shown for the decay $B \to X \ell \nu_\ell$ [106]. This will considerably enlarge the theoretical error represented by the dashed band for $\langle S_H^2 \rangle$ in Fig. 3.15. Fortunately, the coefficient of the $\bar{\Lambda}/m_B$ term in $\langle S_H \rangle$ is large. Hence, a measurement of this moment alone constrains $\bar{\Lambda}$ effectively. Of course, the utility of the hadronic moments calculated above is only in conjunction with the experimental cuts. Since the optimal experimental cuts in $B \to X_s \ell^+ \ell^-$ remain to be defined, we hope to return to this and related issue of doing an improved theoretical error estimate in a future publication. We remark here that care has to be taken in a general HQE calculation with cuts. For an extraction of meaningful observables the calculation must be smeared by integration. If the remaining phase space gets too restricted the OPE, which is based on parton-hadron duality, breaks down. This happens for example near the high-q^2 end-point of the invariant dilepton mass spectrum in $B \to X_s \ell^+ \ell^-$ decay [18].

Related issues in other decays have been studied in literature. The classification of the operators contributing in $\mathcal{O}(1/m_b^3)$, estimates of their matrix elements, and effects on the decay rates and spectra in the decays $B \to X \ell \nu_\ell$ and $B \to (D, D^*) \ell \nu_\ell$ have been studied in [107,108,109]. Spectral moments of the photon energy in the decay $B \to X_s \gamma$ have been studied in [110]. For studies of $\mathcal{O}(1/m_b^3)$ contributions in this decay and the effects of the experimental cut (on the photon energy) on the photon energy moments, see [65]. An HQE analysis of the first two hadronic invariant mass moments with a lepton energy cut has been worked out in ref. [106].
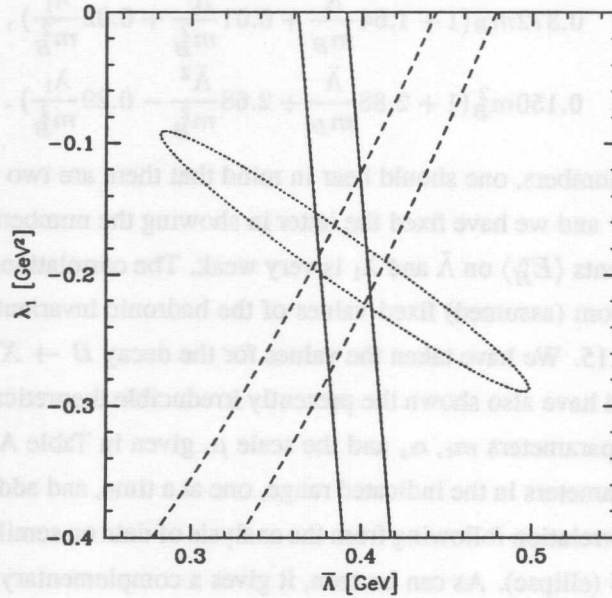

Figure 3.15: $\langle S_H \rangle$ (solid bands) and $\langle S_H^2 \rangle$ (dashed bands) correlation in $(\lambda_1 \text{-} \bar{\Lambda})$ space for fixed values $\langle S_H \rangle = 1.64 \ GeV^2$ and $\langle S_H^2 \rangle = 4.48 \ GeV^4$, corresponding to the central values in Table 3.2. The curves are forced to meet at the point $\lambda_1 = -0.2 \ GeV^2$ and $\bar{\Lambda} = 0.39 \ GeV$. The correlation from $B \to X \ell \nu_\ell$ [31] is also shown here (ellipse).

Finally, concerning the power corrections related to the $c\bar{c}$ loop in $B \to X_s \ell^+ \ell^-$, it has been suggested

HQET	$\langle S_H \rangle$	$\langle S_H^2 \rangle$	$\langle E_H \rangle$	$\langle E_H^2 \rangle$
	(GeV^2)	(GeV^4)	(GeV)	(GeV^2)
$\mu^+\mu^-$	1.64 ± 0.06	4.48 ± 0.29	2.21 ± 0.04	5.14 ± 0.16
e^+e^-	1.79 ± 0.07	4.98 ± 0.29	2.41 ± 0.06	6.09 ± 0.29

Table 3.2: *Hadronic spectral moments for $B \to X_s \mu^+\mu^-$ and $B \to X_s e^+e^-$ in HQET with $\bar{\Lambda} = 0.39\,GeV$, $\lambda_1 = -0.2\,GeV^2$, and $\lambda_2 = 0.12\,GeV^2$. The quoted errors result from varying μ, α_s and the top mass within the ranges given in Table A.1.*

in [27] that an $\mathcal{O}(\Lambda_{QCD}^2/m_c^2)$ expansion in the context of HQET can be carried out to take into account such effects in the invariant mass spectrum away from the resonances. Using the expressions (obtained with $m_s = 0$) for the $1/m_c^2$ amplitude, we have calculated the partonic energy moments $\triangle \langle x_0^n \rangle$, which correct the short-distance result at order λ_2/m_c^2:

$$\triangle \langle x_0^n \rangle \frac{\mathcal{B}}{\mathcal{B}_0} = -\frac{256 C_2 \lambda_2}{27 m_c^2} \int_0^{1/2(1-4\hat{m}_l^2)} dx_0 x_0^{n+2} \text{Re} \left[F(r) \left(C_9^{\text{eff}}(3 - 2x_0) + 2C_7^{\text{eff}} \frac{-3 + 4x_0 + 2x_0^2}{2x_0 - 1} \right) \right],$$
$$r = \frac{1 - 2x_0}{4\hat{m}_c^2}, \tag{3.110}$$

$$F(r) = \frac{3}{2r} \begin{cases} \dfrac{1}{\sqrt{r(1-r)}} \arctan \sqrt{\dfrac{r}{1-r}} - 1 & 0 < r < 1, \\[3mm] \dfrac{1}{2\sqrt{r(r-1)}} \left(\ln \dfrac{1 - \sqrt{1 - 1/r}}{1 + \sqrt{1 - 1/r}} + i\pi \right) - 1 & r > 1. \end{cases} \tag{3.111}$$

The invariant mass and mixed moments give zero contribution in the order we are working, with $m_s = 0$. Thus, the correction to the hadronic mass moments are vanishing, if we further neglect terms proportional to $\frac{\lambda_2}{m_c^2}\bar{\Lambda}$ and $\frac{\lambda_2}{m_c^2}\lambda_i$, with $i = 1, 2$. For the hadron energy moments we obtain numerically

$$\triangle \langle E_H \rangle_{1/m_c^2} = m_B \triangle \langle x_0 \rangle = -0.007\,\text{GeV},$$
$$\triangle \langle E_H^2 \rangle_{1/m_c^2} = m_B^2 \triangle \langle x_0^2 \rangle = -0.013\,\text{GeV}^2, \tag{3.112}$$

leading to a correction of order -0.3% to the short-distance values presented in Table 3.4.

3.9 Hadron Spectra in the Fermi Motion Model

In this section, we study the non-perturbative effects associated with the bound state nature of the B-hadron on the hadronic invariant mass and hadron energy distributions in the decay $B \to X_s \ell^+ \ell^-$. These effects are studied in the Fermi motion model (FM) [22] introduced in section 2.4.2. In the context of rare B decays, this model has been employed to calculate the energy spectra in the decay $B \to X_s + \gamma$ in [6,24], which was used subsequently by the CLEO collaboration in their successful search of this decay [11]. It has also been used in calculating the dilepton invariant mass spectrum and FB asymmetry in $B \to X_s \ell^+ \ell^-$ [18], see section 3.3.

Comparison with HQET

The FM has received a lot of phenomenological attention in B decays, partly boosted by studies in the context of HQET showing that this model can be made to mimic the effects associated with the HQET parameters $\bar{\Lambda}$ and λ_1 [111,16]. We can further quantify this correspondence. The HQET parameters are calculable in terms of the FM parameters p_F and m_q with

$$\bar{\Lambda} = \int_0^\infty dp\, p^2 \phi(p) \sqrt{m_q^2 + p^2},$$

$$\lambda_1 = -\int_0^\infty dp\, p^4 \phi(p) = -\frac{3}{2} p_F^2. \tag{3.113}$$

In addition, for $m_q = 0$, one can show that $\bar{\Lambda} = 2p_F/\sqrt{\pi}$. There is, however, no parameter in the FM model analogous to λ_2 in HQET. Curiously, much of the HQET *malaise* in describing the spectra in the end-point regions is related to λ_2, as also shown in [16,18].

The relation between m_B, m_b, $\bar{\Lambda}$, λ_1 and λ_2 in HQET has already been stated (eq. (2.41)). With the quantity m_b^{eff} defined in eq. (2.47) and the relations in eqs. (3.113) for λ_1 and $\bar{\Lambda}$, the relation

$$m_B = m_b^{\text{eff}} + \bar{\Lambda} - \lambda_1/(2m_b^{\text{eff}}), \tag{3.114}$$

is found to be satisfied in the FM model to a high accuracy (better than 0.7%), which is shown in Table 3.3 for some representative values of the HQET parameters and their FM model equivalents. We shall use the HQET parameters $\bar{\Lambda}$ and λ_1 to characterize also the FM model parameters, with the relations given in eqs. (3.113) and (2.47) and in Table 3.3.

p_F, m_q (MeV,MeV)	m_b^{eff} (GeV)	λ_1 (GeV^2)	$\bar{\Lambda}$ (GeV)
$(450, 0)$	4.76	-0.304	0.507
$(252, 300)$	4.85	-0.095	0.422
$(310, 0)$	4.92	-0.144	0.350
$(450, 150)$	4.73	-0.304	0.534
$(500, 150)$	4.68	-0.375	0.588
$(570, 150)$	4.60	-0.487	0.664

Table 3.3: *Values of non perturbative parameters m_b^{eff}, λ_1 and $\bar{\Lambda}$ for different sets of the FM model parameters (p_F, m_q) taken from various fits of the data on $B \to X_s + (J/\psi, \gamma)$ decays discussed in [14].*

Calculation of the hadron spectra

We turn to discuss the hadron energy spectrum in the decay $B \to X_s \ell^+ \ell^-$ in the FM model including the $\mathcal{O}(\alpha_s)$ QCD corrections. The spectrum $\frac{dB}{dE_H}(B \to X_s \ell^+ \ell^-)$ is composed of a Sudakov improved piece from C_9^2 and the remaining lowest order contribution. The latter is based on the parton model distribution, which is well known and given below for the sake of completeness:

$$\frac{dB}{ds} = B_0 \frac{\hat{u}}{m_b^6} \left\{ \frac{4}{3}(m_b^4 - 2m_s^2 m_b^2 + m_s^4 + m_b^2 s + m_s^2 s - 2s^2) \left(|C_9^{\text{eff}}(s)|^2 + |C_{10}|^2 \right) \right.$$

$$+ \frac{16}{3}(2m_b^6 - 2m_b^4 m_s^2 - 2m_b^2 m_s^4 + 2m_s^6 - m_b^4 s - 14m_b^2 m_s^2 s - m_s^4 s - m_b^2 s^2 - m_s^2 s^2)\frac{|C_7^{\text{eff}}|^2}{s}$$

$$+ \; 16(m_b^4 - 2m_s^2 m_b^2 + m_s^4 - m_b^2 s - m_s^2 s)Re(C_9^{\text{eff}}(s))\,C_7^{\text{eff}} \Big\} \,, \tag{3.115}$$

$$\mathcal{B}_0 = \frac{B_{sl}}{\Gamma_{sl}}\frac{G_F^2|V_{ts}^* V_{tb}|^2}{192\pi^3}\frac{3\alpha^2}{16\pi^2}m_b^5 \,,$$

$$\Gamma_{sl} = \frac{G_F^2 V_{cb}^2 m_b^5}{192\pi^3}f(\hat{m}_c)\kappa(\hat{m}_c) \,, \tag{3.116}$$

where $\hat{u}$ is given in eq. (3.8). Note that in the lowest order expression just given, we have $|C_9^{\text{eff}}(s)|^2 = |Y(s)|^2 + 2C_9 Re(Y(s))$ with the rest of $C_9^{\text{eff}}(s)$ now included in the Sudakov-improved piece as can be seen in eq. (3.84). To be consistent, the total semileptonic width Γ_{sl}, which enters via the normalization constant $\mathcal{B}_0$, has also to be calculated in the FM model with the same set of the model parameters. We implement the correction in the decay width by replacing the b-quark mass in Γ_{sl} given in eq. (3.116) by m_b^{eff} [18]. The hadronic invariant mass spectrum in the decay $B \rightarrow X_s \ell^+ \ell^-$ in this model is calculated very much along the same lines. The kinematically allowed ranges for the distributions are $m_X \leq E_H \leq m_B$ and $m_X^2 \leq S_H \leq m_B^2$, and we recall here that the physical threshold has been implemented by demanding that the lowest hadronic invariant mass produced in the decay $B \rightarrow X_s \ell^+ \ell^-$ satisfies $m_X = max(m_K, m_q + m_s)$. The results for the hadron energy and the hadronic invariant mass spectra are presented in Figs. 3.16 and 3.18, respectively. We do not show the S_H distribution in the entire range, as it tends monotonically to zero for larger values of S_H.
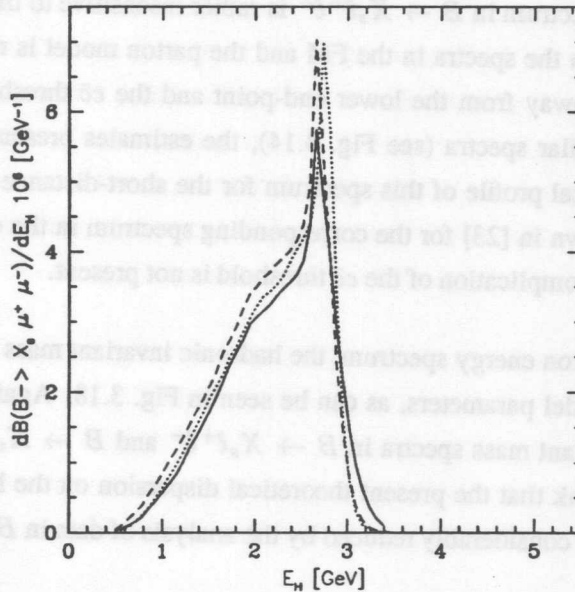

Figure 3.16: *Hadron energy spectrum in* $B \rightarrow X_s \ell^+ \ell^-$ *in the Fermi motion model based on the perturbative contribution only. The solid, dotted, dashed curve corresponds to the parameters* $(\lambda_1, \bar{\Lambda}) = (-0.3, 0.5), (-0.1, 0.4), (-0.15, 0.35)$ *in* (GeV^2, GeV), *respectively.*

A number of remarks is in order:

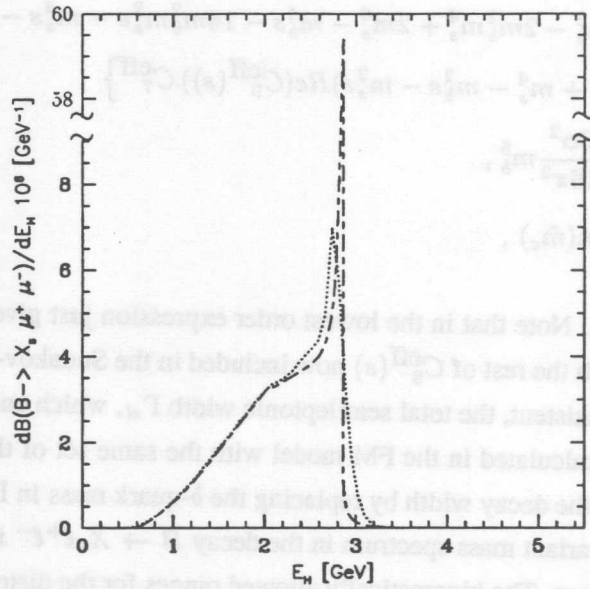**Figure 3.17:** *Hadron energy spectrum in $B \to X_s \ell^+ \ell^-$ based on the perturbative contribution only, in the Fermi motion model (dotted curve) for $(p_F, m_q) = (252, 300)$ (MeV, MeV), yielding $m_b^{eff} = 4.85$ GeV, and in the parton model (long-short dashed curve) for $m_b = 4.85$ GeV.*

- The hadron energy spectrum in $B \to X_s \ell^+ \ell^-$ is rather insensitive to the model parameters. Also, the difference between the spectra in the FM and the parton model is rather small as can be seen in Fig. 3.17. Since, away from the lower end-point and the $c\bar{c}$ threshold, the parton model and HQET have very similar spectra (see Fig. 3.14), the estimates presented in Fig. 3.16 provide a good phenomenological profile of this spectrum for the short-distance contribution. Very similar conclusions were drawn in [23] for the corresponding spectrum in the decay $B \to X_u \ell \nu_\ell$, where, of course, the added complication of the $c\bar{c}$ threshold is not present.

- In contrast to the hadron energy spectrum, the hadronic invariant mass spectrum in $B \to X_s \ell^+ \ell^-$ is sensitive to the model parameters, as can be seen in Fig. 3.18. Again, one sees a close parallel in the hadronic invariant mass spectra in $B \to X_s \ell^+ \ell^-$ and $B \to X_u \ell \nu_\ell$, with the latter worked out in [101]. We think that the present theoretical dispersion on the hadron spectra in the decay $B \to X_s \ell^+ \ell^-$ can be considerably reduced by the analysis of data in $B \to X_u \ell \nu_\ell$.

- The hadronic invariant mass distribution obtained by the $O(\alpha_s)$-corrected partonic spectrum and the HQET mass relation can only be calculated over a limited range of S_H, $S_H > m_B \bar{\Lambda}$, as shown in Fig. 3.12. The larger is the value of $\bar{\Lambda}$, the smaller is this region. Also, in the range where it can be calculated, it depends on the non-perturbative parameter m_b (or $\bar{\Lambda}$). A comparison of this distribution and the one in the FM model may be made for the same values of m_b and m_b^{eff}. This is shown for $m_b = 4.85$ GeV in Fig. 3.18 for HQET (long-short dashed curve) to be compared with the dotted curve in the FM model, which corresponds to $m_b^{\text{eff}} = 4.85$ GeV. We see that the two
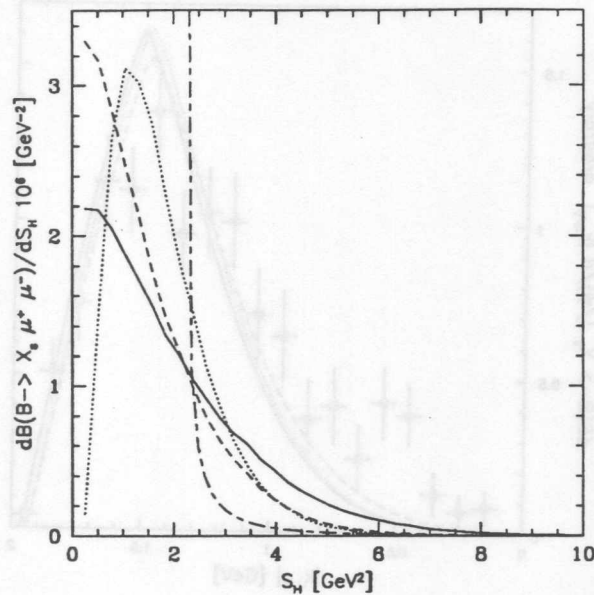
Figure 3.18: *Hadronic invariant mass spectrum in the Fermi motion model and parton model, based on the perturbative contribution only. The solid, dotted, dashed curve corresponds to the parameters* $(\lambda_1, \bar{\Lambda}) = (-0.3, 0.5), (-0.1, 0.4), (-0.15, 0.35)$ *in* (GeV^2, GeV), *respectively. The parton model (long-short dashed) curve is drawn for* $m_b = 4.85$ *GeV.*

distributions differ though they are qualitatively similar for larger values of $S_H > 3\,\text{GeV}^2$.

3.10   LD Contributions in $B \to X_s \ell^+ \ell^-$ (II)

This section is devoted to various aspects of the $c\bar{c}$ resonance effects. Following the procedure adopted in [18], we include the long-distance (LD) resonance effects in the decay $B \to X_s \ell^+ \ell^-$ and *simply add* the $c\bar{c}$ resonant contribution with the perturbative $c\bar{c}$ contribution expressed through the function $g(\hat{m}_c, \hat{s})$ in section 3.1.2 (see, eq. (3.18)). Thus, in our method,

$$C_9^{\text{eff}}(\hat{s}) = C_9 \eta(\hat{s}) + Y(\hat{s}) + Y_{res}(\hat{s}) \,. \tag{3.117}$$

The function $Y_{res}(\hat{s})$ accounts for the $c\bar{c}$ resonance contribution via $B \to X_s(J/\Psi, \Psi', \ldots) \to X_s \ell^+ \ell^-$ and can be seen in eq. (3.73). Note that in this approach, the effective coefficient $C_9^{\text{eff}}(\hat{s})$ has a $\hat{s}$-dependence, which is not entirely due to the propagators in the function $Y_{res}(\hat{s})$ as also the perturbative $c\bar{c}$ contribution $g(\hat{m}_c, \hat{s})$ is a function of $\hat{s}$. In the resonant region, the perturbative part is not noticeable due to the fact that the resonant part in $C_9^{\text{eff}}(\hat{s})$ completely dominates. However, when the $c\bar{c}$ pair is sufficiently off-shell, the $\hat{s}$-dependence of the function $C_9^{\text{eff}}(\hat{s})$ is not (and should not be) entirely determined by the $c\bar{c}$ resonant contribution. This is the motivation of the representation in eq. (3.117).

We start with an analysis of the constraints from existing data on the FM model parameters. Especially the question if the FM reproduces the measured J/ψ momentum distribution in $B \to X_s J/\psi$ will be
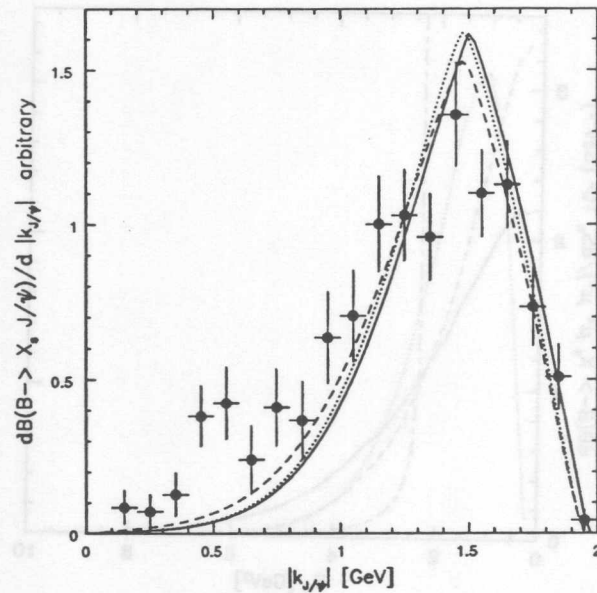
Figure 3.19: *Momentum distribution of J/ψ in the decay $B \to X_s J/\psi$ in the FM model. The solid, dotted, dashed curve corresponds to the parameters $(\lambda_1, \bar{\Lambda}) = (-0.3, 0.5), (-0.3, 0.53), (-0.38, 0.59)$ in (GeV^2, GeV), respectively. The data points are from the CLEO measurements [112].*

investigated. Then we turn to the effect of the Lorentz boost on the hadron spectra including LD effects according to eq. (3.117) and present E_H, S_H distributions for $B \to X_s \ell^+ \ell^-$ decay in the FM. Further, we study the uncertainties in the $B \to X_s \ell^+ \ell^-$ spectra resulting from the ambiguities in the parametrization of the LD effects. Differences in the distributions from different approaches to treat the $c\bar{c}$ resonances are shown as well for hadron spectra as for the q^2 spectra discussed before, namely, the dilepton invariant mass distribution and the FB asymmetry. Finally, the hadronic moments are calculated in the FM and compared with the ones in the HQE approach for identical values of equivalent parameters.

3.10.1   Constraints on the FM model parameters from existing data

The FM model parameters p_F and m_q (equivalently λ_1 and $\bar{\Lambda}$) can, in principle, be determined from an analysis of the energy spectra in the decays $B \to X_u \ell \nu_\ell$ and $B \to X_s + \gamma$, as all of them involve the decay of a b-quark into (an almost) massless (u or s) quark. Assuming that the parameters of the FM models are universal, these parameters can also be constrained from the lepton energy spectrum in the decay $B \to X_c \ell \nu_\ell$ and from the shape of the J/ψ- and ψ'- momentum distributions in the decays $B \to X_s(J/\psi, \psi')$. We review the presently available analyses of the photon- and lepton-energy spectra in B decays in the FM model (and HQET, as the two are very similar) and also present an analysis of the J/ψ-momentum spectrum in $B \to X_s J/\psi$.

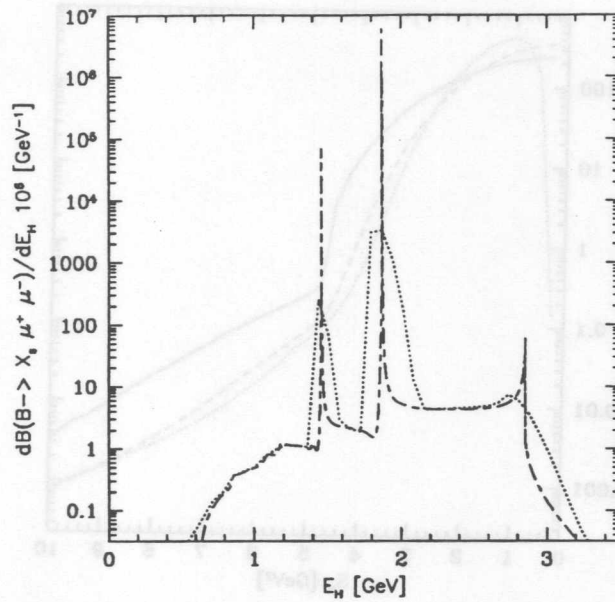• Analysis of the photon energy spectrum in $B \to X_s + \gamma$

Figure 3.20: *Hadron energy spectrum in $B \to X_s \ell^+ \ell^-$ including the resonance and perturbative contributions in the Fermi motion model (dotted curve) for $(\lambda_1, \bar{\Lambda}) = (-0.1 \, GeV^2, 0.4 \, GeV)$, and in the parton model (long-short dashed curve) for $m_b = 4.85 \, GeV$.*

The photon energy- and invariant hadronic mass distributions in $B \to X_s \gamma$ were calculated in the FM model using the leading order (in α_s) corrections in [24,6]. These spectra were used in the analysis of the CLEO data on $B \to X_s + \gamma$ [11], in which the values $p_F = 270 \pm 40$ MeV suggested by the analysis of the CLEO data on $B \to X \ell \nu_\ell$ were used, together with the effective b-quark mass $m_b^{\text{eff}} = 4.87 \pm 0.10$ GeV, which gave reasonable fits to the data. We translate these parameters in terms of λ_1 and $\bar{\Lambda}$ using the relations given in eqs. (3.113) and (3.114), yielding

$$\lambda_1 = -0.11^{-0.035}_{+0.030} \, \text{GeV}^2, \quad \bar{\Lambda} = 0.40 \pm 0.1 \, \text{GeV} . \tag{3.118}$$

The same data was fitted in [94] in the FM model, yielding $(p_F, m_q) = (0.45 \, \text{GeV}, 0 \, \text{GeV})$ as the best-fit solution, with $(p_F, m_q) = (0.310 \, \text{GeV}, 0.3 \, \text{GeV})$ differing from the best-fit solution by one unit in χ^2. The quality of the CLEO data [11] is not good enough to draw very quantitative conclusions. The best-fit values translate into

$$\lambda_1 = -0.3 \, \text{GeV}^2 , \quad \bar{\Lambda} = 0.5 \, \text{GeV} . \tag{3.119}$$

- Analysis of the lepton energy spectrum in $B \to X \ell \nu_\ell$

A fit of the lepton energy spectrum in the semileptonic decay $B \to X \ell \nu_\ell$ in the context of HQET has been performed in [31]. Using the CLEO data [113], the authors of [31] find:

$$\lambda_1 = -0.19 \pm 0.10 \, \text{GeV}^2 , \quad \bar{\Lambda} = 0.39 \pm 0.11 \, \text{GeV} . \tag{3.120}$$

Since the FM model and HQET yield very similar lepton energy spectra apart from the end-point, one can take the analysis of [31] also holding approximately for the FM model.
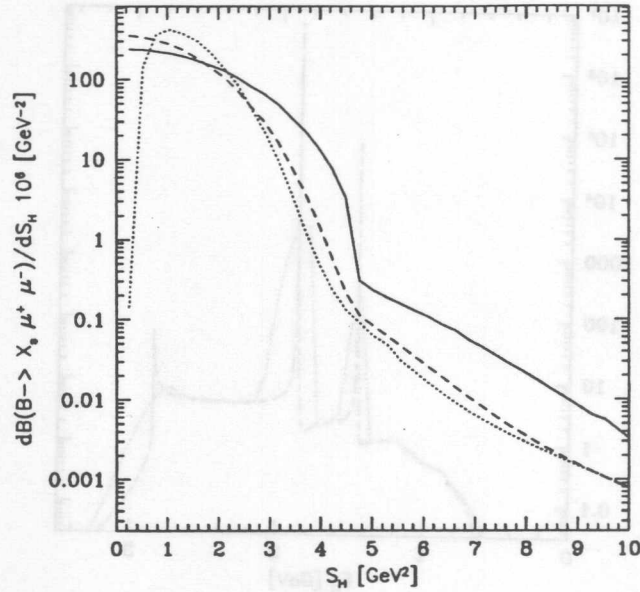
Figure 3.21: *Hadronic invariant mass spectrum in $B \to X_s \ell^+ \ell^-$ including the perturbative and res-onance contributions in the Fermi motion model. The solid, dotted, dashed curve corresponds to the parameters $(\lambda_1, \bar{\Lambda}) = (-0.3, 0.5), (-0.1, 0.4), (-0.15, 0.35)$ in (GeV^2, GeV), respectively.*

- Analysis of the J/ψ-momentum spectrum in $B \to X_s J/\psi$

An analysis of the J/ψ-momentum spectrum in $B \to X_s(J/\psi, \psi')$ measured by the CLEO collaboration [112] in the FM model has been reported in [114]. The authors of [114] addressed both the shape and normalization of the J/ψ-data, using the NRQCD formalism for the inclusive color singlet and color octet charmonium production in $B \to X_s J/\psi$ and the FM model. The preferred FM parameters from this analysis are: $(p_F, m_q) = (0.57 \text{ GeV}, 0.15 \text{ GeV})$, where m_q only plays a role in determining the position of the peak but otherwise does not influence the small momentum tail of the J/ψ momentum distribution. This yields values of the parameter p_F which are consistent with the ones obtained in [115] $p_F = 0.54^{+0.16}_{-0.15}$ GeV based on an analysis of the CLEO data on $B \to X \ell \nu_\ell$ [113]. The central values of p_F in [115] as well as in [114] correspond to $m_b^{\text{eff}} \simeq 4.6$ GeV, which is on the lower side of the present theoretical estimate of m_b pole mass, namely $m_b = 4.8 \pm 0.2$ GeV [64].

We have redone an analysis of the J/ψ-momentum distribution which is shown in Fig. 3.19. As shown in this figure, and also discussed in [114], the low-momentum J/ψ, in particular in the region $|k_{J/\psi}| \leq 0.6$ GeV, are problematic for inclusive decay models, including also the FM model. The $|k_{J/\psi}|$-spectrum appears to have a secondary bump; an inclusive spectrum behaving as a Gaussian tail or having a power-like behavior $\propto |k_{J/\psi}|^{-\delta}$ in this region is hard put to explain this data. There are also suggestions in literature [116] that the spectrum in this region is dominated by the three-body decay $B \to J/\psi \Lambda \bar{p}$ and hence the bump reflects the underlying dynamics of this exclusive decay. In view of this, we have taken out the first six points in the low-$|k_{J/\psi}|$ spectrum and fitted the FM model parameters in the rest of the $|k_{J/\psi}|$-spectrum. The three curves shown correspond to the FM model parameters $(p_F, m_q) =$
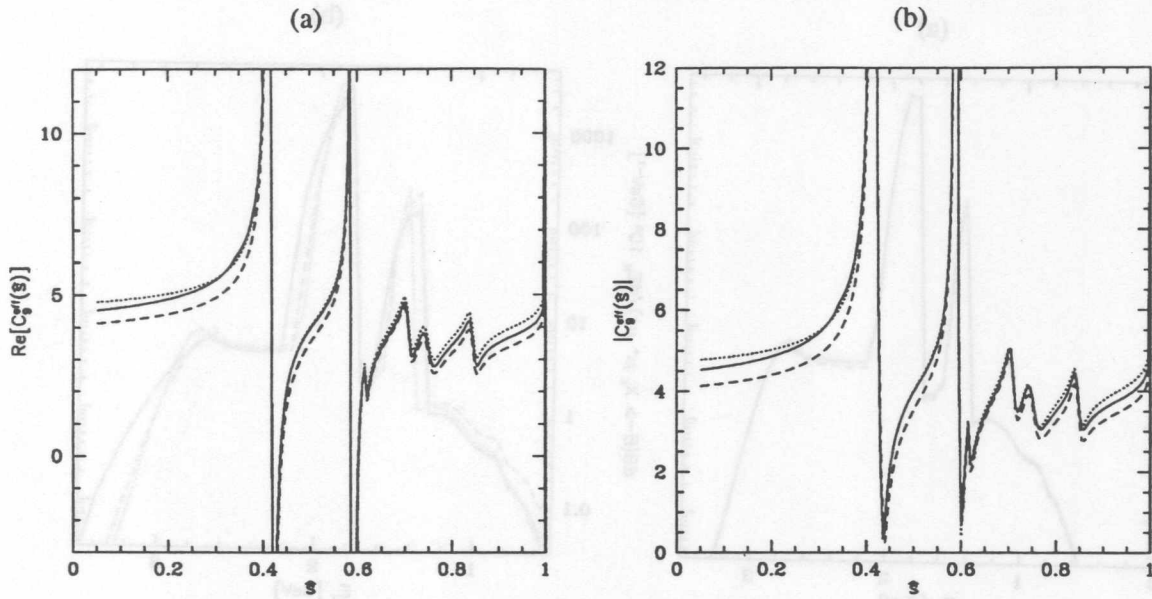
(a)   (b)

Figure 3.22: *The real part (a) and the absolute value (b) of $C_9^{\text{eff}}(\hat{s})$ are shown as a function of $\hat{s}$, where $C_9^{\text{eff}}(\hat{s}) = C_9 \eta(\hat{s}) + Y(\hat{s}) + Y_{res}(\hat{s})$. The solid line corresponds to $Y(\hat{s})$ calculated using the perturbative $c\bar{c}$ contribution $g(\hat{m}_c, \hat{s})$ given in eq. (3.18), and the dotted curve corresponds to using $\tilde{g}(\hat{m}_c, \hat{s})$ in eq. (3.121). The dashed one corresponds to the approach by [28].*

$(0.45 \text{ GeV}, 0 \text{ GeV})$ (solid curve), $(p_F, m_q) = (0.45 \text{ GeV}, 0.15 \text{ GeV})$ (dotted curve) and $(p_F, m_q) = (0.50 \text{ GeV}, 0.15 \text{ GeV})$ (dashed curve). They all have reasonable χ^2, with $\chi^2/dof = 1.6, 1.6$ and 1.1, respectively. Excluding also the seventh lowest point, the χ^2 improves marginally, with the resulting χ^2 being $\chi^2/dof = 1.4, 1.4$ and 0.94. Including the sixth point, the fits become slightly worse. However, they are all acceptable fits. It is interesting that the best-fit solution of the photon energy spectrum in $B \to X_s + \gamma$, $(p_F, m_q) = (0.45 \text{ GeV}, 0 \text{ GeV})$, is also an acceptable fit of the $|k_{J/\psi}|$-data. The corresponding λ_1, $\bar{\Lambda}$ and m_b values from these two analyses are compatible within $\pm 1\sigma$ with the HQET-based constraints from the semileptonic B decays [31], quoted above. Thus, the values in eq. (3.119) appear to be a reasonable guess of the FM model parameters. But, more importantly for the present study, the phenomenological profile of the LD contribution $B \to X_s(J/\psi, \psi', ...) \to X_s \ell^+ \ell^-$ presented here is certainly consistent with present data and theoretical constraints.

3.10.2 Effects of the Lorentz boost on the hadron spectra in $B \to X_s \ell^+ \ell^-$

We now discuss the B-meson wave function effects in the FM model on the hadron spectra in $B \to X_s \ell^+ \ell^-$. Since the resonances in $B \to X_s \ell^+ \ell^-$ are in the dilepton invariant mass variable s and not in S_H, and noting that neither E_0 (partonic energy) nor E_H are Lorentz-invariant quantities, it is expected on general grounds that the effect of the Lorentz boost in the FM model on E_H-and S_H-distributions will be more marked than what was found on the invariant dilepton mass spectrum in [18]. We recall that for the dilepton invariant mass, the Lorentz boost involved in the FM model leaves the spectrum invariant
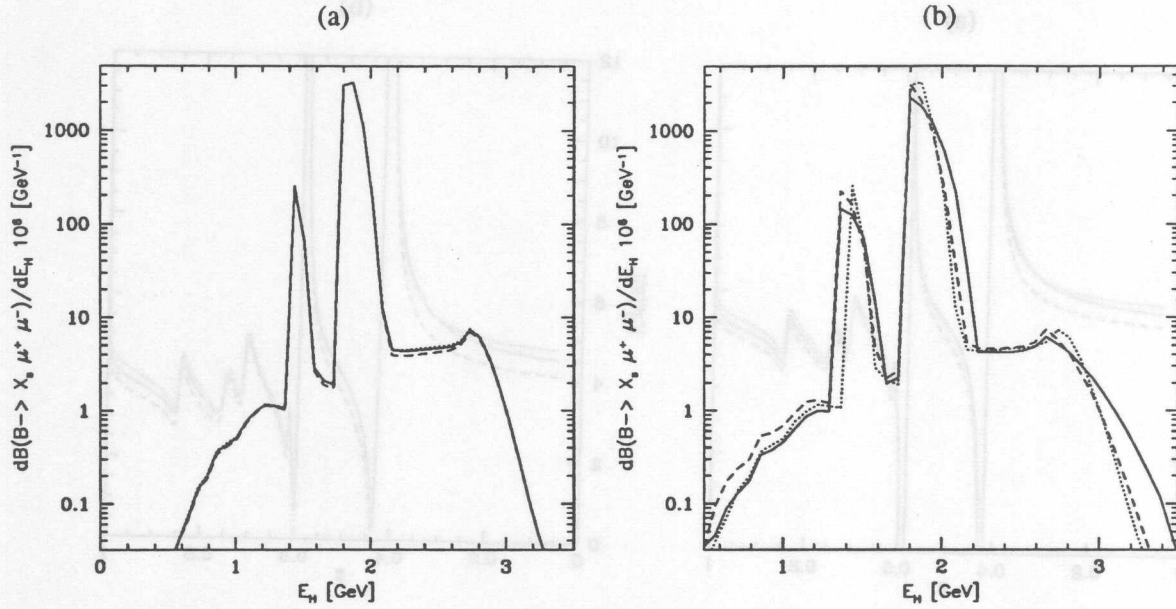
Figure 3.23: *Hadron energy spectrum in $B \to X_s \ell^+ \ell^-$ including the resonance and perturbative contributions in the Fermi motion model. In (a), the FM model parameters are fixed at $(\lambda_1, \bar{\Lambda}) = (-0.1 \, GeV^2, 0.4 \, GeV)$. The almost overlapping curves differ in the perturbative $c\bar{c}$ contribution with the solid curve obtained using eq. (3.18) for $g(\hat{m}_c, \hat{s})$, the dotted curve using $\tilde{g}(\hat{m}_c, \hat{s})$ given in eq. (3.121). The dashed curve corresponds to the approach by [28]. In (b), the solid, dotted, dashed curve corresponds to the parameters $(\lambda_1, \bar{\Lambda}) = (-0.3, 0.5), (-0.1, 0.4), (-0.15, 0.35)$ in (GeV^2, GeV), respectively.*

and there is only a subleading effect due to the momentum dependent b-quark mass. Not so in the hadron spectra. In the hadron energy spectrum, the $c\bar{c}$-resonances, which are narrowly peaked in the parton model, are broadened by the Lorentz boost of the FM model. To show this, the hadron energy spectrum in the FM model is compared with the spectrum in the parton model in Fig. 3.20 for identical values of m_b and m_b^{eff}, taken as 4.85 GeV. In terms of the hadronic invariant mass, the resonance structure is greatly smeared. The reason is that each q^2-bin contributes to a range of E_H and S_H. The different-q^2 regions overlap in S_H resulting in a smearing of the resonances over a wide range. This can be seen in Fig. 3.21 for the hadronic invariant mass. Various curves illustrate the sensitivity of this spectrum on the FM model parameters.

3.10.3   Ambiguities in adding LD and SD contributions in $B \to X_s \ell^+ \ell^-$

Since we are simply adding the short-distance (SD) and resonant charmonium amplitudes, it can not be ruled out that possibly some double counting has crept in in the coefficient $C_9^{\text{eff}}(\hat{s})$, once as a continuum $c\bar{c}$ contribution and then again as $J/\psi, \psi', \dots$ resonances. In the absence of a clear separation of the LD and SD physics in the spectra, we can not plead the case one way or the other. In the meanwhile, the question is whether the addition of the $c\bar{c}$-continuum and resonating pieces as being done here and in [18] compromises the resulting theoretical precision significantly. This can only be studied by comparing the theoretical scenario in question with other trial constructions which have no $c\bar{c}$ double counting. For
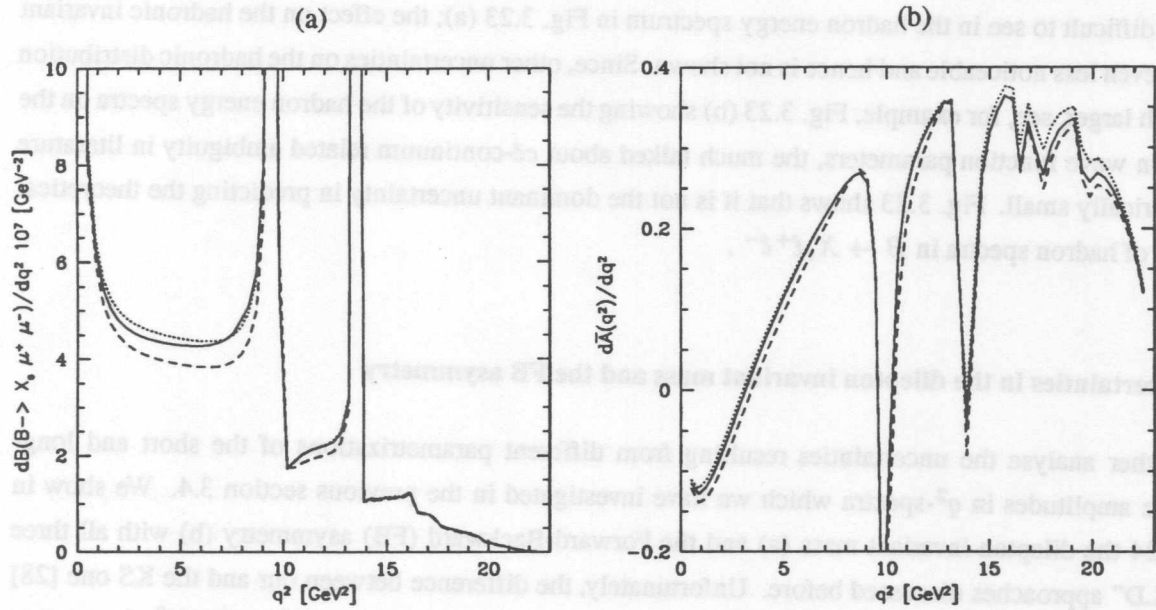
Figure 3.24: *Dilepton invariant spectrum (a) and the (normalized) Forward-Backward asymmetry (b) in* $B \to X_s \ell^+ \ell^-$ *including the resonance and perturbative contributions in the Fermi motion model. The FM model parameters are fixed at* $(\lambda_1, \bar{\Lambda}) = (-0.1 \; GeV^2, 0.4 \; GeV)$. *The curves differ in the perturbative* $c\bar{c}$ *contribution with the solid curve obtained using eq. (3.18) for* $g(\hat{m}_c, \hat{s})$, *and the dotted curve using* $\tilde{g}(\hat{m}_c, \hat{s})$ *given in eq. (3.121). The dashed curve corresponds to the approach given in ref. [28].*

example, one could retain in the perturbative function $g(\hat{m}_c, \hat{s})$ just the constant part in $\hat{s}$ by replacing $g(\hat{m}_c, \hat{s})$ by $\tilde{g}(\hat{m}_c, \hat{s})$, where

$$\tilde{g}(\hat{m}_c, \hat{s}) = -\frac{8}{9} \ln(\frac{m_b}{\mu}) - \frac{8}{9} \ln \hat{m}_c + \frac{8}{27} \, . \tag{3.121}$$

This function (with $\mu = m_b$) has been proposed in [29,28] as an alternative representation of the $c\bar{c}$ perturbative contribution and represents the (minimal) short-distance contribution. We denote this ansatz for C_9^{eff} defined as $C_9^{\text{eff}}(\hat{s}) = C_9\eta(\hat{s}) + Y(\hat{s})(``g(\hat{m}_c, \hat{s}) \to \tilde{g}(\hat{m}_c, \hat{s})") + Y_{res}(\hat{s})$ by LSW. Another approach is based on a dispersion relation, as proposed by [28], here and in the following denoted by KS. The KS parametrization of the $c\bar{c}$ resonant part differs from ours (eq. (3.72)), and the non-resonant part has been extracted from data, see [28] for details. The advantage of the KS procedure is that there is certainly no double counting. To study the difference numerically, we plot both the real part $ReC_9^{\text{eff}}(\hat{s})$ and the absolute value $|C_9^{\text{eff}}(\hat{s})|$ as functions of $\hat{s}$ in Fig. 3.22 by using the complete perturbative expression for $g(\hat{m}_c, \hat{s})$ in eq. (3.16) (our approach) and $\tilde{g}(\hat{m}_c, \hat{s})$ given in eq. (3.121) (LSW) and the KS parametrization. Both figures (a) and (b) show that the KS curve is always below our, which is again always below the LSW one. One sees from Figs. 3.22 (a) and 3.22 (b) that the difference in these functions in the variable $\hat{s}$ is visible. However, the three parametrizations of the perturbative $c\bar{c}$ part give almost identical hadron spectra, with the resulting uncertainty in the hadron energy and the hadronic invariant mass spectra being at most 12.1(4.5)% and 4.1(2.5)%, respectively. The difference between our approach and the KS one (first numbers) is larger than the one between ours and the LSW one, given in parentheses. These differences are

already difficult to see in the hadron energy spectrum in Fig. 3.23 (a); the effect on the hadronic invariant mass is even less noticeable and hence is not shown. Since, other uncertainties on the hadronic distribution are much larger, see, for example, Fig. 3.23 (b) showing the sensitivity of the hadron energy spectra on the B-meson wave function parameters, the much talked about $c\bar{c}$-continuum related ambiguity in literature is numerically small. Fig. 3.23 shows that it is not the dominant uncertainty in predicting the theoretical profiles of hadron spectra in $B \to X_s \ell^+ \ell^-$.

LD uncertainties in the dilepton invariant mass and the FB asymmetry

We further analyse the uncertainties resulting from different parametrizations of the short and long-distance amplitudes in q^2-spectra which we have investigated in the previous section 3.4. We show in Fig. 3.24 the dilepton invariant mass (a) and the Forward-Backward (FB) asymmetry (b) with all three "SD+LD" approaches discussed before. Unfortunately, the difference between our and the KS one [28] in the dilepton spectrum is maximal in the low-q^2 region below the J/ψ-peak, $q^2 < 9\text{GeV}^2$. It amounts up to 15%. In the other distribution, the FB asymmetry, the difference is found to be moderate over the full q^2-range . It does not exceed 5% in the range $5\text{GeV}^2 \leq q^2 \leq 9\text{GeV}^2$. However, we remark here that the position of the first zero of the FB asymmetry is affected by the parametrization of the $c\bar{c}$ states.

3.10.4 Numerical estimates of the hadronic moments in FM model and HQET

To underline the similarity of the HQET and FM descriptions in $B \to X_s \ell^+ \ell^-$, and also to make comparison with data, we have calculated the hadronic moments in the FM model using the spectra which we have presented in the previous sections. The moments based on the SD-contribution are defined as:

$$\langle X_H^n \rangle = (\int X_H^n \frac{dB}{dX_H} dX_H)/B \qquad \text{for } X = S, E .\qquad (3.122)$$

The moments $\langle X_H^n \rangle_{\bar{c}c}$ are defined by taking into account in addition to the SD-contribution also the contributions from the $c\bar{c}$ resonances. The values of the moments in both the HQET approach and the FM for $n = 1, 2$ are shown in Table 3.4, with the numbers in the parentheses corresponding to the former. They are again based on using the central values of the parameters given in Table A.1, and are calculated for the same values of the HQET parameters $\bar{\Lambda}$ and λ_1, using the transcriptions given in eqs. (3.113). Both the HQET and the FM model lead to strikingly similar results for the hadronic moments shown in this table. However, the moments $\langle X_H^n \rangle_{\bar{c}c}$ with $X = S, E$ are significantly lower than their SD-counterparts $\langle X_H^n \rangle$ calculated for the same values of the FM model parameters. This shows, at least in this model study, that the $c\bar{c}$ resonances are important also in moments. The hadronic invariant mass spectra in $B \to X_s \ell^+ \ell^-$ for both the SD and inclusive contributions are expected to be dominated by multi-body states, with $\langle S_H \rangle \simeq (1.5 - 2.1)\,\text{GeV}^2$ and $\langle S_H \rangle_{\bar{c}c} \simeq (1.2 - 1.5)\,\text{GeV}^2$. Note that the difference in the numerical values of the hadronic mass moments $\langle S_H \rangle_{\bar{c}c}$ and $\langle S_H^2 \rangle_{\bar{c}c}$ shown in Table 3.4 caused by different LD parametrizations is less than 0.22%, 0.42%, respectively, as can be see in Table 3.6.

$(\lambda_1, \bar{\Lambda})$ in (GeV^2, GeV)	$\langle S_H \rangle$ (GeV^2)	$\langle S_H \rangle_{\bar{c}c}$	$\langle S_H^2 \rangle$ (GeV^4)	$\langle S_H^2 \rangle_{\bar{c}c}$
$(-0.3, 0.5)$	2.03 (2.09)	1.51	6.43 (6.93)	3.10
$(-0.1, 0.4)$	1.75 (1.80)	1.36	4.04 (4.38)	2.17
$(-0.14, 0.35)$	1.54 (1.49)	1.19	3.65 (3.64)	1.92

$(\lambda_1, \bar{\Lambda})$ in (GeV^2, GeV)	$\langle E_H \rangle$ (GeV)	$\langle E_H \rangle_{\bar{c}c}$	$\langle E_H^2 \rangle$ (GeV^2)	$\langle E_H^2 \rangle_{\bar{c}c}$
$(-0.3, 0.5)$	2.23 (2.28)	1.87	5.27 (5.46)	3.52
$(-0.1, 0.4)$	2.21 (2.22)	1.85	5.19 (5.23)	3.43
$(-0.14, 0.35)$	2.15 (2.18)	1.84	4.94 (5.04)	3.39

Table 3.4: *Hadronic spectral moments for $B \to X_s \mu^+ \mu^-$ in the Fermi motion model (HQET) for the indicated values of the parameters $(\lambda_1, \bar{\Lambda})$.*

3.11 Branching Ratios and Hadron Spectra in $B \to X_s \ell^+ \ell^-$ with Cuts on Invariant Masses

In experimental searches for the decay $B \to X_s \ell^+ \ell^-$, the short-distance contribution is expected to be visible away from the resonances. So, cuts on the invariant dilepton mass are imposed to get rid of the dilepton mass range where the charmonium resonances J/ψ and ψ' are dominant. For example, the cuts imposed in the recent CLEO analysis [30] given below are typical:

$$\text{cut } A \quad : \quad q^2 \leq (m_{J/\psi} - 0.1 \,\text{GeV})^2 = 8.98 \,\text{GeV}^2 ,$$
$$\text{cut } B \quad : \quad q^2 \leq (m_{J/\psi} - 0.3 \,\text{GeV})^2 = 7.82 \,\text{GeV}^2 ,$$
$$\text{cut } C \quad : \quad q^2 \geq (m_{\psi'} + 0.1 \,\text{GeV})^2 = 14.33 \,\text{GeV}^2 . \qquad (3.123)$$

The cuts A and B have been chosen to take into account the QED radiative corrections as these effects are different in the $e^+ e^-$ and $\mu^+ \mu^-$ modes. In the following, we compare the hadron spectra with and without the resonances after imposing these experimental cuts. For the low-q^2 cut for muons (cut A), the hadron energy spectra and the hadronic invariant mass spectra are shown in Fig. 3.25 (a), (b) and Fig. 3.26 (a), (b), respectively. The results for the low-q^2 cut for electrons (cut B), are shown in Fig. 3.25 (c), (d) and Fig. 3.26 (c), (d), respectively. Finally, the hadronic spectra for the high-q^2 cut (cut C) for $e^+ e^-$ and $\mu^+ \mu^-$ can be seen in Fig. 3.25 (e), (f) for the hadronic energy and in Fig. 3.26 (e), (f) for the hadronic invariant mass. We see that the above cuts in q^2 greatly reduce the resonance contributions. Hence, the resulting distributions essentially test the non-resonant $c\bar{c}$ and short-distance contributions. These figures will be used later to quantify the model dependence of the integrated branching ratios in $B \to X_s \ell^+ \ell^-$.

As mentioned in [30], the dominant $B\bar{B}$ background to the decay $B \to X_s \ell^+ \ell^-$ comes from two semileptonic decays of B or D mesons, which produce the lepton pair with two undetected neutrinos. To suppress this $B\bar{B}$ background, it is required that the invariant mass of the final hadronic state is less than

$t = 1.8$ GeV, which approximately equals m_D. We define the survival probability of the $B \to X_s \ell^+ \ell^-$ signal after the hadronic invariant mass cut:

$$S(t) \equiv (\int_{m_X^2}^{t^2} \frac{dB}{dS_H} dS_H)/B \,, \qquad\qquad (3.124)$$

and present $S(t = 1.8$ GeV$))$ as the fraction of the branching ratio for $B \to X_s \ell^+ \ell^-$ surviving these cuts in Table 3.5. To estimate the model dependence of this probability, we vary the FM model parameters. Concentrating on the SD piece, we note that the effect of this cut alone is that between 83% to 92% of the signal for $B \to X_s \mu^+ \mu^-$ and between 79% to 90% of the signal in $B \to X_s e^+ e^-$ survives, depending on the FM model parameters. The corresponding numbers for the inclusive spectrum including the SD and LD contribution, here and in the following abbreviated as tot =SD+LD, is 96% to 99.7% for both the dimuon and dielectron case. This shows that while this cut removes a good fraction of the $B\bar{B}$ background, it allows a very large fraction of the $B \to X_s \ell^+ \ell^-$ signal to survive. However, this cut does not discriminate between the SD and (SD+LD) contributions, for which the cuts A - C are effective. The numbers for the survival probability $S(t = 1.8$ GeV$)$ reflect that the hadronic invariant mass distribution of the LD-contribution is more steep than the one from the SD contribution.

$(\lambda_1, \bar{\Lambda})$ GeV^2, GeV	$B \cdot 10^{-6}$ $\mu^+\mu^-$	$B \cdot 10^{-6}$ e^+e^-	No s-cut $\mu^+\mu^-$	No s-cut e^+e^-	cut A $\mu^+\mu^-$	cut B e^+e^-	cut C $\mu^+\mu^-$	cut C e^+e^-
$(-0.3, 0.5)$	5.8	8.6	83%	79 %	57%	57%	6.4%	4.5%
$(-0.1, 0.4)$	5.7	8.4	93%	91 %	63%	68%	8.3%	5.8%
$(-0.14, 0.35)$	5.6	8.3	92%	90 %	65%	67%	7.9%	5.5%
$(-0.3, 0.5)_{tot}$	562.5	563.9	96%	96 %	0.8%	1.0%	0.06%	0.06%
$(-0.1, 0.4)_{tot}$	564.0	565.6	99.7%	99.7%	0.8%	1.1%	0.08%	0.08%
$(-0.14, 0.35)_{tot}$	566.5	568.2	99%	99 %	0.9%	1.2%	0.08%	0.08%

Table 3.5: *Branching ratios for $B \to X_s \ell^+ \ell^-$, $\ell = \mu, e$ for different FM model parameters are given in the second and third columns. The values given in percentage in the fourth to ninth columns represent the survival probability $S(t = 1.8$ GeV$)$ defined in eq. (3.124) for different FM model parameters and cuts on the dilepton invariant mass as defined in eq. (3.123). The subscript $tot = SD + LD$ denotes that both the short and the long-distance contributions are included in the branching ratios and $S(t)$.*

With the additional cut A (B) imposed on the dimuon (dielectron) invariant mass, between 57% to 65% (57% to 68%) of the $B \to X_s \ell^+ \ell^-$ signal survives the additional cut on the hadronic invariant mass for the SD contribution. However, as expected, the cuts A and B result in drastic reduction of the inclusive branching ratio for the decay $B \to X_s \ell^+ \ell^-$, as they effectively remove the dominant $c\bar{c}$-resonant part. In this case only 0.8% to 0.9% (1.0% to 1.2% of the inclusive signal survives for the cut A (B). The theoretical branching ratios for both the dielectron and dimuon cases, calculated using the central values in Table A.1 are also given in Table 3.5. As estimated in eq. (3.71), the uncertainty on the branching ratios resulting from the errors on the parameters in Table A.1 is about $\pm 23\%$ (for the dielectron mode)

and $\pm 16\%$ (for the dimuon case). The wave function-related uncertainty in the branching ratios is smaller, as can be seen in Table 3.5. With the help of the theoretical branching ratio and the survival probability $S(t = 1.8)$ GeV, calculated for three sets of the FM parameters, the cross section can be calculated for all six cases:

(i) no cut on the dimuon invariant mass [(SD) and (SD + LD)], (ii) no cut on the dielectron invariant mass [(SD) and (SD + LD)], (iii) cut A on the dimuon invariant mass [(SD) and (SD + LD)], (iv) cut B on the dielectron invariant mass [(SD) and (SD + LD)], (v) cut C on the dimuon invariant mass [(SD) and (SD + LD)], (vi) cut C on the dielectron invariant mass [(SD) and (SD + LD)]. This gives a fair estimate of the theoretical uncertainties on the partially integrated branching ratios from the B-meson wave function and $c\bar{c}$ resonances. This table shows that with 10^7 $B\bar{B}$ events, $\mathcal{O}(70)$ dimuon and ($\mathcal{O}(100)$ dielectron) signal events from $B \to X_s \ell^+ \ell^-$ should survive the CLEO cuts A (B) with $m(X_s) < 1.8$ GeV. With cut C, one expects an order of magnitude less events, making this region interesting for the LHC experiments. Given enough data, one can compare the experimental distributions in $B \to X_s \ell^+ \ell^-$ directly with the ones presented here.

3.11.1 Hadronic spectral moments with cuts in the FM

We have calculated the first two moments of the hadronic invariant mass in the FM model by imposing a cut $S_H < t^2$ with $t = 1.8$ GeV and an optional cut on q^2.

$$\langle S_H^n \rangle = \left(\int_{m_X^2}^{t^2} S_H^n \frac{d^2 \mathcal{B}_{cutX}}{dS_H dq^2} dS_H dq^2 \right) / \left(\int_{m_X^2}^{t^2} \frac{d^2 \mathcal{B}_{cutX}}{dS_H dq^2} dS_H dq^2 \right) \qquad \text{for} \quad n = 1, 2 . \qquad (3.125)$$

Here the subscript $cutX$ indicates whether we evaluated $\langle S_H \rangle$ and $\langle S_H^2 \rangle$ with the cuts on the invariant dilepton mass as defined in eq. (3.123), or without any cut on the dilepton mass. The results are collected in Table 3.6. The moments given in Table 3.6 can be compared directly with the data to extract the FM model parameters. The entries in this table give a fairly good idea of what the effects of the experimental cuts on the corresponding moments in HQET will be, as the FM and HQET yield very similar moments for equivalent values of the parameters. The functional dependence of the hadronic moments on the HQET parameters taking into account the experimental cuts still remains to be worked out.

Further, we have calculated $\langle S_H \rangle$ and $\langle S_H^2 \rangle$ with a cut $S_H < 3.24$ GeV^2 and optional ones on q^2 (cut A-C according to eq. (3.123)) with the approaches KS [28] and LSW [29] for $(\lambda_1, \bar{\Lambda}) = (-0.1, 0.4)$ in GeV^2, GeV. They differ from ours (eq. (3.117)) in the parametrization of the resonant and non-resonant $c\bar{c}$ contributions, as discussed in section 3.10.3. We compare the values of the moments for the same set of FM parameters. Denoting our approach by y, we define by Δ the maximal deviation in % between ours and KS and LSW, generically written as: $\Delta = max(|y - \text{LSW}|/|y|, |y - \text{KS}|/|y|)$ and present it in the last row of Table 3.6. We see that the uncertainties in the hadronic mass moments from different "SD+LD" parametrizations are small, namely below 1.6% in the worst case.

3.12 Summary and Concluding Remarks on the Decay $B \to X_s \ell^+ \ell^-$

In this chapter we have investigated distributions, decay rates and moments in rare inclusive $B \to X_s \ell^+ \ell^-$ decay in the standard model. In the first part, we have concentrated mainly on the study of distributions in

FM parameters $(\lambda_1, \bar{\Lambda})$ GeV^2, GeV	No s-cut $\mu^+\mu^-$		No s-cut e^+e^-		cut A $\mu^+\mu^-$		cut B e^+e^-		cut C $\ell^+\ell^-$	
	$\langle S_H \rangle$ GeV^2	$\langle S_H^2 \rangle$ GeV^4	$\langle S_H \rangle$ GeV^2	$\langle S_H^2 \rangle$ GeV^4	$\langle S_H \rangle$ GeV^2	$\langle S_H^2 \rangle$ GeV^4	$\langle S_H \rangle$ GeV^2	$\langle S_H^2 \rangle$ GeV^4	$\langle S_H \rangle$ GeV^2	$\langle S_H^2 \rangle$ GeV^4
$(-0.3, 0.5)$	1.47	2.87	1.52	3.05	1.62	3.37	1.66	3.48	0.74	0.69
$(-0.1, 0.4)$	1.57	2.98	1.69	3.37	1.80	3.71	1.88	3.99	0.74	0.63
$(-0.14, 0.35)$	1.31	2.34	1.38	2.55	1.47	2.83	1.52	2.97	0.66	0.54
$(-0.3, 0.5)_{tot}$	1.41	2.61	1.41	2.62	1.61	3.32	1.66	3.47	0.74	0.68
$(-0.1, 0.4)_{tot}$	1.35	2.14	1.36	2.15	1.77	3.60	1.87	3.94	0.74	0.62
$(-0.14, 0.35)_{tot}$	1.17	1.84	1.18	1.85	1.45	2.76	1.51	2.95	0.66	0.54
Δ (%)	0.15	0.19	0.22	0.42	0.90	1.56	0.32	0.58	0.01	0.32

Table 3.6: $\langle S_H \rangle$ and $\langle S_H^2 \rangle$ for $B \to X_s \ell^+ \ell^-$, $\ell = \mu$, e for different FM model parameters and a hadronic invariant mass cut $S_H < 3.24\,\text{GeV}^2$ are given with and without additional cuts on the dilepton invariant mass as defined in eq. (3.123). The S_H-moments with cuts are defined in eq. (3.125). The subscript $tot = SD + LD$ denotes that both the short and the long-distance contributions are included in these moments. The value of Δ estimates the uncertainty from different approaches to take into account the effect of the $c\bar{c}$ continuum and resonances, see text.

the dilepton invariant mass q^2, the differential branching ratio in this variable and the FB asymmetry. Our findings can be summarized as follows [18]:

- We have calculated the leading $1/m_b$ power corrections with HQE techniques in the dilepton invariant mass distribution in $B \to X_s \ell^+ \ell^-$ decay and have explicitly kept the s-quark dependence. Our calculation is at variance with an earlier one [17] in the limit $m_s = 0$ and has been confirmed recently by [27] for the massless s-quark case.

- We find that the $1/m_b^2$ corrections are stable over a good part of the dilepton mass spectrum. However, near the high q^2 end-point the distribution becomes unphysical due to the HQE parameter λ_2, signaling a breakdown of the heavy quark expansion.

- The $B \to X_s \ell^+ \ell^-$ decay rate in the HQE method decreases by about 4% and the branching ratio by about 1.5% from their corresponding parton model values.

- Alternatively, we have implemented a Gaussian Fermi motion model in the decay $B \to X_s \ell^+ \ell^-$ to model B-meson bound state effects. We have analysed the dilepton invariant mass distribution and the FB asymmetry within this framework, showing the dependence on the parameters of this model. Non-perturbative effects are found to be perceptible in both distributions in the high q^2 region.

- The theoretical uncertainties in the short-distance branching ratios in $B \to X_s \ell^+ \ell^-$ decay are found to be $\pm 23\%$ ($\pm 16\%$) for the electron (muon) case in the FM.

- We have modeled the long-distance contributions from intermediate charmonium resonances with a VMD ansatz and presented the dilepton invariant mass distribution and the FB asymmetry in the FM, including next-to-leading order perturbative QCD corrections in figures.

We have completed the description of final states in $B \to X_s \ell^+ \ell^-$ decay in the second part of this chapter, which is devoted to the study of hadron spectra and hadronic spectral moments. We summarize [25,26,14]:

- We have calculated the $\mathcal{O}(\alpha_s)$ perturbative QCD and leading $\mathcal{O}(1/m_b)$ corrections to the hadron spectra in the decay $B \to X_s \ell^+ \ell^-$, including the Sudakov-improvements in the perturbative part.

- We find that the hadronic invariant mass spectrum is calculable in HQET over a limited range $S_H > m_B \bar{\Lambda}$ and it depends sensitively on the parameter $\bar{\Lambda}$ (equivalently m_b). These features are qualitatively very similar to the ones found for the hadronic invariant mass spectrum in the decay $B \to X_u \ell \nu_\ell$ [101].

- The $1/m_b$-corrections to the parton model hadron energy spectrum in $B \to X_s \ell^+ \ell^-$ are small over most part of this spectrum. However, heavy quark expansion breaks down near the lower end-point of this spectrum and close to the $c\bar{c}$ threshold. The behavior in the former case has a similar origin as the breakdown of HQET near the high end-point in the dilepton invariant mass spectrum, which we have presented here and in ref. [18].

- We have calculated the hadronic spectral moments $\langle S_H^n \rangle$ and $\langle E_H^n \rangle$ for $n = 1, 2$ using HQET. The dependence of these moments on the HQET parameters is worked out numerically. In particular, the moments $\langle S_H^n \rangle$ are sensitive to the parameters $\bar{\Lambda}$ and λ_1 and they provide complementary constraints on them than the ones following from the analysis of the decay $B \to X \ell \nu_\ell$. The simultaneous fit of the data in $B \to X_s \ell^+ \ell^-$ and $B \to X \ell \nu_\ell$ could then be used to determine these parameters very precisely. This is illustrated in Fig. 3.15.

- The corrections to the hadron energy moments $\triangle \langle E_H \rangle_{1/m_c^2}$ and $\triangle \langle E_H^2 \rangle_{1/m_c^2}$ from the leading $\mathcal{O}(\Lambda_{QCD}^2/m_c^2)$ power corrections have been worked out, using the results of [27]. We find that these corrections are very small. The corresponding corrections in $\triangle \langle S_H^n \rangle_{1/m_c^2}$ vanish in the theoretical accuracy we are working.

- We think that the quantitative knowledge of $\bar{\Lambda}$ and λ_1 from the moments can be used to remove much of the theoretical uncertainties in the partially integrated decay rates in $B \to X_u \ell \nu_\ell$ and $B \to X_s \ell^+ \ell^-$. Relating the two decay rates would enable a precise determination of the CKM matrix element V_{ub}.

- As a phenomenological alternative to HQET, we have worked out the hadron spectra and moments in $B \to X_s \ell^+ \ell^-$ in the Fermi motion model. We find that the hadron energy spectrum is stable against the variation of the FM model parameters. However, the hadronic invariant mass is sensitive to the input parameters. Present theoretical dispersion on this spectrum can be reduced with the experimental measurements of the corresponding spectrum in the decay $B \to X_u \ell \nu_\ell$, which will determine these parameters. Conversely, with good measurements of the decay $B \to X_s \ell^+ \ell^-$, one

could fix the input parameters in the decay $B \to X_u \ell \nu_\ell$ and determine the CKM matrix element V_{ub} rather precisely.

- For equivalent values of the FM and HQET parameters, the hadronic spectral moments in $B \to X_s \ell^+ \ell^-$ decay are found to be remarkably close to each other.

- We have worked out the effect of the $c\bar{c}$ resonances in the effective coefficient $C_9^{\text{eff}}(\hat{s})$ on the hadron spectra in $B \to X_s \ell^+ \ell^-$, by parametrizing the present data on the resonant part from the decays $B \to X_s(J/\psi, \psi', ...)$. The resonances are incorporated at the parton level and the broadening of these resonances from the wave function effects in the FM model are then worked out. These spectra will provide an important test of the FM model in $B \to X_s \ell^+ \ell^-$.

- We find that the $c\bar{c}$ long-distance effects in $B \to X_s \ell^+ \ell^-$ decay are also important in the hadronic moments.

- We have quantitatively studied possible double counting effects which may have entered in simply adding the resonant contribution via Breit-Wigner functions and the complete perturbative $c\bar{c}$ contribution in the coefficient $C_9^{\text{eff}}(\hat{s})$ in $B \to X_s \ell^+ \ell^-$. The numerical difference between this approach, followed here [18,14], and alternative ones [28] and [29], are found to be small in the dilepton invariant mass spectrum and negligible in the hadron spectra and moments. Theoretical spectra are found to be more sensitive to the wave function effects, which dominate the uncertainty in the shape.

- We have worked out the hadron spectra by imposing the experimental cuts designed to suppress the resonant $c\bar{c}$ contributions, as well as the dominant $B\bar{B}$ background leading to the final state $B\bar{B} \to X_s \ell^+ \ell^-$ (+ missing energy). The parametric dependences of the resulting spectra are studied in the FM model. In particular, the survival probability of the $B \to X_s \ell^+ \ell^-$ signal by imposing a cut on the hadronic invariant mass $S_H < 3.24$ GeV^2, as used in the CLEO analysis, is estimated and its model dependence studied. This quantifies the statement that with the indicated cuts, these spectra essentially test the physics of the short-distance (and non-resonant $c\bar{c}$) contribution.

The CLEO collaboration has already been searched for inclusive $b \to s\ell^+ \ell^-$ decay with $\ell = e, \mu$. Their results are [30]:

$$\mathcal{B}(b \to se^+e^-)^{\text{CLEO}} < 5.7 \cdot 10^{-5},$$
$$\mathcal{B}(b \to s\mu^+\mu^-)^{\text{CLEO}} < 5.8 \cdot 10^{-5}. \qquad (3.126)$$

Comparing this with our estimates for the SD branching ratios in the decay $B \to X_s \ell^+ \ell^-$ given in eq. (3.71), we see that the above CLEO upper bounds are approximately one order of magnitude away from the theoretical standard model prediction.
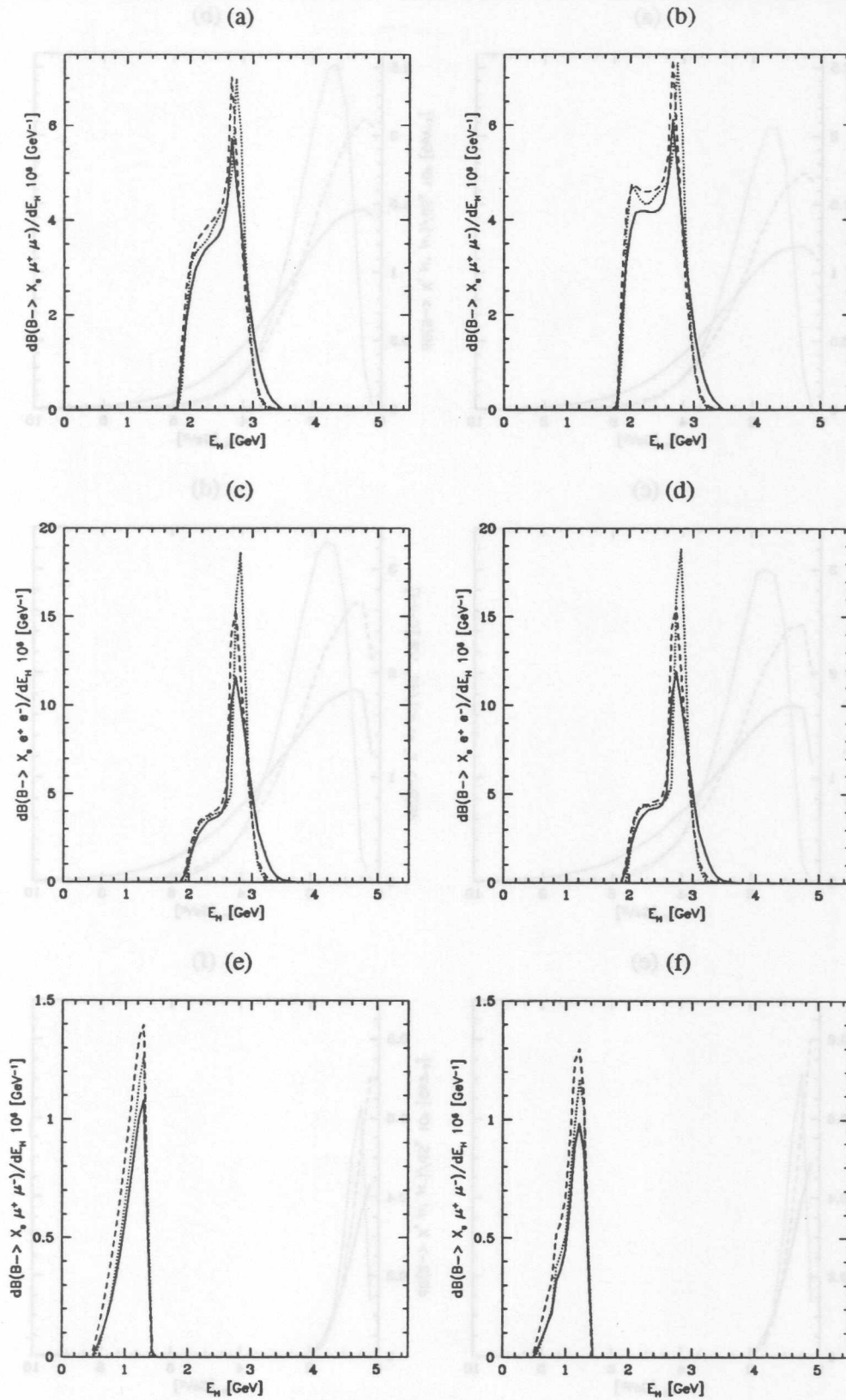
Figure 3.25: *Hadron energy spectrum in $B \to X_s \ell^+ \ell^-$ in the Fermi motion model with the cuts on the dilepton mass defined in eq. (3.123); (a),(c),(e) without and (b),(d),(f) with the $c\bar{c}$-resonance contribution corresponding to cut A,B,C, respectively. The solid, dotted, dashed curves correspond to the parameters $(\lambda_1, \bar{\Lambda}) = (-0.3, 0.5), (-0.1, 0.4), (-0.15, 0.35)$ in (GeV^2, GeV), respectively.*
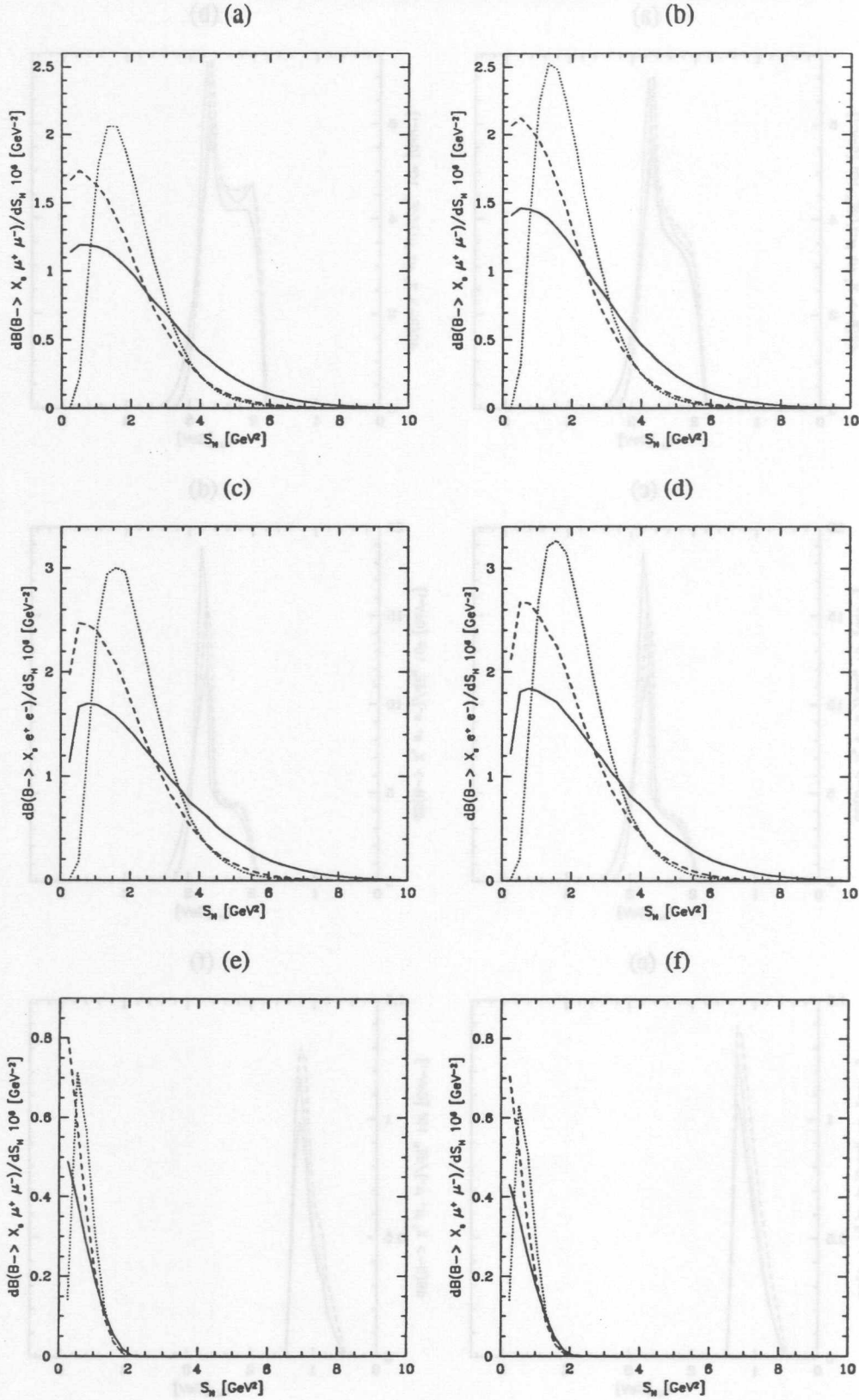
Figure 3.26: *Hadronic invariant mass spectrum in* $B \to X_s \ell^+ \ell^-$ *in the Fermi motion model with the cuts on the dilepton mass defined in eq. (3.123); (a),(c),(e) without and (b),(d),(f) with the* $c\bar{c}$*-resonance contribution corresponding to cut A,B,C, respectively. The solid, dotted, dashed curves correspond to the parameters* $(\lambda_1, \bar{\Lambda}) = (-0.3, 0.5), (-0.1, 0.4), (-0.15, 0.35)$ *in* (GeV^2, GeV)*, respectively.*

Chapter 4

The Decay $B_s \to \gamma\gamma$

Besides the rare decays $B \to X_s\gamma$ and $B \to X_s\ell^+\ell^-$, $B_s \to \gamma\gamma$ is another potential candidate to explore perturbative and non-perturbative aspects of QCD and test the standard model (SM). The L3 collaboration has already been searched for $B_s \to \gamma\gamma$ decay. Their upper bound is the best present limit of this channel [117]

$$\mathcal{B}(B_s \to \gamma\gamma) < 1.48 \cdot 10^{-4} \ . \tag{4.1}$$

The first theoretical analysis of a rare decay into 2 photons is contained in the pioneering work by Gaillard and Lee [118], who considered $K_{S,L} \to \gamma\gamma$. Exclusive $B_s \to \gamma\gamma$ decay has been investigated in the lowest order in refs. [32–35]. The branching ratio found is $4.5 \cdot 10^{-7}$ in the SM context for $m_s = 0.5$ GeV and other parameters given in Table A.1. The large value of the s-quark mass here results from using the constituent quark mass $m_s \sim m_K$. As learned from studies of $B \to X_s\gamma$ decay, the flavour changing neutral current (FCNC) $b \to s\gamma$ vertex receives in leading logarithmic (LLog) QCD approximation a large enhancement about a factor of 2-3. We suggest similar effects for the $b \to s\gamma\gamma$ transition. To see whether $B_s \to \gamma\gamma$ decay is worth more effort to be searched for at future experiments, a more advanced analysis of its branching ratio is required. A branching ratio of order 10^{-6} is a benchmark of a decay to be measured at present B experiments like CLEO or Hera-B with reasonable statistics. Upgrades and planned B-factories will be sensitive to branching ratios of order 10^{-8}. However, the $B_s\bar{B}_s$ pair is too heavy to be produced at the $\Upsilon(4s)$ resonance.

The $B_s \to \gamma\gamma$ final state consists of a CP-odd T^- and a CP-even T^+ amplitude. It offers, besides the branching ratio, another observable, the so called CP ratio $|T^+|^2/|T^-|^2$ [34,35]. With it CP violating effects can be studied.

The work reported in this thesis, which has already been published [37], [38] differs from the previous ones [35,33,32] with respect to three points: a) We calculate and use the QCD-improved LLog amplitudes. b) In contrast to previous works using the constituent quark model we model the bound state effects of the B_s meson through an heavy quark expansion technique (HQET) inspired approach following [16]. This introduces an additional dispersion on the $B_s \to \gamma\gamma$ branching ratio and CP ratio, which serves as an estimate of the hadronic uncertainties. c) We include long distance effects due to decay chains via intermediate vector mesons in our analysis. To be definite, we estimate the additional contribution in the decay $B_s \to \gamma\gamma$ through $B_s \to \phi\gamma$ followed by $\phi \to \gamma$ using Vector Meson Dominance (VMD) [74].

Further, the $B_s \to \phi\psi$ decay is modeled by inclusive $b \to s\psi$ decay. Using the VMD model, the amplitude for the chain process $B_s \to \phi\psi \to \phi\gamma \to \gamma\gamma$ is presented.

Leading logarithmic QCD corrections for the short-distance part of the decay $B_s \to \gamma\gamma$ have also been calculated by Chang et al. [119]. They fix $\bar{\Lambda} = m_{B_s} - m_b$, which corresponds to m_s in the naive constituent quark model, and the renormalization scale $\mu = m_b$. We emphasize here that the decay rate (and the CP ratio) is sensitive to both of these parameters and requires further theoretical investigation. Soni et al. [120] calculated also LLog QCD calculations in $B_s \to \gamma\gamma$ and in addition in the decay $B \to X_s\gamma\gamma$. Analyses of $B_s \to \gamma\gamma$ decay in non standard models have been done in ref. [35] in the lowest order and in ref. [121] including LLog QCD corrections in the two Higgs doublet model (2HDM), in ref. [122] in the minimal supersymmetric model (MSSM) and in ref. [123] in the 2HDM with flavour changing neutral currents allowed at tree level.

4.1 Leading Logarithmic Improved Short-Distance Contributions in $B_s \to \gamma\gamma$ Decay

In this section we present the leading logarithmic QCD-improved rates for exclusive $B_s \to \gamma\gamma$ decay. We use the free quark model and make the connection between quark and mesons states by means of the B_s meson decay constant f_{B_s}. Dot products of kinematical variables, which are not fixed by this are estimated in an approach inspired by HQET.

QCD-improved rates in b-quark decays can in general be obtained through the following procedure: Matching of the full theory with an effective theory at a scale $\mu = m_W$, using an effective Hamiltonian and performing an evolution of the Wilson coefficients from m_W down to $\mu \sim \mathcal{O}(m_b)$, thus resumming all large logarithms of the form $\alpha_s^n(m_b) \ln^m(\frac{m_b}{m_W})$, where $m \leq n$ ($n = 0, 1, 2, \ldots$). In the leading logarithmic approximation, which we use here, $m = n$. In our case, which is $B_s \to \gamma\gamma$ now an enormous short cut is possible from observing that the effective Hamiltonian in eq. (2.18) for $b \to s\gamma$ is identical for $b \to s\gamma\gamma$ to this order of $\frac{1}{m_W^2}$:

$$\mathcal{H}_{eff}(b \to s\gamma) = \mathcal{H}_{eff}(b \to s\gamma\gamma) + \mathcal{O}(\frac{1}{m_W^4}) . \tag{4.2}$$

The proof goes as follows: One can ask, if there are more operators needed for $b \to s\gamma\gamma$ than included in $\mathcal{H}_{eff}(b \to s\gamma)$ and try to find an operator $\bar{s}Xb$ with $dim(X) \leq 3$ and containing two photons! Here X must be a gauge and Lorentz invariant structure made out of quark and photon fields, masses and covariant derivatives $D_\mu = \partial_\mu + ieQ_qA_\mu$. (For the moment we shall work in zeroth order of the strong interactions.) When constructing the full set of physical operators, the equations of motion (EOM) can be used to reduce the operator basis:

$$i\not{D}q = m_q q , \quad D_\mu F^{\mu\nu} = eQ_q\bar{q}\gamma^\nu q , \quad \partial_\mu\tilde{F}^{\mu\nu} = 0 . \tag{4.3}$$

Here $F^{\mu\nu}$, $\tilde{F}^{\mu\nu} = \frac{1}{2}\epsilon^{\mu\nu\alpha\beta}F_{\alpha\beta}$ denote the photon field strength tensor and its dual, respectively. For chiral fermions we have the following EOM, which can be obtained with the identities given in eq. (A.41)

$$i\not{D}b_L = m_b b_R , \quad \overline{s_L}i\not{D} = m_s\bar{s}L = m_s\overline{s_R} . \tag{4.4}$$

Other useful identities in this context are:

$$D^2 = \not{D}^2 - \frac{1}{2}eQ_q\sigma F , \quad D_\mu = \frac{1}{2}(\not{D}\gamma_\mu + \gamma_\mu\not{D}) , \quad [D_\mu, D_\nu] = ieQ_q F_{\mu\nu} . \tag{4.5}$$

As a result, using the EOM gives either a mass, a current or remains in the operator basis $O_{1...8}$ eq. (2.18) or gives contributions to the FCNC self energy. The latter will be absorbed in the on-shell renormalization and does not give any contribution to $b \to s\gamma\gamma$

$$\Sigma(p^2 = m_b^2)b = \bar{s}\Sigma(p'^2 = m_s^2) = 0 . \tag{4.6}$$

Here p, p' is the 4-momentum of the incoming b-quark, outgoing s-quark, respectively. To display the foregoing we give some examples of EOM operator identities:

- $F_{\mu\nu}\overline{s_L}\gamma^\mu D^\nu b_L = \frac{1}{4}\bar{s}\sigma_{\mu\nu}(m_b R + m_s L)bF^{\mu\nu} \sim O_7$

- $\bar{s}(i\not{D})^3 b = m_b^3 \bar{s}b$

- $m_b \bar{s}D^2 b = -m_b^3 \bar{s}b - \frac{m_b}{2}eQ_q\bar{s}\sigma Fb$

- $\bar{s}\gamma_\nu(D_\mu F^{\mu\nu})b = eQ_q\bar{s}\gamma_\nu b\bar{q}\gamma^\nu q$

Since after applying the equations of motion there exists no gauge-invariant FCNC-2-photon operator with field dimension ≤ 6, the set of operators given in eq. (2.18) is a complete basis for both $b \to s\gamma$ and $b \to s\gamma\gamma$ decay [10,51]. Hence all the results obtained for the former, a collection of which can be seen in section 2.2, can be used for the latter, like the LLog evolution of the Wilson coefficients.

4.1.1 $B_s \to \gamma\gamma$ decay in the effective Hamiltonian theory

Having convinced us that the set-up eq. (4.2) is correct, we can now turn to an explicit calculation of LLog improved FCNC 2 photon amplitudes. The amplitude for the decay $B_s \to \gamma\gamma$ can be decomposed as [32,33,35]

$$\mathcal{A}(B_s \to \gamma\gamma) = \epsilon_1^\mu(k_1)\epsilon_2^\nu(k_2)(A^+ g_{\mu\nu} + iA^- \epsilon_{\mu\nu\alpha\beta}k_1^\alpha k_2^\beta) , \tag{4.7}$$

where the k_i and $\epsilon_i^\nu(k_i)$ denote the four-momenta and the polarization vectors of the outgoing photons, respectively [1]. Alternatively, we can write the amplitude in terms of photon field strength tensors:

$$\mathcal{A}(B_s \to \gamma\gamma) = T^+ F_{\mu\nu}^1 F_2^{\mu\nu} + iT^- F_{\mu\nu}^1 \tilde{F}_2^{\mu\nu} . \tag{4.8}$$

We have for real photons $k_i^2 = 0, \epsilon_i.k_i = 0$ with $i = 1, 2, k_1.k_2 = m_{B_s}^2/2$ and further for a B_s decaying at rest the additional conditions $\epsilon_1.k_2 = \epsilon_2.k_1 = 0$. Then the following equations result:

$$A^+ = -m_{B_s}^2 T^+ , \quad A^- = 2T^- . \tag{4.9}$$

Also, in the rest frame of the B_s meson, the $CP = -1$ amplitude A^- is proportional to the perpendicular spin polarization $\vec{\epsilon_1} \times \vec{\epsilon_2}$, and the $CP = 1$ amplitude A^+ is proportional to the parallel spin polarization $\vec{\epsilon_1}.\vec{\epsilon_2}$. The ratio

$$r_{CP} \equiv |T^+|^2/|T^-|^2 = \frac{4|A^+|^2}{m_{B_s}^4|A^-|^2} \tag{4.10}$$

---

[1] We adopt the convention $Tr(\gamma^\mu\gamma^\nu\gamma^\alpha\gamma^\beta\gamma_5) = 4i\epsilon^{\mu\nu\alpha\beta}$, with $\epsilon^{0123} = +1$.

can be used to study CP violating effects in $B_s \to \gamma\gamma$ decays. We will discuss it together with the $B_s \to \gamma\gamma$ branching ratio in section 4.4.

Using the effective Hamiltonian in eq. (2.18), the CP-even (A^+) and CP-odd (A^-) parts in the SM can be written as (for diagrams see Fig. 4.1 and Fig. 4.2) in a HQET inspired approach:

$$A^+ = -\frac{\alpha G_F}{\sqrt{2}\pi} f_{B_s} \lambda_t \left(\frac{1}{3} \frac{m_{B_s}^4 (m_b^{eff} - m_s^{eff})}{\bar{\Lambda}_s (m_{B_s} - \bar{\Lambda}_s)(m_b^{eff} + m_s^{eff})} C_7^{eff}(\mu) \right.$$

$$\left. - \frac{4}{9} \frac{m_{B_s}^2}{m_b^{eff} + m_s^{eff}} (-m_b J(m_b) + m_s J(m_s)) D(\mu) \right) ,$$

$$A^- = -\frac{\alpha G_F}{\sqrt{2}\pi} 2 f_{B_s} \lambda_t \left(\frac{1}{3} \frac{1}{m_{B_s} \bar{\Lambda}_s (m_{B_s} - \bar{\Lambda}_s)} g\_C_7^{eff}(\mu) \right.$$

$$\left. - \frac{1}{9(m_b^{eff} + m_s^{eff})} (m_b \Delta(m_b) + m_s \Delta(m_s)) D(\mu) \right) , \qquad (4.11)$$

$$- \sum_q Q_q^2 I(m_q) C_q(\mu) +$$

where we have used the unitarity of the CKM-matrix $\sum_{i=u,c,t} V_{is}^* V_{ib} = 0$ and have neglected the contribution due to $V_{us}^* V_{ub} \ll V_{ts}^* V_{tb} \equiv \lambda_t$. In eq. (4.11) N_c is the colour factor ($N_c = 3$ for QCD) and $Q_q = \frac{2}{3}$ for $q = u, c$ and $Q_q = -\frac{1}{3}$ for $q = d, s, b$. The QCD-corrected Wilson coefficients in leading logarithmic approximation [6,7], which are discussed in section 2.2, $C_{1...6}(\mu)$ and $C_7^{eff}(\mu)$, enter the amplitudes in the combinations

$$C_u(\mu) = C_d(\mu) = (C_3(\mu) - C_5(\mu))N_c + C_4(\mu) - C_6(\mu) ,$$

$$C_c(\mu) = (C_1(\mu) + C_3(\mu) - C_5(\mu))N_c + C_2(\mu) + C_4(\mu) - C_6(\mu) ,$$

$$C_s(\mu) = C_b(\mu) = (C_3(\mu) + C_4(\mu))(N_c + 1) - N_c C_5(\mu) - C_6(\mu) ,$$

$$D(\mu) = C_5(\mu) + C_6(\mu) N_c . \qquad (4.12)$$

The Feynman rules used are given in appendix A.3. Note that the chromomagnetic operator O_8 does not contribute here in this order of α_s. The functions $I(m_q)$, $J(m_q)$ and $\Delta(m_q)$ come from the irreducible diagrams with an internal q-type quark propagating, see Fig. 4.1, and are defined as

$$I(m_q) = 1 + \frac{m_q^2}{m_{B_s}^2} \Delta(m_q) ,$$

$$J(m_q) = 1 - \frac{m_{B_s}^2 - 4m_q^2}{4m_{B_s}^2} \Delta(m_q) ,$$

$$\Delta(m_q) = \left(\ln(\frac{m_{B_s} + \sqrt{m_{B_s}^2 - 4m_q^2}}{m_{B_s} - \sqrt{m_{B_s}^2 - 4m_q^2}}) - i\pi \right)^2 \quad \text{for } \frac{m_{B_s}^2}{4m_q^2} \geq 1,$$

$$\Delta(m_q) = -\left(2 \arctan(\frac{\sqrt{4m_q^2 - m_{B_s}^2}}{m_{B_s}}) - \pi \right)^2 \quad \text{for } \frac{m_{B_s}^2}{4m_q^2} < 1. \qquad (4.13)$$

Detailed analysis shows that the diagram Fig. 4.1 requires the calculation of three different types of insertions: The current-current operators $O_{1,2}$ only give a contribution to a charm loop. They have the structure $\gamma_\mu L \otimes \gamma_\mu L$, which leads after integration over the internal quark momentum to the function $I(m_q)$ given above. In contrast, each of the penguin operators $O_{3...6}$ has two possible insertions, a "direct" one and one

after Fierz ordering of the fields. In the former just internal b- and s-quarks appear and the operators have to be "turned" by $\pm 90°$ to generate a diagram consisting of one continuous $b \to s$ fermion line. In the latter the four-Fermi operators, which contribute to all 5 active flavours $q = u, d, s, c, b$, are rearranged with the help of the Fierz transformation given in appendix A.3. This simplifies the calculation as it circumvents a trace over γ-matrices. The procedure is legitimate since the resulting amplitude is (IR and UV) finite. The operators $O_{3,4}$ have the same Dirac structure as $O_{1,2} \sim \gamma_\mu L \otimes \gamma_\mu L$ which is reproduced after Fierz transformation, see eq. (A.21). Therefore, here no new integrals appear. The operators $O_{5,6}$ are of $\gamma_\mu L \otimes \gamma_\mu R$ type. "Direct" insertion leads to the functions $\Delta(m_q), J(m_q)$ given above. They contribute to the $B_s \to \gamma\gamma$ amplitude only via an internal s- and b-quark. Here care must be taken of the left-right structure, which is different for the s- and the b-quark and results in the sign difference in the corresponding term proportional to $D(\mu)$ in the CP-even amplitude A^+ given in eq. (4.11). The Fierz transformation of $O_{5,6}$ results in a scalar/pseudoscalar coupling $\sim R \otimes L$, see eq. (A.22). The analytical expression for such an insertion is minus the one for $\gamma_\mu L \otimes \gamma_\mu L$, which can be checked after explicit calculation. From here the minus signs in the functions eq. (4.12) can be understood.

The parameter $\bar{\Lambda}_s$ enters eq. (4.11) through the bound state kinematics. At the quark and meson level, the decay kinematics are given

$$b(p) \to s(p')\gamma(k_1, \epsilon_1)\gamma(k_2, \epsilon_2) , \tag{4.14}$$

$$B_s(P) \to \gamma(k_1, \epsilon_1)\gamma(k_2, \epsilon_2) , \tag{4.15}$$

respectively. A problem lies now in the intermediate propagators of the reducible diagrams, see Fig. 4.2, where we need to evaluate $p.k_i$ and $p'.k_i$, $i = 1, 2$. The answer cannot be given just by using kinematics, energy/momentum conservation in a chosen frame and a model is necessary here. For definiteness, we consider the decay $B_s \equiv (\bar{b}s) \to \gamma\gamma$. We write the momentum of the $\bar{b}$-quark inside the meson as $p = m_b v + k$, where k is a small residual momentum, v is the 4-velocity, which connects the quark with the meson kinematics through $P = m_{B_s} v$ and P is the momentum of the meson. In the B_s rest frame, $v = (1, 0, 0, 0)$. Now following [16], we average the residual momentum of the $\bar{b}$-quark through

$$< k_\alpha > = -\frac{1}{2m_b}(\lambda_1 + 3\lambda_2)v_\alpha ,$$

$$< k_\alpha k_\beta > = \frac{\lambda_1}{3}(g_{\alpha\beta} - v_\alpha v_\beta) , \tag{4.16}$$

where λ_1, λ_2 are matrix elements from the heavy quark expansion. Using $P = p - p'$, $P.k_i = \frac{m_{B_s}^2}{2}$, $v.k_i = \frac{m_{B_s}}{2}$ and the HQET relation [16]

$$m_{B_s} = m_b + \bar{\Lambda}_s - \frac{1}{2m_b}(\lambda_1 + 3\lambda_2) \tag{4.17}$$

one gets:

$$p.k_i = \frac{m_{B_s}}{2}(m_{B_s} - \bar{\Lambda}_s) ,$$

$$p'.k_i = -\frac{m_{B_s}}{2}\bar{\Lambda}_s ,$$

$$(m_b^{eff})^2 \equiv p^2 = m_b^2 - 3\lambda_2 ,$$

$$(m_s^{eff})^2 \equiv p'^2 = (m_b^{eff})^2 - m_{B_s}^2 + 2m_{B_s}\bar{\Lambda}_s . \tag{4.18}$$

The non-perturbative parameter $\bar{\Lambda}_s$ can be related to $\bar{\Lambda}$, which has been extracted (together with λ_1) from data on semileptonic $B^{\pm}$, B^0 decays in ref. [31], and the measured mass difference $\triangle m = m_{B_s} - m_B = 90$ MeV [39], defining $\bar{\Lambda}_s = \bar{\Lambda} + \triangle m$. The matrix element λ_2 is well determined from the $B^*_{(s)} - B_{(s)}$ mass splitting, $\lambda_2 = 0.12$ GeV^2. With the help of eq. (4.17), the correlated values of $\bar{\Lambda}$ and λ_1 can be transcribed into a correlation between $\bar{\Lambda}_{(s)}$ and m_b. We select 3 representative values [2] $(m_b, \bar{\Lambda}_s) = (5.03, 370), (4.91, 480), (4.79, 590)$ in (GeV, MeV) to study the hadronic uncertainties of our approach. Note that we assume here that λ_1, λ_2 are flavour independent. Furthermore, we have used the definition

$$< 0|\bar{s}\gamma_\mu\gamma_5 b|B_s(P) > \; = \; if_{B_s}P_\mu \, , \tag{4.19}$$

which leads together with the off-shellness of the quarks inside the meson to the matrix element of the pseudoscalar current

$$< 0|\bar{s}\gamma_5 b|B_s(P) > \; = \; -if_{B_s}\frac{m_{B_s}^2}{m_b^{eff} + m_s^{eff}} \, . \tag{4.20}$$

The auxiliary function $g_- = g_-(m_b^{eff}, \bar{\Lambda}_s)$ is defined as

$$g_- = m_{B_s}(m_b^{eff} + m_s^{eff})^2 + \bar{\Lambda}_s(m_{B_s}^2 - (m_b^{eff} + m_s^{eff})^2) \, . \tag{4.21}$$

Note that in the limit $\bar{\Lambda}_s \to m_s$, $m_{b,s}^{eff} \to m_{b,s}$ and using $m_{B_s} = m_b + m_s$ we recover the result obtained by the constituent quark model [32,33,35], ignoring QCD corrections. Using the above expressions, the partial decay width is then given by :

$$\Gamma(B_s \to \gamma\gamma) = \frac{1}{32\pi m_{B_s}}(4|A^+|^2 + \frac{1}{2}m_{B_s}^4|A^-|^2) \, . \tag{4.22}$$

Now, there are 2 new observations to be made:

First, the Wilson coefficients in eq. (4.11) depend on the scale μ. Therefore, since the behaviour of these short-distance (SD) coefficients under renormalization is known from the studies of $B \to X_s\gamma$ [43,44,6,7], one can give an improved width for $B_s \to \gamma\gamma$ by including the leading logarithmic QCD corrections by renormalizing the coefficients $C_{1...6}$ and C_7^{eff} from $\mu = m_W$ down to the relevant scale $\mu \approx \mathcal{O}(m_b)$. The explicit $\mathcal{O}(\alpha_s)$ improvement in the decay width $\Gamma(B_s \to \gamma\gamma)$ requires the calculation of a large number of virtual corrections, which we have not taken into account. Varying the scale μ in the range $\frac{m_b}{2} \leq \mu \leq 2m_b$, one introduces an uncertainty, which can be reduced only when the complete next-to-leading order (NLO)-analysis is available, similar to the recently completed calculation for the $B \to X_s\gamma$ decay [43,44].

The second point concerns the strong dependence of the decay width $\Gamma(B_s \to \gamma\gamma)$ on $\bar{\Lambda}_s$, $\Gamma \sim \mathcal{O}(\frac{1}{\bar{\Lambda}_s^2})$ in eq. (4.22). It originates in the s-quark propagator in the diagram with an intermediate s-quark in Fig. 4.2. In the earlier work the authors of e.g. [32] evaluated the decay width with $m_s \approx m_K$, assuming that the constituent quarks are to be treated as static quarks in the meson. This is a questionable assumption. In the HQET inspired approach, this gets replaced by $\bar{\Lambda}_s$, which is well-defined experimentally. This formalism implies, that the decay width $\Gamma(B_d \to \gamma\gamma)$ will involve the parameter $\bar{\Lambda}$, which avoids the unwanted uncertainty on m_d.

---

[2]We choose $(\lambda_1, \bar{\Lambda}) = (-0.09, 280), (-0.19, 390), (-0.29, 500)$ in (GeV^2, MeV) from Fig. 1 in [31].
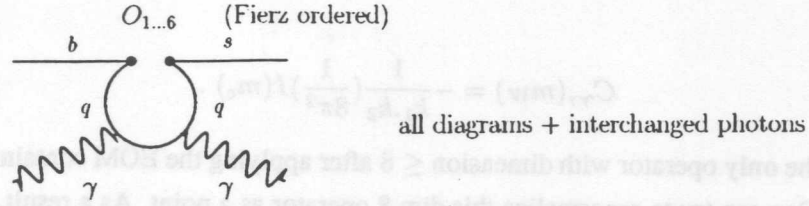
Figure 4.1: *The generic diagram contributing to $b \rightarrow s\gamma\gamma$ in the effective theory due to the (Fierz ordered) four-quark operators. The diagram with interchanged photons is not shown.*
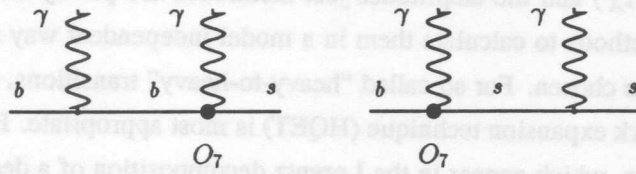

Figure 4.2: *The reducible diagrams contributing to $b \rightarrow s\gamma\gamma$. The blob denotes the FCNC operator O_7. The diagrams with interchanged photons are not shown.*

The branching ratio and the CP ratio as a function of the scale μ for different values of $(m_b, \bar{\Lambda}_s)$ are discussed in section 4.4 including the O_7-type long-distance (LD) estimate.

In the lowest order, which can be recovered at $\mu = m_W$, C_7 and C_2 are the only remaining non-zero Wilson coefficients. The reducible diagram (1PR), which is proportional to C_7, contributes to $A^\pm$, however, the irreducible one (1PI) ($\sim C_2(m_W) = 1$), represented by the charm loop, enters only the CP-odd amplitude A^-. In contrast, in neutral pion decays $\pi^0 \rightarrow \gamma\gamma$ the electromagnetic vector coupling results in an CP-odd amplitude and hence $A^+ = 0$ and the CP ratio $\sim |A^+|^2/|A^-|^2$ vanishes. The authors of [32], analysed the $b \rightarrow s\gamma\gamma$ transition in the lowest order in the full theory (SM). This amounts in the calculation of in total 2×34 diagrams (the factor 2 is due to the diagrams with interchanged photons). They further interpreted the total 1PI amplitude as a (local) FCNC 2 photon operator with canonical field dimension 8:

$$O_{\gamma\gamma} = (Q_c e)^2 \bar{s} \left(F^1_{\mu\nu} \partial^\nu \tilde{F}^{\mu\beta}_2 + F^2_{\nu\mu} \partial^\mu \tilde{F}^{\beta\nu}_1 \right) \gamma_\beta L b \,. \tag{4.23}$$

After applying the EOM to the photonic part of $O_{\gamma\gamma}$ the following Lorentz structure is obtained in the B_s rest frame

$$X = [\epsilon_1.\epsilon_2(\not{k}_1 - \not{k}_2) - \not{\epsilon}_1\not{\epsilon}_2(\not{k}_1 - \not{k}_2)] L \,, \tag{4.24}$$

which leads to the relation $O_{\gamma\gamma} = (Q_c e)^2 k_1.k_2 \bar{s} X b$ and the 1PI amplitude:

$$A(B_s \rightarrow \gamma\gamma)_{1PI}(\mu = m_W) = -\frac{4G_F}{\sqrt{2}} \lambda_t C_{\gamma\gamma}(m_W)\langle O_{\gamma\gamma}\rangle \,. \tag{4.25}$$

Note that we used on-shell conditions for the photons. The initial value of the "Wilson" coefficient is

given as

$$C_{\gamma\gamma}(m_W) = -\frac{1}{k_1.k_2}\left(\frac{1}{8\pi^2}\right)I(m_c) \,. \tag{4.26}$$

Note that $O_{\gamma\gamma}$ is the **only** operator with dimension ≤ 8 after applying the EOM containing 2 photons and 2 fermions [33]. One can try to renormalize this dim 8 operator as a point. As a result, the leading order anomalous dimension of $O_{\gamma\gamma}$ vanishes.

4.2   QCD Sum Rule for the $B_s \to \phi\gamma$ Form Factor

In the description of exclusive B decays hadronic matrix elements $< X|O_i|B >$ are involved. Here X is any hadron (with mass m_X) and the amplitudes just mentioned are purely non-perturbative objects. At present there are two methods to calculate them in a model independent way and, depending on the mass value of X, one can be chosen. For so called "heavy-to-heavy" transitions, where X contains one heavy quark, the heavy quark expansion technique (HQET) is most appropriate. Heavy quark symmetry implies that the form factors, which appear in the Lorentz decomposition of a decay into a hadron with certain spin, are all related to **one** single function, the Isgur-Wise function $\xi(v.v')$ [124]. Here v, v' denote the velocities of the B, X, respectively. Moreover, it can be shown that at the *zero recoil* point, that is where the final hadron is at rest in the rest frame of the decaying B, we have the normalization $\xi(1) = 1$. The behaviour of $\xi(v.v')$ for general values of the argument $v.v' \neq 1$ cannot be calculated. It is of non-perturbative nature. The advantage is that there is just one universal function describing all transitions in the heavy quark limit. From kinematical considerations one can get the possible range of the dot product as $v.v' = (m_B^2 + m_X^2 - q^2)/2m_B m_X$, where $q^2 = (m_B v - m_X v')^2$. The maximal momentum transfer $q_{max}^2 = (m_B - m_X)^2$ corresponds to the minimal value of $v.v' = 1$. The decay under consideration $B_s \to \phi\gamma$ requires $q^2 = 0$ for an on-shell photon, and we have $v.v' = 2.73$. For such "heavy-to-light" decay an extrapolation too far from the zero recoil point is needed, and the QCD sum rule method is more useful.

The decay $B_s \to \phi\gamma$ is CKM allowed and, in the language of the operator basis given in eq. (2.18), involves the operator O_7, (see eq. (4.29) below). It has been studied in the literature in the framework of Light-cone QCD sum rules [125], which is based on the approximate conformal invariance of QCD. Here the sum rule is evaluated in terms of meson wave functions on the light-cone. These universal functions with increasing twist replace the expansion in "classical" QCD sum rules into many vacuum expectation values of operators with increasing dimension. We show the calculation of the form factor F_1 in the decay $B_s \to \phi\gamma$ in the framework of the ordinary QCD sum rules [126], including the contribution from the gluon condensate [37].

4.2.1   Calculation of the sum rule

The amplitude for the $B_s \to \phi\gamma$ transition $\mathcal{A}(B_s \to \phi\gamma) = < \phi\gamma|\mathcal{H}_{eff}|B_s >$ reduces to

$$\mathcal{A}(B_s \to \phi\gamma) = \epsilon^\mu C m_b < \phi(p')|\bar{s}\sigma_{\mu\nu}Rq^\nu b|B_s(p) > \tag{4.27}$$

with the constant C

$$C = \frac{G_F}{\sqrt{2}} \frac{e}{2\pi^2} V_{ts}^* V_{tb} C_7^{\text{eff}}(\mu) \, , \tag{4.28}$$

where we just take the contribution due to the electromagnetic penguin operator O_7

$$O_7 = \frac{e}{16\pi^2} \bar{s}_\alpha \sigma_{\mu\nu} (m_b R + m_s L) b_\alpha F^{\mu\nu} \, , \tag{4.29}$$

into account and put $m_s = 0$, justified by $m_s \ll m_b$. Here ϵ and q are the photon polarization and the (outgoing) photon momentum, respectively. Lorentz decomposition gives further:

$$\begin{aligned}
< \phi(p')|\bar{s}\sigma_{\mu\nu} R q^\nu b|B_s(p) > &= i\epsilon_{\mu\nu\rho\sigma} \epsilon^{\phi\nu} p^\rho p'^\sigma F_1(q^2) \\
&+ (\epsilon_\mu^\phi p.q - p_\mu q.\epsilon^\phi) G(q^2) \, ,
\end{aligned} \tag{4.30}$$

where p, p' denote the four-momenta of the initial B_s-meson and the outgoing ϕ, respectively and ϵ_μ^ϕ is the polarization vector of the ϕ-meson. At $q^2 = 0$ both form factors coincide [127] and it is sufficient to calculate $F_1(0)$. Note, that the form factors introduced above are in general functions of two variables q^2 and p'^2. Since the ϕ is on-shell, we abbreviate here and in the following unless otherwise stated $F_1(q^2) \equiv F_1(q^2, p'^2 = m_\phi^2)$.

The starting point for the sum rule is the three-point function [128]

$$T_{\alpha\mu} = -\int d^4x e^{ipx - ip'y} < 0|T[J_\alpha(x)T_\mu(0)J_5(y)]|0 > \, , \tag{4.31}$$

where $J_\alpha = \bar{s}\gamma_\alpha s$, $J_5 = \bar{s}i\gamma_5 b$ and $T_\mu = \bar{s}\frac{1}{2}\sigma_{\mu\nu}q^\nu b$ correspond to the electromagnetic, pseudoscalar currents and the penguin operator, respectively. Performing now an operator product expansion (OPE) of $T_{\alpha\mu}$, we obtain a perturbative term, the so-called bare loop, and non-perturbative power corrections, diagrammatically shown in Fig. 4.3. The bare loop diagram can be obtained using a double dispersion relation in p^2 and p'^2,

$$T_{bare} = \frac{1}{\pi^2} \int_{m_b^2}^\infty ds \int_0^\infty ds' \frac{\rho(s,s')}{(s-p^2)(s'-p'^2)} + \text{subtractions} \, . \tag{4.32}$$

Technically, the spectral density $\rho(s, s')$ can be calculated by using the Cutkosky rule, namely, by replacing the usual propagator denominator by a delta function: $\frac{1}{k^2 - m^2} \to -2\pi i\delta(k^2 - m^2)\theta(k_0)$. As a result we get

$$\rho(s, s') = \frac{N_c}{8} m_b^4 \frac{s'}{(s-s')^3} \, . \tag{4.33}$$

OPE enables us further to parametrize the non-perturbative effects in terms of vacuum expectation values of gauge-invariant operators up to a certain dimension, the so-called condensates. We consider up to dimension-5 operators; i.e. the quark condensate, gluon condensate and the quark-gluon (mixed) condensate contributions (Fig. 4.3). This calculation is carried out in the fixed point gauge, i.e. $A_\mu x^\mu = 0$. We get

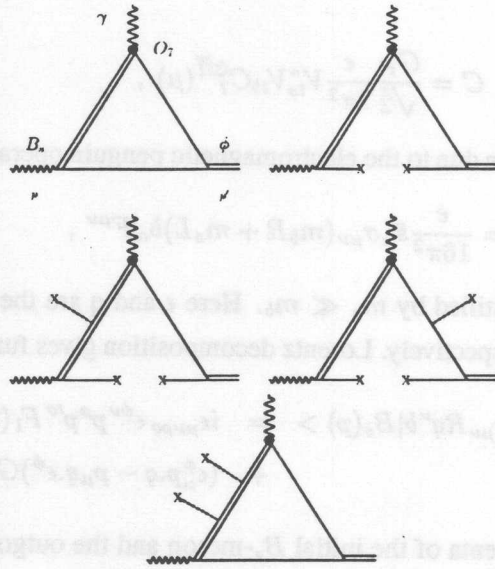$$T_{dim-3} = \frac{-m_b}{2} < \bar{s}s > \frac{1}{(p^2 - m_b^2)p'^2} \, ,$$

Figure 4.3: *Contributions of perturbation theory and of vacuum condensates to the $B_s \rightarrow \phi\gamma$ decay. The dashed lines denote soft gluons.*

$$T_{dim-4} = \frac{\alpha_s}{144\pi} <G^2> \int_0^1 dx \int_0^{1-x} dy \int_0^\infty d\alpha \alpha^3$$
$$\cdot (c_1 + c_2 P^2 + c_3 P'^2)e^{-\alpha(d_1+d_2 P^2+d_3 P'^2)} ,$$
$$T_{dim-5} = \frac{m_b}{2}g <\bar{s}\sigma Gs> [\frac{m_b^2}{2(p^2-m_b^2)^3 p'^2} + \frac{m_b^2}{3(p^2-m_b^2)^2 p'^4}$$
$$+ \frac{1}{2(p^2-m_b^2)^2 p'^2}] ,$$

(4.34)

where

$$c_1 = m_b^4 x^4$$
$$c_2 = m_b^2 x^4(1-x-y) ,$$
$$c_3 = m_b^2 x^3(3+y)(1-x-y) ,$$
$$d_1 = m_b^2 x ,$$
$$d_2 = x(1-x-y) ,$$
$$d_3 = y(1-x-y) .$$

(4.35)

Here we used the exponential representation for the gluon condensate contribution:

$$\frac{1}{D^n} = \frac{1}{(n-1)!} \int_0^\infty d\alpha \, \alpha^{n-1} e^{-\alpha D} .$$

(4.36)

The momenta P, P' in eq. (4.34) are Euclidean.

For the calculation of the physical part of the sum rules we insert a complete set of on-shell states with the same quantum numbers as B_s and ϕ in eq. (4.31) and get a double dispersion relation

$$T_{phys} = \frac{m_{B_s}^2 f_{B_s}}{m_b} f_\phi m_\phi \frac{1}{(p^2-m_{B_s}^2)(p'^2-m_\phi^2)} F_1(0) + \text{continuum} ,$$

(4.37)

where f_ϕ and f_{B_s} are the leptonic decay constants of the ϕ and B_s mesons respectively, defined as usual by

$$
\begin{aligned}
<0|J_\alpha|\phi> &= m_\phi f_\phi \epsilon_\alpha^\phi , \\
<0|J_5|B_s(p)> &= f_{B_s} m_{B_s}^2 / m_b .
\end{aligned}
\tag{4.38}
$$

We have absorbed all higher order states and resonances in the continuum.

Now, we equate the hadron-world with the quark-world by $T_{phys} = T_{bare} + T_3 + T_4 + T_5$. Using quark-hadron duality, we model the continuum contribution by purely perturbative QCD. To be definite, it is the part in eq. (4.32) above the so-called continuum thresholds s_0 and s_0'. To get rid of subtractions and to suppress the contribution of higher order states, we apply a double Borel transformation $\hat{B}$ [126] with respect to p^2 and p'^2. We make use of the following properties of the Borel transform:

$$
\hat{B}\left(\frac{1}{(p^2 - m^2)^n}\right) = \frac{(-1)^n}{(n-1)!} \frac{e^{-m^2/M^2}}{(M^2)^n} ,
\tag{4.39}
$$

$$
\hat{B}(e^{-\alpha p^2}) = \delta(1 - \alpha M^2) .
\tag{4.40}
$$

Finally, this yields the sum rule:

$$
\begin{aligned}
F_1(0) = & \exp\left(\frac{m_{B_s}^2}{M^2} + \frac{m_\phi^2}{M'^2}\right) \frac{m_b}{f_{B_s} f_\phi m_\phi m_{B_s}^2} \left\{ \frac{1}{\pi^2} \int_{m_b^2}^{s_0} ds \int_0^{\bar{s}} ds' \rho(s, s') e^{-s/M^2 - s'/M'^2} \right. \\
& - \frac{m_b}{2} < \bar{s}s > e^{(-m_b^2/M^2)} [1 - m_0^2 (\frac{m_b^2}{4M^4} + \frac{m_b^2}{3M^2 M'^2} - \frac{1}{2M^2})] \\
& \left. + \frac{\alpha_s}{\pi} < G^2 > \int_0^{x_{max}} N(x) dx \right\} ,
\end{aligned}
\tag{4.41}
$$

where $\bar{s} = min(s - m_b^2, s_0')$ and $x_{max} = \frac{M'^2}{M^2 + M'^2}$. Here we used the parametrization

$$
g < \bar{s}\sigma G s > = m_0^2 < \bar{s}s > .
\tag{4.42}
$$

The last term in eq. (4.41) is due to the gluon condensate contribution and the function $N(x)$ is defined by:

$$
\begin{aligned}
N(x) = & \frac{1}{48} \exp\left(-\frac{m_b^2}{M^2(1 - x - xM^2/M'^2)}\right) m_b^2 M'^6 x (m_b^2 M'^4 - 4M^2 M'^4 + 5M^2 M'^4 x \\
& + 5M^4 M'^2 x - M^2 M'^4 x^2 - 2M^4 M'^2 x^2 - M^6 x^2) / (M^4(-M'^2 + M'^2 x + M^2 x)^5)
\end{aligned}
\tag{4.43}
$$

4.2.2 Analysis of the sum rule

First we list the values of the input parameters entering the sum rules (eq. (4.41)), which are not included in Table A.1: $m_0^2 = 0.8$ GeV^2 [129], $< \bar{s}s > = -0.011$ GeV^3 [130], $\frac{\alpha_s}{\pi} < G^2 > = 0.012$ GeV^4 [126], $m_\phi = 1.019$ GeV and $f_\phi = 0.23$ GeV [131].

We do the calculations for two different continuum threshold values $s_0 = 33$ GeV^2 and $s_0 = 35$ GeV^2 and take $s_0' = 1.8$ GeV^2. In Fig. 4.4 we present the dependence of $F_1(0)$ on M^2 and M'^2 for $s_0 = 33$ GeV^2. According to the QCD sum rules method, it is necessary to find a range of M^2 and M'^2, where the dependence of $F_1(0)$ on these parameters is very weak and, at the same time, the power corrections
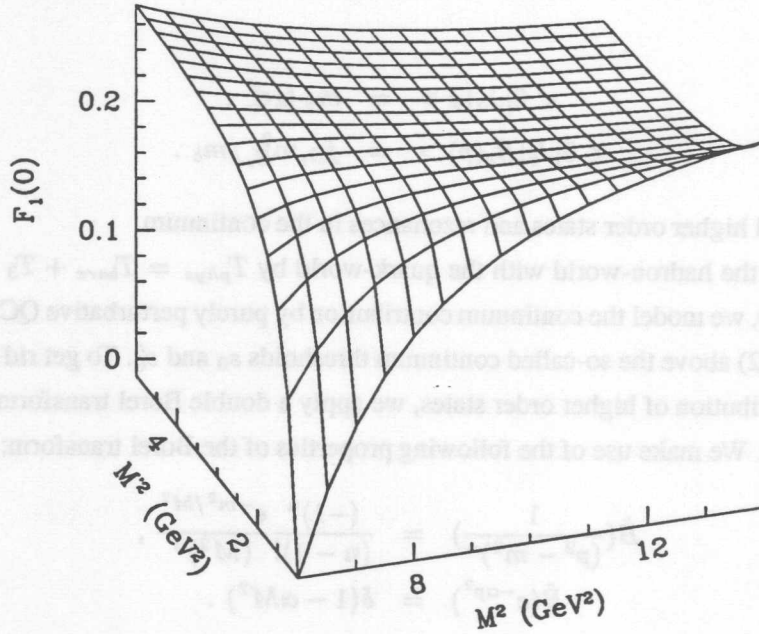
Figure 4.4: *The dependence of the decay constant $F_1(0)$ on the Borel parameters M^2 and M'^2 for $s_0 = 33$ GeV^2.*

and the continuum contribution remain under control. From Fig. 4.4 and Fig. 4.5 follows that the best stability region for $F_1(0)$ is 7 GeV$^2 \leq M^2 \leq 9$ GeV^2, 2 GeV$^2 \leq M'^2 \leq 3$ GeV^2 for $s_0 = 33, 35$ GeV^2. We get:

$$F_1(0) = 0.24 \pm 0.02 \ . \tag{4.44}$$

This agrees for our value of m_b within errors with the result given in the literature, based on Light-cone QCD sum rule calculations [125].

Numerical analysis shows, as also mentioned in [128], that the natural hierarchy of the bare loop, the power corrections and continuum contributions does not hold due to the smallness of the integration region, and the power corrections exceed the bare loop contribution. The gluon condensate contribution is $\leq 1\%$ of the dim-3 + dim-5 condensate contributions and can therefore be safely neglected in numerical calculations.

4.3   The $B_s \to \phi\gamma \to \gamma\gamma$ Amplitude using VMD

Starting with the amplitude for the decay $B_s \to \phi\gamma$ as input, we calculate the CP-odd and CP-even amplitudes in $B_s \to \gamma\gamma$ by using a $\phi \to \gamma$ conversion factor supplied by the VMD model. Here an extrapolation of the $B_s \to \phi\gamma$ decay amplitude from $p'^2 = m_\phi^2$ (needed for $B_s \to \phi\gamma$) to $p'^2 = 0$ (required for $B_s \to \gamma\gamma$) is necessary, such that the ϕ meson propagates as a massless virtual particle before converting into a photon. Note that we suppressed in our notation the dependence of the form factor $F_1(q^2) = F_1(q^2, p'^2 = m_\phi^2)$ on the second argument p'^2. We define here $\bar{F}_1(Q^2) \equiv F_1(q^2 = 0, Q^2)$
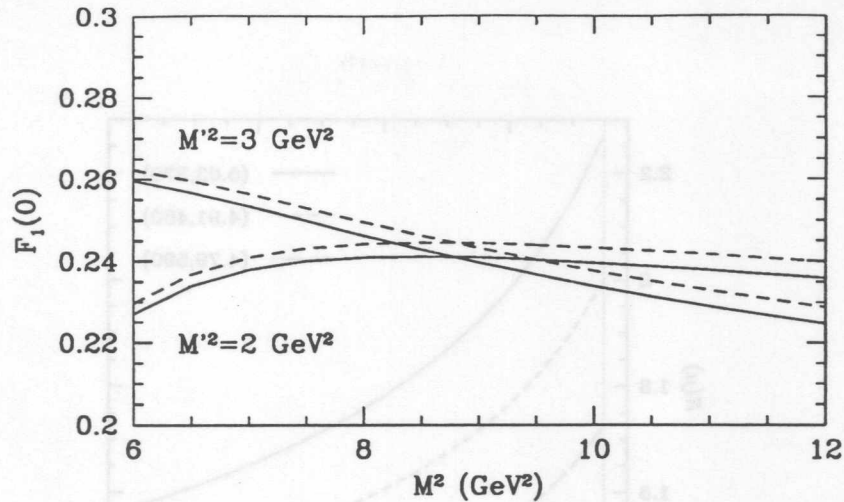
Figure 4.5: *The dependence of the decay constant $F_1(0)$ on the Borel parameter M^2 for fixed M'^2 at $s_0 = 33 \ GeV^2$ (solid) and $s_0 = 35 \ GeV^2$ (dashed).*

for virtual momenta $Q^2 = -p'^2$. We assume, that the form factor $\bar{F}_1(Q^2)$ is dominated by a single pole, which is a good approximation for light mesons and write:

$$\bar{F}_1(Q^2) = \frac{\bar{F}_1(0)}{1 - Q^2/m_{pole}^2} . \tag{4.45}$$

Using an m_{pole} of order $1.7 - 1.9$ GeV, which corresponds to the mass of the higher resonances of the ϕ meson, we estimate $\bar{F}_1(0) = 0.16 \pm 0.02$.

With the help of VMD [74,77,76] and factorization we can now present the amplitude for $B_s \to \gamma\gamma$. Using the intermediate propagator $\frac{-1}{Q^2 + m_\phi^2}$ at $Q^2 = 0$, the $\phi \to \gamma$ conversion vertex from the VMD mechanism

$$< 0|J_{\mu \, em}|\phi(p',\epsilon) >= eQ_s f_\phi(0) m_\phi \epsilon_\mu , \tag{4.46}$$

and the $\mathcal{A}(B_s \to \phi\gamma)$ amplitude, see eq. (4.27), we get:

$$\mathcal{A}(B_s \to \phi\gamma \to \gamma\gamma) = \epsilon_1^\mu(k_1)\epsilon_2^\nu(k_2)\left(A_{LD_{O_7}}^+ g_{\mu\nu} + iA_{LD_{O_7}}^- \epsilon_{\mu\nu\alpha\beta}k_1^\alpha k_2^\beta\right) , \tag{4.47}$$

with the CP-even $(A_{LD_{O_7}}^+)$ and CP-odd $(A_{LD_{O_7}}^-)$ parts:

$$\begin{aligned} A_{LD_{O_7}}^+ &= 2\chi C m_b \frac{m_{B_s}^2 - m_\phi^2}{2}\bar{F}_1(0) \\ &= \sqrt{2}\frac{\alpha G_F}{\pi}\bar{F}_1(0) f_\phi(0)\lambda_t \frac{m_b(m_{B_s}^2 - m_\phi^2)}{3m_\phi}C_7^{\text{eff}}(\mu) , \end{aligned}$$

$$\begin{aligned} A_{LD_{O_7}}^- &= 2\chi C m_b \bar{F}_1(0) \\ &= 2\sqrt{2}\frac{\alpha G_F}{\pi}\bar{F}_1(0) f_\phi(0)\lambda_t \frac{m_b}{3m_\phi}C_7^{\text{eff}}(\mu) , \end{aligned} \tag{4.48}$$

where $f_\phi(0) = 0.18$ GeV [75], $Q_s = -1/3$ and C is defined in eq. (4.28). The factor 2 stems from the addition of the diagrams with interchanged photons. While for the analysis of the sum rule for $B_s \to \phi\gamma$ we have used $f_\phi \equiv f_\phi(m_\phi^2)$, here we take into account the suppression in $f_\phi(Q^2)$ going from $Q^2 = m_\phi^2$ to $Q^2 = 0$. We treated the polarization vector ϵ^ϕ as transversal and replaced $\epsilon \to \epsilon_1$, $\epsilon^\phi \to \epsilon_2$, $q \to k_1$, $p' \to k_2$. The conversion factor χ is defined as $\chi = -eQ_s\frac{f_\phi(0)}{m_\phi}$.
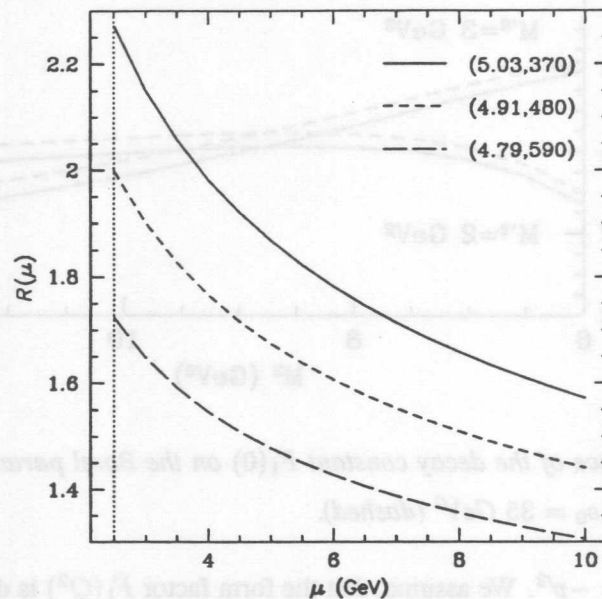
Figure 4.6: *Scale dependence of the ratio $R(\mu)$ defined in eq. (4.50). The solid, short-dashed and long-dashed lines correspond to the values $(m_b, \bar{\Lambda}_s)$ in (GeV, MeV) as indicated in the figure. The dotted line depicts the suggested choice of the scale μ from $B \to X_s\gamma$ studies in NLO [43,44,6,7]. The parameters used are given in Table A.1.*

4.4 Numerical Estimates of the μ, $(m_b, \bar{\Lambda}_s)$ Uncertainties and the O_7 Mediated LD Effects

We combine in this section the results obtained in the previous sections 4.1-4.3, i. e., the LLog QCD corrections, the HQET inspired bound state model and the O_7-type LD effects in $B_s \to \gamma\gamma$ decay. We give numbers for the $B_s \to \gamma\gamma$ branching ratio and CP ratio and discuss the dependences on and the uncertainties due to the renormalization scale μ and the bound state parameters $(m_b, \bar{\Lambda}_s)$.

Adding the O_7-type LD amplitudes (eq. (4.48)) to the short-distance ones (eq. (4.11)), we obtain the $B_s \to \gamma\gamma$ width including the $B_s \to \phi\gamma \to \gamma\gamma$ contribution:

$$\Gamma(B_s \to \gamma\gamma)_{SD+LD_{O_7}} = \frac{1}{32\pi m_{B_s}}\left(4|A^+ + A^+_{LD_{O_7}}|^2 + \frac{1}{2}m^4_{B_s}|A^- + A^-_{LD_{O_7}}|^2\right). \qquad (4.49)$$

Here a comment about double counting is in order. The "LD" amplitudes considered here, which involve the Wilson coefficient C_7, also contain a piece from perturbation theory. It originates in the bare loop diagram in the calculation of the sum rule and enters the value of the form factor F_1. Without this perturbative part, it is not possible to perform an operator product expansion; it corresponds to the leading term in the sum rule and hence there is no way to avoid it. The "SD" amplitudes on the other hand include also contributions from small momenta. As a consequence, by adding the perturbative and the non-perturbative parts in eq. (4.49) there is certainly some double counting present. However, as usual, it is assumed that the SD parts are small in regions where the LD ones are large and hence the effect of this is small.

First we study the leading logarithmic μ-dependence of the ratio

$$R(\mu) = \frac{\Gamma(B_s \rightarrow \gamma\gamma)(\mu)_{SD+LD_{O_7}}}{\Gamma(B_s \rightarrow \gamma\gamma)(m_W)_{SD+LD_{O_7}}} . \tag{4.50}$$

In the numerical analysis we neglect the masses of the light quarks, i. e. we use $I(m_q) = 1$ for $q = u, d, s$ and $m_s \triangle(m_s) = m_s J(m_s) = 0$ in eq. (4.13). From Fig. 4.6 we find an enhancement factor of $1.3 - 2.3$ relative to the lowest order result obtained by setting $\mu = m_W$, depending on the model parameter $(m_b, \bar{\Lambda}_s)$. Varying μ in the range 2.5 GeV $\leq \mu \leq 10.0$ GeV, gives an uncertainty $\triangle R/R(\mu = 5$ GeV$) \approx \pm(17, 19, 22)\%$ for $\bar{\Lambda}_s = (590, 480, 370)$ MeV, respectively. Here one can argue, that the choice $\mu = \frac{m_b}{2}$ takes into account effectively the bulk of the NLO correction as suggested by the NLO calculation for $B \rightarrow X_s \gamma$ [43,44].

Table 4.1 shows the combined μ and model parameter dependence of the branching ratio

$$\mathcal{B}(B_s \rightarrow \gamma\gamma)_{SD+LD_{O_7}} = \frac{\Gamma(B_s \rightarrow \gamma\gamma)_{SD+LD_{O_7}}}{\Gamma_{tot}(B_s)} . \tag{4.51}$$

The dependence of the form factor $\bar{F}_1(m_\phi^2)$ on the b-quark mass has been extrapolated from Fig. 3 [125]. Here $\bar{F}_1(0) = 0.14, 0.15, 0.16$ has been used for $m_b = (5.03, 4.91, 4.79)$ GeV, respectively. Qualitatively,

μ (GeV)	$\bar{\Lambda}_s = 370$ MeV $m_b = 5.03$ GeV	$\bar{\Lambda}_s = 480$ MeV $m_b = 4.91$ GeV	$\bar{\Lambda}_s = 590$ MeV $m_b = 4.79$ GeV
2.5	$1.43 \cdot 10^{-6}$	$8.1 \cdot 10^{-7}$	$5.0 \cdot 10^{-7}$
5.0	$1.18 \cdot 10^{-6}$	$6.8 \cdot 10^{-7}$	$4.3 \cdot 10^{-7}$
10.0	$0.99 \cdot 10^{-6}$	$5.9 \cdot 10^{-7}$	$3.8 \cdot 10^{-7}$

Table 4.1: *Branching ratio $\mathcal{B}(B_s \rightarrow \gamma\gamma)_{SD+LD_{O_7}}$ for selected values $(m_b, \bar{\Lambda}_s)$ and the renormalization scale μ.*

the influence of the LD contribution through $B_s \rightarrow \phi\gamma \rightarrow \gamma\gamma$ reduces the width because of the destructive interference of the LD + SD contributions. To quantify this, we define

$$\kappa \equiv \frac{\mathcal{B}(B_s \rightarrow \gamma\gamma)_{SD+LD_{O_7}} - \mathcal{B}(B_s \rightarrow \gamma\gamma)_{SD}}{\mathcal{B}(B_s \rightarrow \gamma\gamma)_{SD}} , \tag{4.52}$$

with $\Gamma(B_s \rightarrow \gamma\gamma)_{SD}$ given in eq. (4.22). We find, that κ lies in the range:

$$-15\% \leq \kappa \leq -27\% , \tag{4.53}$$

depending mainly on $(m_b, \bar{\Lambda}_s)$. To summarize, lowering the scale μ and $\bar{\Lambda}_s$ enhances the branching ratio $\mathcal{B}(B_s \rightarrow \gamma\gamma)$.

The dependence of the CP ratio [35], [121], here including our LD O_7-type estimate

$$r_{CP\,SD+LD_{O7}} = \frac{4|A^+ + A^+_{LD_{O_7}}|^2}{m_{B_s}^4 |A^- + A^-_{LD_{O_7}}|^2} , \tag{4.54}$$

μ (GeV)	$\bar{\Lambda}_s = 370$ MeV $m_b = 5.03$ GeV	$\bar{\Lambda}_s = 480$ MeV $m_b = 4.91$ GeV	$\bar{\Lambda}_s = 590$ MeV $m_b = 4.79$ GeV
2.5	0.79 (0.80)	0.88 (0.88)	0.89 (0.90)
5.0	0.69 (0.71)	0.73 (0.75)	0.70 (0.73)
10.0	0.61 (0.63)	0.60 (0.63)	0.55 (0.60)
m_W	0.38 (0.41)	0.33 (0.36)	0.26 (0.33)

Table 4.2: *The CP ratio $r_{CP\,SD+LD_{O7}}$ given in eq. (4.54) for selected values $(m_b, \bar{\Lambda}_s)$ and the renormalization scale μ. The values in parentheses correspond to r_{CP} as defined in eq. (4.10) without taking into account the O_7-type LD effects.*

on the renormalization scale and on the bound state parameters can be inferred from Table 4.2. The values of r_{CP} without taking into account the LD contribution from the decay chain $B_s \to \phi\gamma \to \gamma\gamma$ are also shown in parentheses. As can be seen, the O_7-type LD effects reduce the ratio [121]. Further including the LLog QCD corrections enhance $r_{CP\,SD+LD_{O7}}$ by a factor of $1.6 - 3.4$ compared to the lowest order result ($\mu = m_W$), depending on the $(m_b, \bar{\Lambda}_s)$ parameter set. As a rule, both lowering μ and increasing $\bar{\Lambda}_s$ enlarge the value of the CP ratio.

4.5   Estimate of the Long-Distance Contribution through $b \to s\psi$ in $B_s \to \gamma\gamma$ Decay

In this section we estimate the additional LD effect due to the dominant four-quark operators O_1 and O_2 (see eq. (4.56)) through the $B_s \to \phi\psi \to \phi\gamma \to \gamma\gamma$ chain decay. We use at quark level $b \to s\psi$ followed by $b \to s\gamma$ decay [76] and we pass to the hadronic level using the transition form factor $F_1(0)$ from the amplitude $\mathcal{A}(B_s \to \phi)$ [37], [127] given in eq. (4.44). For both the conversions $\psi \to \gamma$ and $\phi \to \gamma$ we employ the Vector Meson Dominance (VMD) model [76]. The conversion $\psi \to \gamma$ needs further manipulation because of the strong contribution from the longitudinal part of the ψ meson. We extract the transverse part using the Golowich-Pakvasa procedure [76], [77]. Further, we calculate the $O_{1,2}$-type LD effect to the $B_s \to \phi\gamma$ decay using the method given in ref. [36], namely, by taking into account the virtual c-quark loop instead of the hadronization of the $\bar{c}c$ pair. This procedure was originally applied to estimate the LD effect in $B \to K^*\gamma$ decay and uses operator product expansion and QCD sum rule techniques. Finally we present amplitudes for the decay chain $B_s \to \phi\psi \to \phi\gamma \to \gamma\gamma$.

4.5.1   The chain process $B_s \to \phi\psi \to \phi\gamma \to \gamma\gamma$

We first consider the additional contribution to $b \to s\gamma$ from $b \to s\psi_i \to s\gamma$, where ψ_i are all $\bar{c}c$ $J = 1$ bound states, see Fig. 4.7. The relevant part of the effective Hamiltonian describing this process is given

as

$$\mathcal{H}_{eff} = 4\frac{G_F}{\sqrt{2}}V_{cs}^*V_{cb}(C_1(\mu)O_1(\mu) + C_2(\mu)O_2(\mu)) \,, \tag{4.55}$$

with the dominant four-Fermi operators

$$O_1 = \bar{s}_\alpha\gamma_\mu\frac{1-\gamma_5}{2}c_\beta\ \bar{c}_\beta\gamma_\mu\frac{1-\gamma_5}{2}b_\alpha \,,$$
$$O_2 = \bar{s}\gamma_\mu\frac{1-\gamma_5}{2}c\ \bar{c}\gamma_\mu\frac{1-\gamma_5}{2}b \,. \tag{4.56}$$

Here α, β are $SU(3)$ colour indices and $V_{ij}^{(*)}$ are the relevant elements of the quark mixing matrix. The initial values of the corresponding Wilson coefficients are $C_1(m_W) = 0$ and $C_2(m_W) = 1$. To include leading logarithmic QCD corrections we evaluate $C_{1,2}(\mu)$ at the relevant scale, $\mu \approx m_b$ for B-decays, and this takes into account short-distance effects from single gluon exchange. The analytical expressions can be found in [6,7]. Further we have used the unitarity of the CKM matrix $V_{cs}^*V_{cb} = -V_{ts}^*V_{tb} - V_{us}^*V_{ub}$ and
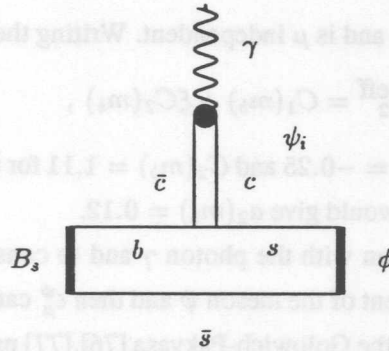

Figure 4.7: *The diagram contributing to $B_s \to \phi\psi \to \phi\gamma$.*

have neglected the contribution due to an internal u-quark, since $V_{us}^*V_{ub} \ll V_{ts}^*V_{tb} = \lambda_t$.

Using factorization, we obtain the inclusive decay amplitude for the process $b \to s\psi$ [76] as

$$\mathcal{A}(b \to s\,\psi(k_1, \epsilon^\psi)) = -i\bar{C}f_\psi(m_\psi^2)m_\psi\bar{s}\gamma^\mu(1-\gamma_5)b\,\epsilon_\mu^\psi \,. \tag{4.57}$$

Here

$$\bar{C} = -\frac{G_F}{\sqrt{2}}\lambda_t a_2(\mu) \tag{4.58}$$

with, assuming naive factorization,

$$a_2(\mu) = C_1(\mu) + \frac{C_2(\mu)}{N_c} \,, \tag{4.59}$$

where $N_c = 3$ in colour $SU(3)$ and k_1, ϵ^ψ are the momentum and the polarization vector of the ψ, respectively. In eq. (4.57) we used the matrix element

$$< 0|\bar{c}\gamma_\mu c|\psi(k_1, \epsilon^\psi) > = f_\psi(m_\psi^2)m_\psi\epsilon_\mu^\psi \,. \tag{4.60}$$

At this stage there is a critical remark about factorization in order, concerning the value of $a_2(\mu)$ used. The decay under consideration is a class II decay following the classification of [132]. In general eq. (4.59) is written as

$$a_2^{\text{eff}} = (C_1(\mu) + \frac{C_2(\mu)}{N_c}) \left[1 + \epsilon_1(\mu)\right] + C_2(\mu)\epsilon_2(\mu) , \tag{4.61}$$

where $\epsilon_1(\mu)$ and $\epsilon_2(\mu)$ parametrize the non-factorizable contributions to the hadronic matrix elements. a_2^{eff} takes into account all contributions of the matrix elements in contrast to $a_2(\mu)$, which assumes naive factorization $\epsilon_1(\mu) = \epsilon_2(\mu) = 0$. Especially $\epsilon_2(\mu)$, which is the colour octet piece, has sizable contributions to naive factorization in class II decays [99]. Furthermore, the additional problem is not to know the correct factorization scale. In order to include the non-factorizable corrections we use the effective coefficient a_2^{eff}, which is determined experimentally from the world average branching ratio of $\bar{B} \to \bar{K}^{(*)}\psi$ as [99]

$$a_2^{\text{eff}} = 0.21 . \tag{4.62}$$

This choice restores the correct scale and is μ independent. Writing the ansatz

$$a_2^{\text{eff}} = C_1(m_b) + \xi C_2(m_b) , \tag{4.63}$$

it follows that $\xi \approx 0.41$ with $C_1(m_b) = -0.25$ and $C_2(m_b) = 1.11$ for the input values given in Table A.1. For comparison, naive factorization would give $a_2(m_b) = 0.12$.

Our aim is to replace the ψ meson with the photon γ and to construct a gauge invariant amplitude. We remove the longitudinal component of the meson ψ and then ϵ_μ^ψ can be converted into the polarization vector ϵ_μ^γ of the photon γ. We utilize the Golowich-Pakvasa [76],[77] procedure making use of the Gordon identity, namely $\gamma_\mu\gamma_\alpha = g_{\mu\alpha} - i\sigma_{\mu\alpha}$. We start with the vertex $\bar{s}\gamma_\mu(1 - \gamma_5)b$ and using the equation of motion $\not{p}b = m_b b$ and momentum conservation $p = p' + k_1$, we get

$$\bar{s}\gamma_\mu(1 - \gamma_5)b = \frac{1}{m_b}\{\bar{s}\gamma_\mu\not{p}'(1 + \gamma_5)b + \bar{s}\gamma_\mu\not{k}_1(1 + \gamma_5)b\} , \tag{4.64}$$

where p, p' are the momenta of the b- and s-quark, respectively. We neglect the first term in eq. (4.64) since $\frac{m_s}{m_b} \ll 1$ and $p'^\mu\epsilon_\mu^T = 0$, which follows from $\epsilon_\mu^T p^\mu = 0$ in the rest frame of the b-quark and the transversality condition $\epsilon_\mu^T k_1^\mu = 0$, where ϵ_μ^T is the transversal polarization vector of the ψ meson [76]. The second term can be written as

$$\frac{1}{m_b}\bar{s}\gamma_\mu\not{k}_1(1 + \gamma_5)b = \frac{1}{m_b}\{\bar{s}(1 + \gamma_5)k_{1\mu}b - i\bar{s}\sigma_{\mu\alpha}k_1^\alpha(1 + \gamma_5)b\} . \tag{4.65}$$

Only the $\sigma_{\mu\alpha}$ term in eq. (4.65) couples to the transversal component of the ψ and we obtain the corresponding amplitude as

$$A(b \to s\psi^T) = -2\bar{C}f_\psi(m_\psi^2)\frac{m_\psi}{m_b}\bar{s}\sigma_{\mu\alpha}k_1^\alpha R b\epsilon_\mu^T , \tag{4.66}$$

where $R = \frac{1+\gamma_5}{2}$ denotes the chiral right projection. Note that the coupling structure is the same as due to a direct use of $O_7 = \frac{e}{16\pi^2}\bar{s}\sigma_{\mu\nu}m_b R b F^{\mu\nu}$ [6,7] with the photon field strength tensor $F^{\mu\nu}$ and $m_s = 0$. For the $\psi^T \to \gamma$ conversion following the VMD mechanism we have

$$< 0|J_{\mu,el}|\psi^T(k_1, \epsilon^T) > = eQ_c f_\psi(0)m_\psi\epsilon_\mu^T , \tag{4.67}$$

where $Q_c = 2/3$ and $f_\psi(0)$ is the coupling at $k_1^2 = 0$, see eq. (4.71). Using the intermediate propagator of the ψ meson at $k_1^2 = 0$, we get

$$\mathcal{A}(b \to s\psi^T \to s\gamma) = 2\bar{C}f_\psi^2(0)\frac{eQ_c}{m_b}\bar{s}\sigma_{\mu\alpha}k_1^\alpha\, R\, b\, \epsilon_\mu^T \,. \tag{4.68}$$

The expression for the amplitude eq. (4.68) can be completed by summing over all $\bar{c}c$ resonant states $\psi(1S), \psi(2S), \psi(3770), \psi(4040), \psi(4160)$ and $\psi(4415)$

$$\mathcal{A}(b \to s\psi_i^T \to s\gamma) = 2\bar{C}\sum_i f_{\psi_i}^2(0)\frac{eQ_c}{m_b}\bar{s}\sigma_{\mu\alpha}k_1^\alpha\, R\, b\epsilon_\mu^T \,. \tag{4.69}$$

The various decay couplings $f_{\psi_i} = f_{\psi_i}(m_{\psi_i}^2)$ are calculated using

$$f_{\psi_i}^2 = \Gamma(\psi_i \to e^+e^-)\frac{3m_{\psi_i}}{Q_c^2 4\pi\alpha^2} \,, \tag{4.70}$$

and the measured widths from [39] and given in Table 4.3.

ψ_i	f_{ψ_i}[GeV]
$f_{\psi(1S)}$	0.405
$f_{\psi(2S)}$	0.282
$f_{\psi(3770)}$	0.099
$f_{\psi(4040)}$	0.175
$f_{\psi(4160)}$	0.180
$f_{\psi(4415)}$	0.145

Table 4.3: *Vector meson coupling constants used in the numerical calculations.*

Now we have to extrapolate the couplings $f_{\psi_i}(k_1^2)$ from $k_1^2 = m_{\psi_i}^2$ to $k_1^2 = 0$. We use the suppression factor [76]

$$\kappa = f_{\psi(1S)}^2(0)/f_{\psi(1S)}^2(m_\psi^2) = 0.12 \tag{4.71}$$

obtained from data on photo production of the ψ and assume κ to be universal for the other (higher) resonances. [3] We now use eq. (4.69) to find the matrix element of $B_s \to \phi\gamma$ through the $b \to s\psi^T \to s\gamma$ transition at quark level. The matrix element [127] is given as

$$<\phi(p')|\bar{s}\sigma_{\mu\alpha}R\,k_1^\alpha b|B_s(p)> = i\epsilon_{\mu\nu\rho\sigma}\epsilon^{\phi\nu}p^\rho p'^\sigma F_1(k_1^2)$$
$$+ (\epsilon_\mu^\phi p.k_1 - p_\mu k_1.\epsilon^\phi)G(k_1^2) \,, \tag{4.72}$$

and we get the amplitude

$$\mathcal{A}(B_s \to \phi\gamma) = 2\bar{C}\epsilon_1^\mu\epsilon^{\phi\nu}\sum_i \frac{f_{\psi_i}^2(0)}{m_b}eQ_c\{i\epsilon_{\mu\nu\rho\sigma}k_1^\rho p'^\sigma$$
$$+ g_{\mu\nu}\frac{m_{B_s}^2 - m_\phi^2}{2}\}F_1(0) \,, \tag{4.73}$$

---

[3]This is consistent with $\kappa = 0.11$ [75] based on a dispersion relation calculation.

where $\epsilon_{1\mu}$, ϵ_ν^ϕ are the polarization vectors and k_1, p' are the momenta of the photon and ϕ meson, respectively. We used $G(k_1^2 = 0) = F_1(k_1^2 = 0)$ [127]. Note, that the form factors introduced above are in general functions of two variables k_1^2 and p'^2. We abbreviated here $F_1(k_1^2) \equiv F_1(k_1^2, p'^2 = m_\phi^2)$ and use the value $F_1(0) = 0.24 \pm 0.02$ [37] obtained in section 4.2.2.

VMD vs soft gluon interaction

Now we want to compare our result for $\mathcal{A}(B_s \to \phi\gamma)$ eq. (4.73) with the same amplitude calculated by the method worked out in [36]. This method is based on the new effective quark-gluon operator obtained by the interaction of the virtual charm quark loop with soft gluons, in contrast to a phenomenological description in terms of ψ resonances converting into a photon, as we used. In this approach, the operator O_1 does not give any contribution to the matrix element of $B_s \to \phi\gamma$ for an on-shell photon. The Fierz transformation of the operator O_2 reads (using eq. (A.13) and eq. (A.21))

$$O_2 = 1/N_c O_1 + 1/2\, O_{octet}\ , \tag{4.74}$$

where

$$O_{octet} = 4(\bar{c}\gamma_\mu \frac{1-\gamma_5}{2}T^a c)(\bar{s}\gamma_\mu \frac{1-\gamma_5}{2}T^a b)\ , \tag{4.75}$$

and $T^a = \lambda^a/2$ are the $SU(3)$ colour generators. Then the only contribution comes from the colour octet part O_{octet}. Using the operator O_{octet} as a vertex of the virtual charm quark loop, which emits a real photon, and taking into account the c-quark-soft gluon interaction, a new effective operator is obtained. The matrix element of this operator between B_s and ϕ meson states gives the long distance amplitude of $B_s \to \phi\gamma$ decay due to the $O_{1,2}$ operators and it is written as (see [36] for details; there the decay amplitude for the decay $B \to K^*\gamma$ is given)

$$\mathcal{A}'(B_s \to \phi\gamma) = 2C'\epsilon_1^\mu \epsilon^{\phi\,\nu}\{i\epsilon_{\mu\nu\rho\sigma}k_1^\rho p'^\sigma L + \frac{m_{B_s}^2 - m_\phi^2}{2}g_{\mu\nu}\tilde{L}\}\ , \tag{4.76}$$

where $C' = \frac{eG_F\lambda_t}{8\sqrt{2}\pi^2}\frac{C_2(\mu)}{9m_c^2}$. The form factors L and $\tilde{L}$ are calculated using QCD sum rules [36],

$$L = \frac{m_b}{m_\phi m_{B_s}^2 f_{B_s} f_\phi}\exp(\frac{m_{B_s}^2}{M^2} + \frac{m_\phi^2}{M'^2})$$

$$\cdot \{\frac{m_b}{48}\{\frac{\alpha_s}{\pi}<G^2>\int_{m_b^2/M^2}^\infty ds\, e^{-s}[\frac{m_b^2}{s} - \frac{M^4}{M^2 + M'^2}(1 - \frac{m_b^2}{sM^2})(1 + \frac{M'^2}{sM^2})]$$

$$- [\frac{m_0^2 <\bar{s}s> m_b^2}{12} - \frac{4\pi\alpha_s <\bar{s}s>^2 m_b}{27}(1 + \frac{m_b^2}{M'^2})]\exp(-\frac{m_b^2}{M^2})\}\ ,$$

$$\tilde{L} = \frac{m_b}{m_\phi m_{B_s}^2 f_{B_s} f_\phi}\exp(\frac{m_{B_s}^2}{M^2} + \frac{m_\phi^2}{M'^2})$$

$$\cdot \{\frac{m_b}{48}\{\frac{\alpha_s}{\pi}<G^2>\int_{m_b^2/M^2}^\infty ds\, e^{-s}[\frac{m_b^2}{s} + \frac{M^4}{M^2 + M'^2}(1 - \frac{m_b^2}{sM^2})(1 + \frac{M'^2}{sM^2})]$$

$$- [\frac{m_0^2 <\bar{s}s> m_b^2}{12} - \frac{16\pi\alpha_s <\bar{s}s>^2 m_b}{27}(1 + \frac{m_b^2}{M'^2})]\exp(-\frac{m_b^2}{M^2})\}\ . \tag{4.77}$$

The Borel parameters M and M' are varied to find the stability region for L and $\tilde{L}$. We use in the evaluation of the sum rules the input parameters given at the beginning of section 4.2.2 and Table A.1. The stability region is reached for $6\,\text{GeV}^2 \le M^2 \le 9\,\text{GeV}^2$ and $2\,\text{GeV}^2 \le M'^2 \le 4\,\text{GeV}^2$ and we get

$$
\begin{aligned}
L &= (0.30 \pm 0.05)\,\text{GeV}^3\,, \\
\tilde{L} &= (0.35 \pm 0.05)\,\text{GeV}^3\,.
\end{aligned}
\tag{4.78}
$$

Writing the amplitude for $B_s \to \phi\gamma$ as

$$
\mathcal{A}^{(')}(B_s \to \phi\gamma) = \epsilon_1^\mu \epsilon^{\phi\,\nu}(i\epsilon_{\mu\nu\rho\sigma}k_1^\rho p'^\sigma\, A^{-(')} + g_{\mu\nu}\,A^{+(')})\,,
\tag{4.79}
$$

and using eq. (4.73), (4.76) and (4.78), we can compare the coefficients obtained by the two different methods and get

$$
\begin{aligned}
\frac{|A^- - A'^-|}{A^-} &\le 10\%\,, \\
\frac{|A^+ - A'^+|}{A^+} &\le 5\%\,.
\end{aligned}
\tag{4.80}
$$

This means, that the amplitudes agree within 10%.

In our approach, the structure of the transition $b \to s\psi^T \to s\gamma$ is proportional to $\sigma_{\mu\alpha}\frac{1+\gamma_5}{2}k_1^\alpha$ (see eq. 4.66), since we removed the longitudinal part of the ψ meson from the amplitude. Further, the form factors $F_1(k_1^2)$ and $G(k_1^2)$ in eq. (4.72) are related for a real photon ($k_1^2 = 0$), $F_1(0) = G(0)$. Therefore, in the amplitude $\mathcal{A}(B_s \to \phi\gamma)$ only one form factor appears, which is $F_1(0)$ in eq. (4.73). However, the form factors L and $\tilde{L}$ in $\mathcal{A}'(B_s \to \phi\gamma)$ given in eq. (4.76) are not related. They are calculated separately using QCD sum rules and this causes the difference between the ratios in eq. (4.80). In spite of the fact that the amplitudes $A^\pm$ and $A'^\pm$ are different from each other, they coincide within the given approximation and theoretical uncertainties lying in both methods.

$O_{1,2}$-type LD amplitudes in $B_s \to \gamma\gamma$

We can now present the amplitude for $B_s \to \gamma\gamma$ due to the chain reaction $B_s \to \phi\psi \to \phi\gamma \to \gamma\gamma$. We use the intermediate propagator at zero momentum transfer and the $\phi \to \gamma$ conversion vertex from the VMD model,

$$
< 0|J_{\mu\,el}|\phi(p',\epsilon^\phi) > = eQ_s f_\phi(0) m_\phi \epsilon_\mu^\phi\,,
\tag{4.81}
$$

where the polarization vector ϵ_μ^ϕ is treated as transversal. To apply the VMD mechanism to the amplitude eq. (4.73), we have to know the form factor at $F_1(k_1^2 = 0, p'^2 = 0)$. We employ the extrapolated value $\bar{F}_1(0) \equiv F_1(0,0) = 0.16 \pm 0.02$ [37] from section 4.3. Then the amplitude can be written with $p' \to k_2$, $\epsilon^\phi \to \epsilon_2$ as

$$
\mathcal{A}(B_s \to \phi\psi \to \phi\gamma \to \gamma\gamma) = \epsilon_1^\mu(k_1)\epsilon_2^\nu(k_2)(g_{\mu\nu}A_{LD_{O_2}}^+ + i\epsilon_{\mu\nu\alpha\beta}k_1^\alpha k_2^\beta A_{LD_{O_2}}^-)\,,
\tag{4.82}
$$

with the CP-even A^+ and CP-odd A^- parts

$$
\begin{aligned}
A_{LD_{O_2}}^+ &= 4\chi\frac{\bar{C}}{m_b}\bar{F}_1(0)\sum_i f_{\psi_i}^2(0)eQ_c\frac{m_{B_s}^2 - m_\phi^2}{2}\,, \\
A_{LD_{O_2}}^- &= 4\chi\frac{\bar{C}}{m_b}\bar{F}_1(0)\sum_i f_{\psi_i}^2(0)eQ_c\,,
\end{aligned}
\tag{4.83}
$$

where $\bar{C}$ is defined in eq. (4.58) and the conversion factor χ is given as $\chi = -eQ_s \frac{f_\phi(0)}{m_\phi}$. Here $f_\phi(0) =$ 0.18 GeV [75] and $Q_s = -1/3$. The extra factor 2 comes from the addition of the diagram with interchanged photons.

4.6   Final Numbers and Conclusion on the Decay $B_s \to \gamma\gamma$

In conclusion, we have reanalysed the decay rate $B_s \to \gamma\gamma$ in the SM and we included leading logarithmic QCD corrections. Our model to incorporate the bound state effects in the B_s meson is inspired by HQET, resulting in the parameters $(m_b, \bar{\Lambda}_s)$. The strong parametric dependence of the decay rate $\Gamma(B_s \to \gamma\gamma)$ and the CP ratio r_{CP} on $(m_b, \bar{\Lambda}_s)$ and on the renormalization scale μ has been studied by us. Further we investigated the influence of the LD contributions due to the chain $B_s \to \phi\gamma \to \gamma\gamma$. Depending on $\bar{\Lambda}_s$, the LD-contributions induced by the operator O_7 become sizeable.

For typical values $(m_b, \bar{\Lambda}_s) = (5\,\text{GeV}, 370\,\text{MeV})$ and $\mu = 5$ GeV, we get (including long-distance effects through O_7) the branching ratio $\mathcal{B}(B_s \to \gamma\gamma)_{SD+LD_{O_7}} = 1.18 \cdot 10^{-6}$, which is a factor 1.9 larger compared to the lowest order estimate for the same values of the parameters. However, varying $(m_b, \bar{\Lambda}_s)$ and μ in the allowed range results in significant variation on the branching ratio (see Table 4.1), yielding

$$0.38 \cdot 10^{-6} \leq \mathcal{B}(B_s \to \gamma\gamma)_{SD+LD_{O_7}} \leq 1.43 \cdot 10^{-6} \ . \tag{4.84}$$

Improving this requires NLO calculation in the decay rate $B_s \to \gamma\gamma$ and further study of the bound state effects. The present best limit on the branching ratio in $B_s \to \gamma\gamma$ decay [117] given in eq. (4.1) is still a factor $\approx 100 - 400$ away from the estimates given here.

Likewise the CP ratio $r_{CP\,SD+LD_{O_7}}$ is rather uncertain. Varying $m_b/2 \leq \mu \leq 2m_b$ and $(m_b, \bar{\Lambda}_s)$ in the allowed range, we get in the SM

$$0.55 \leq r_{CP\,SD+LD_{O7}} \leq 0.89 \ . \tag{4.85}$$

Further we presented a VMD model based calculation of the LD contribution to CP-even A^+ and CP-odd A^- decay amplitudes for $B_s \to \gamma\gamma$ decay due to the inclusive process $b \to s\psi$ via $B_s \to \phi\psi \to \phi\gamma \to \gamma\gamma$ decay. The conversions to photons from both the ψ_i resonances and the ϕ meson lead to two suppressions and make the amplitudes in eq. (4.83) smaller than the ones from the LD effect from the $B_s \to \phi\gamma \to \gamma\gamma$ chain decay [37]. To quantify this we estimated the ratio

$$\rho = \left| \frac{A_{LD_{O_2}}^{+(-)}(B_s \to \phi\psi \to \phi\gamma \to \gamma\gamma)}{A_{LD_{O_7}}^{+(-)}(B_s \to \phi\gamma \to \gamma\gamma)} \right| = 4\pi^2 Q_c \frac{a_2^{\text{eff}}}{|C_7^{\text{eff}}(\mu)|} \sum_i \frac{f_{\psi_i}^2(0)}{m_b^2} \tag{4.86}$$

and found

$$2\% \leq \rho \leq 4\% \ , \tag{4.87}$$

while varying $\frac{m_b}{2} \leq \mu \leq 2m_b$ and allowing a_2^{eff} to have a theoretical error of 25% as stated in [99]. We compared the LD-contribution to $B_s \to \gamma\gamma$ decay resulting from intermediate ψ_i production with the one obtained by the interaction of the virtual charm loop with soft gluons [36]. We see that both amplitudes

are in good agreement within the accuracy of the calculation. The new LD contribution resulting from the four-quark operators O_1 and O_2 is smaller compared to the one of the operator O_7 [37] and affects our old estimate given in eq (4.84) for the branching ratio $\mathcal{B}(B_s \to \gamma\gamma)_{SD+LD_{O_7}}$ [37] by less than 1%.

Another LD effect in $B_s \to \gamma\gamma$ decay is the one due to intermediate D_s, D_s^* mesons [133]. At quark level this involves the four-Fermi operator transition $b \to c\bar{c}s$. The calculation cannot be done by first principles and hence is not straight forward, as the diagrammatic structure is the one of charmed mesons in a loop, which are no fundamental particles. The $B_s D_s^{(*)} D_s^{(*)}$ vertex can be treated with a factorization approach, which is an approximation. The next task is to give a prescription of the electromagnetic coupling of the (charged) $D_s^{(*)}$ mesons, which can be solved by *minimal substitution* as a first approximation. The authors of [133] found a contribution to the branching ratio $B_s \to \gamma\gamma$, which is even **larger** than the SM short-distant one. The channel $B_s \xrightarrow{D_s^{(*)} D_s^{(*)}} \gamma\gamma$ surely needs further investigation.

"New physics"-effects in $B_s \to \gamma\gamma$ decay are found to be small as in $b \to s\gamma\gamma$ they are mainly driven by the Wilson coefficient C_7^{eff}, for which a strong constraint from data on $B \to X_s\gamma$ decay exists. This has accordingly been studied in ref. [121] in the 2HDM and ref. [122] in the MSSM. However, a small enhancement of the branching ratio $\mathcal{B}(B_s \to \gamma\gamma)$ compared to the SM one is still possible in some regions of the parameter space. In models with an extended operator basis the branching ratio and the CP ratio can be much larger than the SM estimates [123].

Once the necessary machines are running, $B_s \to \gamma\gamma$ will certainly get the same attention as the single photon decay $b \to s\gamma$ has at present. In particular, the branching ratio $\mathcal{B}(B_s \to \gamma\gamma) \sim \mathcal{O}(10^{-6})$ is large enough to be observed at the LHC.

Chapter 5
Summary & Future

Rare B decays are one of the most active fields in recent particle physics. Its main theoretical principles and developments of the last 40 years, which are still used, are roughly given as: Of course, the standard model (SM) (1961) [1] and the quark mixing (CKM) matrix (1963) [5]; further phenomenological approaches like vector meson dominance (VMD)(1969) [74] and the Fermi motion model (FM) (1979) [22]. The description of low energy weak processes (1981) [134] made progress with the inclusion of QCD improved perturbative corrections by using renormalization group equation methods yielding the effective Hamiltonian theory (1991) [6–8], [10], together with the onset of the heavy quark expansion (HQE) (1990)[15].

We outlined these methods and applied them to the decays $B \to X_s \ell^+ \ell^-$ with $\ell = e, \mu$ and (partly) to exclusive $B_s \to \gamma\gamma$ decay. We presented quantitative SM based results in terms of distributions, decay rates and moments which can be compared with experimental results.

Concerning $B \to X_s \ell^+ \ell^-$ decays, the invariant dilepton mass spectrum and the Forward-Backward (FB) asymmetry can be used to extract the short-distance coefficients from data in conjunction with the branching ratio in $B \to X_s \gamma$ decay. In this work we have analysed these spectra and their present uncertainties.

Further, apart from being a test of the SM, the decay $B \to X_s \ell^+ \ell^-$ can help to improve our knowledge in certain aspects of long-distance effects:

a) HQE enables a description of B-meson bound state effects in terms of higher dimensional operator matrix elements. We proposed in this thesis the determination of the non-perturbative HQE parameters $\bar\Lambda$ and λ_1 from moments of the hadronic invariant mass in $B \to X_s \ell^+ \ell^-$ decays, as it has been done for the charged current induced decays $B \to X \ell \nu_\ell$ [66]. Given enough data, these parameters can be extracted from $B \to X_s \ell^+ \ell^-$ decays and assuming universality, can be used in the analysis of, e.g., the decay $B \to X_u \ell \nu_\ell$. Likewise, $B \to X_s \ell^+ \ell^-$ decay can be used to test the FM, which can be seen as a model dependent resummation of the theory into a so-called shape function [19,135], and/or to determine its parameters. We remark here that some of the HQE and FM parameters are related.

b) Long-distance (LD) effects occur in $B \to X_s \ell^+ \ell^-$ decays via the decay chain $B \to X_s (J/\Psi, \Psi', \ldots)$ $\to X_s \ell^+ \ell^-$, which we have taken into account with a VMD ansatz. Since in the literature there is no agreement about the implementation of this LD contribution together with the short-distance one, we compared

our approach [18] with alternative ones [28,29] and estimated the resulting uncertainties in the observables. We find that these uncertainties are not the dominant ones in $B \to X_s \ell^+ \ell^-$ decay. Further we have shown, that one can reduce the influence of the $c\bar{c}$ resonances by kinematical cuts. At present, only an experimental analysis can identify the correct procedure to implement the charmonium resonances into an a parton model based calculation in the decays $b \to s \ell^+ \ell^-$.

Finally, by means of building appropriate ratios of (partly) integrated spectra of rare $B \to X_s \ell^+ \ell^-$ and semileptonic $B \to X_{u,c} \ell \nu_\ell$ decays, the uncertainties resulting from bound state effects in the individual decays are expected to cancel out to a large extent.

The essential points reported in this thesis are:

- The calculation of leading power corrections in spectra and hadronic spectral moments in the decay $B \to X_s \ell^+ \ell^-$, including next-to-leading order perturbative $\mathcal{O}(\alpha_s)$ corrections [18,25,26,14].

- The presentation of leading logarithmic QCD corrections to $B_s \to \gamma\gamma$ decay and an estimate of the long-distance effects due to intermediate neutral vector mesons in $B_s \to \gamma\gamma$ decay [37,38].

Besides $B_s \to \gamma\gamma$, other exclusive decay modes relevant for future B-experiments are $B_s \to \ell^+ \ell^-$, $B_s \to \nu\bar{\nu}$ and, of course, $B \to (K, K^*) \ell^+ \ell^-$, $B \to (K, K^*) \nu\bar{\nu}$. The transitions $b \to s \nu\bar{\nu}$ are the cleanest theoretically among other $b \to s$ decays. The expected branching ratio is larger ($\sim 4 \cdot 10^{-5}$ [136]; note, that one has summed over all neutrino flavours) than the one from $b \to s \ell^+ \ell^-$. However, the decay $b \to s \nu\bar{\nu}$ is difficult to observe. Moreover, the inclusive $B \to X_s \tau^+ \tau^-$ channel is interesting. In the SM, its branching ratio is smaller than the one involving light lepton species (e, μ), however, in non-standard multi-Higgs models it can be enhanced through large Higgs coupling of the τ-lepton.

Upgrades of present experiments and planned B-facilities like Hera-B, CLEO, BaBar and Belle are about to start soon and they will be sensitive to branching ratios of order 10^{-6} and below. For an overview see Table 5.1.

This work will help the search for flavour changing neutral current $B \to X_s \ell^+ \ell^-$ and $B_s \to \gamma\gamma$ decays and in particular, will contribute to precise determinations of the HQET parameters and V_{ub} using the inclusive decays $B \to X_s \ell^+ \ell^-$ and $B \to X_u \ell \nu_\ell$ in forthcoming B-facilities.

Expt.	Collider	Beams	$\sqrt{s}$ (GeV)	Year online	$\mathcal{L}$ (10^{33} $cm^{-1}s^{-1}$)	$\sigma(b\bar{b})$ (nb)	$b\bar{b}$ pairs (10^7/yr)	$\beta\gamma c\tau$ (μm)	$\sigma(b\bar{b})$ /$\sigma(q\bar{q})$
CLEO III	CESR	e^+e^-	10	1999	1.2	1	1.2	30	$3 \cdot 10^{-1}$
	CESR-IV		10	?	30	1	30	30	$3 \cdot 10^{-1}$
BaBar	PEP-II	e^+e^- †	10	1999	3-10	1	3-10	270	$3 \cdot 10^{-1}$
Belle	KEK-B	e^+e^- †	10	1999	3-10	1	3-10	200	$3 \cdot 10^{-1}$
HERA-B	HERA	pN	40	1998	—	6-12	50-100	9000	$1 \cdot 10^{-6}$
CDF II D0	Tevatron	$p\bar{p}$	1800	2000	0.2-1.0	10^5	20000	500	$1 \cdot 10^{-3}$
BTeV ‡				2004	0.2			5000	
LHC-B ‡	LHC	pp	14000	2005	0.15	$5 \cdot 10^5$	75000	7000	$5 \cdot 10^{-3}$
Atlas CMS								500	

Table 5.1: *Future B experiments. Parameters which do not change between different experiments at the same collider are entered only once.* † *asymmetric beam energies,* ‡ *forward detector. [3]*

Acknowledgments

I would like to thank Ahmed Ali, who suggested this work. I have benefited from his strong interest in this work and advice in numerous clarifying discussions.

Further the DESY theory group members and visitors are gratefully acknowledged for instructive discussions and practical help, especially Sven Moch, Ulrich Nierste, Tilman Plehn, Michael Plümacher and Mathias Vogt.

Also I would like to thank Erhan Iltan for intense collaboration on $B_s \rightarrow \gamma\gamma$ decay.

Appendix A

Generalities

A.1   Input Parameters

Parameter	Value	Parameter	Value
m_W	80.26 GeV	α^{-1}	129
m_Z	91.19 GeV	$\alpha_s(m_Z)$	0.117 ± 0.005
$\sin^2\theta_W$	0.2325	$|V_{ts}^* V_{tb}|/|V_{cb}|$	1
m_s	0.2 GeV	$\mathcal{B}_{sl}$	$(10.4 \pm 0.4)\,\%$
m_c	1.4 GeV	λ_1	$-0.20\ \text{GeV}^2$
m_b	4.8 GeV	λ_2	$+0.12\ \text{GeV}^2$
m_t	175 ± 5 GeV	$\Gamma_{tot}(B_s)$	$4.09 \cdot 10^{-13}$ GeV
μ	$m_b{}^{+m_b}_{-m_b/2}$	f_{B_s}	0.2 GeV
$\Lambda^{(5)}_{QCD}$	$0.214^{+0.066}_{-0.054}$ GeV	m_{B_s}	5.369 GeV

Table A.1: *Values of the input parameters used in the numerical calculations, unless otherwise specified.*

A.2   QCD

The QCD Lagrangian reads in covariant gauge [137] (A^a_μ: gluon field)

$$\mathcal{L}_{QCD} = \sum_{q=u,d,s,c,b,t} \bar{q}(i\not{D} - m_q)q - \frac{1}{4}G^a_{\mu\nu}G^{a\,\mu\nu} + \mathcal{L}_{fix} + \mathcal{L}_{ghosts}\,, \tag{A.1}$$

where the gauge fixing term and the one for ghosts c^a, $\bar{c}^a$ are given as

$$\mathcal{L}_{fix} = -\frac{1}{2\xi}(\partial \cdot A^a)^2\,, \tag{A.2}$$

$$\mathcal{L}_{ghosts} = \bar{c}^a \partial \cdot D^{ab} c^b\,. \tag{A.3}$$

The chromomagnetic field strength tensor and covariant derivative are written as

$$G^a_{\mu\nu} = \partial_\mu A^a_\nu - \partial_\nu A^a_\mu + g f^{axy} A^x_\mu A^y_\nu\,, \tag{A.4}$$

$$D_\mu = \partial_\mu - ig T^x A_\mu^x , \tag{A.5}$$

$$D_\mu^{ab} = \delta^{ab}\partial_\mu - g f^{abx} A_\mu^x , \tag{A.6}$$

where f^{abx} are the structure constants of $SU(3)$, defined by

$$[T^a, T^b] = i f^{abx} T^x . \tag{A.7}$$

We have the identities

$$[D_\mu, D_\nu] = -ig T^x G_{\mu\nu}^x , \tag{A.8}$$

$$D_\mu^{ax} D_\nu^{xb} - D_\nu^{ax} D_\mu^{xb} = -g f^{abx} G_{\mu\nu}^x . \tag{A.9}$$

Often the abbreviation is used

$$G_{\mu\nu} = G_{\mu\nu}^a T^a . \tag{A.10}$$

T^a, $a = 1, \ldots, 8$ are the generators of QCD. They are related to the Gell-Mann (3×3) matrices λ^a through $T^a = \frac{\lambda^a}{2}$. The T^a obey the following relations $(i, j, k = 1, 2, 3)$

$$Sp(T_a) = 0 , \tag{A.11}$$

$$Sp(T_a T_b) = \delta_{ab}/2 , \tag{A.12}$$

$$T_{ij}^a T_{kl}^a = -\frac{1}{2N_c}\delta_{ij}\delta_{kl} + \frac{1}{2}\delta_{ik}\delta_{jl} , \tag{A.13}$$

$$T_{il}^a T_{lk}^a = \delta_{ik} C_F , \tag{A.14}$$

with the invariant C_F is in an arbitrary $SU(N_c)$ given as

$$C_F = \frac{N_c^2 - 1}{2N_c} \ \left(= \frac{4}{3} \text{ for } N_c = 3\right) . \tag{A.15}$$

The coefficients of the QCD beta function (see eq. (2.30)) are written as:

$$\beta_0 = \frac{11N_c - 2N_f}{3} , \tag{A.16}$$

$$\beta_1 = \frac{34N_c^2 - 10N_c N_f - 6C_F N_f}{3} . \tag{A.17}$$

Here, N_c denotes the number of colours ($N_c = 3$ for QCD) and N_f denotes the number of *active* flavours ($N_f = 5$ for the effective Hamiltonian theory relevant for b decays).

A.3 Feynman Rules

The covariant derivative consistent with our definition of the operator basis and the corresponding Wilson coefficients given in section 2.2 is [51]

$$D_\mu \equiv \partial_\mu + ig T^a A_\mu^a + ie Q A_\mu , \tag{A.18}$$

where A^a, A denote the polarization four-vectors of the gluon, photon respectively. Note that the sign convention of the strong coupling here is opposite to the usual one appearing in QCD text books [137,

138] given in eq. (A.5), but can be made coincident with the substitution $g \to -g$. The Feynman rules consistent with eq. (A.18) are given here with boson propagators in Feynman gauge. In a general gauge with gauge parameter ξ they are written as:

$$-i\frac{g_{\mu\nu} + (\xi - 1)k_\mu k_\nu/(k^2 + i\epsilon)}{k^2 + i\epsilon}\,, \tag{A.19}$$

with $\xi = 1, 0$ corresponding to Feynman, Landau gauge, respectively. The rules should be complemented

$$i\frac{1}{\not{p} - m_q + i\epsilon}\delta_{jk}$$

$$-i\frac{g_{\mu\nu}}{k^2 + i\epsilon}\delta_{ab}$$

$$-ieQ\gamma_\mu, -igT^a_{kj}\gamma_\mu$$

by

- evaluate fermion lines **against** the momentum flow

- add a (-1) for a closed fermion loop and perform the trace over the string of γ matrices

The rule for an O_7 operator insertion is, using $\partial_\mu = iq_\mu$ for an **out going** photon and further $\epsilon \cdot q = 0$ for a real photon, and $F^{\mu\nu} = \partial^\mu A^\nu - \partial^\nu A^\mu$

$$\sigma F = \sigma_{\mu\nu} F^{\mu\nu} = i[\not{\partial}, \not{A}] = 2\gamma_\mu \not{q} \epsilon^\mu\,. \tag{A.20}$$

The Fierz transformation in $d = 4$ dimensions is defined as:

$$(\bar{q}_1 \gamma_\mu L q_2)(\bar{q}_3 \gamma_\mu L q_4) = +(\bar{q}_1 \gamma_\mu L q_4)(\bar{q}_3 \gamma_\mu L q_2)\,, \tag{A.21}$$

$$(\bar{q}_1 \gamma_\mu L(R) q_2)(\bar{q}_3 \gamma_\mu R(L) q_4) = (-2)(\bar{q}_1 R(L) q_4)(\bar{q}_3 L(R) q_2)\,. \tag{A.22}$$

A.3.1 Feynman Rules in the Heavy Quark Limit of QCD

The effective Lagrangian in the limit of an infinitely heavy quark h with mass $m_Q \to \infty$ is given by $\mathcal{L}_{HQET} = \bar{h}iv.Dh$. Here v denotes the velocity ($v^2 = 1$) of a heavy quark h with momentum $p = m_Q v + k$ and small residual momentum k of order Λ_{QCD}. These rules are consistent with the definition of the covariant QCD derivative in eq. (A.5), which causes a sign difference in the quark gluon/photon coupling compared to the weak effective Hamiltonian rules above, based on the convention eq. (A.18). A heavy quark h is represented by a double line.

$$\xrightarrow{\quad h \quad}_{j \qquad k} \qquad i\frac{1+\not{v}}{2}\frac{1}{v\cdot k+i\epsilon}\delta_{jk}$$

$$\xrightarrow{\quad \mu \quad}_{j \qquad k} \qquad +ieQv_\mu, \ +igT^a_{kj}v_\mu$$

A.4 Utilities

A variety of tools for 1-loop calculations is collected in the appendix of ref. [138].

Distributions

$$\delta(x) = \frac{1}{2\pi}\int_{\mathbf{R}} dq e^{iqx} dq , \tag{A.23}$$

$$\theta(x) = \lim_{\epsilon\to 0}\frac{-i}{2\pi}\int_{\mathbf{R}} dq \frac{e^{iqx}}{q-i\epsilon} dq , \tag{A.24}$$

$$\frac{d\theta}{dx}(x) = \delta(x) . \tag{A.25}$$

Geometrical series

$$\frac{1}{1\pm x} = 1 \mp x + x^2 + \sum_{n=3}^{\infty}(\mp x)^n . \tag{A.26}$$

Fit quality χ^2 (see also [39] statistics section), dof: degrees of freedom

$$\chi^2 = \sum_{\text{data points}} |\frac{\text{data-curve}}{\text{error}}|^2 , \tag{A.27}$$

$$\frac{\chi^2}{dof} = \frac{\chi^2}{N_{\text{data points}} - N_{\text{Fit parameters}}} . \tag{A.28}$$

$\frac{\chi^2}{dof}$ should be around 1, if it is much smaller, the errors are underestimated, if it is large, the model fails.

Special Functions useful for loops

Poly logarithms:

$$Li_n(z) = \sum_{k=1}^{\infty}\frac{z^k}{k^n}; \ |z| < 1 , \tag{A.29}$$

$$Li_2(z) = -\int_0^z \frac{dt}{t}\ln(1-t) . \tag{A.30}$$

Spence function

$$Sp(z) \equiv Li_2(z) = -\int_0^1 \frac{dt}{t}\ln(1-zt) , \tag{A.31}$$

$$Sp(0) = 0 , \ Sp(1) = \frac{\pi^2}{6} , \ Sp(-1) = \frac{\pi^2}{12} , \tag{A.32}$$

$$Sp(z) = -Sp(1-z) + \frac{\pi^2}{6} - \ln(z)\ln(1-z) , \qquad (A.33)$$

$$Sp(z) = -Sp(\frac{1}{z}) - \frac{\pi^2}{6} - \frac{1}{2}\ln^2(-z) . \qquad (A.34)$$

Useful identities for loops:

$$\arctan(z) = \frac{1}{2i}\ln\frac{1+iz}{1-iz} , \quad \operatorname{arctanh}(z) = \frac{1}{2}\ln\frac{1+z}{1-z} . \qquad (A.35)$$

Phase space element, $d^3\vec{p} = |\vec{p}|^2 d|\vec{p}| d\cos\theta d\phi$, $\cos\theta \in [-1,+1]$, $\phi \in [0,2\pi[$.

$$\frac{d^3\vec{p}}{2E} = \int d^4p\,\delta(p^2-m^2)\theta(E) \ ; \ E = \sqrt{\vec{p}^2+m^2} . \qquad (A.36)$$

Dirac algebra identities, for more see ref. [139], especially the appendix.

$$\{\gamma_\mu,\gamma_\nu\} = 2g_{\mu\nu} , \ \ \sigma_{\mu\nu} = \frac{i}{2}[\gamma_\mu,\gamma_\nu] , \ \ \gamma_\mu\gamma_\nu = g_{\mu\nu} - i\sigma_{\mu\nu} . \qquad (A.37)$$

A useful tool within this context is the TRACER routine [140] running under the symbolic algebra program mathematica.

Chiral projectors $L(R) \equiv (1 \mp \gamma_5)/2$:

$$\gamma_5^2 = 1 , \ \gamma_5^\dagger = \gamma_5 , \qquad (A.38)$$

$$(L(R))^2 = L(R) , \ LR = RL = 0 , \ (L(R))^\dagger = L(R) . \qquad (A.39)$$

Further we have

$$\gamma_0^2 = 1 , \ \gamma_0^\dagger = \gamma_0 . \qquad (A.40)$$

Fermion fields

$$\overline{\psi} \equiv \psi^\dagger\gamma_0 = (\psi^*)^T\gamma_0 , \ \ \psi_{L(R)} \equiv L(R)\psi ,$$
$$\overline{\psi_{L(R)}} = \overline{L(R)\psi} = (L(R)\psi)^\dagger\gamma_0 = \psi^\dagger(L(R))^\dagger\gamma_0 = \psi^\dagger\gamma_0 R(L) = \overline{\psi}R(L) . \qquad (A.41)$$

Appendix B

$B \to X_s \ell^+ \ell^-$ Dilepton Invariant Mass Distributions and FB Asymmetry

B.1 The Functions $T_i^{(j)}(v.\hat{q}, \hat{s})$

In this appendix we list the functions $T_i^{(j)}(v.\hat{q}, \hat{s})$, $(i = 1, 2, 3)$ with $j = 0, 1, 2, s, g, \delta$, (defined in eq. (3.55)), representing the power corrections in $b \to s\ell^+\ell^-$ up to and including terms of order m_B/m_b^3. The parton model contributions $T_i^{(0)}$ are given in eqs. (B.1) - (B.3).

$$T_1^{(0)L/R} = -\frac{1}{x}\frac{m_B}{m_b}\left\{(1 - v\cdot\hat{q})|C_9^{\text{eff}} \mp C_{10}|^2\right.$$
$$+\frac{4}{\hat{s}^2}\left[\left(1 + \hat{m}_s^2\right)\left(2(v\cdot\hat{q})^2 - \hat{s}(v\cdot\hat{q}) - \hat{s}\right) - 2\hat{m}_s^2\,\hat{s}\right]|C_7^{\text{eff}}|^2$$
$$\left.+\frac{4}{\hat{s}}\left[v\cdot\hat{q} - \hat{s} - \hat{m}_s^2(v\cdot\hat{q})\right]\text{Re}\left[(C_9^{\text{eff}} \mp C_{10})^*C_7^{\text{eff}}\right]\right\}, \tag{B.1}$$

$$T_2^{(0)L/R} = -\frac{2}{x}\frac{m_B}{m_b}\left\{|C_9^{\text{eff}} \mp C_{10}|^2 - \frac{4}{\hat{s}}\left(1 + \hat{m}_s^2\right)|C_7^{\text{eff}}|^2\right\}, \tag{B.2}$$

$$T_3^{(0)L/R} = \frac{1}{x}\frac{m_B}{m_b}\left\{-|C_9^{\text{eff}} \mp C_{10}|^2 - \frac{4}{\hat{s}^2}\left[2(v\cdot\hat{q}) - \hat{s}\right]\left[1 - \hat{m}_s^2\right]|C_7^{\text{eff}}|^2\right.$$
$$\left.-\frac{4}{\hat{s}}\left(\hat{m}_s^2 + 1\right)\text{Re}\left[(C_9^{\text{eff}} \mp C_{10})^*C_7^{\text{eff}}\right]\right\}, \tag{B.3}$$

$$T_1^{(1)L/R} = -\frac{1}{3}\frac{m_B}{m_b^3}(\lambda_1 + 3\lambda_2)\left\{\left[\frac{1}{x} - \frac{2}{x^2}\left(\hat{s} - (v\cdot\hat{q})^2\right)\right]|C_9^{\text{eff}} \mp C_{10}|^2\right. \tag{B.4}$$
$$+\frac{4}{\hat{s}^2}\left[\frac{1}{x}\left(\hat{s} - 2(v\cdot\hat{q})^2\right) - \frac{2}{x^2}\left(\hat{s}^2 - 2\hat{s}(v\cdot\hat{q}) - \hat{s}(v\cdot\hat{q})^2 + 2(v\cdot\hat{q})^3\right)\right](1 + \hat{m}_s^2)|C_7^{\text{eff}}|^2$$
$$\left.-(\hat{s} - v\cdot\hat{q}^2)\,\hat{m}_s^2\frac{8}{\hat{s}x^2}\,\text{Re}(C_9^{\text{eff}} \mp C_{10})^*C_7^{\text{eff}}\right\},$$

$$T_2^{(1)L/R} = -\frac{2}{3}\frac{m_B}{m_b^3}(\lambda_1 + 3\lambda_2)\left[\frac{1}{x} + \frac{2}{x^2}v\cdot\hat{q}\right]\left[-|C_9^{\text{eff}} \mp C_{10}|^2 + \frac{4}{\hat{s}}(1 + \hat{m}_s^2)|C_7^{\text{eff}}|^2\right], \tag{B.5}$$

$$T_3^{(1)L/R} = -\frac{2}{3}\frac{m_B}{m_b^3}(\lambda_1 + 3\lambda_2)\left\{\frac{1}{x^2}(1 - v\cdot\hat{q})|C_9^{\text{eff}} \mp C_{10}|^2\right.$$
$$\left.-\frac{4}{\hat{s}^2}\left[\frac{1}{x}v\cdot\hat{q} - \frac{1}{x^2}\left(\hat{s} + \hat{s}(v\cdot\hat{q}) - 2(v\cdot\hat{q})^2\right)\right](1 - \hat{m}_s^2)|C_7^{\text{eff}}|^2\right.$$

$$-v \cdot \hat{q}\, \hat{m}_s^2 \frac{4}{\hat{s} x^2}\, \mathrm{Re}(C_9^{\mathrm{eff}} \mp C_{10})^* C_7^{\mathrm{eff}} \Big\} \, , \tag{B.6}$$

$$T_1^{(2)L/R} = \frac{1}{3}\frac{m_B}{m_b^3}\lambda_1 \left\{ \left[-\frac{4}{x^3}\left(\hat{s} - (v\cdot\hat{q})^2\right) + \frac{3}{x^2} \right](1 - v\cdot\hat{q})|C_9^{\mathrm{eff}} \mp C_{10}|^2 \right.$$
$$-\frac{4}{\hat{s}^2 x^3}\Big[-4\hat{s}^2 - 12\hat{m}_s^2\hat{s}^2 + 3\hat{s}x + 9\hat{m}_s^2\hat{s}x - 4\hat{s}^2 v\cdot\hat{q} - 4\hat{m}_s^2\hat{s}^2 v\cdot\hat{q} + 7\hat{s}x v\cdot\hat{q}$$
$$+7\hat{m}_s^2\hat{s}x v\cdot\hat{q} + 12\hat{s}v\cdot\hat{q}^2 + 20\hat{m}_s^2\hat{s}v\cdot\hat{q}^2 - 6x v\cdot\hat{q}^2 - 6\hat{m}_s^2 x v\cdot\hat{q}^2 + 4\hat{s}v\cdot\hat{q}^3$$
$$+4\hat{m}_s^2 v\cdot\hat{q}^3\hat{s} - 4x v\cdot\hat{q}^3 - 4\hat{m}_s^2 x v\cdot\hat{q}^3 - 8v\cdot\hat{q}^4 - 8\hat{m}_s^2 v\cdot\hat{q}^4 \Big]|C_7^{\mathrm{eff}}|^2$$
$$+\frac{4}{\hat{s}x^3}\Big[4\hat{s}^2 - 5\hat{s}x - 4\hat{s}v\cdot\hat{q} + 4\hat{m}_s^2\hat{s}v\cdot\hat{q} + 3x v\cdot\hat{q} - 3\hat{m}_s^2 x v\cdot\hat{q} - 4\hat{s}v\cdot\hat{q}^2 + 2x v\cdot\hat{q}^2$$
$$\left. +4v\cdot\hat{q}^3 - 4\hat{m}_s^2 v\cdot\hat{q}^3 \Big] \mathrm{Re}\left[(C_9^{\mathrm{eff}} \mp C_{10})^* C_7^{\mathrm{eff}}\right] \right\} \, , \tag{B.7}$$

$$T_2^{(2)L/R} = -\frac{2}{3}\frac{m_B}{m_b^3}\lambda_1 \left[\frac{4}{x^3}\left(\hat{s} - (v\cdot\hat{q})^2\right) - \frac{3}{x^2} - \frac{2}{x^2}v\cdot\hat{q} \right]$$
$$\left(|C_9^{\mathrm{eff}} \mp C_{10}|^2 - \frac{4}{\hat{s}}(1 + \hat{m}_s^2)\, |C_7^{\mathrm{eff}}|^2 \right) \, , \tag{B.8}$$

$$T_3^{(2)L/R} = -\frac{1}{3}\frac{m_B}{m_b^3}\lambda_1 \left\{ \left[\frac{4}{x^3}\left(\hat{s} - (v\cdot\hat{q})^2\right) - \frac{5}{x^2} \right]|C_9^{\mathrm{eff}} \mp C_{10}|^2 \right.$$
$$+\frac{4}{\hat{s}^2 x^3}\Big[-4\hat{s}^2 + 5\hat{s}x + 8\hat{s}v\cdot\hat{q} - 6x v\cdot\hat{q} + 4\hat{s}v\cdot\hat{q}^2 - 4x v\cdot\hat{q}^2 - 8v\cdot\hat{q}^3 \Big](1 - \hat{m}_s^2)|C_7^{\mathrm{eff}}|^2$$
$$\left. +\frac{4}{\hat{s}x^3}\Big[(4\hat{s} - 3x - 4v\cdot\hat{q}^2)(1 + \hat{m}_s^2) - 2x v\cdot\hat{q} \Big] \mathrm{Re}\left[(C_9^{\mathrm{eff}} \mp C_{10})^* C_7^{\mathrm{eff}}\right] \right\} \, , \tag{B.9}$$

$$T_1^{(s)L/R} = \frac{2}{\hat{s}}\frac{m_B}{x\, m_b^3}(\lambda_1 + 3\lambda_2)\left[(\hat{s} - v\cdot\hat{q})\mathrm{Re}\left[(C_9^{\mathrm{eff}} \mp C_{10})^* C_7^{\mathrm{eff}}\right] + 2\hat{m}_s^2|C_7^{\mathrm{eff}}|^2 \right] \, , \tag{B.10}$$

$$T_2^{(s)L/R} = 0 \, , \tag{B.11}$$

$$T_3^{(s)L/R} = -\frac{2}{\hat{s}}\frac{m_B}{x\, m_b^3}(\lambda_1 + 3\lambda_2)\mathrm{Re}\left[(C_9^{\mathrm{eff}} \mp C_{10})^* C_7^{\mathrm{eff}}\right] \, , \tag{B.12}$$

$$T_1^{(g)L/R} = \frac{1}{x^2}\frac{m_B}{m_b^3}\lambda_2 \left\{ -(1 - v\cdot\hat{q})|C_9^{\mathrm{eff}} \mp C_{10}|^2 \right.$$
$$+\frac{4}{\hat{s}^2}\Big[\hat{s} + 3\hat{m}_s^2\hat{s} + \hat{s}(v\cdot\hat{q})(1 + \hat{m}_s^2) - 2(v\cdot\hat{q})^2(1 + \hat{m}_s^2) \Big]|C_7^{\mathrm{eff}}|^2$$
$$\left. +\frac{4}{\hat{s}}(\hat{s} - v\cdot\hat{q}(1 - \hat{m}_s^2))\mathrm{Re}\left[(C_9^{\mathrm{eff}} \mp C_{10})^* C_7^{\mathrm{eff}}\right] \right\} \, , \tag{B.13}$$

$$T_2^{(g)L/R} = \frac{-2}{x^2}\frac{m_B}{m_b^3}\lambda_2 \left\{ -|C_9^{\mathrm{eff}} \mp C_{10}|^2 - \frac{4}{\hat{s}}(1 + \hat{m}_s^2)|C_7^{\mathrm{eff}}|^2 - 4\mathrm{Re}\left[(C_9^{\mathrm{eff}} \mp C_{10})^* C_7^{\mathrm{eff}}\right] \right\} \, , \tag{B.14}$$

$$T_3^{(g)L/R} = \frac{-1}{x^2}\frac{m_B}{m_b^3}\lambda_2 \left\{ |C_9^{\mathrm{eff}} \mp C_{10}|^2 + \frac{4}{\hat{s}^2}[2(v\cdot\hat{q}) - \hat{s}](1 - \hat{m}_s^2)|C_7^{\mathrm{eff}}|^2 \right.$$
$$\left. +\frac{4}{\hat{s}}(1 + \hat{m}_s^2)\mathrm{Re}\left[(C_9^{\mathrm{eff}} \mp C_{10})^* C_7^{\mathrm{eff}}\right] \right\} \, , \tag{B.15}$$

$$T_1^{(\delta)L/R} = \frac{1}{2}\frac{m_B}{m_b^3}(\lambda_1 + 3\lambda_2)\left\{ \left[\frac{1}{x} - \frac{2}{x^2}(1 - v\cdot\hat{q})^2 \right]|C_9^{\mathrm{eff}} \mp C_{10}|^2 \right.$$
$$-\frac{4}{\hat{s}^2 x^2}\Big[-2\hat{s} - 6\hat{m}_s^2\hat{s} + \hat{s}x + \hat{m}_s^2\hat{s}x + 4\hat{m}_s^2\hat{s}v\cdot\hat{q} + 4v\cdot\hat{q}^2 + 4\hat{m}_s^2 v\cdot\hat{q} + 2\hat{s}v\cdot\hat{q}^2$$
$$+2\hat{m}_s^2\hat{s}v\cdot\hat{q}^2 - 2x v\cdot\hat{q}^2 - 2\hat{m}_s^2 x v\cdot\hat{q}^2 - 4v\cdot\hat{q}^3 - 4\hat{m}_s^2 v\cdot\hat{q}^3 \Big]|C_7^{\mathrm{eff}}|^2$$
$$-\frac{4}{\hat{s}x^2}\Big[-2\hat{s} + 2v\cdot\hat{q} - 2\hat{m}_s^2 v\cdot\hat{q} + 2\hat{s}v\cdot\hat{q} - x v\cdot\hat{q} - 2v\cdot\hat{q}^2$$
$$\left. +2\hat{m}_s^2 v\cdot\hat{q}^2 \Big] \mathrm{Re}\left[(C_9^{\mathrm{eff}} \mp C_{10})^* C_7^{\mathrm{eff}}\right] \right\} \, , \tag{B.16}$$

$$T_2^{(\delta)L/R} = \frac{m_B}{m_b^3} (\lambda_1 + 3\lambda_2) \left[\frac{1}{x} - \frac{2}{x^2} (1 - v \cdot \hat{q}) \right] \left[|C_9^{\text{eff}} \mp C_{10}|^2 - \frac{4}{\hat{s}} (1 + \hat{m}_s^2) |C_7^{\text{eff}}|^2 \right] , \qquad \text{(B.17)}$$

$$T_3^{(\delta)L/R} = \frac{m_B}{m_b^3} (\lambda_1 + 3\lambda_2) \left\{ -\frac{1}{x^2} (1 - v \cdot \hat{q}) |C_9^{\text{eff}} \mp C_{10}|^2 \right.$$

$$+ \frac{4}{\hat{s}^2} \left[\frac{1}{x} v \cdot \hat{q} - \frac{1}{x^2} (1 - v \cdot \hat{q}) (2 (v \cdot \hat{q}) - \hat{s}) \right] (1 - \hat{m}_s^2) |C_7^{\text{eff}}|^2$$

$$\left. - \frac{2}{\hat{s}x^2} \left[2 + 2\hat{m}_s^2 - x - 2v \cdot \hat{q} - 2\hat{m}_s^2 v \cdot \hat{q} \right] \text{Re} \left[(C_9^{\text{eff}} \mp C_{10})^* C_7^{\text{eff}} \right] \right\} . \qquad \text{(B.18)}$$

Here the variable x is defined as $x \equiv 1 + \hat{s} - 2 (v \cdot \hat{q}) - \hat{m}_s^2 + i \epsilon$.

B.2   Auxiliary Functions $E_1(\hat{s}, \hat{u})$ and $E_2(\hat{s}, \hat{u})$

In this appendix we give the auxiliary functions $E_1(\hat{s}, \hat{u})$ and $E_2(\hat{s}, \hat{u})$, multiplying the delta-function $\delta[\hat{u}(\hat{s}, \hat{m}_s) - \hat{u}^2]$ and its first derivative $\delta'[\hat{u}(\hat{s}, \hat{m}_s) - \hat{u}^2]$, respectively, appearing in the power corrected Dalitz distribution $d^2B/d\hat{s}d\hat{u}(b \to s\ell^+\ell^-)$ in the HQE approach given in eq. (3.60).

$$E_1(\hat{s}, \hat{u}) = \frac{1}{3} \left\{ 2 \hat{\lambda}_1 \left[1 - 4\hat{m}_s^2 + 6\hat{m}_s^4 - 4\hat{m}_s^6 + \hat{m}_s^8 - 2\hat{m}_s^2\hat{s} + 4\hat{m}_s^4\hat{s} - 2\hat{m}_s^6\hat{s} + 2\hat{m}_s^2\hat{s}^3 - \hat{s}^4 \right. \right.$$

$$\left. + \hat{u}^2 \left(1 - 2\hat{m}_s^2 + \hat{m}_s^4 - 2\hat{m}_s^2\hat{s} + 4\,\hat{s} + \hat{s}^2 \right) \right]$$

$$+ 3 \hat{\lambda}_2 (1 - \hat{m}_s^2 + \hat{s}) \left[-1 + 7\hat{m}_s^2 - 11\hat{m}_s^4 + 5\hat{m}_s^6 + 11\,\hat{s} + 10\hat{m}_s^2\hat{s} - 5\hat{m}_s^4\hat{s} - 15\,\hat{s}^2 \right.$$

$$\left. -5\hat{m}_s^2\hat{s}^2 + 5\hat{s}^3 + \hat{u}^2 \left(1 - 5\hat{m}_s^2 + 5\,\hat{s} \right) \right] \Big\}$$

$$\times \left(|C_9^{\text{eff}}|^2 + |C_{10}|^2 \right)$$

$$+ \frac{4}{3\,\hat{s}} \left\{ 2 \hat{\lambda}_1 \left[1 - 3\hat{m}_s^2 + 2\hat{m}_s^4 + 2\hat{m}_s^6 - 3\hat{m}_s^8 + \hat{m}_s^{10} - 10\hat{m}_s^2\hat{s} + 18\hat{m}_s^4\hat{s} - 6\hat{m}_s^6\hat{s} - 2\hat{m}_s^8\hat{s} \right. \right.$$

$$\left. + 16\hat{m}_s^4\hat{s}^2 - 6\hat{m}_s^2\hat{s}^3 + 2\hat{m}_s^4\hat{s}^3 - \hat{s}^4 - \hat{m}_s^2\hat{s}^4 \right.$$

$$\left. - \hat{u}^2 \left(1 - \hat{m}_s^2 - \hat{m}_s^4 + \hat{m}_s^6 + 4\hat{s} + 2\hat{m}_s^2\hat{s} - 2\hat{m}_s^4\hat{s} + \hat{s}^2 + \hat{m}_s^2\hat{s}^2 \right) \right]$$

$$+ 3 \hat{\lambda}_2 (1 - \hat{m}_s^2 + \hat{s}) \left[3 + 2\hat{m}_s^2 - 8\hat{m}_s^4 - 2\hat{m}_s^6 + 5\hat{m}_s^8 + 3\hat{s} - 35\hat{m}_s^2\hat{s} - 27\hat{m}_s^4\hat{s} - 5\hat{m}_s^6\hat{s} \right.$$

$$\left. -11\hat{s}^2 + 8\hat{m}_s^2\hat{s}^2 - 5\hat{m}_s^4\hat{s}^2 + 5\hat{s}^3 + 5\hat{m}_s^2\hat{s}^3 \right.$$

$$\left. + \hat{u}^2 \left(3 + 8\hat{m}_s^2 + 5\hat{m}_s^4 - 5\hat{s} - 5\hat{m}_s^2\hat{s} \right) \right] \Big\} |C_7^{\text{eff}}|^2$$

$$+ 8 \left\{ \frac{2}{3} \hat{\lambda}_1 (1 - 4\hat{m}_s^2 + 6\hat{m}_s^4 - 4\hat{m}_s^6 + \hat{m}_s^8 - \hat{s} - \hat{m}_s^2\hat{s} + 5\hat{m}_s^4\hat{s} - 3\hat{m}_s^6\hat{s} + \hat{s}^2 + 3\hat{m}_s^4\hat{s}^2 \right.$$

$$\left. -\hat{s}^3 - \hat{m}_s^2\hat{s}^3) \right.$$

$$\left. + \hat{\lambda}_2(1 - \hat{m}_s^2 + \hat{s}) \left[4 - 3\hat{m}_s^2 - 6\hat{m}_s^4 + 5\hat{m}_s^6 - 6\hat{s} - 4\hat{m}_s^2\hat{s} - 10\hat{m}_s^4\hat{s} + 2\hat{s}^2 + 5\hat{m}_s^2\hat{s}^2 + \hat{u}^2 \right] \right\}$$

$$Re(C_9^{\text{eff}}) \, C_7^{\text{eff}}$$

$$+ 4\,\hat{s}\,\hat{u} \left[-\frac{4}{3} \hat{\lambda}_1 \hat{s} + \hat{\lambda}_2 \left(7 - 2\hat{m}_s^2 - 5\hat{m}_s^4 + 2\,\hat{s} + 10\hat{m}_s^2\hat{s} - 5\,\hat{s}^2 \right) \right] Re(C_9^{\text{eff}}) \, C_{10}$$

$$+ \frac{8}{3} \hat{u} \left[-4 \hat{\lambda}_1 \hat{s} (1 + \hat{m}_s^2) \right.$$

$$\left. + 3\hat{\lambda}_2 \left(5 + \hat{m}_s^2 - \hat{m}_s^4 - 5\hat{m}_s^6 + 2\hat{s} + 4\hat{m}_s^2\hat{s} + 10\hat{m}_s^4\hat{s} - 3\,\hat{s}^2 - 5\hat{m}_s^2\hat{s}^2 \right) \right] C_{10}^* C_7^{\text{eff}}, \qquad \text{(B.1)}$$

$$E_2(\hat{s}, \hat{u}) = \frac{2}{3} \hat{\lambda}_1 \left(1 - \hat{m}_s^2 + \hat{s} \right)^2 \hat{u}(\hat{s}, \hat{m}_s)^2 \left[\left(1 - 2\hat{m}_s^2 + \hat{m}_s^4 - \hat{s}^2 - \hat{u}^2 \right) \left(|C_9^{\text{eff}}|^2 + |C_{10}|^2 \right) \right.$$

$$+4 \left(1 - \hat{m}_s^2 - \hat{m}_s^4 + \hat{m}_s^6 - 8\hat{m}_s^2\hat{s} - \hat{s}^2 - \hat{m}_s^2\hat{s}^2 + \hat{u}^2 + \hat{m}_s^2\hat{u}^2\right) \frac{|C_7^{\text{eff}}|^2}{\hat{s}}$$

$$+8 \left(1 - 2\hat{m}_s^2 + \hat{m}_s^4 - \hat{s} - \hat{m}_s^2\hat{s}\right) Re(C_9^{\text{eff}}) \, C_7^{\text{eff}}$$

$$+4 \, \hat{s} \, \hat{u} \, Re(C_9^{\text{eff}}) \, C_{10} + 8 \, \hat{u} \left(1 + \hat{m}_s^2\right) Re(C_{10}) \, C_7^{\text{eff}} \Big] \, . \tag{B.2}$$

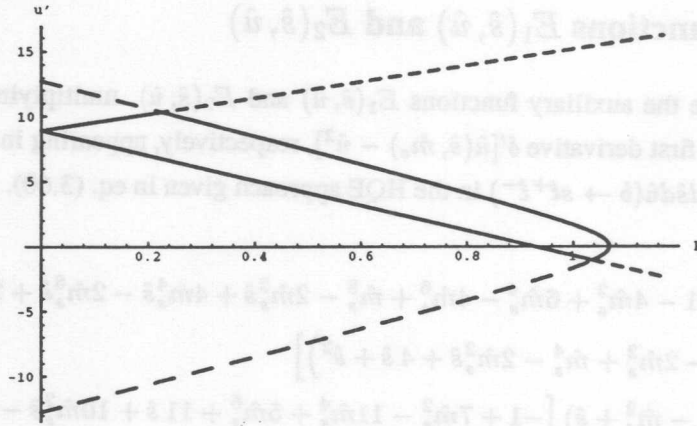## B.3   Dalitz Distribution $d^2\Gamma(B \to X_s \ell^+\ell^-)/ds\,du$ and FB Asymmetry in the Fermi Motion Model

Figure B.1: *Phase space boundaries for the u' and p integrations with fixed values of s and u drawn for $s = 15 \, GeV^2$ and $u = 8.9 \, GeV^2$. The integration region (solid curve) is given by the intersection of $u'_{\pm}$ (short dashed) and $\pm u(s,p)$ (long dashed curve). The Fermi motion parameters used are $(p_F, m_q) = (450, 0)$ in MeV.*

We start with the differential decay rate $d^3\Gamma_B/ds\,du\,dp$, describing the decay $b \to s\ell^+\ell^-$ of a moving b-quark having a mass $m_b \equiv m_b(p)$ and three momentum $|p| \equiv p$ with a distribution $\phi(p)$, which will be taken as a Gaussian [22],

$$\frac{d\Gamma_B}{ds\,du\,dp} = \int_{u'_{\min}}^{u'_{\max}} du' \, \frac{m_b{}^2}{m_B} \, p \, \phi(p) \, \frac{1}{\sqrt{u'^2 + 4\,m_b{}^2\,s}} \left[\frac{d^2\Gamma_b}{ds\,du'}\right] . \tag{B.1}$$

Here, $d^2\Gamma_b/ds\,du'$ is the double differential decay rate of a b-quark at rest and can be written in the case of $b \to s\ell^+\ell^-$ as,

$$\frac{d^2\Gamma_b}{ds\,du'} = |V_{ts}^* V_{tb}|^2 \, \frac{G_F{}^2}{192\,\pi^3} \, \frac{1}{m_b{}^3} \, \frac{3\,\alpha^2}{16\,\pi^2} \left[F_1(s,p) + F_2(s,p) \, u' + F_3(s,p) \, u'^2\right] , \tag{B.2}$$

and the three functions have the following expressions,

$$F_1(s,p) = \left[\left(m_b{}^2 - m_s{}^2\right)^2 - s^2\right] \left(|C_9^{\text{eff}}|^2 + |C_{10}|^2\right)$$

$$+ \, 4 \left[m_b{}^4 - m_s{}^2 m_b{}^2 - m_s{}^4 + \frac{m_s{}^6}{m_b{}^2} - 8\,s\,m_s{}^2 - s^2\left(1 + \frac{m_s{}^2}{m_b{}^2}\right)\right] \frac{m_b{}^2}{s} \, |C_7^{\text{eff}}|^2$$

$$- \, 8 \left[s \left(m_b{}^2 + m_s{}^2\right) - \left(m_b{}^2 - m_s{}^2\right)^2\right] Re(C_7^{\text{eff}} C_9^{\text{eff}}) , \tag{B.3}$$

$$F_2(s,p) = 4 s \operatorname{Re}(C_9^{\text{eff}} C_{10}) + 8 \left(m_b^2 + m_s^2 \right) C_{10} C_7^{\text{eff}}, \tag{B.4}$$

$$F_3(s,p) = - \left(|C_9^{\text{eff}}|^2 + |C_{10}|^2 \right) + 4 \left[1 + \left(\frac{m_s^2}{m_b^2} \right)^2 \right] \frac{m_b^2}{s} |C_7^{\text{eff}}|^2, \tag{B.5}$$

which can be read off directly from eq. (3.60) in the limit $\lambda_i = 0$; $i = 1, 2$. Note that the Wilson coefficient C_9^{eff} also has an implicit m_b dependence, as can be seen in the text. The integration limit for u' is determined through the equations

$$u'_{\text{max}} \equiv \operatorname{Min} \left[u'_+, u(s,p) \right], \tag{B.6}$$

$$u'_{\text{min}} \equiv \operatorname{Max} \left[u'_-, -u(s,p) \right], \tag{B.7}$$

where

$$u'_\pm \equiv \frac{E_b}{m_B} u \pm \frac{p}{m_B} \sqrt{4 s m_B^2 + u^2}, \tag{B.8}$$

$$E_b = \sqrt{m_b^2 + p^2}, \tag{B.9}$$

and

$$u(s,p) \equiv \sqrt{\left[s - (m_b + m_s)^2 \right] \left[s - (m_b - m_s)^2 \right]}. \tag{B.10}$$

A typical situation in the phase space is displayed in Fig. B.1. Integration over p gives the double differential decay rate including the Fermi motion. The result is,

$$
\begin{aligned}
\frac{\mathrm{d}^2 \Gamma_B}{\mathrm{d}s\, \mathrm{d}u} = & |V_{ts}^* V_{tb}|^2 \frac{G_F^2}{192 \pi^3} \frac{3 \alpha^2}{16 \pi^2} \int_0^{p_{\text{max}}} \mathrm{d}p \frac{1}{m_b 2 m_B} p\, \phi(p) \\
& \left\{ F_1(s,p) \ln \left| \frac{u'_{\text{max}} + \sqrt{{u'_{\text{max}}}^2 + 4 m_b^2 s}}{u'_{\text{min}} + \sqrt{{u'_{\text{min}}}^2 + 4 m_b^2 s}} \right| \right. \\
& + F_2(s,p) \left[\sqrt{{u'_{\text{max}}}^2 + 4 m_b^2 s} - \sqrt{{u'_{\text{min}}}^2 + 4 m_b^2 s} \right] \\
& + F_3(s,p) \frac{1}{2} \left[u'_{\text{max}} \sqrt{{u'_{\text{max}}}^2 + 4 m_b^2 s} - u'_{\text{min}} \sqrt{{u'_{\text{min}}}^2 + 4 m_b^2 s} \right. \\
& \left. \left. - 4 m_b^2 s \ln \left| \frac{u'_{\text{max}} + \sqrt{{u'_{\text{max}}}^2 + 4 m_b^2 s}}{u'_{\text{min}} + \sqrt{{u'_{\text{min}}}^2 + 4 m_b^2 s}} \right| \right] \right\}. \tag{B.11}
\end{aligned}
$$

Note that the upper limit in p integration, p_{max} is determined such that p satisfies,

$$u'_{\text{max}}(p_{\text{max}}, s, u) = u'_{\text{min}}(p_{\text{max}}, s, u). \tag{B.12}$$

Lastly, the normalized differential FB asymmetry including the Fermi motion becomes,

$$\frac{\mathrm{d}\overline{\mathcal{A}}}{\mathrm{d}s} = \frac{\int_{-u_{\text{ph}}}^0 \frac{\mathrm{d}\Gamma_B}{\mathrm{d}s\, \mathrm{d}u} \mathrm{d}u - \int_0^{u_{\text{ph}}} \frac{\mathrm{d}\Gamma_B}{\mathrm{d}s\, \mathrm{d}u} \mathrm{d}u}{\int_{-u_{\text{ph}}}^0 \frac{\mathrm{d}\Gamma_B}{\mathrm{d}s\, \mathrm{d}u} \mathrm{d}u + \int_0^{u_{\text{ph}}} \frac{\mathrm{d}\Gamma_B}{\mathrm{d}s\, \mathrm{d}u} \mathrm{d}u}, \tag{B.13}$$

where

$$u_{\text{ph}} \equiv \sqrt{\left[s - (m_B + m_X)^2 \right] \left[s - (m_B - m_X)^2 \right]}, \tag{B.14}$$

and

$$m_X \equiv \operatorname{Max} \left[m_K, m_s + m_{\text{q}} \right], \tag{B.15}$$

with m_q the spectator quark mass and m_K the kaon mass. Since the calculations are being done for an inclusive decay $B \to X_s \ell^+ \ell^-$, we should have put this threshold higher, say starting from $m_K + m_\pi$, but as this effects the very end of a steeply falling dilepton mass spectrum, we have kept the threshold in $B \to X_s \ell^+ \ell^-$ at $m(X_s) = m_K$.

Appendix C

$B \to X_s \ell^+ \ell^-$ Hadron Spectra and Moments

C.1 Coefficient Functions $g_i^{(9,10)}, g_i^{(7)}, g_i^{(7,9)}, h_i^{(9)}, h_i^{(7,9)}, k_1^{(9)}, k_1^{(7,9)}$

These functions enter in the derivation of the leading $(1/m_b^2)$ corrections to the hadron energy spectrum in $B \to X_s \ell^+ \ell^-$, given in eq. (3.95).

$$g_0^{(9,10)} = \sqrt{x_0^2 - \hat{m}_s^2} \frac{32}{3}(-2\hat{m}_s^2 + 3x_0 + 3\hat{m}_s^2 x_0 - 4x_0^2) , \tag{C.1}$$

$$g_1^{(9,10)} = \frac{1}{\sqrt{x_0^2 - \hat{m}_s^2}} \frac{16}{9}(9\hat{m}_s^2 + 23\hat{m}_s^4 - 18\hat{m}_s^2 x_0 - 18x_0^2 - 52\hat{m}_s^2 x_0^2 + 36x_0^3 + 20x_0^4) , \tag{C.2}$$

$$g_2^{(9,10)} = \frac{1}{\sqrt{x_0^2 - \hat{m}_s^2}} \frac{16}{3}(3\hat{m}_s^2 + 23\hat{m}_s^4 - 3x_0 - 21\hat{m}_s^2 x_0 - 6x_0^2 - 52\hat{m}_s^2 x_0^2 + 36x_0^3 + 20x_0^4) , \tag{C.3}$$

$$g_0^{(7)} = \sqrt{x_0^2 - \hat{m}_s^2} \frac{64}{3}(10\hat{m}_s^2 + 10\hat{m}_s^4 - 3x_0 - 18\hat{m}_s^2 x_0 - 3\hat{m}_s^4 x_0 + 2x_0^2 + 2\hat{m}_s^2 x_0^2) , \tag{C.4}$$

$$\begin{aligned} g_1^{(7)} = {} & \frac{1}{\sqrt{x_0^2 - \hat{m}_s^2}} \frac{1}{(x_0 - \frac{1}{2}(1 + \hat{m}_s^2))^2} \frac{-8}{9}(9\hat{m}_s^2 + 34\hat{m}_s^4 + 104\hat{m}_s^6 + 110\hat{m}_s^8 + 31\hat{m}_s^{10} \\ & - 132\hat{m}_s^4 x_0 - 312\hat{m}_s^6 x_0 - 180\hat{m}_s^8 x_0 - 18x_0^2 - 170\hat{m}_s^2 x_0^2 - 58\hat{m}_s^4 x_0^2 + 74\hat{m}_s^6 x_0^2 - 20\hat{m}_s^8 x_0^2 \\ & + 72x_0^3 + 564\hat{m}_s^2 x_0^3 + 576\hat{m}_s^4 x_0^3 + 228\hat{m}_s^6 x_0^3 - 116x_0^4 - 676\hat{m}_s^2 x_0^4 - 436\hat{m}_s^4 x_0^4 - 20\hat{m}_s^6 x_0^4 \\ & + 72x_0^5 + 240\hat{m}_s^2 x_0^5 + 24\hat{m}_s^4 x_0^5) , \end{aligned} \tag{C.5}$$

$$\begin{aligned} g_2^{(7)} = {} & \frac{1}{\sqrt{x_0^2 - \hat{m}_s^2}} \frac{1}{x_0 - \frac{1}{2}(1 + \hat{m}_s^2)} \frac{16}{3}(27\hat{m}_s^2 + 93\hat{m}_s^4 + 97\hat{m}_s^6 + 31\hat{m}_s^8 - 3x_0 - 63\hat{m}_s^2 x_0 \\ & - 189\hat{m}_s^4 x_0 - 129\hat{m}_s^6 x_0 - 18x_0^2 - 108\hat{m}_s^2 x_0^2 - 62\hat{m}_s^4 x_0^2 - 20\hat{m}_s^6 x_0^2 + 72x_0^3 + 324\hat{m}_s^2 x_0^3 \\ & + 180\hat{m}_s^4 x_0^3 - 60x_0^4 - 152\hat{m}_s^2 x_0^4 - 20\hat{m}_s^4 x_0^4) , \end{aligned} \tag{C.6}$$

$$g_0^{(7,9)} = \sqrt{x_0^2 - \hat{m}_s^2} 128(-2\hat{m}_s^2 + x_0 + \hat{m}_s^2 x_0) , \tag{C.7}$$

$$g_1^{(7,9)} = \frac{1}{\sqrt{x_0^2 - \hat{m}_s^2}} 64(\hat{m}_s^2 + 3\hat{m}_s^4 + 2\hat{m}_s^2 x_0 - 2x_0^2 - 4\hat{m}_s^2 x_0^2) , \tag{C.8}$$

$$g_2^{(7,9)} = \frac{1}{\sqrt{x_0^2 - \hat{m}_s^2}} 64(5\hat{m}_s^2 + 9\hat{m}_s^4 - x_0 + 5\hat{m}_s^2 x_0 - 6x_0^2 - 12\hat{m}_s^2 x_0^2) , \tag{C.9}$$

$$h_1^{(9,10)} = \frac{32}{9}\sqrt{x_0^2 - \hat{m}_s^2}(-12\hat{m}_s^2 - 6\hat{m}_s^4 + 9x_0 + 19\hat{m}_s^2 x_0 + 3x_0^2 + 15\hat{m}_s^2 x_0^2 - 28x_0^3) , \tag{C.10}$$

$$h_2^{(9,10)} = \frac{32}{3}\sqrt{x_0^2 - \hat{m}_s^2}(-6\hat{m}_s^4 + 3x_0 + 5\hat{m}_s^2 x_0 + 3x_0^2 + 15\hat{m}_s^2 x_0^2 - 20x_0^3) , \tag{C.11}$$

$$h_1^{(7,9)} = \frac{128}{3}\sqrt{x_0^2 - \hat{m}_s^2}(-8\hat{m}_s^2 - 2\hat{m}_s^4 + 3x_0 - 3\hat{m}_s^2 x_0 + 5x_0^2 + 5\hat{m}_s^2 x_0^2) , \tag{C.12}$$

$$h_2^{(7,9)} = \frac{128}{3}\sqrt{x_0^2 - \hat{m}_s^2}(-4\hat{m}_s^2 - 6\hat{m}_s^4 + 3x_0 - 15\hat{m}_s^2 x_0 + 7x_0^2 + 15\hat{m}_s^2 x_0^2) , \tag{C.13}$$

$$k_1^{(9,10)} = \frac{64}{9}\sqrt{x_0^2 - \hat{m}_s^2}^3 (2\hat{m}_s^2 - 3x_0 - 3\hat{m}_s^2 x_0 + 4x_0^2) , \tag{C.14}$$

$$k_1^{(7,9)} = \frac{-256}{3}\sqrt{x_0^2 - \hat{m}_s^2}^3 (-2\hat{m}_s^2 + x_0 + \hat{m}_s^2 x_0) . \tag{C.15}$$

C.2   Auxiliary Functions $f_\delta(\hat{\lambda}_1, \hat{\lambda}_2)$, $f_{\delta'}(\hat{\lambda}_1, \hat{\lambda}_2)$

The auxiliary functions given below are the coefficients of the singular terms in the derivation of the leading $(1/m_b^2)$ corrections to the hadron energy spectrum in $B \to X_s \ell^+ \ell^-$, given in eq. (3.95).

$$\begin{aligned}
f_\delta(\hat{\lambda}_1, \hat{\lambda}_2) = B_0 &\left\{ \left[\frac{2}{9}(1 - \hat{m}_s^2)^3(5 - \hat{m}_s^2)\hat{\lambda}_1 \right. \right. \\
&+ \left. \frac{2}{3}(1 - \hat{m}_s^2)^3(-1 + 5\hat{m}_s^2)\hat{\lambda}_2 \right] \left(|C_9^{\text{eff}}|^2 + |C_{10}|^2 \right) \\
&+ \left[\frac{1}{9}(1 + 12\hat{m}_l^2 - 88\hat{m}_l^4 - 4\hat{m}_s^2 - 36\hat{m}_l^2\hat{m}_s^2 - 736\hat{m}_l^4\hat{m}_s^2 + 5\hat{m}_s^4 + 24\hat{m}_l^2\hat{m}_s^4 + 720\hat{m}_l^4\hat{m}_s^4 \right. \\
&+ 24\hat{m}_l^2\hat{m}_s^6 + 160\hat{m}_l^4\hat{m}_s^6 - 5\hat{m}_s^8 - 36\hat{m}_l^2\hat{m}_s^8 - 56\hat{m}_l^4\hat{m}_s^8)\frac{\hat{\lambda}_1}{\hat{m}_l^2} + \frac{4}{3}(-1 + \hat{m}_s^2)(-3 \\
&+ 14\hat{m}_l^2 - 2\hat{m}_s^2 + 166\hat{m}_l^2\hat{m}_s^2 + 8\hat{m}_s^4 + 154\hat{m}_l^2\hat{m}_s^4 + 2\hat{m}_s^6 + 50\hat{m}_l^2\hat{m}_s^6 - 5\hat{m}_s^8)\hat{\lambda}_2 \left. \right] \frac{|C_7^{\text{eff}}|^2}{\hat{m}_l^2} \\
&+ \left[\frac{8}{3}(1 - \hat{m}_s^2)^3(7 + \hat{m}_s^2)\hat{\lambda}_1 + \frac{8}{3}(1 - \hat{m}_s^2)^3(13 + 15\hat{m}_s^2)\hat{\lambda}_2 \right] Re(C_9^{\text{eff}}) C_7^{\text{eff}} \\
&+ \left. \hat{\lambda}_1(-1 + \hat{m}_s^2)^5 (\frac{2}{9}\frac{d|C_9^{\text{eff}}|^2}{d\hat{s}_0} + \frac{8}{3}\frac{dRe(C_9^{\text{eff}})}{d\hat{s}_0} C_7^{\text{eff}}) \right\}.
\end{aligned} \tag{C.16}$$

$$\begin{aligned}
f_{\delta'}(\hat{\lambda}_1, \hat{\lambda}_2) = B_0\hat{\lambda}_1 &\left\{ \frac{1}{9}(1 - \hat{m}_s^2)^5 \left(|C_9^{\text{eff}}|^2 + |C_{10}|^2 \right) \right. \\
&+ \frac{2}{9}(-1 + \hat{m}_s^2)^3(-1 + 14\hat{m}_l^2 + \hat{m}_s^2 + 52\hat{m}_l^2\hat{m}_s^2 + \hat{m}_s^4 + 14\hat{m}_l^2\hat{m}_s^4 - \hat{m}_s^6)\frac{|C_7^{\text{eff}}|^2}{\hat{m}_l^2} \\
&+ \left. \frac{4}{3}(1 - \hat{m}_s^2)^5 Re(C_9^{\text{eff}}) C_7^{\text{eff}} \right\}.
\end{aligned} \tag{C.17}$$

C.3   The Functions $\alpha_i, \beta_i, \gamma_i, \delta_i$

The functions entering in the definition of the hadron moments in eq. (3.99) are given in this appendix. Note that the functions $\alpha_i^{(n,m)}$ and $\beta_i^{(n,m)}$ multiply the Wilson coefficients $|C_7^{\text{eff}}|^2$ and C_{10}^2, respec-

tively. The functions $\gamma_i^{(n,m)}, \delta_i^{(n,m)}$ result from the Wilson coefficients $C_7^{\text{eff}} Re(C_9^{\text{eff}}), |C_9^{\text{eff}}|^2$, respectively. They cannot be given in a closed form since C_9^{eff} is an implicit function of x_0.

The functions $\alpha_i^{(n,m)}$

$$\alpha_0^{(0,0)} = \frac{16}{9}(-8 - 26\hat{m}_s^2 + 18\hat{m}_s^4 + 22\hat{m}_s^6 - 11\hat{m}_s^8) + \frac{32}{3}(-1 + \hat{m}_s^2)^3(1 + \hat{m}_s^2)\ln(4\hat{m}_l^2)$$
$$+ \frac{64}{3}\hat{m}_s^4(-9 - 2\hat{m}_s^2 + \hat{m}_s^4)\ln(\hat{m}_s) , \tag{C.18}$$

$$\alpha_1^{(0,0)} = \frac{1}{2}\alpha_0^{(0,0)} , \tag{C.19}$$

$$\alpha_2^{(0,0)} = \frac{8}{3}(-4 + 38\hat{m}_s^2 - 42\hat{m}_s^4 - 26\hat{m}_s^6 - 15\hat{m}_s^8) + 16(-1 + \hat{m}_s^2)^2(3 + 8\hat{m}_s^2 + 5\hat{m}_s^4)\ln(4\hat{m}_l^2)$$
$$+ 32\hat{m}_s^2(-8 - 17\hat{m}_s^2 - 2\hat{m}_s^4 + 5\hat{m}_s^6)\ln(\hat{m}_s) , \tag{C.20}$$

$$\alpha_0^{(0,1)} = \frac{2}{9}(-41 - 49\hat{m}_s^2 + 256\hat{m}_s^4 - 128\hat{m}_s^6 - 43\hat{m}_s^8) + \frac{16}{3}(-1 + \hat{m}_s^2)^3(1 + \hat{m}_s^2)^2\ln(4\hat{m}_l^2)$$
$$+ \frac{16}{3}\hat{m}_s^4(3 - \hat{m}_s^2 - 2\hat{m}_s^4)\ln(\hat{m}_s) , \tag{C.21}$$

$$\alpha_1^{(0,1)} = \alpha_1^{(0,0)} , \tag{C.22}$$

$$\alpha_2^{(0,1)} = \frac{4}{9}(21 + 167\hat{m}_s^2 + 128\hat{m}_s^4 - 276\hat{m}_s^6 - 319\hat{m}_s^8) + \frac{16}{3}(-1 + \hat{m}_s^2)^2(3 + 14\hat{m}_s^2 + 21\hat{m}_s^4$$
$$+ 10\hat{m}_s^6)\ln(4\hat{m}_l^2) + \frac{32}{3}\hat{m}_s^2(3 - 24\hat{m}_s^2 - 18\hat{m}_s^4 + \hat{m}_s^6)\ln(\hat{m}_s) , \tag{C.23}$$

$$\alpha_0^{(0,2)} = \frac{2}{45}(-119 - 144\hat{m}_s^2 + 45\hat{m}_s^4 + 320\hat{m}_s^6 + 45\hat{m}_s^8) + \frac{8}{3}(-1 + \hat{m}_s^4)^3\ln(4\hat{m}_l^2)$$
$$- \frac{16}{3}\hat{m}_s^6(8 + 3\hat{m}_s^2)\ln(\hat{m}_s) , \tag{C.24}$$

$$\alpha_1^{(0,2)} = \frac{1}{27}(-127 - 278\hat{m}_s^2 + 1075\hat{m}_s^4 - 800\hat{m}_s^6 + 49\hat{m}_s^8) + \frac{4}{9}(1 - \hat{m}_s^2)^3(-7 - 17\hat{m}_s^2$$
$$- 5\hat{m}_s^4 + 5\hat{m}_s^6)\ln(4\hat{m}_l^2) + \frac{8}{9}\hat{m}_s^4(18 - 38\hat{m}_s^2 - 13\hat{m}_s^4)\ln(\hat{m}_s) , \tag{C.25}$$

$$\alpha_2^{(0,2)} = \frac{1}{9}(27 - 46\hat{m}_s^2 + 1681\hat{m}_s^4 - 688\hat{m}_s^6 - 1189\hat{m}_s^8) + \frac{4}{3}(-1 + \hat{m}_s^4)^2(3 + 20\hat{m}_s^2 + 25\hat{m}_s^4)\ln(4\hat{m}_l^2)$$
$$- \frac{8}{3}\hat{m}_s^4(18 + 54\hat{m}_s^2 + 47\hat{m}_s^4)\ln(\hat{m}_s) , \tag{C.26}$$

$$\alpha_0^{(1,0)} = 0 , \tag{C.27}$$

$$\alpha_1^{(1,0)} = \frac{2}{9}(-23 - 159\hat{m}_s^2 - 112\hat{m}_s^4 + 304\hat{m}_s^6 - 45\hat{m}_s^8) - \frac{16}{3}(-1 + \hat{m}_s^2)^4(1 + \hat{m}_s^2)\ln(4\hat{m}_l^2)$$
$$+ \frac{16}{3}\hat{m}_s^4(-39 - 7\hat{m}_s^2 + 6\hat{m}_s^4)\ln(\hat{m}_s) , \tag{C.28}$$

$$\alpha_2^{(1,0)} = \frac{2}{9}(-93 - 469\hat{m}_s^2 + 704\hat{m}_s^4 - 127\hat{m}_s^8) + \frac{16}{3}(-1 + \hat{m}_s^2)^3(3 + 8\hat{m}_s^2 + 5\hat{m}_s^4)\ln(4\hat{m}_l^2)$$
$$- \frac{112}{3}\hat{m}_s^4(3 + 3\hat{m}_s^2 + 2\hat{m}_s^4)\ln(\hat{m}_s) , \tag{C.29}$$

$$\alpha_0^{(1,1)} = 0 , \tag{C.30}$$

$$\alpha_1^{(1,1)} = \frac{2}{27}(-4 - 131\hat{m}_s^2 + 307\hat{m}_s^4 - 416\hat{m}_s^6 + 178\hat{m}_s^8) - \frac{8}{9}(-1 + \hat{m}_s^2)^4(1 + 6\hat{m}_s^2 + 5\hat{m}_s^4)\ln(4\hat{m}_l^2)$$
$$+ \frac{16}{9}\hat{m}_s^4(9 - 35\hat{m}_s^2 - 7\hat{m}_s^4)\ln(\hat{m}_s) , \tag{C.31}$$

$$\alpha_2^{(1,1)} = \frac{2}{9}(-60 - 185\hat{m}_s^2 + 173\hat{m}_s^4 + 160\hat{m}_s^6 + 70\hat{m}_s^8) + \frac{8}{3}(-1 + \hat{m}_s^2)^3(1 + \hat{m}_s^2)^2(3 + 5\hat{m}_s^2)\ln(4\hat{m}_l^2)$$

$$+ \frac{16}{3} \hat{m}_s^4 (3 - 21 \hat{m}_s^2 - 13 \hat{m}_s^4) \ln(\hat{m}_s) \,, \tag{C.32}$$

$$\alpha_0^{(2,0)} = 0 \,, \tag{C.33}$$

$$\alpha_1^{(2,0)} = \frac{8}{135}(119 - 176\hat{m}_s^2 - 1085\hat{m}_s^4 + 400\hat{m}_s^6 + 835\hat{m}_s^8) + \frac{32}{9}(1 - \hat{m}_s^2)^5(1 + \hat{m}_s^2)\ln(4\hat{m}_l^2)$$

$$- \frac{64}{9} \hat{m}_s^6 (28 + 5\hat{m}_s^2) \ln(\hat{m}_s) \,, \tag{C.34}$$

$$\alpha_2^{(2,0)} = 0 \,. \tag{C.35}$$

The functions $\beta_i^{(n,m)}$

$$\beta_0^{(0,0)} = \frac{2}{3}(1 - 8\hat{m}_s^2 + 8\hat{m}_s^6 - \hat{m}_s^8 - 24\hat{m}_s^4 \ln(\hat{m}_s)) \,, \tag{C.36}$$

$$\beta_1^{(0,0)} = \frac{1}{2}\beta_0^{(0,0)} \,, \tag{C.37}$$

$$\beta_2^{(0,0)} = -3 + 8\hat{m}_s^2 - 24\hat{m}_s^4 + 24\hat{m}_s^6 - 5\hat{m}_s^8 - 24\hat{m}_s^4 \ln(\hat{m}_s) \,, \tag{C.38}$$

$$\beta_0^{(0,1)} = \frac{1}{30}(7 - 25\hat{m}_s^2 + 160\hat{m}_s^4 - 160\hat{m}_s^6 + 25\hat{m}_s^8 - 7\hat{m}_s^{10} + 120\hat{m}_s^4 \ln(\hat{m}_s) + 120\hat{m}_s^6 \ln(\hat{m}_s)) \,, \tag{C.39}$$

$$\beta_1^{(0,1)} = \beta_1^{(0,0)} \,, \tag{C.40}$$

$$\beta_2^{(0,1)} = \frac{1}{3}\hat{m}_s^2(7 - 20\hat{m}_s^2 + 20\hat{m}_s^6 - 7\hat{m}_s^8 + 24\ln(\hat{m}_s) - 48\hat{m}_s^2 \ln(\hat{m}_s)) \,, \tag{C.41}$$

$$\beta_0^{(0,2)} = \frac{2}{45}(2 - 3\hat{m}_s^2 - 30\hat{m}_s^4 + 30\hat{m}_s^8 + 3\hat{m}_s^{10} - 2\hat{m}_s^{12} - 120\hat{m}_s^6 \ln(\hat{m}_s)) \,, \tag{C.42}$$

$$\beta_1^{(0,2)} = \frac{1}{270}(43 - 135\hat{m}_s^2 + 1260\hat{m}_s^4 - 1440\hat{m}_s^6 + 405\hat{m}_s^8 - 153\hat{m}_s^{10} + 20\hat{m}_s^{12} + 1080\hat{m}_s^4 \ln(\hat{m}_s)$$

$$+ 840\hat{m}_s^6 \ln(\hat{m}_s)) \,, \tag{C.43}$$

$$\beta_2^{(0,2)} = \frac{1}{90}(13 - 315\hat{m}_s^2 + 1500\hat{m}_s^4 - 1560\hat{m}_s^6 + 315\hat{m}_s^8 + 147\hat{m}_s^{10} - 100\hat{m}_s^{12} + 360\hat{m}_s^4 \ln(\hat{m}_s)$$

$$+ 840\hat{m}_s^6 \ln(\hat{m}_s)) \,, \tag{C.44}$$

$$\beta_0^{(1,0)} = 0 \,, \tag{C.45}$$

$$\beta_1^{(1,0)} = \frac{1}{30}(13 - 135\hat{m}_s^2 - 160\hat{m}_s^4 + 320\hat{m}_s^6 - 45\hat{m}_s^8 + 7\hat{m}_s^{10} - 600\hat{m}_s^4 \ln(\hat{m}_s) - 120\hat{m}_s^6 \ln(\hat{m}_s)) \,, \tag{C.46}$$

$$\beta_2^{(1,0)} = \frac{1}{6}(3 - 9\hat{m}_s^2 + 16\hat{m}_s^4 - 48\hat{m}_s^6 + 45\hat{m}_s^8 - 7\hat{m}_s^{10} + 24\hat{m}_s^4 \ln(\hat{m}_s) - 72\hat{m}_s^6 \ln(\hat{m}_s)) \,, \tag{C.47}$$

$$\beta_0^{(1,1)} = 0 \,, \tag{C.48}$$

$$\beta_1^{(1,1)} = \frac{1}{270}(23 - 45\hat{m}_s^2 + 1080\hat{m}_s^4 - 1440\hat{m}_s^6 + 585\hat{m}_s^8 - 243\hat{m}_s^{10} + 40\hat{m}_s^{12} + 1080\hat{m}_s^4 \ln(\hat{m}_s)$$

$$+ 600\hat{m}_s^6 \ln(\hat{m}_s)) \,, \tag{C.49}$$

$$\beta_2^{(1,1)} = \frac{1}{90}(13 + 45\hat{m}_s^2 - 120\hat{m}_s^4 - 45\hat{m}_s^8 + 147\hat{m}_s^{10} - 40\hat{m}_s^{12} + 360\hat{m}_s^4 \ln(\hat{m}_s)$$

$$- 600\hat{m}_s^6 \ln(\hat{m}_s)) \,, \tag{C.50}$$

$$\beta_0^{(2,0)} = 0 \,, \tag{C.51}$$

$$\beta_1^{(2,0)} = \frac{16}{135}(-1 + 9\hat{m}_s^2 - 45\hat{m}_s^4 + 45\hat{m}_s^8 - 9\hat{m}_s^{10} + \hat{m}_s^{12} - 120\hat{m}_s^6 \ln(\hat{m}_s)) \,, \tag{C.52}$$

$$\beta_2^{(2,0)} = 0 \,. \tag{C.53}$$

The functions $\gamma_i^{(n,m)}$

Note that in the expressions given below $C_9^{\text{eff}} \equiv C_9^{\text{eff}}(\hat{s} = 1 - 2x_0 + \hat{m}_s^2)$. The lower and upper limits

of the x_0-integrals are: $x_0^{min} = \hat{m}_s$ and $x_0^{max} = \frac{1}{2}(1 + \hat{m}_s^2 - 4\hat{m}_l^2)$.

$$\gamma_0^{(0,0)} = 128 \int_{x_0^{min}}^{x_0^{max}} dx_0 \sqrt{x_0^2 - \hat{m}_s^2}(-2\hat{m}_s^2 + x_0 + \hat{m}_s^2 x_0) Re(C_9^{\text{eff}}) , \tag{C.54}$$

$$\gamma_1^{(0,0)} = \frac{1}{2}\gamma_0^{(0,0)} , \tag{C.55}$$

$$\gamma_2^{(0,0)} = \int_{x_0^{min}}^{x_0^{max}} dx_0 \frac{64}{\sqrt{x_0^2 - \hat{m}_s^2}}(4\hat{m}_s^2 + 14\hat{m}_s^4 - x_0 - \hat{m}_s^2 x_0 - 12\hat{m}_s^4 x_0 - 4x_0^2 - 22\hat{m}_s^2 x_0^2 + 7x_0^3$$

$$+ \ 15\hat{m}_s^2 x_0^3) Re(C_9^{\text{eff}}) , \tag{C.56}$$

$$\gamma_0^{(0,1)} = 128 \int_{x_0^{min}}^{x_0^{max}} dx_0 x_0 \sqrt{x_0^2 - \hat{m}_s^2}(-2\hat{m}_s^2 + x_0 + \hat{m}_s^2 x_0) Re(C_9^{\text{eff}}) , \tag{C.57}$$

$$\gamma_1^{(0,1)} = \gamma_1^{(0,0)} , \tag{C.58}$$

$$\gamma_2^{(0,1)} = \frac{64}{3} \int_{x_0^{min}}^{x_0^{max}} dx_0 \frac{1}{\sqrt{x_0^2 - \hat{m}_s^2}}(4\hat{m}_s^4 + 6\hat{m}_s^6 + 9\hat{m}_s^2 x_0 + 57\hat{m}_s^4 x_0 - 3x_0^2 - 14\hat{m}_s^2 x_0^2 - 57\hat{m}_s^4 x_0^2$$

$$- \ 9x_0^3 - 81\hat{m}_s^2 x_0^3 + 28x_0^4 + 60\hat{m}_s^2 x_0^4) Re(C_9^{\text{eff}}) , \tag{C.59}$$

$$\gamma_0^{(0,2)} = 128 \int_{x_0^{min}}^{x_0^{max}} dx_0 x_0^2 \sqrt{x_0^2 - \hat{m}_s^2}(-2\hat{m}_s^2 + x_0 + \hat{m}_s^2 x_0) Re(C_9^{\text{eff}}) , \tag{C.60}$$

$$\gamma_1^{(0,2)} = \frac{64}{3} \int_{x_0^{min}}^{x_0^{max}} dx_0 \sqrt{x_0^2 - \hat{m}_s^2}(-4\hat{m}_s^4 - 10\hat{m}_s^2 x_0 + 2\hat{m}_s^4 x_0 + 6x_0^2 + 16\hat{m}_s^2 x_0^2 - 5x_0^3$$

$$- \ 5\hat{m}_s^2 x_0^3) Re(C_9^{\text{eff}}) , \tag{C.61}$$

$$\gamma_2^{(0,2)} = \frac{64}{3} \int_{x_0^{min}}^{x_0^{max}} dx_0 \frac{x_0}{\sqrt{x_0^2 - \hat{m}_s^2}}(8\hat{m}_s^4 + 12\hat{m}_s^6 + 6\hat{m}_s^2 x_0 + 72\hat{m}_s^4 x_0 - 3x_0^2 - 25\hat{m}_s^2 x_0^2 - 78\hat{m}_s^4 x_0^2$$

$$- \ 6x_0^3 - 96\hat{m}_s^2 x_0^3 + 35x_0^4 + 75\hat{m}_s^2 x_0^4) Re(C_9^{\text{eff}}) , \tag{C.62}$$

$$\gamma_0^{(1,0)} = 0 , \tag{C.63}$$

$$\gamma_1^{(1,0)} = 128 \int_{x_0^{min}}^{x_0^{max}} dx_0 \frac{(x_0 - 1)}{\sqrt{x_0^2 - \hat{m}_s^2}}(-2\hat{m}_s^4 + \hat{m}_s^2 x_0 + \hat{m}_s^4 x_0 + 2\hat{m}_s^2 x_0^2 - x_0^3 - \hat{m}_s^2 x_0^3) Re(C_9^{\text{eff}}) , \tag{C.64}$$

$$\gamma_2^{(1,0)} = \frac{128}{3} \int_{x_0^{min}}^{x_0^{max}} dx_0 \sqrt{x_0^2 - \hat{m}_s^2}(-4\hat{m}_s^2 - 6\hat{m}_s^4 + 3x_0 - 15\hat{m}_s^2 x_0 + 7x_0^2 + 15\hat{m}_s^2 x_0^2) Re(C_9^{\text{eff}}) , \tag{C.65}$$

$$\gamma_0^{(1,1)} = 0 , \tag{C.66}$$

$$\gamma_1^{(1,1)} = \frac{128}{3} \int_{x_0^{min}}^{x_0^{max}} dx_0 \frac{1}{\sqrt{x_0^2 - \hat{m}_s^2}}(4\hat{m}_s^6 + 4\hat{m}_s^4 x_0 - 2\hat{m}_s^6 x_0 - 3\hat{m}_s^2 x_0^2 - 17\hat{m}_s^4 x_0^2 + \hat{m}_s^2 x_0^3 + 7\hat{m}_s^4 x_0^3$$

$$+ \ 3x_0^4 + 13\hat{m}_s^2 x_0^4 - 5x_0^5 - 5\hat{m}_s^2 x_0^5) Re(C_9^{\text{eff}}) , \tag{C.67}$$

$$\gamma_2^{(1,1)} = \frac{128}{3} \int_{x_0^{min}}^{x_0^{max}} dx_0 x_0 \sqrt{x_0^2 - \hat{m}_s^2}(-4\hat{m}_s^2 - 6\hat{m}_s^4 + 3x_0 - 15\hat{m}_s^2 x_0 + 7x_0^2 + 15\hat{m}_s^2 x_0^2) Re(C_9^{\text{eff}}) , \tag{C.68}$$

$$\gamma_0^{(2,0)} = 0 , \tag{C.69}$$

$$\gamma_1^{(2,0)} = \frac{512}{3} \int_{x_0^{min}}^{x_0^{max}} dx_0 \sqrt{x_0^2 - \hat{m}_s^2}(-2\hat{m}_s^4 + \hat{m}_s^2 x_0 + \hat{m}_s^4 x_0 + 2\hat{m}_s^2 x_0^2 - x_0^3 - \hat{m}_s^2 x_0^3) Re(C_9^{\text{eff}}) , \tag{C.70}$$

$$\gamma_2^{(2,0)} = 0 . \tag{C.71}$$

The functions $\delta_i^{(n,m)}$

$$\delta_0^{(0,0)} = \frac{32}{3} \int_{x_0^{min}}^{x_0^{max}} dx_0 \sqrt{x_0^2 - \hat{m}_s^2}(-2\hat{m}_s^2 + 3x_0 + 3\hat{m}_s^2 x_0 - 4x_0^2)|C_9^{\text{eff}}|^2 , \tag{C.72}$$

$$\delta_1^{(0,0)} = \frac{1}{2}\delta_0^{(0,0)} , \tag{C.73}$$

$$\delta_2^{(0,0)} = \int_{x_0^{min}}^{x_0^{max}} dx_0 \frac{16}{\sqrt{x_0^2 - \hat{m}_s^2}}(6\hat{m}_s^4 - x_0 - 9\hat{m}_s^2 x_0 - 12\hat{m}_s^4 x_0 + 6\hat{m}_s^2 x_0^2 + 15x_0^3 + 15\hat{m}_s^2 x_0^3$$

$$- 20x_0^4)|C_9^{\text{eff}}|^2 , \tag{C.74}$$

$$\delta_0^{(0,1)} = \frac{32}{3} \int_{x_0^{min}}^{x_0^{max}} dx_0 x_0 \sqrt{x_0^2 - \hat{m}_s^2}(-2\hat{m}_s^2 + 3x_0 + 3\hat{m}_s^2 x_0 - 4x_0^2)|C_9^{\text{eff}}|^2 , \tag{C.75}$$

$$\delta_1^{(0,1)} = \delta_1^{(0,0)} , \tag{C.76}$$

$$\delta_2^{(0,1)} = \frac{16}{3} \int_{x_0^{min}}^{x_0^{max}} dx_0 \frac{1}{\sqrt{x_0^2 - \hat{m}_s^2}}(6\hat{m}_s^6 - 3\hat{m}_s^2 x_0 + 13\hat{m}_s^4 x_0 - 3x_0^2 - 30\hat{m}_s^2 x_0^2 - 57\hat{m}_s^4 x_0^2 + 3x_0^3$$

$$+ 43\hat{m}_s^2 x_0^3 + 48x_0^4 + 60\hat{m}_s^2 x_0^4 - 80x_0^5)|C_9^{\text{eff}}|^2 , \tag{C.77}$$

$$\delta_0^{(0,2)} = \frac{32}{3} \int_{x_0^{min}}^{x_0^{max}} dx_0 x_0^2 \sqrt{x_0^2 - \hat{m}_s^2}(-2\hat{m}_s^2 + 3x_0 + 3\hat{m}_s^2 x_0 - 4x_0^2)|C_9^{\text{eff}}|^2 , \tag{C.78}$$

$$\delta_1^{(0,2)} = \frac{16}{9} \int_{x_0^{min}}^{x_0^{max}} dx_0 \sqrt{x_0^2 - \hat{m}_s^2}(-4\hat{m}_s^4 - 6\hat{m}_s^2 x_0 + 6\hat{m}_s^4 x_0 + 18x_0^2 + 20\hat{m}_s^2 x_0^2 - 39x_0^3 - 15\hat{m}_s^2 x_0^3$$

$$+ 20x_0^4)|C_9^{\text{eff}}|^2 , \tag{C.79}$$

$$\delta_2^{(0,2)} = \frac{16}{3} \int_{x_0^{min}}^{x_0^{max}} dx_0 \frac{x_0}{\sqrt{x_0^2 - \hat{m}_s^2}}(12\hat{m}_s^6 - 6\hat{m}_s^2 x_0 + 8\hat{m}_s^4 x_0 - 3x_0^2 - 33\hat{m}_s^2 x_0^2 - 78\hat{m}_s^4 x_0^2 + 6x_0^3$$

$$+ 68\hat{m}_s^2 x_0^3 + 51x_0^4 + 75\hat{m}_s^2 x_0^4 - 100x_0^5)|C_9^{\text{eff}}|^2 , \tag{C.80}$$

$$\delta_0^{(1,0)} = 0 , \tag{C.81}$$

$$\delta_1^{(1,0)} = \frac{32}{3} \int_{x_0^{min}}^{x_0^{max}} dx_0 \frac{(x_0 - 1)}{\sqrt{x_0^2 - \hat{m}_s^2}}(-2\hat{m}_s^4 + 3\hat{m}_s^2 x_0 + 3\hat{m}_s^4 x_0 - 2\hat{m}_s^2 x_0^2 - 3x_0^3 - 3\hat{m}_s^2 x_0^3$$

$$+ 4x_0^4)|C_9^{\text{eff}}|^2 , \tag{C.82}$$

$$\delta_2^{(1,0)} = \frac{32}{3} \int_{x_0^{min}}^{x_0^{max}} dx_0 \sqrt{x_0^2 - \hat{m}_s^2}(-6\hat{m}_s^4 + 3x_0 + 5\hat{m}_s^2 x_0 + 3x_0^2 + 15\hat{m}_s^2 x_0^2 - 20x_0^3)|C_9^{\text{eff}}|^2 , \tag{C.83}$$

$$\delta_0^{(1,1)} = 0 , \tag{C.84}$$

$$\delta_1^{(1,1)} = \frac{32}{9} \int_{x_0^{min}}^{x_0^{max}} dx_0 \frac{1}{\sqrt{x_0^2 - \hat{m}_s^2}}(4\hat{m}_s^6 - 6\hat{m}_s^6 x_0 - 9\hat{m}_s^2 x_0^2 - 15\hat{m}_s^4 x_0^2 + 27\hat{m}_s^2 x_0^3 + 21\hat{m}_s^4 x_0^3$$

$$+ 9x_0^4 - 9\hat{m}_s^2 x_0^4 - 27x_0^5 - 15\hat{m}_s^2 x_0^5 + 20x_0^6)|C_9^{\text{eff}}|^2 , \tag{C.85}$$

$$\delta_2^{(1,1)} = \frac{32}{3} \int_{x_0^{min}}^{x_0^{max}} dx_0 x_0 \sqrt{x_0^2 - \hat{m}_s^2}(-6\hat{m}_s^4 + 3x_0 + 5\hat{m}_s^2 x_0 + 3x_0^2 + 15\hat{m}_s^2 x_0^2 - 20x_0^3)|C_9^{\text{eff}}|^2 , \tag{C.86}$$

$$\delta_0^{(2,0)} = 0 , \tag{C.87}$$

$$\delta_1^{(2,0)} = \frac{128}{9} \int_{x_0^{min}}^{x_0^{max}} dx_0 \sqrt{x_0^2 - \hat{m}_s^2}(-2\hat{m}_s^4 + 3\hat{m}_s^2 x_0 + 3\hat{m}_s^4 x_0 - 2\hat{m}_s^2 x_0^2 - 3x_0^3$$

$$- 3\hat{m}_s^2 x_0^3 + 4x_0^4)|C_9^{\text{eff}}|^2 , \tag{C.88}$$

$$\delta_2^{(2,0)} = 0 . \tag{C.89}$$

C.4 Lowest Hadronic Moments (Parton Level)

$$\langle x_0 \rangle \frac{\mathcal{B}}{\mathcal{B}_0} = \frac{2}{9m_B^2}(-41m_B^2 - 49m_s^2 - 24(m_B^2 - m_s^2)\ln(4\frac{m_l^2}{m_B^2}))C_7^{\text{eff}^2} + \frac{1}{30m_B^2}(7m_B^2 - 25m_s^2)C_{10}^2$$

$$+ \int_{m_s/m_B}^{\frac{1}{2}(1+m_s^2/m_B^2)} dx_0 \frac{64}{m_B^2}x_0(-m_s^2 - 4m_s^2x_0 + 2m_B^2x_0^2 + 2m_s^2x_0^2)Re(C_9^{\text{eff}})C_7^{\text{eff}}$$

$$+ \int_{m_s/m_B}^{\frac{1}{2}(1+m_s^2/m_B^2)} dx_0 \frac{16}{3m_B^2}x_0(-3m_s^2 + 6m_B^2x_0^2 + 6m_s^2x_0^2 - 8m_B^2x_0^3)|C_9^{\text{eff}}|^2$$

$$+ \frac{\alpha_s}{\pi}A^{(0,1)}C_9^2 + \frac{-32}{3}C_7^{\text{eff}^2}\frac{\bar{\Lambda}}{m_B} + \frac{-16}{3}C_7^{\text{eff}^2}\frac{\bar{\Lambda}^2}{m_B^2} + \left[\frac{-16}{9}(1 + 3\ln(4\frac{m_l^2}{m_B^2}))C_7^{\text{eff}^2} + \frac{C_{10}^2}{3}\right.$$

$$+ \left.\int_0^{\frac{1}{2}} dx_0(64x_0^2 Re(C_9^{\text{eff}})C_7^{\text{eff}} + \frac{16}{3}(3 - 4x_0)x_0^2|C_9^{\text{eff}}|^2)\right]\frac{\lambda_1}{m_B^2} +$$

$$+ \left[\frac{4}{3}(19 + 12\ln(4\frac{m_l^2}{m_B^2}))C_7^{\text{eff}^2} + \int_0^{\frac{1}{2}} dx_0(\frac{64}{3}x_0(-3 - 9x_0 + 28x_0^2)Re(C_9^{\text{eff}})C_7^{\text{eff}}\right.$$

$$+ \left.\frac{16}{3}x_0(-3 + 3x_0 + 48x_0^2 - 80x_0^3)|C_9^{\text{eff}}|^2\right]\frac{\lambda_2}{m_B^2}, \tag{C.90}$$

$$\langle x_0^2 \rangle \frac{\mathcal{B}}{\mathcal{B}_0} = \frac{2}{45m_B^{12}}(-119m_B^{12} - 144m_B^{10}m_s^2 - 60(m_B^{12} - m_s^{12})\ln(4\frac{m_l^2}{m_B^2}))C_7^{\text{eff}^2} + \frac{2}{45m_B^2}(2m_B^2 - 3m_s^2)C_{10}^2$$

$$+ \int_{m_s/m_B}^{\frac{1}{2}(1+m_s^2/m_B^2)} dx_0 \frac{64}{m_B^2}x_0^2(-m_s^2 - 4m_s^2x_0 + 2m_B^2x_0^2 + 2m_s^2x_0^2)Re(C_9^{\text{eff}})C_7^{\text{eff}}$$

$$+ \int_{m_s/m_B}^{\frac{1}{2}(1+m_s^2/m_B^2)} dx_0 \frac{16}{3m_B^2}x_0^2(-3m_s^2 + 6m_B^2x_0^2 + 6m_s^2x_0^2 - 8m_B^2x_0^3)|C_9^{\text{eff}}|^2$$

$$+ \frac{\alpha_s}{\pi}A^{(0,2)}C_9^2 + \frac{-16}{3}C_7^{\text{eff}^2}\frac{\bar{\Lambda}}{m_B} + \frac{-8}{3}C_7^{\text{eff}^2}\frac{\bar{\Lambda}^2}{m_B^2} + \left[\frac{-1}{27}(55 + 84\ln(4\frac{m_l^2}{m_B^2}))C_7^{\text{eff}^2} + 43\frac{C_{10}^2}{270}\right.$$

$$+ \left.\int_0^{\frac{1}{2}} dx_0(\frac{64}{3}(6 - 5x_0)x_0^3 Re(C_9^{\text{eff}})C_7^{\text{eff}} + \frac{16}{9}(18 - 39x_0 + 20x_0^2)x_0^3|C_9^{\text{eff}}|^2)\right]\frac{\lambda_1}{m_B^2}$$

$$+ \left[(11 + 4\ln(4\frac{m_l^2}{m_B^2}))C_7^{\text{eff}^2} + 13\frac{C_{10}^2}{90} + \int_0^{\frac{1}{2}} dx_0(\frac{64}{3}x_0^2(-3 - 6x_0 + 35x_0^2)Re(C_9^{\text{eff}})C_7^{\text{eff}}\right.$$

$$+ \left.\frac{16}{3}x_0^2(-3 + 6x_0 + 51x_0^2 - 100x_0^3)|C_9^{\text{eff}}|^2\right]\frac{\lambda_2}{m_B^2}, \tag{C.91}$$

$$\langle x_0(\hat{s}_0 - \hat{m}_s^2) \rangle \frac{\mathcal{B}}{\mathcal{B}_0} = \frac{\alpha_s}{\pi}A^{(1,1)}C_9^2 + \left[\frac{-8}{27}(1 + 3\ln(4\frac{m_l^2}{m_B^2}))C_7^{\text{eff}^2} + 23\frac{C_{10}^2}{270}\right.$$

$$+ \left.\int_0^{\frac{1}{2}} dx_0(\frac{128}{3}(3 - 5x_0)x_0^3 Re(C_9^{\text{eff}})C_7^{\text{eff}} + \frac{32}{9}(9 - 27x_0 + 20x_0^2)x_0^3|C_9^{\text{eff}}|^2)\right]\frac{\lambda_1}{m_B^2}$$

$$+ \left[\frac{-8}{3}(5 + 3\ln(4\frac{m_l^2}{m_B^2}))C_7^{\text{eff}^2} + 13\frac{C_{10}^2}{90}\right. \tag{C.92}$$

$$+ \left.\int_0^{\frac{1}{2}} dx_0(\frac{128}{3}x_0^3(3 + 7x_0)Re(C_9^{\text{eff}})C_7^{\text{eff}} + \frac{32}{3}x_0^3(3 + 3x_0 - 20x_0^2)|C_9^{\text{eff}}|^2)\right]\frac{\lambda_2}{m_B^2},$$

$$\langle \hat{s}_0 - \hat{m}_s^2 \rangle \frac{\mathcal{B}}{\mathcal{B}_0} = \frac{\alpha_s}{\pi}A^{(1,0)}C_9^2 + \left[\frac{-2}{9}(23 + 24\ln(4\frac{m_l^2}{m_B^2}))C_7^{\text{eff}^2} + 13\frac{C_{10}^2}{30}\right.$$

$$+ \left. \int_0^{\frac{1}{2}} dx_0 (128(1-x_0)x_0^2 Re(C_9^{\text{eff}})C_7^{\text{eff}} + \frac{32}{3}(3 - 7x_0 + 4x_0^2)x_0^2 |C_9^{\text{eff}}|^2) \right] \frac{\lambda_1}{m_B^2}$$

$$+ \left[\frac{-2}{3}(31 + 24 \ln(4\frac{m_l^2}{m_B^2}))C_7^{\text{eff}^2} + \frac{C_{10}^2}{2} \right. \tag{C.93}$$

$$+ \left. \int_0^{\frac{1}{2}} dx_0 (\frac{128}{3}x_0^2(3 + 7x_0)Re(C_9^{\text{eff}})C_7^{\text{eff}} + \frac{32}{3}x_0^2(3 + 3x_0 - 20x_0^2)|C_9^{\text{eff}}|^2) \right] \frac{\lambda_2}{m_B^2},$$

$$\langle (\hat{s}_0 - \hat{m}_s^2)^2 \rangle \frac{\mathcal{B}}{\mathcal{B}_0} = \frac{\alpha_s}{\pi} A^{(2,0)} C_9^2 + \left[\frac{8}{135}(119 + 60 \ln(4\frac{m_l^2}{m_B^2}))C_7^{\text{eff}^2} - 16\frac{C_{10}^2}{135} \right. \tag{C.94}$$

$$+ \left. \int_0^{\frac{1}{2}} dx_0 (\frac{-512}{3}x_0^4 Re(C_9^{\text{eff}})C_7^{\text{eff}} + \frac{128}{9}(-3 + 4x_0)x_0^4 |C_9^{\text{eff}}|^2) \right] \frac{\lambda_1}{m_B^2} .$$

Bibliography

[1] S.L. Glashow, Nucl. Phys. **22** (1961) 579; S. Weinberg, Phys. Rev. Lett. **19** (1967) 1264; A. Salam, in *Elementary Particle Theory*, ed. N. Svartholm (Almqvist and Wiksell, Stockholm) (1968).

[2] R. Ammar et al. (CLEO Collaboration), Phys. Rev. Lett. **71** (1993) 674.

[3] T. Skwarnicki, preprint HEPSY 97-03, hep-ph/9712253; to be published in Proc. of the Seventh Int. Symp. on Heavy Flavor Physics, UC Santa Barbara, California, July 7-11, 1997; K. Lingel, T. Skwarnicki and J.G. Smith, hep-ex/9804015.

[4] A. Ali, preprint DESY 97-256, hep-ph/9801270, to appear in Proc. of the First APCTP Workshop, Pacific Particle Physics Phenomenology, Seoul, South Korea, Oct. 31 - Nov. 2, 1997.

[5] N. Cabibbo, Phys. Rev. Lett. **10** (1963) 531;
M. Kobayashi and K. Maskawa, Prog. Theor. Phys. **49** (1973) 652.

[6] A. Ali and C. Greub, Z. Phys. C **49** (1991) 431.

[7] A. J. Buras et al., Nucl. Phys. B **424** (1994) 374.

[8] M. Ciuchini et al., Phys. Lett. **B316** (1993) 127; Nucl. Phys. **B415** (1994) 403;
G. Cella et al., Phys. Lett. **B325** (1994) 227; M. Ciuchini et al., Phys. Lett. B **334** (1994) 137.

[9] M. Misiak, Nucl. Phys. B **393** (1993) 23 [E. B **439** (1995) 461].

[10] B. Grinstein, R. Springer and M. Wise, Phys. Lett. B **202** (1988) 138.

[11] M.S. Alam et al. (CLEO Collaboration), Phys. Rev. Lett. **74** (1995) 2885.

[12] A. Ali, G. F. Giudice and T. Mannel, Z. Phys. C **67** (1995) 417.

[13] A. Ali, T. Mannel and T. Morozumi, Phys. Lett. B **273** (1991) 505.

[14] A. Ali and G. Hiller, DESY Report 98-031.

[15] J. Chay, H. Georgi and B. Grinstein, Phys. Lett. B **247** (1990) 399; I.I. Bigi, N.G. Uraltsev and A.I. Vainshtein, Phys. Lett. B **293** (1992) 430 [E. B **297** (1993) 477]; I.I. Bigi et al., Phys. Rev. Lett. **71** (1993) 496; B. Blok et al., Phys. Rev. D **49** (1994) 3356 [E. D **50** (1994) 3572].

[16] A. Manohar and M. B. Wise, Phys. Rev. D **49** (1994) 1310.

[17] A. F. Falk, M. Luke and M. J. Savage, Phys. Rev. D **49** (1994) 3367.

[18] A. Ali, L. T. Handoko, G. Hiller and T. Morozumi, Phys. Rev. D **55** (1997) 4105.

[19] I. Bigi et al., Int. J. Mod. Phys. A **9** (1994) 2467.

[20] A. Falk et al., Phys. Rev. D **49** (1994) 4553.

[21] R. Jaffe and L. Randall, Nucl. Phys. B **412** (1994) 79.

[22] A. Ali and E. Pietarinen, Nucl. Phys. B **154** (1979) 519;
      G. Altarelli et al., Nucl. Phys. B **208** (1982) 365.

[23] C. Greub and S.-J. Rey, Phys. Rev. D **56** (1997) 4250.

[24] A. Ali and C. Greub, Phys. Lett. B **259** (1991) 182.

[25] A. Ali and G. Hiller, DESY Report 98-025, hep-ph/9803407 (submitted to Physical Review Letters).

[26] A. Ali and G. Hiller, DESY Report 98-030, hep-ph/9803428 (submitted to Physical Review D).

[27] G. Buchalla, G. Isidori and S. -J. -Rey, Nucl. Phys. B **511** (1998) 594.

[28] F. Krüger and L.M. Sehgal, Phys. Lett. B **380** (1996) 199.

[29] Z. Ligeti, I.W. Stewart and M.B. Wise, preprint CALT-68-2141, hep-ph/9711248.

[30] S. Glenn et al. (CLEO Collaboration), Phys. Rev. Lett. **80** (1998) 2289.

[31] M. Gremm, A. Kapustin, Z. Ligeti and M.B. Wise, Phys. Rev. Lett. **77** (1996) 20.

[32] G.-L. Lin, J. Liu and Y.-P. Yao, Phys. Rev. Lett. **64** (1990) 1498;
      G.-L. Lin, J. Liu and Y.-P. Yao, Phys. Rev. D **42** (1990) 2314.

[33] H. Simma and D. Wyler, Nucl. Phys. B **344** (1990) 283.

[34] S. Herrlich and J. Kalinowski, Nucl. Phys. B **381** (1992) 501.

[35] T. M. Aliev and G. Turan, Phys. Rev. D **48** (1993) 1176.

[36] A. Khodjamirian, R. Rückl, G. Stoll and D. Wyler, Phys. Lett. B **402** (1997) 167.

[37] G. Hiller and E. O. Iltan, Phys. Lett. B **409** (1997) 425.

[38] G. Hiller and E. O. Iltan, Mod. Phys. Lett. A **12** (1997) 2837.

[39] R. M. Barnett et al., Review of Particle Properties, Phys Rev D **54** (1996) 1.

[40] L. Wolfenstein, Phys. Rev. Lett. **51** (1983) 1845.

[41] C. Jarlskog and R. Stora, Phys. Lett. B **208** (1988) 268.

[42] P. Colrain and M. Williams (AEPH COllaboration), contributed to the International Europhysics Conference on High-Energy Physics, Jerusalem, Israel, 19-26 August 1997, (unpublished).

[43] C. Greub, T. Hurth and D. Wyler, Phys. Lett.B **380** (1996) 385; Phys. Rev. D **54** (1996) 3350.

[44] K. Chetyrkin, M. Misiak and M. Münz, hep-ph/9612313.

[45] S.L. Glashow, J. Iliopoulos and L. Maiani, Phys. Rev. **D2** (1970) 1285.

[46] G. Buchalla, A.J. Buras and M.E. Lautenbacher, Rev. Mod. Phys. **68** (1996).

[47] A. J. Buras and M. Münz, Phys. Rev. D **52** (1995) 186.

[48] P. Cho and M. Misiak, Phys. Rev. D **49** (1994) 5894.

[49] T.G. Rizzo, hep-ph/9802401.

[50] J. Hewett, hep-ph/9803370.

[51] B. Grinstein, R. Springer and M.B. Wise, Nucl. Phys. B **339** (1990) 269.

[52] S. Bertolini et. al., Nucl. Phys. B **353** (1991) 591; F. Borzumati, Z. Phys.C **63** (1994) 291.

[53] A. Ali and C. Greub, Z. Phys. C **60** (1993) 433.

[54] N. Pott, Phys. Rev. D **54** (1996) 938.

[55] K. Adel and Y.-P. Yao, Phys. Rev. D **49** (1994) 4945.

[56] C. Greub and T. Hurth, Phys.Rev. D **56** (1997) 2934.

[57] A.J. Buras, A. Kwiatkowski and N. Pott, Phys. Lett. B **414** (1997) 157.

[58] H. Georgi, Boulder, TASI 1991.

[59] A. F. Falk, hep-ph/9610363, to appear in the Proceedings of the XXIVth SLAC Summer Institute on Particle Physics, Stanford, 1996.

[60] M. Luke, Phys. Lett. B **252** (1990) 447; A.F. Falk and M. Neubert, Phys. Rev. D **47** (1993) 2965.

[61] P. Ball and V.M. Braun, Phys. Rev. D **49** (1994) 2472; V. Eletsky and E. Shuryak, Phys. Lett. B **276** (1992) 191; M. Neubert, Phys. Lett. B **322** (1994) 419.

[62] M. Neubert, Phys. Lett. B **389** (1996) 727.

[63] M. Neubert, preprint CERN-TH/98-2, hep-ph/9801269; to be published in Proc. of the Int. Europhys. Conf. on High Energy Physics, Jerusalem, Israel, 19 - 26 August, 1997.

[64] M. Neubert, C. Sachrajda, Nucl. Phys. B **483** (1997) 339.

[65] C. Bauer, preprint UTPT-97-19, hep-ph/9710513.

[66] A. F. Falk, M. Luke and M. J. Savage, Phys. Rev. D **53** (1996) 6316.

[67] V. Chernyak, Phys. Lett. B **387** (1996) 173.

[68] M. Gremm and I. Stewart, Phys. Rev. D **55** (1997) 1226.

[69] H. Li and H.-L. Yu, Phys. Rev. D **55** (1997) 2833.

[70] M.B. Voloshin, Phys. Lett. B **397** (1997) 275.

[71] A.K. Grant et.al., Phys. Rev. D **56** (1997) 3151.

[72] A.K. Grant, hep-ph/9801337.

[73] Z. Ligeti, L. Randall and M.B. Wise, Phys. Lett. B **402** (1997) 178.

[74] J. J. Sakurai, Currents and Mesons (University of Chicago Press, Chicago, 1969).

[75] K. Terasaki, Nuovo Cim. Vol. **66** A, No. **4** (1981) 475.

[76] N. G. Deshpande, Xiao-Gang He and J. Trampetic, Phys. Lett. B **367** (1996) 362.

[77] E. Golowich and S. Pakvasa, Phys. Rev. D **51** (1995) 1215.

[78] W.S. Hou, R.I. Willey and A. Soni, Phys. Rev. Lett. **58** (1987) 1608.

[79] B. Grinstein, M.J. Savage and M.B. Wise, Nucl. Phys. B **319** (1989) 271.

[80] W. Jaus and D. Wyler, Phys. Rev. D **41** (1990) 3405.

[81] P. Cho, M. Misiak and D. Wyler, Phys. Rev. D **54** (1996) 3329.

[82] T. Goto, Y. Okada, Y. Shimizu and M. Tanaka, Phys. Rev. D **55** (1997) 4273.

[83] J.L. Hewett and J. Wells, Phys. Rev. D **55** (1997) 55.

[84] D.S. Liu and R. Delbourgo, Phys. Rev. D **55** (1997) 7044.

[85] O. Bär and N. Pott, Phys. Rev. D **55** (1997) 1684.

[86] G. Buchalla and G. Isidori, preprint CERN-TH/97-374, LNF-98/003(P), hep-ph/9801456.

[87] J.L. Hewett, Phys. Rev. D **53** (1996) 4964.

[88] J.-W. Chen, G. Rupak and M. J. Savage, Phys Lett B **410** (1997) 285.

[89] C. S. Lim, T. Morozumi and A. I. Sanda, Phys. Lett. **218** (1989) 343; N. G. Deshpande, J. Trampetic and K. Panose, Phys. Rev. D **39** (1989) 1461; P. J. O'Donnell and H. K. K. Tung, Phys. Rev. D **43** (1991) R2067; N. Paver and Riazuddin, Phys. Rev. D **45** (1992) 978.

[90] M.R. Ahmady, Phys. Rev. D **53** (1996) 2843.

[91] A. Czarnecki, M. Jeżabek and J. H. Kühn, Acta. Phys. Pol. B **20** (1989) 961;
M. Jeżabek and J. H. Kühn, Nucl. Phys. B **320** (1989) 20.

[92] N. Cabibbo and L. Maiani, Phys. Lett. B **79** (1978) 109.

[93] A. F. Falk, M. Luke and M. J. Savage, Phys. Rev. D **53** (1996) 2491.

[94] A. Ali and C. Greub, Phys. Lett. B **361** (1995) 146.

[95] M. Barish et al. (CLEO Collaboration), Phys. Rev. Lett. **76** (1996) 1570; Ed. Thorndike (private communication).

[96] Z. Ligeti and M.B. Wise, Phys. Rev. D **53** (1996) 4937.

[97] J.M. Soares, Phys. Rev. D **53** (1996) 241; J. Milana, Phys. Rev. D **53** (1996) 1403; G. Ricciardi, Phys. Lett. B **355** (1995) 313.

[98] G. Eilam et al., Phys. Rev. D **53** (1996) 3629.

[99] M. Neubert and B. Stech, hep-ph/9705292, to appear in the Second Edition of Heavy Flavours, edited by A. J. Buras and M. Lindner (World Scientific, Singapore).

[100] T.E. Browder, K. Honscheid and D. Pedrini, Ann. Rev. Nucl. Part. Sci. **46** (1996) 395.

[101] A. F. Falk, Z. Ligeti and M.B. Wise, Phys. Lett. B **406** (1997) 225.

[102] V. Barger, C.S. Kim and R.J.N. Philips, Phys. Lett. B **251** (1990) 629.

[103] R.D. Dikeman and N.G. Uraltsev, Nucl. Phys. B **509** (1998) 378; see also, I.I. Bigi, R.D. Dikeman and N.G. Uraltsev, preprint TPI-MINN-97-21, hep-ph/9706520.

[104] A. Ali, Z. Physik C **1** (1979) 25.

[105] S. Brodsky, G.P. Lepage and P. Mackenzie, Phys. Rev. D **28** (1983) 228.

[106] A.F. Falk and M. Luke, Phys. Rev. D **57** (1998) 424.

[107] I. I. Bigi, M. Shifman, N.G. Uraltsev and A. Vainshtein, Phys. Rev. D **52** (1995) 196.

[108] T. Mannel, Phys. Rev. D **50** (1994) 428.

[109] M. Gremm and A. Kapustin, Phys. Rev. D **55** (1997) 6924.

[110] A. Kapustin and Z. Ligeti, Phys. Lett. B **355** (1995) 318.

[111] I.I. Bigi et al., Phys. Lett. B **328** (1994) 431.

[112] R. Balest et al. (CLEO Collaboration), Phys. Rev. D **52** (1995) 2661, and references quoted therein for earlier measurements.

[113] J. Bartelt et al. (CLEO Collaboration), CLEO/CONF 93-19;
      B. Barish et al. (CLEO Collaboration), Phys. Rev. Lett. **76** (1996) 1570;
      R.Wang, Ph. D. Thesis, University of Minnesota (1994).

[114] W.F. Palmer, E.A. Paschos and P.H. Soldan, Phys. Rev. D **56** (1997) 5794.

[115] D.S. Hwang, C.S. Kim and W. Namgung, Z. Phys. C **60** (1996) 107; Phys. Rev. D **54** (1996) 5620.

[116] S.J. Brodsky and F.S. Navarra, Phys. Lett. B **411** (1997) 152.

[117] M. Acciarri et al. (L3 Collaboration), Phys. Lett. B **363** (1995) 137.

[118] M. K. Gaillard and B. W. Lee, Phys. Rev. D**10** (1974) 897.

[119] Chia-Hung V. Chang, Guey-Lin Lin and York-Peng Yao, Phys. Lett. B **415** (1997) 395.

[120] L. Reina, G. Ricciardi and A. Soni, Phys. Rev. D **56** (1997) 5805.

[121] T.M. Aliev, G. Hiller and E.O. Iltan, Nucl. Phys. B **515** (1998) 321.

[122] S. Bertolini and J. Matias, Phys. Rev. D **57** (1998) 4197.

[123] T.M. Aliev and E.O. Iltan, hep-ph/9803459.

[124] N. Isgur and M.B. Wise, Phys. Lett. B **232** (1989) 113; **237** (1990) 527.

[125] A. Ali, V. M. Braun and H. Simma, Z. Phys. C **63** (1994) 437.

[126] M. A. Shifman, A. I. Vainshtein and V. I. Zakharov, Nucl. Phys. B **147** (1979) 385.

[127] A. Ali and V. M. Braun, Phys. Lett. B **359** (1995) 223.

[128] P. Colangelo et al., Phys. Lett. B **317** (1993) 183.

[129] V.M. Belyaev, B.L. Ioffe, Sov. JETP **83** (1982) 876.

[130] B.L. Ioffe, A.V. Smilga, Phys.Let. B **133** (1985) 436.

[131] V. L. Chernyak and A. R. Zhitnitsky, Phys. Rep. **112** (1984) 173.

[132] M. Bauer, B. Stech and M. Wirbel, Z. Phys C **34** (1987) 103.

[133] D. Choudhury and J. Ellis, hep-ph-9804300.

[134] T. Inami and C.S. Lim, Prog. Theor. Phys. **65** (1981) 297; [E. **65** (1981) 1772].

[135] M. Neubert, Phys. Rev. D **49** (1994) 4623.

[136] A. Ali, DESY Report 96-106 [hep-ph/9606324]; to appear in: *Proceedings of the XX International Summer College on Physics and Contemporary Needs*, Bhurban, Pakistan, June 24 - July 13, 1995 (Nova Science Publishers, New York).

[137] P. Pascual and R. Tarrach, *QCD: Renormalization for the practitioner*, Springer 1984.

[138] F. J. Yndurain, *quantum chromodynamics*, Springer, Heidelberg, 1983.

[139] C. Itzykson and J.-B. Zuber, *quantum field theory*, McGraw-Hill, 1980.

[140] M. Jamin and M. E. Lautenbacher, Comp. Phys. Comm **74** (1993) 265.

[137] P. Pascual and R. Tarrach, QCD: Renormalization for the practitioner, Springer 1984.

[138] F. J. Ynduráin, quantum chromodynamics, Springer, Heidelberg, 1983.

[139] C. Itzykson and J.-B. Zuber, quantum field theory, McGraw-Hill, 1980.

[140] M. Jamin and M. E. Lautenbacher, Comp. Phys. Comm 74 (1993) 265.